

A SYSTEMATIC SEARCH FOR LOW MASS COMPANIONS
ORBITING NEARBY STARS AND THE CALIBRATION
OF THE END OF THE STELLAR MAIN SEQUENCE

by

Todd Jackson Henry

A Dissertation Submitted to the Faculty of the
DEPARTMENT OF ASTRONOMY
In Partial Fulfillment of the Requirements
For the Degree of
DOCTOR OF PHILOSOPHY
In the Graduate College
THE UNIVERSITY OF ARIZONA

1 9 9 1

THE UNIVERSITY OF ARIZONA
GRADUATE COLLEGE

As members of the Final Examination Committee, we certify that we have

read the dissertation prepared by Todd Jackson Henry

entitled A SYSTEMATIC SEARCH FOR LOW MASS COMPANIONS ORBITING

NEARBY STARS AND THE CALIBRATION OF THE END OF THE

STELLAR MAIN SEQUENCE

and recommend that it be accepted as fulfilling the dissertation

requirement for the Degree of Doctor of Philosophy

<u>Donald W. McCarthy, Jr.</u>	<u>11/11/91</u>
Donald W. McCarthy, Jr.	Date
<u>Marcia J. Rieke</u>	<u>11/11/91</u>
Marcia J. Rieke	Date
<u>James W. Liebert</u>	<u>11/11/91</u>
James W. Liebert	Date
<u>Jonathan Lunine</u>	<u>11/11/91</u>
Jonathan Lunine	Date
_____	<u>11/11/91</u>
	Date

Final approval and acceptance of this dissertation is contingent upon the candidate's submission of the final copy of the dissertation to the Graduate College.

I hereby certify that I have read this dissertation prepared under my direction and recommend that it be accepted as fulfilling the dissertation requirement.

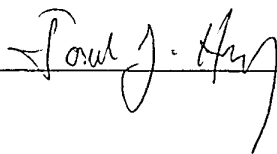
<u>Donald W. McCarthy, Jr.</u>	<u>11/11/91</u>
Dissertation Director Donald W. McCarthy, Jr.	Date

STATEMENT BY AUTHOR

This dissertation has been submitted in partial fulfillment of requirements for an advanced degree at the University of Arizona and is deposited in the University Library to be made available to borrowers under the rules of the Library.

Brief quotations from this dissertation are allowable without special permission, provided that accurate acknowledgement of source is made. Requests for permission for extended quotation from or reproduction of this manuscript in whole or in part may be granted by the head of the major department or the Dean of the Graduate College when in his or her judgment the proposed use of the material is in the interests of scholarship. In all other instances, however, permission must be obtained from the author.

SIGNED: _____

A handwritten signature in cursive script, appearing to read "Paul J. Hing", is written over a horizontal line.

DEDICATION

What would I ever have done without you?

To Mother, Dad, Betty, Deb, Val, Curt, and Matt, I cannot say how much your support has meant. You never doubted, you never pushed, you never judged (well, maybe a little, but that's ok — we're awfully good at giving advice in our family, no?). When I was twelve years old I said I wanted to get a Ph.D. in astronomy. I didn't even know what it was. Okay, so maybe I didn't know what I was getting myself into, but you always gave me the freedom to find out for myself, and that has made all the difference. It has been a long haul to get to this point, and you have stuck with me all the way. You don't know how much that means. This work is dedicated to you. I love you all.

I remember a night some fifteen years ago, when at the ripe age of twelve I was taken out on a dark night by a very special person to really look at the stars for the first time. My dear Linda, this is what you started. I don't think that either of us knew then that a decade and a half later I'd be here. I still remember the jingle you talk me that wintry night about the zodiac, and use it to this day. And every time I use it, I think of you.

Finally, although this may be a bit unusual, this work is also dedicated to my advisor, Don McCarthy. I have nothing but respect and admiration for you, Don, and always will. You have offered me so many things during the last five years that many never get, especially the freedom to do what I could, and the patience to help me get there. You have also given me opportunities that many never have. We have spent much more time together than most advisors and their students, whether at the observatory, on the mountain, in the gym, or at a camp or conference, and I am hard-pressed to find any moment that wasn't a good one. I think, to say the least, that this is unusual. You are the main reason why I decided to stick it out here in Tucson, although there were many times when I thought I had had enough. I am very glad I stayed. And best of all, you have not only been a fine mentor, but I have come to think of you as a great friend. Here's to you!

ACKNOWLEDGMENTS

I am indebted to my colleagues in the speckle group — Julian Christou, Jonathan Freeman and Brian McLeod, without whom the truly monumental task of tackling the piles of speckle data would have been utterly impossible. And of course, the help I've had from Diana Johnson has been outstanding, and I sometimes wonder if she didn't handle the data better than I. I would also like to thank Jim Liebert, Jon Lunine and Marcia Rieke for their guidance over the past years, and would like to acknowledge the support of the National Science Foundation, which has made this thesis possible.

Some of my more interesting moments in Tucson have come in the company of Grace Wolf, Pat Hartigan, Barry and Bridgett Meyers-Rice, Rex and Janet Saffer, Liz Alvarez, Rich Roberts, and Joe Haller. I seem to recall seedy dives, outdoor adventures, tennis, dancing of various sorts — some proper, some entirely improper and a whole lot more fun — and even a time (the only time in Tucson, I'll have you know) when I was absolutely abashed. I shall not forget. I must not forget, either, the wild ones — Joan Morrill, Jennifer Gangel, Sally Oey and Mark English, who always guarantee an interesting time, regardless of the locale.

Over the past years, Kim Dow and Davy Kirkpatrick have convinced me that astronomers can be fun, have listened to me rant and rave, watched me ride a never-ending roller coaster of sanity, and endured to tell about it. They are remarkable. They also happen to be two of the most conscientious, caring individuals I know, and have always been there when I needed them. Thanks, you guys, for everything.

Then there are the runners. Without the likes of Ted Fotinos, Wayne Smith, Brent Johnson, Diane Engler and Bill Latter (yes, Bill, I think of you more as a running buddy than a geeky astronomer) life in Tucson would have been unbearable. Fortunately, there are also those borderline fanatics like myself (although I think we've lost sight of the border at this point!), Danny Burns and Ray Dunn, without whom I would have gone truly mad. You two have dragged my butt up and down A Mountain and the Phoneline more times than I care to count, and the runs we've done will be among my fondest memories of Tucson. You've been two of the best confidants, counselors, compatriots, and friends any man could want or hope for, and I will miss your daily comradeship dearly.....until, of course, we end up again in the same part of this planet we call home.

There is a special group of people who have made their indelible marks on my psyche over the past years, and who have helped me learn a very important lesson — how to really live. You are exciting, motivating, thoughtful, and thought-provoking. Above all else, you don't make a habit of letting life get the upper hand, but lead it yourself instead, and I thank you for sharing your secrets with me. So, to you Katy Moore, Johnny Gerrick, and Marty Salvato, I owe the world. You have taught me lessons that I will use forever, and I love you all for it.

Thanks.

TABLE OF CONTENTS

List of Illustrations	10
List of Tables	15
Abstract	16
1 Introduction: M Dwarfs, Brown Dwarfs and Planets	18
1.1 Extrasolar Planetary Systems	19
1.2 Research Objectives of this Thesis	20
1.3 Personal Motivation	21
1.4 Brown Dwarfs	21
1.4.1 History and Characterization of Brown Dwarfs	22
1.4.2 The Semantics of Brown Dwarfs	27
1.4.3 The Semantics of Planetary Systems	28
1.5 Recent Events	30
1.6 Systematic Searches for Brown Dwarfs	31
1.6.1 Indirect Methods — Astrometry and Radial Velocity	32
1.6.2 Direct Methods — Deep Imaging and Speckle	36
1.7 M Dwarfs	40
1.7.1 Empirical Definitions of M Dwarfs and Brown Dwarfs	40
1.7.2 Luminosity and Mass Functions	42
1.7.3 Binarity	43
1.7.4 Contribution to the Galactic Missing Mass	44
1.8 Organization of this Thesis	44
2 Infrared Speckle Imaging	52
2.1 Diffraction-Limited Imaging from the Earth's Surface	53
2.1.1 Atmospheric Seeing	53

	7
2.1.2 Speckle Imaging	54
2.1.3 Application of Speckle Techniques	59
2.2 One-Dimensional Infrared Speckle Imaging	63
2.2.1 The History of 1D Scanning	63
2.2.2 The Steward Observatory 1D Scanner	64
2.2.3 Observing Technique with the 1D Scanner	67
2.3 Two-Dimensional Infrared Imaging	68
2.3.1 The (Brief) History of 2D Speckle Imaging	68
2.3.2 The Steward Observatory 2D Infrared Speckle Camera	69
2.3.3 Observing Technique with the 2D Camera	73
2.4 Data Reduction	76
2.4.1 One-Dimensional Data	76
2.4.2 Two-Dimensional Data	78
3 A Systematic Search for Low Mass Companions	
Orbiting Nearby Stars	95
3.1 An Infrared Speckle Search for Brown Dwarfs	96
3.1.1 Scientific Rationale for an Infrared Speckle Search ...	96
3.1.2 Why M Dwarfs?	99
3.2 The Sample	100
3.2.1 Parallaxes and their Distribution	101
3.2.2 Photometry	103
3.2.3 Age	106
3.3 The Visibility Curves	106
3.3.1 Determining Visibility Curves for Resolved Sources .	108
3.3.2 Comparison of 1D and 2D Techniques — Gliese 67AB	112
3.4 Six New Companions — Resolved Targets	114

3.4.1 The Companions	114
3.4.2 Mass Determinations	118
3.5 Determining Detection Limits for Unresolved Sources	121
3.5.1 Limits at 1, 2, 5 and 10 AU	121
3.5.2 Flux Limits for the Survey as a Whole	126
3.5.3 Mass Limits for the Survey as a Whole	128
3.6 Missed Objects	130
3.6.1 Missed Primary Targets	130
3.6.2 Orbital Presentation Selection	131
3.6.3 Stellar Companions Missed due to Bright Limits	133
3.7 Binaries	133
3.7.1 All Secondaries	133
3.7.2 Binary Frequency	134
3.7.3 Semimajor Axis Distribution	136
3.8 Characteristics of All Survey Constituents	137
3.8.1 Absolute Magnitudes	137
3.8.2 Spectral Types	139
3.9 The Nearby Star Census	140
3.10 Objects Worthy of Special Note	141
4 Characterizing the Population of Low Mass Dwarfs ...	270
4.1 The Mass-Infrared Luminosity Relations	271
4.1.1 Selection of Systems	272
4.1.2 Mass Determinations	273
4.1.3 Systems with Very Low Mass Components	274
4.1.4 Luminosity Determinations	276
4.1.5 The Relations at J, H and K	277

4.1.6 Absolute Infrared Magnitudes at the 80 Jupiter Border	280
4.2 A Mass–Spectral Type Relation	280
4.3 The Luminosity Function	282
4.3.1 The Infrared Luminosity Function	284
4.3.2 The Visual Luminosity Function	286
4.3.3 The Effect of Binaries	287
4.4 The Mass–Luminosity–Age Diagram	289
4.5 The Mass Function	289
4.6 The Contribution of Low Mass Objects to the Galactic Disk	291
5 The End of the Main Sequence and Brown Dwarfs Today	325
5.1 The Empirical Definition of the End of the Main Sequence	326
5.1.1 Absolute Magnitudes and Colors	326
5.1.2 Spectral Type	327
5.1.3 The End of the Main Sequence	328
5.2 Brown Dwarfs Today	329
5.2.1 Candidates with Mass Determinations	330
5.2.2 Intrinsically Faint, Red Candidates	332
5.2.3 Cluster Candidates	334
5.2.4 Serendipitous Discoveries of Brown Dwarf Candidates	335
5.2.5 The Two Best Brown Dwarf Bets	337
5.3 Summary	338
5.4 The Future	341
References	347

LIST OF ILLUSTRATIONS

1.1 Masses of Stars, Brown Dwarfs and Planets	50
1.2 Regions Searched for Companions by Various Techniques ...	51
2.1 Schematics of 1D and 2D Speckle Techniques	88
2.2 Flatfield and Badpixel Map for the 2D Camera Array	89
2.3 Three Successive Speckle Frames of GL 873	90
2.4 Three Successive Speckle Frames of GL 704AB	91
2.5 Several Examinations of Speckle Observations of GL 22AC .	92
2.6 Processing Steps of a Single Frame of GL 623AB	93
2.7 Seeing Plots for 500 Frames taken of GL 873	94
3.1 Visibility Curves for GJ 1005AB	177
3.2 Visibility Curves for GL 65AB	178
3.3 Visibility Curves for GL 185AB	179
3.4 Visibility Curves for GL 234AB	180
3.5 Visibility Curves for GJ 1116AB	181
3.6 Visibility Curves for GL 570BC	182
3.7 Visibility Curves for GL 623AB	183
3.8 Visibility Curves for GL 644AB	184
3.9 Visibility Curves for GL 661AB	185
3.10 Visibility Curves for GL 831AB	186
3.11 Visibility Curves for GL 860AB	187
3.12 Comparison of 1D and 2D Speckle Data of GL 67AB	188
3.13 Residual Visibility Curves from 2D Data of GL 67AB	189

3.14 Visibility Curves for GJ 1002	190
3.15 Visibility Curves for GL 15A	191
3.16 Visibility Curves for GL 15B	192
3.17 Visibility Curves for GL 34B	193
3.18 Visibility Curves for GL 54.1	194
3.19 Visibility Curves for GL 83.1	195
3.20 Visibility Curves for GL 105B	196
3.21 Visibility Curves for GL 109	197
3.22 Visibility Curves for GL 166C	198
3.23 Visibility Curves for GL 169.1A	199
3.24 Visibility Curves for GL 205	200
3.25 Visibility Curves for GL 213	201
3.26 Visibility Curves for GL 229	202
3.27 Visibility Curves for GL 251	203
3.28 Visibility Curves for GJ 1093	204
3.29 Visibility Curves for GL 268	205
3.30 Visibility Curves for GL 273	206
3.31 Visibility Curves for GL 283B	207
3.32 Visibility Curves for GL 285	208
3.33 Visibility Curves for GL 299	209
3.34 Visibility Curves for GL 300	210
3.35 Visibility Curves for GJ 1111	211
3.36 Visibility Curves for GL 338A	212
3.37 Visibility Curves for GL 338B	213
3.38 Visibility Curves for GL 388	214

3.39 Visibility Curves for LHS 292	215
3.40 Visibility Curves for GL 393	216
3.41 Visibility Curves for GL 402	217
3.42 Visibility Curves for GL 406	218
3.43 Visibility Curves for GL 408	219
3.44 Visibility Curves for GL 411	220
3.45 Visibility Curves for GL 412A	221
3.46 Visibility Curves for GL 412B	222
3.47 Visibility Curves for GL 445	223
3.48 Visibility Curves for GL 447	224
3.49 Visibility Curves for GL 450	225
3.50 Visibility Curves for GJ 1156	226
3.51 Visibility Curves for GL 493.1	227
3.52 Visibility Curves for GL 514	228
3.53 Visibility Curves for GL 526	229
3.54 Visibility Curves for GL 555	230
3.55 Visibility Curves for GL 581	231
3.56 Visibility Curves for GL 625	232
3.57 Visibility Curves for GL 628	233
3.58 Visibility Curves for GL 643	234
3.59 Visibility Curves for GL 644C	235
3.60 Visibility Curves for GL 687	236
3.61 Visibility Curves for GL 699	237
3.62 Visibility Curves for GL 701	238
3.63 Visibility Curves for GJ 1224	239

3.64 Visibility Curves for GJ 1230A	240
3.65 Visibility Curves for GL 725A	241
3.66 Visibility Curves for GL 725B	242
3.67 Visibility Curves for GL 729	243
3.68 Visibility Curves for GL 752A	244
3.69 Visibility Curves for GL 752B	245
3.70 Visibility Curves for GL 809	246
3.71 Visibility Curves for GL 829	247
3.72 Visibility Curves for GL 873	248
3.73 Visibility Curves for GL 876	249
3.74 Visibility Curves for GL 880	250
3.75 Visibility Curves for GL 884	251
3.76 Visibility Curves for GL 896A	252
3.77 Visibility Curves for GL 896B	253
3.78 Visibility Curves for GJ 1286	254
3.79 Visibility Curves for GL 905	255
3.80 Visibility Curves for GL 908	256
3.81 Limit Tests for GL 67AB at H	257
3.82 Limit Tests for GL 67AB at K	258
3.83 Limit Tests for GL 623AB at H	259
3.84 Survey Limits for Blackbodies of Various Radii	260
3.85 Survey Limits in the Mass–Luminosity–Age Diagram	261
3.86 Resolution Probabilities of Binaries 2 to 8 Parsecs	262
3.87 Superresolution Probabilities of Binaries 2 to 8 Parsecs ..	263
3.88 Standard Spectral Sequence for M0 to M9 Dwarfs	264

3.89 Spectral Features for M 0.0, M4.5 and M 9.0 Dwarfs	268
3.90 The Nearby Star Census during the Last 45 Years	269
4.1 Visibility Curves for GL 22AC	303
4.2 Visibility Curves for GL 25AB	304
4.3 Visibility Curves for GL 67AB	305
4.4 Visibility Curves for ADS 3475AB	306
4.5 Visibility Curves for GL 340AB	307
4.6 Visibility Curves for GL 352AB	308
4.7 Visibility Curves for GL 508AB	309
4.8 Visibility Curves for GL 677AB	310
4.9 Visibility Curves for GL 702AB	311
4.10 Visibility Curves for GL 704AB	312
4.11 Mass–Luminosity Relation at K	313
4.12 Mass–Luminosity Relation at H	314
4.13 Mass–Luminosity Relation at J	315
4.14 Mass–Spectral Type Relation for Late-Type Dwarfs	316
4.15 Luminosity Functions at K for the Survey Members	317
4.16 Luminosity Functions at H for the Survey Members	318
4.17 Luminosity Functions at J for the Survey Members	319
4.18 Luminosity Functions at V for the Survey Members	320
4.19 True and False Luminosity Functions at V	321
4.20 True and False Luminosity Functions at K	322
4.21 Mass–Luminosity–Age Diagram for Very Low Mass Objects	323
4.22 Mass Function for the Survey Members	324
5.1 Color–Absolute Magnitude Diagram for the Survey Members	346

LIST OF TABLES

1.1 Brown Dwarf Searches	46
1.2 Astrometric Companions	48
2.1 Observing Parameters Encountered During the Survey	87
3.1 Photometry of M Dwarfs within 8 Parsecs	149
3.2 Infrared Speckle Observations of M Dwarf Survey Binaries	158
3.3 Companion Magnitude Limits for M Dwarfs	163
3.4 Characteristic Survey Limits	167
3.5 M Dwarf Secondaries within 8 Parsecs	168
3.6 Distribution of M Dwarf Secondaries	169
3.7 Characteristics of All 99 Survey Members	170
3.8 The Nearby Star Census during the Last 45 Years	176
4.1 Orbital Parameters and Masses for Close Binaries	293
4.2 Infrared Speckle Observations of Non-Survey Binaries	296
4.3 Absolute Magnitudes for Mass–Luminosity Relation Objects	298
4.4 Spectral Types for Stars with Well-Determined Masses	301
4.5 Mass Estimates for All 99 Survey Members	302
5.1 Brown Dwarf Candidates	344

ABSTRACT

We have completed a search for low luminosity companions, including high mass brown dwarfs, to all M dwarfs known within eight parsecs of the sun, and north of -25° . A region 1 to 10 AU in radius around 74 M dwarfs has been searched using one-dimensional and, since October 1989, two-dimensional infrared speckle imaging. We are able to detect companions as faint as $M_K \sim 10.8$ at a separation of 1 AU around most targets, and to fainter limits at larger separations.

We found six new companions orbiting the survey stars. Because we are working at resolution scales where rapid orbital motion can be followed, we are able to determine accurately the crucial parameter defining whether or not an object is a brown dwarf — its mass — when the speckle data is combined with astrometric or spectroscopic data. We find that the masses of the six new secondaries fall between 0.39 and 0.05 M_\odot . Three of the new companions, G208-44B, GL 623B and LHS 1047B, and one previously known secondary in the survey, Ross 614B, are brown dwarf candidates with masses ~ 80 Jupiters ($0.08 M_\odot$), the dividing line between stars and brown dwarfs. Including the new companions and all previously known close multiples, the survey now contains 99 red objects, none of which has $M_K = 10-11$. This break occurs at the precipitous drop in luminosity near 80 Jupiter masses predicted by the theoretical models, and indicates that high mass brown dwarfs may be much fainter than very low mass stars.

In addition, we provide infrared photometry at J, H and K for all 99 survey members, and spectral types on a standard system for half. Analysis of the entire sample indicates that 50% of the stars in the more distant half of the survey volume remain undetected, as is supported by the steadily growing M dwarf census over the last 45 years. The binary fraction of M dwarfs, 30–40%, is lower than that of earlier type main sequence stars, and there are more companions to M dwarfs found between 1 and 10 AU than in any other decade interval. We find that the luminosity function of the lowest mass stars is flat or rising to the end of the main sequence, and that the mass function undoubtedly rises to the stellar/substellar break. We illustrate that the resolution of close binaries is crucial if accurate luminosity and mass functions are to be determined. Finally, we estimate $0.02 \text{ M}_{\odot}/\text{pc}^3$ to be the amount of mass contributed by M dwarfs to the galactic mass.

Based upon new mass-luminosity relations developed at infrared wavelengths using a sample of stars with well-determined masses between 1.2 and 0.08 M_{\odot} , we are able to define empirically the end of the main sequence. We present absolute magnitudes, colors and spectral types for objects at the theoretical lowest stellar mass. Using these relations, we conclude that a few brown dwarfs may have already been discovered.

CHAPTER 1

Introduction:

M Dwarfs, Brown Dwarfs and Planets

1.1 Extrasolar Planetary Systems

“...’tis a consummation devoutly to be wished.”

Hamlet Act III, Scene I

That is my reply to my sister Val’s ever-present question, “Find any brown dwarfs, yet, little brother?”

We have now ventured, by the poking and prodding of our mechanical extensions, to eight of the nine known planets in our own solar system — only Pluto remains. We have found that each of these worlds, and many of their moons, has a personality all its own. Yet, this is only a beginning. Countless worlds may circle distant suns, and each of these will be undoubtedly unique.

A brown dwarf is one type of world that may be called a planet. The discovery of the elusive brown dwarf was a goal of the search I began five years ago. It is my attempt to unearth evidence of planetary systems other than our own, and although I did not find a multitude of brown dwarfs, a few interesting candidates were revealed. I hope that this work gives a much better idea of what a brown dwarf is, and that it is at least a step toward finding worlds circling other stars.

The technology available to astronomers today allows us to begin, in

earnest, searches for planets orbiting other stars. Methods ranging from the study of photographic plates to the use of state-of-the-art infrared arrays, now grant us the ability to probe the neighborhoods of many types of stellar hosts for companions smaller than stars. We have uncovered great disks of matter around some stars, which may be in the process of coalescing into planetary systems, but as yet, *no definite extrasolar planets have been discovered.*

1.2 Research Objectives of this Thesis

The primary goal of the work presented here has been the discovery of brown dwarfs orbiting nearby stars. This has been carried out through a systematic search of M dwarf stars known within eight parsecs of the sun. As the search progressed, it became obvious that developing an *empirical* definition of a brown dwarf was crucial, so that I would know if I found one. During the past five years, a working definition for objects which may be brown dwarfs has been developed using measurable characteristics — fluxes, colors, and spectral types based upon mass.

In addition, a wealth of information about the most populous stars, the M dwarfs, has been collected. Their luminosity and mass functions (in the infrared and visible) can be determined using the sample of stars nearest the sun — those that have been studied the most thoroughly — and the effect of binaries on those functions can be addressed. We also provide stellar infrared mass-luminosity relations that have been calibrated to the end of the main sequence. Based upon the comprehensive survey and the empirical definition of the stellar/substellar boundary, we can now

determine whether there is a conspicuous break in the luminosity function at the point of stellar ignition, and test current theoretical models for objects of mass ~ 80 Jupiters. We also provide quantitative data on the binarity of the smallest stars, and estimate the amount of mass contributed to the galaxy by the M dwarfs.

1.3 Personal Motivation

On a more personal level, I entered graduate school in 1986 with the desire to contribute to the search for planets orbiting other stars, and this seemed to be the best bet at the time. I see this survey as a step toward characterizing what a planet is, and understanding how our solar system got here. It is also a step toward our own future, as someday (probably not too soon) I believe we will go there. And finally, it is a step, albeit a small one, toward finding life of some unimaginable sort somewhere else, should it be there to be found. These reasons may appear somewhat far-sighted, or perhaps a bit romantic, but if nothing else, at least they are all mine.

1.4 Brown Dwarfs

Brown dwarfs are bodies roughly the size of Jupiter that have masses between 10 and 80 Jupiter masses. They burn deuterium briefly, but are not capable of self-support at any time during their lives by fusing hydrogen into helium.

A *star* is a self-luminous body that is capable of energy output because of nuclear reactions in its core. A *planet* shines by reflected light, or, as in the case of the Jovian planets in our solar system,

may emit additional radiation due to continuing gravitational contraction, differentiation or elemental radioactive decay. At no time during its life, however, does a planet experience a significant phase of thermonuclear reactions. In between the realms of stars and planets is a domain where the not-quite-stars/not-quite-planets exist. These objects have been dubbed *brown dwarfs*, alias BDs.

For this discussion, we define BDs to be objects with masses in the range 10 to 80 Jupiters, thereby including all “substellar” bodies with masses below that needed to spark hydrogen burning, but which do burn deuterium early in their lives for a short period of time.

1.4.1 History and Characterization of Brown Dwarfs

The term “brown dwarf” was coined by Jill Tarter in her Ph.D. thesis in 1975. At the *Astrophysics of Brown Dwarfs Conference* held in October 1985, she defended her rationale for the name against other possible names including, but certainly not limited to, Lilliputian stars, black dwarfs, infrared dwarfs and Super-Jupiters. In reference to the name brown dwarf, she humorously pointed out in a talk entitled “Brown is Not a Color” that “I am convinced that the non-color brown most aptly describes these bodies of questionable existence, whose formation probably has to do with a fragmentation process, and not the existence of a planetary system, whose opacities are unknown and whose appearance is therefore unpredictable...As a last word, I think that it will be this workshop that will have settled the name question” (Tarter 1986). And so the conference did.

In 1963, modelling fully convective, collapsing stars, Kumar first

recognized that at very low masses, stable nuclear fusion could not occur in objects where electron degeneracy set in, resulting in central temperatures and densities too low to spark hydrogen. Such a failed star, as a BD is often called, will never reach the main sequence, and once it evolves beyond the stage of maximum central temperature, is doomed through further contraction to approach a state of complete degeneracy. Early steps in defining BDs were made by Tarter (1975) and Stevenson (1978).

Progress in describing the elusive BD has been made since. A great deal of theoretical work has been done to characterize very low mass stars (Grossman *et al.* 1974 [interiors]; Mould 1976 [atmospheres]; VandenBerg *et al.* 1983 [interiors]) which provided a stepping stone to determinations of the luminosities, temperatures, radii and masses of BDs. The most detailed BD models include those by D'Antona and Mazzitelli (1985), Nelson *et al.* (1986), Lunine *et al.* (1986, 1989), and Burrows *et al.* (1989). The current definition of a BD includes any body that is not capable of doing what a star does — burning simple hydrogen into helium — but that can experience for a brief time (at most 10^8 years early in its life) an episodic burst of deuterium burning. The upper mass limit for BDs (and, by definition, the lower mass limit for stars) is consistently found to be ~ 80 Jupiters in the BD models, although in some combinations of abundances, opacities, and mixing lengths, the limit shifts slightly (70 to 90 Jupiters). The minimum luminosity and surface temperature for a stabilized hydrogen burning star are $\sim 10^{-4} L_{\odot}$ and 1700–3500 K respectively, again, depending on the model. Deuterium burning can occur at a core temperature of $7\text{--}8 \times 10^5$ K, and sets the lower mass limit for a BD at 12 Jupiters (Grossman

and Graboske 1973), although the exact value is sensitive to the adopted deuterium abundance.

We can estimate crudely the mass that defines the star/BD border as follows. By equating the pressure for the equation of state for an ideal gas, P_i (roughly true for collapsing protostars) with electron degeneracy pressure, P_e (the support mechanism that takes over if stellar ignition fails), we can solve for the mass as function of radius. We begin with the basic equations

$$P_i = nkT = \frac{\rho kT}{m_p} \quad (1.1)$$

$$P_e = 0.0485 \cdot \frac{h^2 \rho^{5/3}}{m_e m_p^{5/3}} \quad (1.2)$$

$$P_i = P_e \quad (1.3)$$

where n is the particle number density, k is Boltzmann's constant, T is the temperature, ρ is the mass density, h is Planck's constant, and m_e and m_p are the masses of the electron and proton. Setting the two pressures equal,

$$\frac{\rho kT}{m_p} = 0.0485 \cdot \frac{h^2 \rho^{5/3}}{m_e m_p^{5/3}} \quad (1.4)$$

and solving for the density yields

$$\rho = 93.6 \cdot \frac{(kTm_e)^{3/2} m_p}{h^3}. \quad (1.5)$$

At this point we substitute the mean density of the contracting cloud, characterized by mass M and radius R , for the ambient mass density,

$$\rho \sim \frac{M}{\frac{4\pi R^3}{3}} \quad (1.6)$$

and solve for M as a function of R , where we have chosen the hydrogen ignition temperature, T , to be 3.4×10^6 K

$$M = 630 \cdot R^3. \quad (1.7)$$

BD models indicate that their radii are typically 7—10% of the sun's radius (70—100% of Jupiter's radius). Assuming a middle value of $R \sim 6 \times 10^9$ cm, we find the minimum mass for hydrogen burning to be 65 Jupiters, a value not far from the canonical 80 Jupiter cutoff.

Figure 1.1 illustrates schematically the realms of stars, BDs and planets. The horizontal scale is logarithmic in mass, and illustrates the narrow range of masses in which BDs lie — narrower, in fact, than any of the other divisions. Plotted for reference are the solar system objects Pluto (a pseudo-terrestrial world), Mercury and Earth (the terrestrial mass extremes), Uranus and Jupiter (the Jovian mass extremes), and the Sun.

The first stage of a BD's life is spent in hydrodynamic collapse at roughly constant temperature and with decreasing radius, eventually leading to the brief phase of deuterium burning. Following the deuterium burning

stage, they will still glow, due to the release of gravitational and thermal energy, and may be detectable in the near infrared (1-5 μm) as they cool and slowly contract. Because they are small and cool, it is plausible that large numbers of BDs have remained essentially invisible, and that they may contribute significantly to the mass of the galaxy.

Recent advances in observing techniques utilized at infrared wavelengths have allowed progress to be made in determining the characteristics of the lowest mass and lowest luminosity objects known. The faintest, least massive objects we are now finding encroach upon the theoretical border between stars and BDs, and some masses actually fall below the 80 Jupiter limit, although the errors are not sufficiently small to allow them to be called definitive BDs.

One must ask whether such objects exist at all, since no absolutely proven BD is known currently, and if they do exist, are there many of them? These questions are of fundamental importance to considerations of other planetary systems and what may comprise the proposed missing mass of the galactic disk. Do stars form by one scenario, and planetary systems in an entirely different way? Objects may exist which span the range of sizes and masses in between stars and planets, lending impetus to a unified theory of many-body system formation, whether they be stars, BDs, or planets, of which only the details differ. We have now reached a point when the scientific results are exciting and predictably controversial. As a final word about the history of BDs, we point out that the term "brown dwarf" was first used only sixteen years ago, and today we are capable of rigorous searches for such objects.

1.4.2 The Semantics of Brown Dwarfs

We are confronted with the following question of semantics: Should a brown dwarf be called a planet or a star? A *star* burns hydrogen into helium — that is what stars spend their main sequence lives doing. For most of their lives stars maintain a relatively steady output of energy, and generally brighten a little. BDs do not burn hydrogen, gradually cool, and slowly grow fainter. While a high mass BD may appear similar to a low mass star, a low mass BD may appear similar to a high mass Jovian planet. Yet, both the high mass BD and the low mass BD are BDs. Thus, the process of definition by similarity can lean either way, and therefore remains indeterminate.

The definition of the word *planet*, as originally used by the Greeks, is wanderer. BDs can certainly be seen to wander across the sky by an observer on a planet orbiting some distant star, thereby satisfying the original definition. In our solar system there are two entirely different classes of worlds, Jovian and terrestrial. Yet, for all their differences, both classes are called planets. According to current theory, a BD has more physical similarities to a Jovian planet than a Jovian has to a terrestrial planet. In fact, BDs glow (in the long term) for the same reason the Jovian planets do — the release of gravitational energy. Jupiter, for example, emits 60% more energy than it receives from the sun, and would radiate as a blackbody of temperature 95 K if it were removed from the solar system (Black 1980). There is no logical reason, then, why a third class of planet, more similar to one of the two accepted classes than those two are to one another, cannot be defined — brown dwarf.

The reason most often given for *not* calling a BD a planet is that it does not form in a disk of matter surrounding a star, the way the planets in our solar system presumably did (see, for example, Black 1985). One is then faced with the quandary: what is a free-floating Jupiter, not in the presence of a star, called? To complicate matters further, if two bodies orbit one another, but neither is a star, is either a planet? We must also consider the likely possibility that a BD *can* form in the disk of matter surrounding a protostar. Unless we are then willing to define an entirely new class of object for each situation (a cumbersome and unappealing solution), a BD should then be called a type of planet.

In summary, a brown dwarf can be a planet, but it cannot be a star. For the reasons given, it is the opinion of the author that a brown dwarf should be called a third class of planet.

1.4.3 The Semantics of Planetary Systems

Because this thesis involves a search for objects that may be called planets orbiting nearby stars, it is appropriate to discuss what a planetary system *is*. Groundwork for defining a planetary system has been laid by Huang (1973), and some of the following discussion parallels his. Currently, our working definition of a planetary system is naturally limited because our sun and its retinue of nine known planets comprise the only example we have. (Whether or not a star with a single planet orbiting it makes up a planetary *system* is purely a matter of semantics at this point.) Thus, the discussion of the meaning of the term “planetary system” remains somewhat academic because of the limited data, and as is often the case, the definition

will be cast and recast as examples are found to fit it. Such has been the case in the latter part of this century with attempts to define the concepts of "life" (viruses make this difficult) and "intelligence" (dolphins and chimpanzees complicate matters here). As we approach the twenty-first century, we find that the stage is now set for the thought-provoking process of defining "planetary system."

Today, conventional facets of the definition include characteristics evident in our own solar system — a large concentration of matter at its center which has evolved into a star, and bodies that orbit the central mass in roughly circular, coplanar, corevolving orbits. The subtle points which include terrestrial versus Jovian planets, minor planets, cometary clouds, etc. are unimportant in the basic definition.

An important distinction may be made between a planetary system and a binary system if one considers the way in which either developed. We now believe that our solar system formed from a rotating disk of gas and dust, where the planets coalesced from small condensations in the disk. Because of the shape and rotation of the disk, the bodies orbit in paths that are nearly circular, lie in the same plane, and follow the same direction. However, this need not always be the case. There is no requirement that the planetary objects *must* form in a disk near the star; they could be captured, for example, however unlikely that may be. In contrast, a binary system may form from masses condensing in a molecular cloud, or from the fissure of a developing central mass. Either situation can result in eccentric orbits. There is no reason, however, why a binary system *cannot* form from a primordial disk. It is clear, then, that while the guidelines for defining

planetary and binary systems may include stipulations involving formation processes, there will always be exceptions.

The broadest definitions shall be adopted here. A *planetary system* is any collection of gravitationally bound objects which includes at least one star and one planetary body, regardless of formation processes. A *binary system* is more easily defined as any system which consists of exactly two objects gravitationally bound to one another, regardless of their character. By this definition, the Earth-Moon system is a binary system. A *multiple system* possesses the same boundedness criterion, but may be made up of more than two members. Our solar system is both a planetary system and a multiple system.

1.5 Recent Events

We have now reached a crucial point in the search for extrasolar planetary systems. During the past few decades, claims have been made that planets have been “found” orbiting around stars in the solar neighborhood. The astrometrists have led the way, and their years of painstaking work should not be taken for granted. Perhaps the most famous report is the long-term work of van de Kamp (1986) and the possibility that there are two Jovian planets circling Barnard’s Star. This star remains interesting, and the existence of its planets is still unresolved (Gatewood, unpublished). Reports using other techniques include: the infrared speckle discovery of a companion to VB 8 (McCarthy *et al.* 1985), which has not been confirmed in follow-up work (Perrier and Mariotti 1987, and this thesis), a companion to the solar-type star HD114762 (Latham *et*

al. 1989) discovered by radial velocity techniques (thus, the mass remains undetermined), the companion to the white dwarf GD 165 (Becklin and Zuckerman 1988), and the recent announcement of a very low mass companion to the pulsar PSR 1829-10 (Bailes *et al.* 1991). The simple fact that such reports happen, and the tenacity with which they catch the attention of the public, is proof that the discovery of another star with its own planet(s) will not only cause a revolution in the astronomical community, it will at least create a stir in the general public as well. Within the last decade in particular, available technology has reached a level of sophistication in sensitivity and precision that permits realistic searches for substellar companions to be accomplished.

1.6 Systematic Searches for Brown Dwarfs

Through the use of indirect and direct search techniques, brown dwarf candidates are being discovered, and their characteristics revealed.

The motivation to search for very low mass objects has many facets. The nature of BDs, and the M dwarfs themselves, merits a great deal of work. First and foremost, what actually delineates a BD from an M dwarf is a matter of considerable importance, at least to the astronomical community — more than a few hours have been spent by the author and others, in impromptu gatherings at meetings, in hallways and offices, defining what a BD is, regardless of whether or not any *bona fide* examples are known. A variety of observational techniques, including both indirect and direct methods, has been applied to and sometimes invented exclusively for the purpose of finding very low mass objects. Systematic searches for

BDs are discussed below and are summarized in Table 1.1. (BD candidates discovered serendipitously are mentioned in the final chapter, see §5.2.4). Through systematic searches, whether by imaging, photometric, or kinematic techniques, we have begun to investigate whether other solar systems exist, and with the application of direct imaging at small and large scales in addition to astrometric and radial velocity techniques, the prevalence of BDs orbiting stellar primaries can begin to be assessed.

1.6.1 Indirect Methods — Astrometry and Radial Velocity

The indirect methods used to find companions to stars are those which do not directly detect the secondary body. Rather, it is the companion's gravitational effect on its primary that is measured. The two methods which have been applied to systematic searches of stars for low mass companions are the astrometric and radial velocity techniques.

The astrometric technique involves the high-precision measurement of wobbles induced in a stellar image by an unseen companion over long time periods. Typically, decades of photographic plates are analyzed for perturbations of candidate stars located in fields of background stars. Orbital periods of a few years to decades can be defined, with separations between the primary and its companion typically a few AU to tens of AU for nearby stars. Astrometry results in some of the most fundamental measurements in astronomy, including parallaxes and proper motions, in addition to orbital determinations.

Long-term astrometric programs have uncovered dark companions orbiting dozens of stars of various types in the solar neighborhood.

Lippincott (1978) and van de Kamp (1986) provide comprehensive reviews, which describe the astrometric technique and the coverage of nearby stars. To date, there have been ~ 50 astrometrically-discovered binaries — the first was Ross 614, which is included in the speckle survey discussed in this thesis. Many of these companions have now been revealed by infrared speckle and visual techniques. In Table 1.2 we give a comprehensive list of the known astrometric binaries and their current status (IR YES = resolved using infrared speckle, IR NO = not resolved, VIS YES = resolved using visual techniques, unseen = no attempt made to resolve by infrared speckle). The list has been compiled using the Lippincott and van de Kamp reviews, the USNO Catalog of Orbits of Visual Binary Stars by Worley and Heintz (1983), and recent articles forwarded to the author.

Note the predominance of northern hemisphere binaries, evidence that long-term astrometric programs have been underway only in the United States. Many of the still-unresolved companions, if real, are of very low mass. Stars with very uncertain astrometric orbits, which have been called into question (Heintz 1984, for example) are indicated by daggers in the table. In general, we have found astrometric orbits with photocentric amplitudes less than $0.05''$ to be unreliable, in that rarely do they turn out to have detectable companions. Conversely, it is possible that these companions are simply beyond the capability of current infrared speckle techniques. Stars with astrometric perturbations that remain unresolved and possess potential BD companions include GL 169.1A, GJ 1215, GL 699 and GL 791.2. BD candidates resolved using infrared speckle include GJ 1005B, GL 234B, GL 623B and GJ 1245C.

Figure 1.2 outlines the regions most effectively searched by astrometric and other techniques. The illustration is scaled logarithmically in separation along the horizontal axis. For reference, the semi-major axes of several solar system objects (Mercury, Earth, Jupiter and Pluto) are shown. Also plotted is the nearest star to the sun, Proxima Centauri, at its current separation from its primary, Alpha Centauri (itself a binary). Because of the large separation, it is not clear that Proxima is actually in orbit around the close binary, and we use this as an example of the outer limit for low mass secondary detection. Beyond this limit, it is difficult to confirm, by any technique, whether or not a companion is gravitationally bound to its “primary.”

The inner regions illustrated in Figure 1.2 can be reached by radial velocity techniques. The inner cutoff is chosen somewhat arbitrarily to be 0.001 AU, corresponding to $0.2 R_{\odot}$. Radial velocity studies quantify the reflex of a star’s motion along the line-of-sight due to the tugs of an unseen companion. As the secondary orbits the target star, the star’s spectrum is shifted from blue to red and back. The resultant curve yields information about the period, shape and size of the orbit. The major drawback of radial velocity work is that the inclination cannot be determined unless the system eclipses, or can be resolved by other techniques, and while the mass function is obtained, individual masses for the system components cannot be found.

Campbell *et al.* (1988) searched twelve dwarfs and four subgiants of spectral types F, G and K for velocity variations over a period of six years. They found two stellar companions, and allude to the possibility that seven

of the remaining fourteen show long period trends, which may be due to companions of mass ≤ 10 Jupiters, although as they discuss, some other cause such as convective granulation patterns, may be operative. One of the stellar companions, χ^1 Ori B has been observed by this group using infrared speckle techniques; the other has not been attempted. No good BD candidates were found.

The most extensive radial velocity search done for BDs circling nearby stars is the excellent work of Marcy and Benitz (1989). In the process of examining 70 nearby, primarily M dwarf stars over periods up to 3.8 years, they uncovered four definitely stellar companions to GL 206, 268, 735 and 829 which are double-lined spectroscopic binaries, one stellar companion to GL 570B, and one companion near the hydrogen burning minimum mass at 80 Jupiters, GL 623B. The latter two were also discovered concurrently by infrared speckle observations — Mariotti *et al.* (1990) and our speckle survey for GL 570B, and McCarthy and Henry (1987) for GL 623, which remains a BD candidate.

Latham *et al.* (1989 and references therein) have reported one of the most interesting BD candidates, using radial velocity techniques with the original intent of manufacturing a list of new IAU radial velocity standards. The solar-type star HD114762 was found to possess a periodic trend with an 84 day duration. The minimum mass for the companion is 11 Jupiters, with a 99% chance that it has mass less than 80 Jupiters, making it a very good BD candidate.

Finally, McMillan (1991) has a five year observing baseline for 16

solar-type stars in a high-precision (≤ 10 m/s) radial velocity study which is still in progress. Preliminary results indicate suspicious data in a few cases, but longer time coverage is required for confirmation.

1.6.2 Direct Methods — Deep Imaging and Speckle

Direct methods used to search for companions are those that measure first-hand some parameter of the secondary object. These methods all utilize imaging techniques, including deep photographic, spectroscopic and speckle, and they all measure the radiative flux from the low mass companion.

Deep photographic studies sometimes target specific stars, probing the space around them for wide (a few arcseconds to a few arcminutes) companions, or are conducted in young stellar clusters. Before the age of the charge-coupled devices (CCDs) which are used now, searches done at visible wavelengths made use of photographic plates. With the advent of large-format infrared arrays, the most recent searches have been done in the near-infrared J, H and K bands ($1.0\text{--}2.5\ \mu\text{m}$), which are more favorable to the detection of very red, low luminosity objects. Usually, fields are imaged at several wavelengths so that the colors and temperatures of the candidates can be determined. Spectroscopic searches, typically done in the red ($0.6\text{--}0.9\ \mu\text{m}$), and recently in the near-infrared, are often used as follow-up steps to the first-stage photometric searches in order to further define an object's character.

Many deep imaging surveys have been done to evaluate the luminosity function of the faintest stars. Most notably, the proper motion surveys of Luyten and Giclas have covered the full sky photographically.

Vysotsky and Uppgren have done large-scale objective prism surveys to remove the kinematical bias inherent to proper motion surveys, and have concentrated on the galactic poles. The reader is directed to Liebert and Probst (1987) for the relevant references. These surveys in general, however, were not done specifically to detect BDs, and will not be discussed further here.

Deep imaging surveys which have the primary purpose of finding BDs naturally fall into four general areas — young star clusters, field searches, white dwarfs, and nearby stars. While the cluster searches possess the advantage that BDs are brighter at younger ages and therefore easier to detect, they suffer from four problems which are always difficult to address — cluster membership of the candidates, reddening in the cluster field, accurate photometry for faint objects in crowded fields, and the true age of an individual source. Even if the age of the cluster can be estimated, a single object may not have that age, and fitting a specific candidate to the models at those ages is problematic. Nonetheless, some of the surveys have proven fruitful, revealing BD candidates: Jameson and Skillen 1989 [5 candidates]; Stauffer *et al.* 1989 [4 candidates]; Rieke and Rieke 1990 [3 candidates]; Hambly and Jameson 1991 [~ 30 candidates]; Simons 1991 [~ 20 candidates]). Other studies have proven to be boondoggles (Forrest *et al.* 1989; follow-up by Stauffer *et al.* 1991). These discoveries challenge the theoretical models, but in no reported instance is there evidence of binarity in the candidates. Thus, the eventual determination of the crucial parameter that defines a BD, its mass, is impossible.

Field searches are similar, and although the problems of cluster

membership, reddening and difficult photometry are eliminated, an age estimate for a solitary body is unreliable. Again, the problem ends in an uncertain mass estimate based upon model-fitting. Efforts in this category have sometimes ended in no candidates (Boeshaar *et al.* 1985), or a few (Hawkins and Bessell 1988, [2 candidates]; Kirkpatrick 1991 [1 candidate]).

At longer wavelengths, IRAS has provided a database which can be searched for BD candidates. Examination of ~ 5000 $12\ \mu\text{m}$ sources present in the IRAS Point Source Catalog has resulted in no candidates (Beichman 1987 and references therein) — all were identified as SAO stars, faint M giants, carbon stars, or in one case, an infrared quasar. Similar results were obtained when follow-up work was done on 47 uncataloged objects (Beichman *et al.* 1990). Two candidates were found during a check of ~ 1200 $12\ \mu\text{m}$ sources in the more sensitive Serendipitous Survey (Cutri *et al.* 1985), but neither proved to be a brown dwarf.

Infrared photometric measurements of white dwarfs have been procured in an effort to detect the excess flux due to a low mass, red companion. Probst (1983) first attempted this, and found no excess due to a BD in over 100 white dwarfs. Kumar (1987) similarly found none around 20 stars. At the same time, Zuckerman and Becklin (1987) probed 14 white dwarfs in the Hyades and Pleiades for low mass companions where BDs would presumably be younger and brighter, and came up empty. Their effort in a larger survey of 200+ white dwarfs is still in progress (Zuckerman and Becklin 1991), and the results are more encouraging. So far, the search has uncovered two infrared excesses which could be BD companions (Zuckerman and Becklin 1987; Becklin and Zuckerman 1988),

at least one of which, GD 165B, is a spatially-resolved, very red object. Finally, Shipman (1986) has examined 21 nearby white dwarfs for BD excesses using coadded IRAS data and found no candidates.

For objects in the solar neighborhood, the fundamental work by van Biesbroeck (1944, 1961) done using photographic plates taken of the regions surrounding nearby stars revealed what have become two benchmarks of the lower main sequence, if not BDs themselves, VB 8 and VB 10. Other comprehensive searches that target nearby stars have been done in the near-infrared and together have resulted in only one BD candidate (Jameson *et al.* 1983 [no candidates]; Skrutskie *et al.* 1989 [1 candidate]; Rieke and Rieke, unpublished [no candidates]).

In addition to the deep photometric work, speckle searches, implemented in the infrared for low mass secondaries, permit the direct measurement of a companion's characteristics. Speckle imaging is done when high resolution information is desired. It is the only technique that can probe within 20 AU of nearby stars and recover information about the secondary directly. Recent advances in infrared arrays have permitted the expansion from one-dimensional scanning to two-dimensional frame-snapping techniques.

This thesis discusses an infrared speckle search for low mass companions orbiting nearby M dwarfs. The initial stage of the systematic search began in 1986 using a one-dimensional scanner, and eventually expanded to include all M dwarfs within eight parsecs north of -25° after the development of a two-dimensional speckle camera. The speckle

search techniques are discussed in detail in Chapter 2, and the search results in Chapters 3, 4 and 5.

1.7 M Dwarfs

The M dwarfs dominate the galactic population, yet they remain among the most poorly understood members of all astronomical species.

Although the mundane red dwarfs comprise roughly 70% of our galaxy's population, we know little about them. In fact, many of the most basic scientific questions concerning these runts of the stellar family remain unanswered because they may be as much as ten thousand times fainter than our sun. Their masses, radii and temperatures are poorly determined, their luminosity and mass functions, which describe them as a group, are ill-defined, and whether or not there is a conspicuous break in the star formation process at the point of stellar ignition is not understood. Furthermore, what fraction of red dwarfs are in multiple systems remains unknown.

1.7.1 Empirical Definitions of M Dwarfs and Brown Dwarfs

During the survey, frustration in knowing if an object could be considered a viable BD candidate or whether it fell in with the rest of the stellar M dwarfs led me to the following question: Are there any empirical guidelines that can be used to tell a very low mass M dwarf from a high mass BD? A large body of data was collected on M dwarfs and BD candidates during the search, including absolute magnitudes in the near-infrared bands, colors, spectral types and spectral features. Few attempts had been made before this work to delineate *empirically* the M dwarfs from

the BDs. One of the primary goals of this thesis has been to develop an empirical definition of a BD, or alternately, what would a BD look like if you found one?

Today, the single agreed-upon diagnostic that separates the BDs from the stars is mass. Current models of stars and BDs show the end of the main sequence to be at ~ 80 Jupiter masses, as discussed in §1.4.1. Direct imaging by infrared speckle splits a binary system's total flux into its component fluxes. The combination of the speckle-determined separation with an astrometric or spectroscopic orbit allows the direct calculation of the masses, and with accurate infrared photometry and trigonometric parallaxes, the absolute magnitudes and colors can be found for the components. A mass–luminosity relation defined in the infrared, where low mass stars and BDs are brightest, is more easily obtained, and more useful, than it is in the visible where the objects are difficult to study.

Although close binary systems were not split in the work of Veeder (1974), empirical relations for bolometric and absolute infrared magnitudes, colors, emission properties and masses were given. Since that work, the masses of known binary components have been revised, several close binaries have been resolved for the first time, and many more very low mass companions have been found. Marcy and Moore (1989) and Henry and McCarthy (1990) provided preliminary M_K vs. mass relations, which can now be improved substantially. Extensive databases now allow us to calibrate observed quantities — absolute magnitudes at J, H, K and V, colors, spectral type, and spectral features — with mass.

1.7.2 Luminosity and Mass Functions

Recent work on the luminosity function (LF) of very low mass stars has been extensive, and nearly every conceivable answer has been found. Much of the work is summarized in Liebert and Probst (1987). The shape of the LF is wavelength-dependent, assuming a different character in the visible than in the infrared, because of the extreme redness of the fainter stars. In the visible (surveys done in the V through I bands), the LF is reported to turn over (Luyten 1968; Probst and O’Connell 1983; Gilmore and Reid 1983; Reid 1987 and references therein; Hawkins and Bessell 1988; Leggett and Hawkins 1988; Stobie *et al.* 1989; Stauffer *et al.* 1989; Hambly and Jameson 1991), be flat (Dahn *et al.* 1986; Fahlman *et al.* 1989), or rise (Simons 1991). Among the infrared LFs, some studies find a LF that turns over at low masses (Hawkins and Bessell 1988; Leggett and Hawkins 1988; Skrutskie 1989) and some find that it rises (Henry and McCarthy 1990; Zuckerman and Becklin 1991). A few studies also indicate that the LF rises again after a decline, but the statistics in all cases are so small and unreliable as to warrant only minor consideration. All studies which indicate falling LFs (typically the turnover occurs near $0.2 M_{\odot}$) suffer from the contamination of field binaries that are counted as single stars.

We present determinations of the LF found in the infrared using the nearby stars, in which all binaries are resolved, and known infrared fluxes and color relations are used to transform the infrared LF into a visible LF. We also investigate the effects of unresolved binaries on determinations of the LF from field and cluster studies.

A well-determined mass function (MF) at low stellar masses is crucial to our current understanding of the purported unseen mass in the galactic disk, what types of objects comprise it, and how it is distributed. The conversion of a LF to a MF requires an accurate mass–luminosity relation for the M dwarfs, which until now has been unavailable. Here we provide much needed mass–luminosity relations at J, H and K for dwarfs of mass 1.2 to 0.08 M_{\odot} . Scalo (1986) derived a MF that peaks near 0.3 M_{\odot} and decreases rapidly at lower masses. His conclusion is based on the assumption that the mass–luminosity relation is a power law for low masses. Kroupa *et al.* (1991) use the slope of the mass–luminosity relation and the poorly-defined visible LF to find the MF. Hubbard *et al.* (1990) have found that the initial MF for very low mass stars in the Hyades does not increase with decreasing mass. As with the LF, it is perhaps more useful to find the mass function in the infrared, where the objects of concern are more easily observed. We examine the MF in detail here, using infrared observations of the survey members and the new calibration of the mass–luminosity relation.

1.7.3 Binarity

Very little work has concentrated on the binary fraction of the lowest mass stars. Abt (1983) reviews the binary frequencies in various stellar populations, including dwarfs of types O, B, A, F and G, but passes over the M dwarfs for lack of data. Liebert and Probst (1987) discuss other searches for binaries among the M dwarfs, but to date, no comprehensive study has been published. We provide quantitative data on M dwarf binarity using our survey M dwarfs.

1.7.4 Contribution to the Galactic Missing Mass

On a grand scale, low mass stars and BDs may account for the so-called “missing mass” of the galactic disk. Although some studies (Kuijken 1989a, 1989b) indicate that there may be no mass actually “missing,” it remains possible that astronomers do not observe $\sim 0.1 \text{ M}_{\odot}/\text{pc}^3$, or 50% of the local mass density (Bahcall 1984a, 1984b). It has been proposed that the lack of visible mass (stars, dust and gas) required to explain the dynamics of stars in the solar neighborhood may be comprised of distinct substellar mass objects, which may exist as solitary bodies, single companions to stars, or systems of objects. Furthermore, BDs may play a role in globular clusters, the Galactic halo, and at the greater scales of galaxy clusters, where larger fractions of mass evade detection.

Of immediate concern is the calibration of masses for M dwarfs, which is crucial for interpreting a luminosity function as a mass function, let alone how much total mass they contribute to the galaxy. We provide mass estimates for every M dwarf in the survey, determine the mass function of the survey members, and proceed to find the total mass contributed to the galactic disk in the solar neighborhood by the smallest stars.

1.8 Organization of this Thesis

In Chapter 2 we discuss the principles behind the infrared speckle technique, the observational methods, and the data reduction procedures used in the survey. Chapter 3 details the infrared speckle search conducted during the past five years, and includes discussion of new companions, detection limits, missed objects, and M dwarf binarity. In addition,

we report the absolute magnitudes, colors and spectral types for the survey constituents, and give a census of low mass objects in the solar neighborhood, as it stands today. In Chapter 4 the mass–luminosity calibration of low mass stars, from $1.2 M_{\odot}$ to the end of the main sequence is enumerated. The luminosity and mass functions are also discussed. Using the empirical mass–luminosity relations, we give mass estimates for all 99 of the survey members, and calculate their contribution to the mass of the galaxy. Chapter 5 outlines the empirical guidelines that can be used to determine when you’ve got a possible brown dwarf. Using these guidelines, we provide a summary of current brown dwarf candidates.

TABLE 1.1
BROWN DWARF SEARCHES

Reference	Search Method	Targets or Region	Coverage	R	T
Lippincott 1978	Astrometry	28 nearby dK, dM	decades	4	2 ^g
Lippincott 1978 and van de Kamp 1986	Astrometry	31 others all types	decades	11	4 ^g
Campbell <i>et al.</i> 1988	Radial Vel.	12 dF,dG,dK 4 subgiants	6 years 6 years	0 0	0 0
Marcy & Benitz 1989	Radial Vel.	70 dM	3 years	1	1
Latham <i>et al.</i> 1989	Radial Vel.	~50	10 years	1	1
McMillan 1991	Radial Vel.	16 dF,dG,dK	5 years	p	p
van Biesbroeck 1961	Deep VIS	650 nearby	10 arcmin ^r	1	1
Boeshaar <i>et al.</i> 1986	Deep VIS	Field	72 arcmin ²	0	0
Hawkins & Bessell 1988	Deep VIS	Field	85 degrees ²	2	2
Jameson & Skillen 1989	Deep VIS	Pleiades	175 arcmin ²	5	5
Hambly & Jameson 1991	Deep VIS	Pleiades	7 degrees ²	30 ^s	30 ^s
Kirkpatrick 1991	Deep VIS	Field	45 degrees ²	1	1
Stauffer <i>et al.</i> 1989	Deep IR	Pleiades	870 arcmin ²	4	4
Forrest <i>et al.</i> 1989	Deep IR	26 T-Tauri	12 arcsec ^r	4	0
Rieke & Rieke 1990	Deep IR	ρ Oph	200 arcmin ²	3	3
Simons & Becklin 1991	Deep IR	Pleiades	200 arcmin ²	22 ^s	22 ^s
Cutri <i>et al.</i> 1985	IRAS Seren.	~1200 sources	$ b \geq 30^\circ$	2	0
Shipman 1986	IRAS PSC	21 WD	1.5 arcmin ^r	0	0
Beichman 1987	IRAS PSC	~5000 sources	$ b \geq 50^\circ$	0	0
Beichman <i>et al.</i> 1990	IRAS PSC	47 uncataloged	$ b \geq 50^\circ$	0	0

TABLE 1.1 (continued)

Reference	Search Method	Targets or Region	Coverage	R	T
Probst 1983	Phot IR	106 WD	a few arcsec ^r	0	0
Kumar 1987	Phot IR	20 WD	3 arcsec ^r	0	0
Zuckerman & Becklin 1987	Phot IR	14 WD	6 arcsec ^r	0	0
Zuckerman & Becklin 1991	Phot IR	~200 WD	3 or 6 arcsec ^r	2	1
Jameson <i>et al.</i> 1983	Deep IR	21 nearby dK,dM	10–32 arcsec ^r	0	0
Skrutskie <i>et al.</i> 1989	Deep IR	55 nearby dK,dM,WD	2–7 arcsec ^r	1	1
Rieke & Rieke (unpub.)	Deep IR	25 nearby dM	3–50 arcsec ^r	0	0
this work	IR Speckle	74 nearby dM	0.2–2 arcsec ^r	3	3

^g “good” candidates, strong perturbations not yet eliminated by detection

^s statistical numbers of candidates

^r radius searched around target star

p indicates work in progress

Columns: “R” = number reported, “T” = number today.

TABLE 1.2
ASTROMETRIC COMPANIONS

Gliese No.	Other Name	RA	DEC	Status	Reference
GJ 1005	LHS 1047	00 13	-16 24	IR YES	IRM 88, *
GL 22A	BD +66 34A	00 29	+66 58	IR YES	MHMC 91
GL 53	μ Cas	01 05	+54 41	IR YES	M 84
GL 67	BD +41 328	01 39	+42 22	IR YES	HMFC 91
—	ι Cas	02 25	+67 11	unseen	—
GL 105A	BD +6 398	02 33	+06 39	IR NO	M 86
—	Algol	03 05	+40 46	VIS YES	LBSG 74
GL 164†	Ross 28	04 09	+52 30	unseen	—
GL 169.1A	Stein 2051A	04 27	+58 54	IR NO	*
—	ϵ Aur†	04 58	+43 46	unseen	—
GJ 1081	G 96-45	05 30	+44 47	IR YES	M 86
GL 222	χ^1 Ori	05 51	+20 16	IR YES	M 86
GL 234	Ross 614	06 27	-02 46	VIS YES	P 77
—	γ Gem	06 35	+16 27	IR NO	M 86
—	G 250-29	06 50	+60 57	IR YES	M 86
GL 275.2A†	G 107-69	07 27	+48 19	IR NO	M 86
GL 295†	BD +29 1664	07 57	+29 22	unseen	—
—	ζ Cnc C	08 09	+17 48	IR YES	M 86
GL 310	BD +67 552	08 32	+67 28	IR YES	M 86
GL 388†	BD +20 2465	10 17	+20 07	IR NO	*
GL 395†	36 UMa	10 27	+56 14	IR NO	M 86
—	G 146-72	10 52	+47 31	IR NO	M 86
GL 423A	ξ UMa A	11 16	+31 49	unseen	—
GL 568	Ross 52	14 52	+23 46	VIS YES	V 86
—	G 152-31	15 27	-07 41	unseen	—
GL 623	CC 20,986	16 23	+48 28	IR YES	MH 88
GL 644AB†	BD -08 4352	16 53	-08 15	unseen	—
GL 644C†	VB 8	16 53	-08 18	IR NO	*
GJ 1215	G 139-29	17 15	+11 44	IR NO	M 86
GL 681	α Oph	17 33	+12 36	IR YES	KLM 89
GL 687†	BD +68 946	17 37	+68 23	IR NO	*
—	Kuiper 84	17 54	+04 28	IR YES	M 86
GL 699†	Barnard's Star	17 55	+04 33	IR NO	*

TABLE 1.2 (continued)

Gliese No.	Other Name	RA	DEC	Status	Reference
GL 713	χ Dra	18 22	+72 43	VIS YES	LBSG 74
GL 735†		18 53	+08 20	unseen	—
GL 748	Wolf 1062	19 10	+02 49	IR YES	M 86
GL 752B†	VB 10	19 15	+05 05	IR NO	*
GL 760	δ Aqu	19 23	+03 01	unseen	—
GJ 1245A	G 208-44	19 52	+44 18	IR YES	MHFSLC 88
	Furuhjelm 54	20 08	+39 53	VIS YES	L 78
GL 791.2	G 24-16	20 27	+09 31	IR YES	*
	VW Cep	20 38	+75 25	VIS YES	V 86
GL 806†	CC 1228	20 43	+44 19	IR NO	M 86
GL 831	Wolf 922	21 29	-10 01	IR YES	*
GL 835	BD +27 4120	21 36	+27 30	IR YES	M 86
GL 835.1	ν Oct	21 36	-77 37	unseen	—
—	VV Cep	21 55	+63 23	unseen	—
—	α Tuc	22 15	-60 30	unseen	—
—	ζ Aqr B	22 26	-00 17	IR YES	M 86
—	STF 2934	22 39	+21 10	unseen	—
—	η Peg	22 41	+29 58	unseen	—
GL 873†	BD +43 4305	22 45	+44 05	IR NO	*

† very weak perturbation, possibly spurious

HMFC 91 = Henry *et al.* (1991),

IRM 88 = Ianna *et al.* (1988),

KLM 89 = Kamper *et al.* (1989),

LBSG 74 = Labeyrie *et al.* (1974),

L 78 = Lippincott (1978),

M 84 = McCarthy (1984),

M 86 = McCarthy (1986),

MH 88 = McCarthy and Henry (1988),

MHFSLC 88 = McCarthy *et al.* (1988),

MHMC 91 = McCarthy *et al.* (1991),

P = Probst (1977),

V = van de Kamp (1986),

* = this work

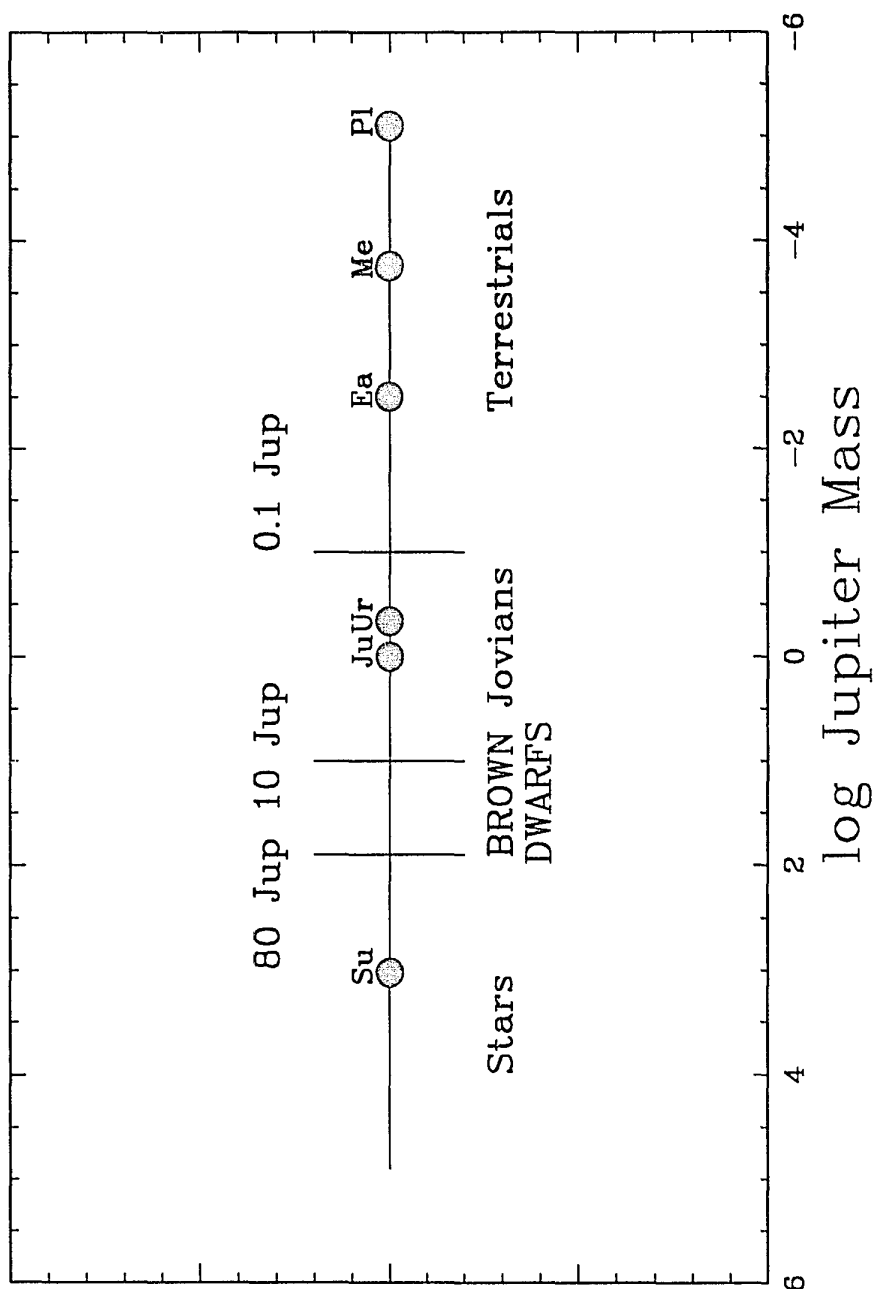


Figure 1.1 Schematic representation of masses for stars, brown dwarfs and planets. Note the narrow range of masses spanned by brown dwarfs. The sun, Jupiter, Uranus, Earth, Mercury and Pluto are labelled at their respective masses.

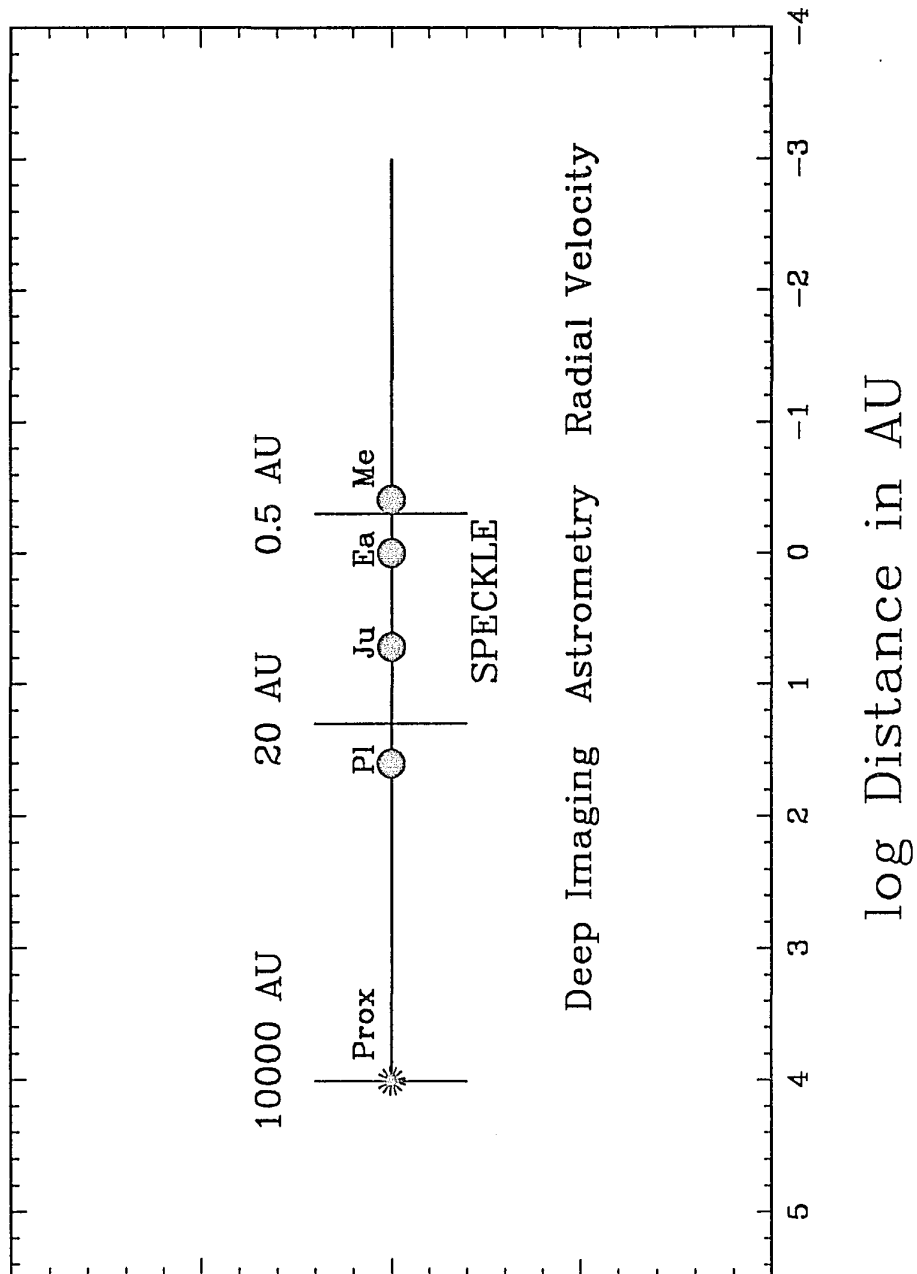


Figure 1.2 Schematic representation of the regions searched by various companion detection techniques. The planets Pluto, Jupiter, Earth and Mercury are labelled at their respective semimajor axes, as is the nearby star Proxima Centauri at its current separation from Alpha Centauri.

CHAPTER 2

Infrared Speckle Imaging

2.1. Diffraction-Limited Imaging from the Earth's Surface

The goal of speckle techniques is to remove the image-degrading effects of the Earth's atmosphere.

2.1.1. Atmospheric Seeing

While the Earth's atmosphere is useful for meteorological and biological functions, it is a hindrance to astronomical research. The atmosphere typically limits image quality to 1'' on good "seeing" nights from an excellent location. This limit in resolution can be reached in visible light ($0.55\ \mu\text{m}$) by a telescope with a primary diameter of only 10 cm. Although a larger aperture can theoretically reduce the size of an instantaneous image, the atmosphere will blur the image into a spot the size of the seeing disk in an amount of time which depends upon the wavelength of the light being observed. Typically this time is a few tens to a few hundreds of milliseconds in the infrared, and shorter in the visible.

As the size of the aperture increases, the instantaneous image breaks into smaller sections, producing a cloud of "speckles". Very short exposure times will effectively image the structure contained in the individual speckles and permit high spatial frequency information to be obtained. As the integration time is increased, one can imagine the long-exposure image to be composed of a sequence of short-exposure frames each with a different speckle cloud — thus, details in the light distribution are blurred. Unfortunately, few astronomical sources are bright enough to allow useful signal to noise measurements to be made in a single, short-exposure frame, and therefore, many frames must be taken. Speckle imaging is one technique

that satisfies the requirements that brief integrations be made in order to “freeze” the atmosphere, and that many integrations must be accomplished in order to build up sufficient signal to noise. This technique is the one utilized in both one and two dimensions for the work described here.

2.1.2 Speckle Imaging

The following discussion addresses those parameters of speckle imaging which are experimental, rather than theoretical in nature. Here we use the term speckle *imaging* rather than speckle *interferometry*, since phase information has been available throughout the survey detailed in this thesis, and with phase information it is possible to reconstruct images in either one or two dimensions. Because the speckle technique has now gained acceptance within the astronomical community, we believe that a discussion of its *application* is in order — specifically, a brief synopsis of relevant measurements which must be considered when making speckle observations. For a more detailed discussion of the theory of speckle techniques, the reader is referred to Dainty (1979) and Roddier (1988) and references therein, upon which much of the following discussion is based.

Various parameters relevant to speckle observations will be detailed below. As a useful reference, the reader is directed to Table 2.1, which lists values for the parameters in the best and worst situations encountered during the survey. The worst set of observing conditions (barring inclement weather, of course) is encountered when looking at a target at the shortest wavelength, J ($1.24\ \mu\text{m}$) in this case, and at high airmass ($z = 60^\circ$), both leading to poor seeing. The best case, which is more typical of the survey

as a whole, is represented by an observation taken at K ($2.19 \mu\text{m}$) where the seeing is generally better, and when pointed toward the zenith.

The principles of speckle imaging rely upon the fact that as a wavefront of light emitted by a distant object encounters the Earth's atmosphere, that wavefront is disturbed. Labeyrie (1970) first elaborated on the possible extension of Michelson stellar interferometry to use the full aperture of a large telescope. He pointed out that individual speckles form at the focus of a telescope, and contain spatial information to the theoretical diffraction limit. The speckles are caused by the interference effects in a coherent beam with random spatial phase fluctuations. In astronomical applications, phase fluctuations are introduced into the wavefront of a distant source by the Earth's atmosphere. Some parts of the wavefront will, however, remain in phase with one another as they pass through the layers of the atmosphere, and their interference will be constructive. The resulting images formed in these speckles will retain the original light-distribution information of the source, to the resolution limit of the telescope. Thus, one can gain information about the source to the diffraction limit, L (in arcseconds, $''$), of the telescope with diameter D (in meters), depending upon the wavelength of light observed, λ (in microns), as determined by interferometric theory:

$$L(\prime\prime) = \frac{206265}{10^6} \cdot \left(\frac{\lambda}{D}\right). \quad (2.1)$$

This limit represents the smallest spatial scale to which information can be obtained due to the coherent interference of light from the edges of

the telescope aperture. It is *not* the core size of the classic Airy pattern which is due to an *entire* circular aperture, which has a constant of 1.22 multiplying the right hand side.

The simplest experiment which forms the backbone of speckle theory, and gives rise to the above equation, is Young's double slit experiment, in which a single pinpoint of light is used to illuminate two slits at some distance from the pinhole. When a screen is placed beyond the slits, a pattern of bright and dark fringes is seen. The angular separation of the fringes is λ/D , where D is the separation of the slits. The key is that the single pinhole provides mutually coherent light to be passed from the slits, and thus interference can occur. The link to speckle techniques is direct because the pinpoint is mimicked by a distant stellar point source, and individual speckles are formed from coherent patches of light occurring at various separations on the primary mirror of the telescope. However, one must imagine sets of slits covering the telescope aperture at all position angles and all separations out to the telescope diameter. In this way two-dimensional information can be obtained at all spatial frequencies.

A speckle cloud is formed by the various coherent parts of the wavefront, and its characteristics have been described in detail by Dainty (1979). The number of speckles, N , can be estimated from

$$N(\#speckles) = 23000 \cdot \left(\frac{D}{r_o}\right)^2 \quad (2.2)$$

where D is the telescope diameter (in meters), and r_o (in cm) is the Fried parameter (Fried 1966). This parameter is defined to be equal to the

diameter of the diffraction-limited telescope whose Airy disc has the same area as the seeing disk, and can be thought of as the size of a bubble in the atmosphere at the telescope over which the light interferes coherently. The constant has been determined theoretically assuming a Kolmogorov spectrum of turbulence. It has been determined empirically that at a zenith angle, z ,

$$r_o(cm) \approx 20 \cdot \lambda^{6/5} (\cos z)^{3/5}. \quad (2.3)$$

Note that at longer wavelengths, r_o increases, N decreases, and thus fewer, higher intensity speckles are found. Intuitively, the $(D/r_o)^2$ portion of Eq. 2.2 can be thought of as a ratio yielding the number of ways the area of a telescope primary can be subdivided, given the sizes of the portions which are coherent. Experience shows that under excellent seeing conditions on a 1.8 meter telescope, the light in a star image may be contained in a single speckle at L ($3.4 \mu m$).

The integration time allowed before speckles become blurred and lose an unacceptably large amount of their high resolution information is critically dependent upon seeing. This parameter is perhaps the most important that can be controlled at the telescope. The atmosphere correlation time, τ_c , describes the time during which the speckles are not seriously degraded, and can be estimated from

$$\tau_c(msec) \approx 22 \cdot \left(\frac{r_o}{v}\right) \approx 450 \cdot \frac{\lambda^{6/5} (\cos z)^{3/5}}{v} \quad (2.4)$$

where v (in mi/hr) is the speed at which "bubbles" are blown past the

telescope aperture.

Another consideration which must be made when making speckle observations is the field size over which the distribution of the image intensity is correlated. Expressed as an angle, this field is termed the isoplanatic patch, and represents the angular diameter of the piece of sky across which two stars' speckle clouds will remain coherent. If the components of a binary star, for example, are separated by more than the scale of the isoplanatic patch, then the two speckle clouds will not be coherent, resulting in an overestimate of the magnitude difference (Roddier 1988). In tests of the isoplanatic patch sizes done at visible wavelengths near the zenith, the scale ranges from 1.5'' to 5''. The isoplanatic angle, Θ , increases proportionally with r_o (and therefore with λ) and is a strong function of the zenith angle (Young 1974):

$$\Theta(\mu) \approx 0.29 \cdot \frac{r_o}{\sec z} = 6.7 \cdot \lambda^{6/5} (\cos z)^{8/5}. \quad (2.5)$$

From this equation, we see that in the infrared two stars within a field up to 20'' in diameter will have coherent speckle clouds, a significantly larger region than is found at visible wavelengths.

Finally, in order to build signal to noise, observations are usually made using a bandpass of full width $\Delta\lambda$. Because the speckle pattern is wavelength-dependent, smearing of the multichromatic speckle cloud will lead to a loss of information for two reasons. The first is the loss of coherence caused by optical path differences of the various wavelengths of light within the bandpass as they travel through the atmosphere. A straightforward

criterion that is useful when considering acceptable bandwidths determined by coherence considerations is given by Dainty (1979):

$$\left(\frac{\Delta\lambda}{\lambda}\right)_{coh} < 0.052 \cdot \left(\frac{r_o}{D}\right)^{5/6}. \quad (2.6)$$

The second effect of finite bandwidth is due to the wavelength-dependent *magnification* of the speckle pattern. The spread in wavelengths, $\Delta\lambda/\lambda$, causes a spread in diffraction angles equal to $\Delta\Theta/\Theta$, in the same way a grating produces dispersion. The angle Θ corresponds roughly to the size of the total seeing disk λ/r_o , which is parcelled into subunits the size of the diffraction limit in speckle applications, so $\Delta\Theta$ can be set equal to λ/D . We then find the criterion

$$\left(\frac{\Delta\lambda}{\lambda}\right)_{mag} < 0.01 \cdot \left(\frac{r_o}{D}\right). \quad (2.7)$$

where in the last two equations, r_o is measured in cm, and D in meters.

2.1.3. Application of Speckle Techniques

In this section we discuss the application of the above experimental parameters to the primary study of the thesis, the infrared speckle search of nearby M dwarf stars for low mass companions (see Chapter 3). Nearly all of the observations reported in this dissertation were made on the Steward Observatory “90 inch” Telescope (hereafter SO 2.3m) which has a primary aperture of 2.26 meters. At the wavelengths of observation used here, J ($\lambda_o = 1.24 \mu\text{m}$), H ($\lambda_o = 1.62 \mu\text{m}$) and K ($\lambda_o = 2.19 \mu\text{m}$), the diffraction limits (Eq. 2.1) of the telescope are $0.11''$, $0.15''$ and $0.20''$, respectively.

The most distant sources targetted in the main survey are found at 8 parsecs, resulting in resolution limits of 0.9, 1.2 and 1.6 AU from the target star at the three wavelengths. In fact, the ability to “super-resolve” companions to half the diffraction limit — i.e. a companion is detected, although a unique solution to the separation and flux ratio is impossible — allows us to probe within 1 AU, even for a star at eight parsecs. It is important to point out that without speckle techniques, observations made in 1'' seeing at K, where cool companions are brightest relative to their primaries, do not allow us to probe any closer than 8 AU around the most distant survey stars. We find that many companions to M dwarfs lie between 1 and 10 AU (see §3.7.3), and without the use of high-resolution techniques, such as speckle imaging, we miss a crucial region around the stars where low mass companions exist.

Table 2.1 lists values for the various parameters discussed above, as applied to the best and worst observing situations encountered during the survey reported here. The Fried parameter (Eq. 2.3) varies from 17–50 cm through the near-infrared wavelengths used, and covering the full range of zenith angles at which observations were made, 0°–60°. We estimate the theoretical number of speckles from Eq. 2.2 to be 50–400 total. In practice, perhaps only 10% as many speckles are seen, indicating a larger r_o , a smaller constant in Eq. 2.2, and/or an integration time greater than the atmospheric coherence time, which leads to speckle blurring.

On a typical night of observation when useful data were acquired, the wind speed would rarely be much higher than 15 mi/hr at telescope level. It is almost certainly true that several layers in the atmosphere should

be considered when determining the coherence time, but as a first estimate we take the ground air speed. This estimate is probably not wildly wrong, as the speckle pattern has been seen to “freeze” often when the wind speed is lower than 15 mi/hr, but seldom when it is higher. Using this speed, the coherence time (Eq. 2.4) for an observation is found to be 25–75 msec. The trick is to choose an exposure time which allows sufficient signal to noise, but does not permit significant speckle blurring. Dainty (1979) has reported that the maximum SNR is reached in exposure times of length $\sim 1.5\text{--}2.0 \tau_c$, permitting integration times under good conditions of 40–150 msec in the near-infrared. Both the scanning times in the one-dimensional technique (100–125 msec in duration) and the integration times in the two-dimensional imaging (usually 80–200 msec) roughly satisfy this constraint, although some speckle blurring may occur.

The isoplanatic patch diameter over which the speckle patterns for the components of a binary star do not suffer serious dissimilarities is found from Eq. 2.5. We find that this field size in the worst case (an observation taken at J at $z = 60^\circ$) is $2.8''$, whereas for a more typical survey observation (at K with $z = 0^\circ$) the field expands to $17''$. The one-dimensional scans were usually $8''\text{--}10''$ in length, and the two-dimensional camera field $4''\text{--}8''$ in size.

Finally, we consider the two bandwidth requirements for speckle coherence and magnification discussed above. At J, H and K in the case of coherence loss (Eq. 2.6, $z = 60^\circ$), we find $(\Delta\lambda/\lambda)_{coh} = 0.28, 0.37$ and 0.50 , respectively. The full bandpasses used in the 1D scanner are $\Delta\lambda_J = 0.27 \mu\text{m}$, $\Delta\lambda_H = 0.52 \mu\text{m}$, and $\Delta\lambda_K = 0.71 \mu\text{m}$, which yield $(\Delta\lambda/\lambda)_{obs}$

values of 0.22 at J, 0.32 at H and 0.33 at K. In the 2D camera, the filters have $\Delta\lambda_J = 0.32 \mu\text{m}$, $\Delta\lambda_H = 0.39 \mu\text{m}$, and $\Delta\lambda_K = 0.47 \mu\text{m}$, which results in $(\Delta\lambda/\lambda)_{obs}$ values of 0.25 at J, 0.24 at H and 0.22 at K. Thus, in no case should there be a problem with coherence loss in the speckle cloud due to a finite bandwidth. However, Eq. 2.7, which describes the magnification of the speckle cloud caused by many overlapping clouds of various wavelengths, may be a problem. In this case, we find (again, at $z = 60^\circ$) $(\Delta\lambda/\lambda)_{mag} = 0.08, 0.11$ and 0.15 at J, H and K. However, the effects of the large bandwidth in the case of magnification should be identical for both the target object and reference point source, and can therefore be calibrated.

The empirical equations described by Eqs. 2.1 to 2.7 must be considered in the application of both one-dimensional (hereafter 1D) and two-dimensional (hereafter 2D) infrared speckle techniques. In 1D speckle thousands of scans are taken across a target and its point source, with the light scanned across a single pixel detector. In 2D speckle, thousands of frames are taken of the region around a target star and a nearby point source, with the light falling upon an array of pixels.

Obviously, there are several factors which must be considered when making any speckle observation. In fact, the technique becomes an exercise in struggling to answer simultaneously a host of questions for each scientific application of the technique, even if all of the targets are nearby stars. A suitable compromise is reached (or approached as closely as possible) when the following questions are answered satisfactorily: What integration time is optimal to allow sufficient signal-to-noise for this source, yet is not so long

as to blur the speckles, and still allows us to answer the scientific question at hand? At what wavelength should I make the observation in order to gain enough spatial frequency information, yet maintain the required signal-to-noise to get a useful answer? How many scans or frames can I take on a source to determine definitively a magnitude difference for a binary, or a limit to which it is unresolved, and still observe all stars in the survey? By balancing the night-to-night changes in weather, seeing fluctuations and observing programs (the nearby star survey, objects for the mass-luminosity relations, system calibration, and photometric program), one can hope to get useful information of some sort on nearly every night.

2.2. One-Dimensional Infrared Speckle Imaging

In one-dimensional infrared speckle techniques, the speckle cloud is scanned across a slit, and the intensity measured as a function of position.

2.2.1. The History of One-Dimensional Scanning

The application of speckle interferometry to astronomical sources was first done at visible wavelengths. In the visible, a wide range of sources has been examined, including the sun, asteroids, moons of the Jovian planets, the Pluto-Charon system, binary stars, star clusters, and evolved stars (see Dainty (1979) and Roddier (1988) for references). The expansion of speckle techniques from the visible to the infrared, where atmospheric coherence time is longer, has opened up new classes of objects for study.

McCarthy (1976) pioneered at Arizona the application of Michelson spatial interferometry (one spatial frequency point at a time) to infrared wavelengths ($5\text{ }\mu\text{m}$) in his study of evolved stars. Sibille *et al.* (1979)

first discussed expanding these infrared *spatial* techniques, which involved two small, widely-separated apertures as in Michelson's interferometer, to infrared *speckle* techniques, where all spatial frequencies to the diffraction limit of a single aperture are sampled simultaneously. They first applied the technique to the bright infrared source NML Cyg. Concurrently, Howell (1980) extended the work at Arizona to include simultaneous coverage of many spatial frequencies. Six years later, McCarthy (1986) reported the first infrared speckle work on the study of nearby stars for very low mass stellar and brown dwarf companions.

Until 1987 when the first 2D Speckle Cameras using infrared arrays came on-line, telescope images were scanned rapidly across a narrow slit, and the light allowed to fall upon a single detector. This 1D infrared technique has since expanded to other groups including those at UCLA, Wyoming, Cornell, Hawaii, and in France and Germany. In addition to extensive work on binary stars, published studies have examined solar system objects, pre-main sequence stars (T Tauri stars), evolved stars, and galaxies. The infrared speckle technique, now a dozen years old, has slowly gained acceptance in the astronomical community and produces important scientific results using 1D, and recently, 2D techniques.

2.2.2. The Steward Observatory 1D Scanner

The Steward Observatory Infrared Speckle 1D Scanner was operated during the initial stage of the survey until June 1989. Thereafter, the 2D Camera, discussed in §2.3.2, was used. Nearly all of the 1D observations were made on the SO 2.3m telescope located on Kitt Peak. A few

observations included in the survey were made on the Mayall 3.8m telescope, also on Kitt Peak. A schematic representation of the observing setup is shown in Figure 2.1a.

Scanning of the speckle cloud across the slit was accomplished by tilting the infrared secondary mirror of the SO 2.3m (f/45), following a triangular waveform. The scanlength was 6'' to 11'', with most nights 8'' to 10'', and was sufficiently rapid to “freeze” the seeing. The scanlength was set at the beginning of an observing run by measuring the distance between two star images on a television camera screen while the secondary was chopped back and forth, and was then calibrated accurately by observing double stars with well-determined orbits. We estimate maximum errors of 10% in the scale determination due to scanlength calibration. In excellent seeing conditions, the scanlength was shortened in order to spend more time on the object, and less on blank sky.

The slit effectively integrates the starlight in one dimension, and therefore allows visibility information to be acquired about the source at only one position angle at a time — along the scan direction. For the survey, all reported data are for scans taken in the north-south (NS) and east-west (EW) scan directions, although scans in other position angles can be made. Information about objects with more complicated structures than binary stars is gained by taking cuts across the object at many position angles, and permits better image reconstruction than NS/EW scans only. The scan motion must be highly linear, with distortions less than 0.02'', and the single pixel detector must have a flat frequency response over a broad bandwidth (0-500 Hz).

The dewar which houses the single pixel detector was bolted to the Cassegrain focus of the telescope. The telescope image first passes through the dewar window which is a flat BaF₂ lens. The light then passes through one of several interference filters. Those used during the survey were OCLI standard near-infrared filters, which are similar, but not identical, to those used in the 2D camera. Operated at 4K, the filters in the 1D scanner have full width bandpasses of: J ($\lambda\lambda = 1.11\text{--}1.38$, $\lambda_o = 1.24\ \mu\text{m}$), H ($\lambda\lambda = 1.35\text{--}1.87$, $\lambda_o = 1.62\ \mu\text{m}$), and K ($\lambda\lambda = 1.77\text{--}2.48$, $\lambda_o = 2.17\ \mu\text{m}$). The slit across which the speckle cloud is scanned is next in the optical path, and is located at the initial focal plane. Several slits are available for use; the ones used for survey work were $\sim 8''$ long, and $0.1''$ to $0.4''$ wide. The slit width was designed to be as close to $\leq \lambda/D$ as possible in order to permit sampling of the speckle cloud to the diffraction limit. In practice, however, the slits were often slightly larger to allow more light to pass through, and to prevent diffraction through the slit.

A field mirror images the telescope's infrared secondary mirror onto the single element detector. The $300\ \mu\text{m}$ -square detector is made of InSb, has a quantum efficiency of $\sim 70\%$ from $1\text{--}5\ \mu\text{m}$, and was operated at liquid helium temperature (4K). The individual scans were displayed in real-time on a monitor, which allowed the observer to notice changes in source intensity due to clouds, fluctuations in seeing, and focus drift. Before data were taken, the signal was focussed by peaking-up the real-time scans displayed on the monitor. The detector signal was read out 128 times per scan, and there were 8–10 scans made per second. The signal was amplified, passed through an anti-aliasing filter, a 12 bit A–D converter,

and into a VME/10 microcomputer. The raw data were then recorded on magnetic tape. On-line processing during observing included the coaddition of power spectra (for the sky, target and point source), phase computation, and shift-and-add scans. Calculations of photometric brightness and scan sharpness were also done.

2.2.3. Observing Technique with the 1D Scanner

For each object in the survey, a minimum of two scans was made, one each in the NS and EW directions in order to sample the entire plane of the sky around the target stars. Centered on the star, the 8'' to 10'' scans formed a search area 4'' to 5'' to each side. Scan rates across the objects were typically 80'' per second, fast enough to freeze the seeing fluctuations. Blocks of 512 scans were taken alternately between an object and a nearby ($\leq 2^\circ$) point source. The proximity of the reference star is crucial, because we wish to calibrate the effects of atmospheric turbulence using a source which undergoes seeing fluctuations similar to the target. Ideally, one would choose a point source within the isoplanatic patch, but the likelihood of a source of similar brightness so close to the target is small, unless the target is in a relatively close binary ($\leq 10''$). Point sources were chosen from the SAO Catalog to be roughly the same brightness as the target in the infrared so that similar amplifier gains could be used as the telescope was nodded between the two sources. Occasionally, the "point sources" proved to be binary systems themselves, and the observation was restarted with a new reference star.

Twenty-six stars were searched using 1D techniques, at either K

or H. Faint objects were observed at H when more signal was required. During an observation, real-time data processing, which included object visibility and phase computation, permitted the observer to play an active role in deciding when a sufficient amount of data had been taken on a particular object. Typically, more than 8000 total scans were taken in each scan direction for an object and a similar number for its reference. The point source scans and those of blank sky were used to calibrate seeing and detector noise, respectively. All objects were scanned at K and/or H, and all doubles in the survey at J as well. We were able to search stars with $3.4 \leq K \leq 8.0$ ($3.6 \leq H \leq 8.3$). On average, eight objects were observed per night, each in one scan direction.

2.3. Two-Dimensional Infrared Imaging

In two-dimensional infrared speckle imaging, frames are snapped of the entire speckle cloud and individual speckles can be observed directly.

2.3.1. The (Brief) History of Two-Dimensional Speckle Imaging

The extension of infrared speckle techniques to two dimensions has only recently been realized. At present, there are only three operational 2D Speckle Cameras — the NOAO (Beckers *et al.* 1988) and the California Institute of Technology (Ghez *et al.* 1990) cameras have been used primarily for studies of pre-main sequence and evolved stars, as well as a few binary systems. The Steward Observatory camera has primarily targetted solar system objects, including Io (McLeod *et al.* 1991), the asteroids Ceres and Vesta, evolved stars such as IRC +10216, and has been used for the large survey of nearby stars for low mass companions reported here (Henry and

McCarthy 1990, McCarthy *et al.* 1991, Henry *et al.* 1991a, 1991b).

In October 1989 we implemented the new 2D Infrared Speckle Camera which allows us to examine the close environs of nearby M dwarfs for low luminosity companions. The obvious benefit of the 2D Camera is that the entire area around a target star can be searched in one observation. In addition, we have found that we are able to probe to fainter companions using the 2D Camera than we were able to reach using 1D techniques (see the discussion of GL 67 in §3.3.2). The first published scientific result from 2D speckle techniques was a study of the nearby multiple star system GL 22 (McCarthy *et al.* 1991).

2.3.2. The Steward Observatory 2D Infrared Speckle Camera

Unlike infrared cameras built by the National Optical Astronomy Observatories and for the United Kingdom Infrared Telescope, the Steward Observatory 2D Infrared Speckle Camera is specifically designed for speckle imaging, involving very short exposures covering small fields. The camera has been constructed to be operable on both conventional single aperture and multiple aperture telescopes. The design allows Nyquist-sampled ($\lambda/2D$ pixels) imaging at three magnifications throughout the near-infrared, and can perform diffraction-limited observations on the SO 1.5m and 2.3m, the KPNO 3.8m, and the cophased Multiple Mirror (6.96m) telescopes. The 2D camera operates at the telescope's Cassegrain focus, where the dewar holding the detector array, the preamplifier electronics, and the camera's optical elements is attached, along with the drive electronics, temperature control, and shutter driver.

The dewar was manufactured by Infrared Laboratories, Inc. It is arranged in a double-shelled cryogenic configuration, with an inner liquid helium tank (4 K) surrounded by a liquid nitrogen (77 K) filled vessel. A Lake Shore 805 temperature controller allows the temperature of the detector to be held within 0.2 K over the range 4.2 to 50 K. We have found the optimal operating temperature, defined by the lowest readout noise, to be 37 K. The interchangeable lenses, filters and coronagraphic mask are cooled inside the dewar in order to reduce the thermal background evident in the near-infrared. Figure 2.1b illustrates schematically the arrangement of the dewar elements.

Five actuators penetrate the vacuum seal, providing access to a field stop mask, an interference filter wheel, a reimaging lens wheel, pathfolding mirrors, and a mechanical heat switch. The dewar window consists of a BaF₂/LiF achromatic doublet which receives the f/45 beam of the SO 2.3m telescope. The doublet causes the light to come to an initial focus where a cold shutter, coronagraphic mask and various field stops are located. An external warm shutter, located before the dewar window, is often used. The light then passes through one of eight interference filters (OCLI filters with full widths at J ($\lambda\lambda = 1.07\text{--}1.39$, $\lambda_o = 1.24\ \mu\text{m}$), H ($\lambda\lambda = 1.44\text{--}1.82$, $\lambda_o = 1.62\ \mu\text{m}$), and K ($\lambda\lambda = 1.96\text{--}2.43$, $\lambda_o = 2.19\ \mu\text{m}$) were used for survey work) and one of four CaF₂ reimaging lenses. (We note here that attempts to correct for different bandpasses in the infrared bands between the 1D and 2D filter sets have not been attempted, primarily because any corrections would be minor relative to the error in magnitude differences between similar type objects in a binary system.) In the lens wheel there

is also a dark mask which is used to blank off all signal in order to take dark frames. The lenses work in combination with gold-coated pathfolding mirrors, which are found next in the optical path, to provide magnifications of 0.3X, 1.0X, 2.0X and 2.8X. The resulting field sizes on the SO 2.3m are $31'' \times 29''$, $8.1'' \times 7.6''$, $4.0'' \times 3.8''$, and $2.8'' \times 2.7''$, providing pixel scales of $0.499''$, $0.131''$, $0.0652''$ ($\lambda/2D$ pixels at H and K), and $0.0458''$ ($\lambda/2D$ pixels at J). The field sizes have been measured using the binary stars ς Aqr, ξ Boo, α Gem, ξ UMa, GL 501, GL 702, and GL 704. The distortion through the optical system is $\leq \lambda/10D$. The two largest fields were used for photometry, the 1.0X configuration for faint stars in the survey, and the 2.0X magnification for the bulk of the speckle work.

The heart of the camera is the 58 X 62 InSb focal plane array (#160) manufactured by the Santa Barbara Research Center. The array is of high quantum efficiency in the near-infrared ($\sim 80\%$) and has a single frame read noise of 280 electrons (system gain 70 electrons per analog-to-digital unit, ADU). The upper right corner of the array suffers from high dark current, including high quantum efficiency “tree rings” symptomatic of the thinning process, and there are a few hot pixels located near the array’s center. An example of a flatfield taken at K showing the tree rings is illustrated in Figure 2.2(a), with its surface plot in panel (b). High background conditions lead to excess noise (caused by the resetting process) from the center hot pixels, right corner and edges. A map of the array’s bad pixels showing the hot upper right corner is shown in Figure 2.2(c) and (d). Most observations were made with a detector bias voltage of 0.1 V and used a surface potential, $v_{gate} = -1.8$ to -1.5 V, which balances

the effects of dark current and excess noise related to imperfections in the resetting process when under high background conditions.

The readout of the array is accomplished in a 96 msec cycle which includes three 32 msec readouts of all pixels — pixel reset, pedestal read, (shutter opens, integration occurs), signal read. Thus, for a typical observation with an integration time of 150 msec, the camera snaps frames at 4 Hz. Exposures can be as short as 4 msec, for a maximum frame rate of 10 Hz. A multiple readout scheme has been developed which reduces the readout noise by $N^{1/2}$, where N is the number of reads done during the pedestal and signal portions of the cycle. At four reads each for the pedestal and signal, we then operate at 2 Hz, which limits the amount of data acquired, but it is of higher quality. The camera also has non-destructive readout capability which is useful for active/adaptive optics applications.

The readout electronics consist of the Hughes CRC 228 MOSFET readout array that is bump bonded to the InSb array, a signal fanout board, a clock signal transient protection board, and a dual preamp board all located inside the dewar. Two electronics control boxes from SBRC, the Dewar Interface Electronics (DIE) and Computer Interface Electronics (CIE), are located next to the dewar when observing. The DIE outputs the sampled analog signals to two 16-bit A/D converters via 80-foot cables which provide the path into the observing chamber, where a VMEbus computer manufactured by Io, Inc. digitizes and records the raw data. The system includes a 68020-based CPU board, a 20 Mflop coprocessor, and 5 Mbytes of fast memory, which can hold up to 582 data frames. Once a block

of data made-up of 500 frames is taken, the memory is dumped onto an Exabyte 8 mm tape, which can hold 2 Gbytes of data.

While observing, the speckle frames are displayed on a monitor which allows the observer to participate actively in data quality-control. The incoming frames are evaluated for seeing, telescope drift and weather. In addition, rough data analysis is possible at the telescope because the system is capable of arithmetic image calculations, as well as 2D FFT computation. Target, point source and sky power spectra, and the resultant visibilities are computed and coadded as blocks of data are taken, allowing the observer to know whether more time needs to be spent on an object.

Further details concerning the camera can be found in McCarthy *et al.* (1990).

2.3.3. Observing Technique with the 2D Camera

Two-dimensional speckle observations were made between October 1989 and August 1991 on the SO 2.3m telescope, the same used during the 1D phase of the survey. A few supplemental observations utilized the cophased (6.86m effective aperture when used for speckle work) Multiple Mirror Telescope on Mt. Hopkins. The telescope is pointed alternately at the program object and a nearby point source where blocks of 500 frames each are recorded. As in 1D, the point sources are chosen from the SAO Catalog, their proximity to the program star is crucial, and the observation is restarted with a new SAO star if the first proves to be resolved. In order to calibrate the sky at near-infrared wavelengths, blocks of 500 sky frames are taken before and after a series of object/point source blocks.

Because identical observing conditions are used for the target, point source and sky frames, dark frames were not required (except for the flatfields), as the dark current was included in the sky frames as well as the source frames. The exposure times depend upon seeing and source brightness, but are usually between 80 and 200 msec, fast enough to freeze the seeing (see §2.1.2). Thousands of frames (2000 – 10000) are taken of the target star and its nearby, unresolved point source.

Figures 2.3 and 2.4 illustrate sequential frames of a single survey star and a binary used in determining the infrared mass-luminosity relations discussed in §4.1. In the figures, north is right and east to the bottom. Three frames of the unresolved star GL 873 are shown in Figure 2.3, with their surface plots. The data were taken at K using the 4'' field on UT 30 Nov 1990 with an integration time of 200 msec. This was a night of superb seeing, as can be seen by the obvious diffraction core of the image, which is 4–5 pixels in width (0.2–0.3''). Shown in Figure 2.4 are three consecutive frames taken on UT 28 Apr 1991 of the double star GL 704AB. The observation was made using the 8'' field at J, with an integration time of 24 msec. Although the seeing was poor ($> 2''$), we still can see both components in some frames, at a separation of only 0.97'', and a magnitude difference of 2.5 mag.

In order to remove the pixel-to-pixel variation in quantum efficiency across the array during data processing, flatfield frames were taken at the end of the night. Flatfield frames from several observing runs have been compared, and minor variations do occur, although the basic structure of the flatfield has not appeared to change over two years. Division of flatfields

taken at J, H and K during different runs typically results in variations $\leq 10\%$ across the array, except for the upper right corner. Several different flatfield acquisition procedures were tested, and we have found that dome flats with the chamber lights on works well. The final calibration frames required were bad pixel maps, which were taken periodically throughout the night to permit bad pixel correction. Bad pixels were identified by computing the standard deviation of each pixel for 50 to 100 dark frames, and selecting a threshold above which pixels were deemed to be too noisy to reliably measure signal. In addition to noisy pixels, the few dead pixels in the array were also added to the bad pixel map.

The faint object limit of the camera is limited by read noise and atmospheric seeing. The read noise of the detector can be reduced by employing the multiple readout scheme (see §2.3.2). Usually, four pedestal and four signal reads were done. The stars observed in the nearby star survey with 2D techniques fall into two groups. The first, containing 31 stars, was observed at 2X magnification at K (29 stars) or H (2 stars). The brightnesses of these stars cover the range of $3.9 \leq K \leq 6.7$, and integration times were 80–200 msec. The brightest star in the survey, GL 411 (Lalande 21185) has $K = 3.4$, but has been examined using 1D techniques. In an effort to build up signal, we observed the fainter survey stars at H in the 1X magnification camera configuration, in which the pixels cover an area of the sky four times larger than in 2X, and at longer integration times (200–300 msec). This second group includes 11 stars with $H \geq 7.8$ ($K \geq 7.5$) except for GL 300 ($H = 6.9$) which could only be observed at high airmass. Although the highest frequency information is lost at this lower

magnification due to pixel size, we are able to examine stars as faint as GL 283B, the faintest star in the survey ($H = 9.3$, $K = 9.6$). The 2X and 1X scales provide search fields of $4.04'' \times 3.78''$ and $8.10'' \times 7.57''$, respectively. Typically, four or five survey objects could be examined a night.

2.4. Data Reduction

The infrared speckle data have been Fourier analyzed in order to recover both visibility (modulus squared) and phase information so that the source may be fully described.

In the following sections we outline the procedures used during reduction of the 1D and 2D speckle data. This is by no means an extensive discussion of the mathematical formalism behind the processing of speckle data, but is provided in order to give a broad idea of how the data are handled. For more detailed descriptions of the 1D and 2D reduction techniques, see Freeman (1988) and Christou (1991), respectively. In the next sections, the methods are described through the point of obtaining the Fourier elements, the modulus and phase, of the target. The procedures used to fit the data are described in §3.3.

2.4.1. One-Dimensional Data

The 1D scans have been analyzed using the complex bispectrum, as discussed by Freeman *et al.* (1988). The bispectrum has been found to be superior to both simple shift-and-add and Knox-Thompson algorithms (Freeman 1989), and utilizes the technique of phase closure. The closure phases are used to calculate the object phases. When applied specifically to

speckle data, the complex visibility (modulus and phase) is found from the computed bispectrum. The steps involved in computing the power spectra and cross spectra for the sky, object and point source (and subsequently, the visibility of the program star) are discussed in detail in the following section, in the expanded 2D regime. Here we briefly outline the reduction process used for 1D speckle data to the point of modulus and phase recovery.

The 1D scans for both the target and point source are centered, the bispectrum computed for each scan, and the bispectra are coadded for each object to build up signal-to-noise. Bispectra are also computed for the corresponding blank sky scans taken near the target and reference in order to calibrate the sky background and the detector noise. Generally, the bispectrum is the time-averaged triple product of the Fourier transform of the speckle scans:

$$\langle I^{(3)}(f_1, f_2) \rangle = \langle I(f_1) \cdot I(f_2) \cdot I^*(f_1 + f_2) \rangle \quad (2.8)$$

where f_1 and f_2 are spatial frequencies, $*$ indicates the complex conjugate, and the Fourier transform is written

$$I(f) = |I(f)|e^{\pm i\phi(f)}. \quad (2.9)$$

Both the Fourier modulus — the quantity $|I(f)|$ — and the phases, $\phi(f)$, are functions of spatial frequency.

The observed intensity distribution of a star is actually the combination of three terms: the actual object distribution $s(f)$, the

instantaneous point spread function of the telescope and atmosphere $p(f)$, and zero-mean additive noise terms. These three terms together produce the observed image, $i(f)$. The equation describing the observed image over many frames (time-averaged quantities enclosed in $\langle \dots \rangle$) can be written, with the bispectrum of X denoted $X^{(3)}$ (where X can be I , S or P),

$$\langle I^{(3)}(f_1, f_2) \rangle = S^{(3)}(f_1, f_2) \cdot \langle P^{(3)}(f_1, f_2) \rangle + noise. \quad (2.10)$$

Thus, the observed image bispectrum, $I^{(3)}(f)$, is simply the object bispectrum, $S^{(3)}(f)$, multiplied by the effects of the telescope and atmosphere in the form of the point spread function bispectrum, $P^{(3)}(f)$, with added noise terms. Once noise terms are removed, the moduli (phases) are recovered separately for the target star and its point source, and the results divided (subtracted) to calibrate for the telescope/atmosphere function, thereby yielding the object's structure in one dimension.

2.4.2. Two-Dimensional Data

The reduction techniques used for the 2D infrared speckle data are essentially the same as those developed for the NOAO IR Speckle Camera (Beckers *et al.* 1988), and are discussed in detail by Christou (1991). The primary data reduction algorithm used is a modified version of the extended Knox-Thompson cross-spectrum analysis (Knox 1976), which provides both the moduli and phases required for image reconstruction.

During data reduction, long-exposure and shift-and-add images are found, in addition to the extensive Fourier processing that results in the Fourier elements. As an example, Figure 2.5 illustrates several ways of

examining the binary star GL 22AC as it was observed on UT 12 Oct 1989 at K. The $4''$ field was used with frame integrations lasting 120 msec. This system is included in the list of binaries used for the mass-luminosity relations discussed in §4.1. Surface plots have north to the right, and east to the front. Contour plots have north to the right, east to the bottom. Panels (a) and (b) show the “long exposure” images (the summation of 7000 centroided frames each) of the point source, SAO 11207, and GL 22AC, respectively, and illustrate the resolution obtainable by removing wavefront tilt and telescope drift (FWHM $0.8''$). Panels (c) and (d) show the shift-and-add images obtained by stacking the frames on the brightest pixel in each frame. A comparison of the two sets of images begins to reveal the the companion of GL 22A to the northeast, and brings out the Airy diffraction pattern characteristic of a point source. The bump in the Airy ring to the south of the central peak in both images appears to be an aberration caused by the optical system of the SO 2.3m.

The Fourier moduli and phases of the resolved pair, GL 22AC, are shown in (e) and (f), respectively. Note the fringe structure which is the signature of a binary star. Panel (g) shows the image obtained by inverting the Fourier components, in which the secondary can be seen clearly. Finally, (h) shows the same image after applying an iterative deconvolution algorithm. The image reconstruction is accomplished by using both the modulus and phase of the object, and during iterative deconvolution (Christou 1991) is constrained by the errors in the measured elements. The modulus and phase are allowed to vary only within 3σ of their values, as determined by the formal measurement errors that are accumulated along

with the elements.

Now that the various products in the data reduction process have been shown, we elaborate upon the steps taken to arrive at the answers. Figure 2.6 shows the processing steps done on a single frame taken on the survey star GL 623, which was examined at H on UT 27 Apr 1991 using the 4'' field with a frame rate of 150 msec. The raw data frame is shown in panel (a), and its surface plot in panel (e). Note the spikes due to hot pixels and the bad upper right corner. The preprocessing stage of the individual speckle frames involves the calibration of each short exposure for bias correction, flat fielding, and noisy and dead detector pixels. An average sky frame, which includes dark current, is subtracted from all sky, target and point source frames (product shown in panel (b)). Next, each frame is divided by a flatfield frame constructed from many 1 to 10 sec exposures of the dome taken at the wavelength of observation (see, for example, Figure 2.2(a) and (b)), or for some of the earlier data, taken at L ($3.5\ \mu\text{m}$) on the sky. After testing several flatfielding techniques, the former proves best, although we have discovered that K and L flats are very similar, so no large systematic errors should have been introduced by the use of L flats. In some datasets, residual flatfielding stripes which pass from the upper right to the lower left in the Fourier modulus plane exist, and are caused by imperfect flatfielding of the tree rings in the array. However, we have found that imperfect flatfielding is preferable to no flatfielding. After dividing by the flatfield frame (c), noisy and dead pixels inherent to the detector are smoothed using nearby pixel values in each frame (an example is shown in Figure 2.2(c) and (d)), and the frame is apodized to prevent

aliasing (d). A surface plot of the final frame is shown in (f).

After preprocessing, all blocks of data are checked quantitatively for bad frames. Bad frames can be caused by detector flashing, cosmic rays, cloud cover, or telescope drift (including battering of the secondary by wind) which causes the speckle cloud to wander far from the detector center. Figure 2.7 shows the calculated values for the total frame power (a), frame maximum (b) and location of the centroid in x and y coordinates (c) for a block of data on the survey star GL 873, which was examined at K using the 4'' field during excellent seeing on UT 30 Nov 1990. The integration time was 200 msec. The vertical scales for panels (a) and (b) are arbitrary units, and for (c) the scale represents the number of pixels that the centroid of the speckle cloud is shifted from center. For this block of 500 frames, there are no problems evident in the frame power or maximum, which are used to check for flashing and cloud cover. When spikes are seen, the cutoff is chosen to eliminate the bad frames. A few frames will not meet the centroid criterion, however, as the drift from the array center is greater than the adopted 15 pixel cutoff (the shortest detector length from center to edge is 29 pixels).

Next, program and reference star frames are centroided on their center-of-light, and each frame is multiplied by a rectangular apodization window with a 10 pixel wide cosine bell roll-off to ensure that the data go smoothly to zero at the original frame boundary. The blank sky frames are not centroided, but are apodized. The apodization is done in order to prevent aliasing effects caused by the sharp cutoff of the detector field. Prior to Fourier transforming, the specklegram is inserted into a 128×128

array so that its centroid is in the middle of the larger field. The Fourier transform of each frame is then computed, and the appropriate Fourier spectra and their variances are accumulated. In addition, long exposure images of the object and point source are found from the straight sums of the centroided images (effectively, autoguided images which are the result of wavefront tilt and telescope drift removal), and shift-and-add images are found by stacking the individual frames on the brightest pixel.

To fully describe an object, both the Fourier moduli and Fourier phases are required. In cases of resolved binaries, both the moduli and phases are used to determine the brightness ratio, separation, and relative position angle of the components. For unresolved sources, only the modulus has been used, as it has proven sufficient for purposes of assigning detection limits for unseen companions. The fitting procedures for both resolved and unresolved sources are discussed in Chapter 3, where the results are presented. Here we outline the scheme used for the reduction of the infrared speckle data as discussed by Christou (1991).

As discussed for the 1D data, a 2D specklegram can be described as the convolution of the program star's light distribution in two dimensions, $s_o(x,y)$, with an instantaneous function that defines the combined effects on the light distribution of the telescope and the atmosphere, $p(x,y)$. Contamination by additive noise in the detector must also be considered, $n(x,y)$, yielding the final images for the star, $s(x,y)$, and reference, $r(x,y)$:

$$s(x,y) = [s_o(x,y) \otimes p(x,y)] + n(x,y) \quad (2.11a)$$

$$r(x, y) = [r_o(x, y) \otimes p(x, y)] + n(x, y) \quad (2.11b)$$

where \otimes denotes convolution. The quantities $s(x, y)$ and $r(x, y)$ are the measured intensity distributions which change with $p(x, y)$. The original light distributions of the program star and reference, $s_o(x, y)$ and $r_o(x, y)$ are to be recovered. Although $p(x, y)$ varies from frame to frame as the atmosphere boils, over time (i.e. thousands of frames) the average $p(x, y)$ for the program star and reference is similar and can be calibrated. The transforms in the (u, v) Fourier domain for the star and reference from a single frame can be written

$$S(u, v) = [S_o(u, v) \cdot P(u, v)] + N(u, v) \quad (2.12a)$$

$$R(u, v) = [R_o(u, v) \cdot P(u, v)] + N(u, v). \quad (2.12b)$$

The power spectra are determined by multiplying the Fourier transforms of the light distributions by their complex conjugates (denoted by $*$):

$$\begin{aligned} PS_S(u, v) = [S_o^*(u, v) \cdot S_o(u, v) \cdot P^*(u, v) \cdot P(u, v)] \\ + N^*(u, v) \cdot N(u, v) \end{aligned} \quad (2.13a)$$

$$PS_R(u, v) = [R_o^*(u, v) \cdot R_o(u, v) \cdot P^*(u, v) \cdot P(u, v)]$$

$$+N^*(u, v) \cdot N(u, v). \quad (2.13b)$$

As many frames are accumulated, the ensemble average of power spectra can be described by

$$\begin{aligned} \langle PS_S(u, v) \rangle &= [S_o^*(u, v) \cdot S_o(u, v) \cdot \langle P^*(u, v) \cdot P(u, v) \rangle] \\ &+ \langle N^*(u, v) \cdot N(u, v) \rangle \end{aligned} \quad (2.14a)$$

$$\begin{aligned} \langle PS_R(u, v) \rangle &= [R_o^*(u, v) \cdot R_o(u, v) \cdot \langle P^*(u, v) \cdot P(u, v) \rangle] \\ &+ \langle N^*(u, v) \cdot N(u, v) \rangle \end{aligned} \quad (2.14b)$$

By taking blank sky frames which include detector noise, the final terms in the above two equations can be eliminated, provided that the sky near the two objects is the same. Furthermore, the ensemble average of the telescope/atmosphere function, $\langle (P^*(u, v) \cdot P(u, v)) \rangle$, can also be calibrated over thousands of frames, effectively “removing the atmosphere.” This term includes any aberrations introduced by the optical system, which are assumed to be the same for both the star and its reference. The visibility of the source in two dimensions is found by dividing the power spectra and taking the square root:

$$\begin{aligned}
V(u, v) &= \left[\frac{\langle PS_S(u, v) \rangle}{\langle PS_R(u, v) \rangle} \right]^{1/2} \\
&= \left[\frac{S_o^*(u, v) \cdot S_o(u, v)}{R_o^*(u, v) \cdot R_o(u, v)} \right]^{1/2}. \tag{2.15}
\end{aligned}$$

In the case of a true point source, the power spectrum equals unity at all spatial frequencies at all angles, so $(R_o^*(u, v) \cdot R_o(u, v)) = 1$, and we have an equation relating the visibility of the program star to the square root of the power spectrum of the star with telescope, atmosphere and noise effects removed:

$$V(u, v) = [S_o^*(u, v) \cdot S_o(u, v)]^{1/2}. \tag{2.16}$$

It is this equation in 2D that gives rise to the modulus fringes familiar in the study of binary systems.

Phase recovery is more difficult. The phases have been invoked in order to reconstruct an image only when a companion was detected. The speckle reduction routines accumulate a multi-plane variant of the Knox-Thompson cross-spectra (Knox and Thompson 1974) for the phase determination. The cross-spectrum is a complex quantity which retains the phases in the form of phase differences. A pair of cross-spectra is necessary for the phase determination:

$$KT(u, v, \Delta u, 0) = \langle I^*(u, v) \cdot I(u + \Delta u, v) \rangle \tag{2.17a}$$

$$KT(u, v, 0, \Delta v) = \langle I^*(u, v) \cdot I(u, v + \Delta v) \rangle. \quad (2.17b)$$

Δu and Δv are orthogonal shifts in the Fourier plane. For $\Delta u = \Delta v = 0$, the pair of equations 2.17 reduces to the power spectrum, $\langle |I(u, v)|^2 \rangle$. The reductions done for the survey stars used 5 pairs of phase planes: $1 \leq \Delta u, \Delta v \leq 5$ pixels in Fourier space.

Returning to the basic equation of the Fourier transform (Eq. 2.9), we see that the complex visibility, $V(u, v)$, is made up of the modulus and phase — both of which are functions of spatial frequency. The results in Fourier space are fringes in the modulus plane and steps in the phase plane for resolved sources, and flat planes for both the modulus and phase for unresolved sources. We have noted that in some cases, particularly widely-separated binaries examined on nights of poor seeing, that there is evidence of damping along a modulus fringe. We attribute this to a difference in the seeing characteristics between an object and its point source which results in different overall shapes in the power spectra, and note that the same effect has been found by others (Ghez, private communication).

In summary, the object's Fourier modulus is obtained by taking the quotient of the target and point source power spectra and computing the square root, thereby correcting the final modulus for the atmospheric and telescope transfer functions. The Fourier phases are found from the phase differences contained within the cross-spectra. The final reconstructed image is obtained by inverting the final Fourier modulus and phase. Further details of the 2D data reduction procedure can be found in Christou (1991).

TABLE 2.1
OBSERVING PARAMETERS ENCOUNTERED DURING THE SURVEY

Parameter	Worst Case J at $z = 60$	Best Case K at $z = 0$
L (arcsec)	0.113	0.200
r_0 (cm)	17.1	51.2
N (speckles)	402	45
τ_c (msec)	25	75
τ_c observable (msec)	38	150
Θ (arcsec)	2.5	14.9
$(\Delta\lambda/\lambda)_{\text{coh}}$	0.28	0.70
$(\Delta\lambda/\lambda)_{\text{mag}}$	0.08	0.23

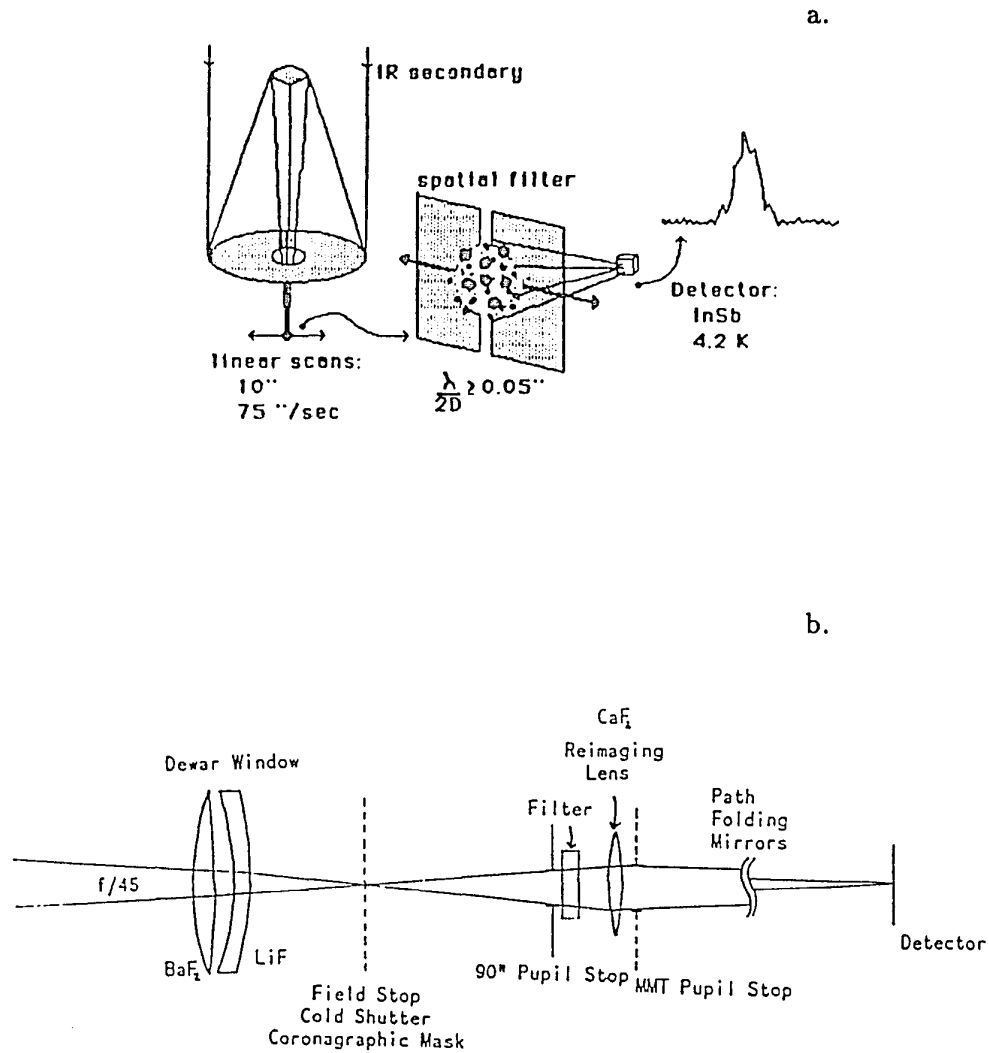


Figure 2.1 (a) Schematic representation of the 1D infrared speckle imaging technique, illustrating the scanning secondary mirror of the telescope, the passage of the speckle cloud across a slit, and the measured intensity during a scan. (b) A blow-up of the 2D infrared speckle camera's optical system.

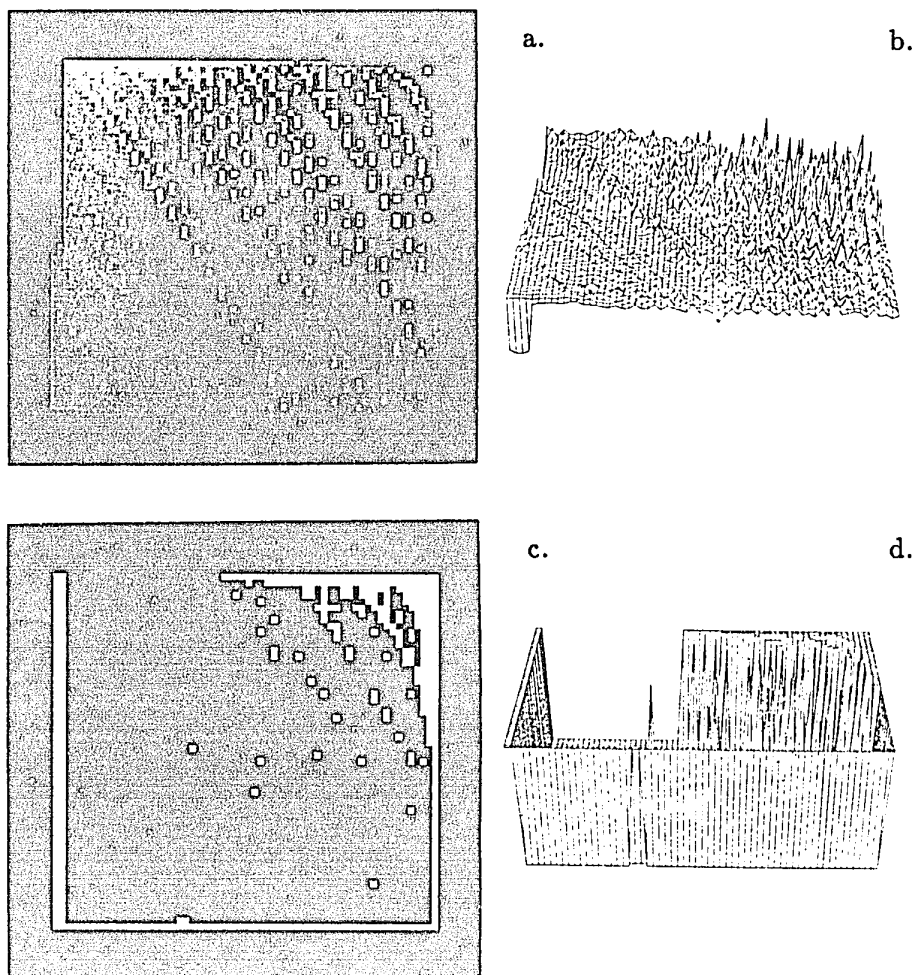


Figure 2.2 (a) A typical flatfield for the 58×62 InSb array, taken at K. (b) Surface plot of the flatfield. (c) A representative bad pixel map for the array. Note the bad upper right corner, edges and "treerings." (d) Surface plot of the bad pixel map.

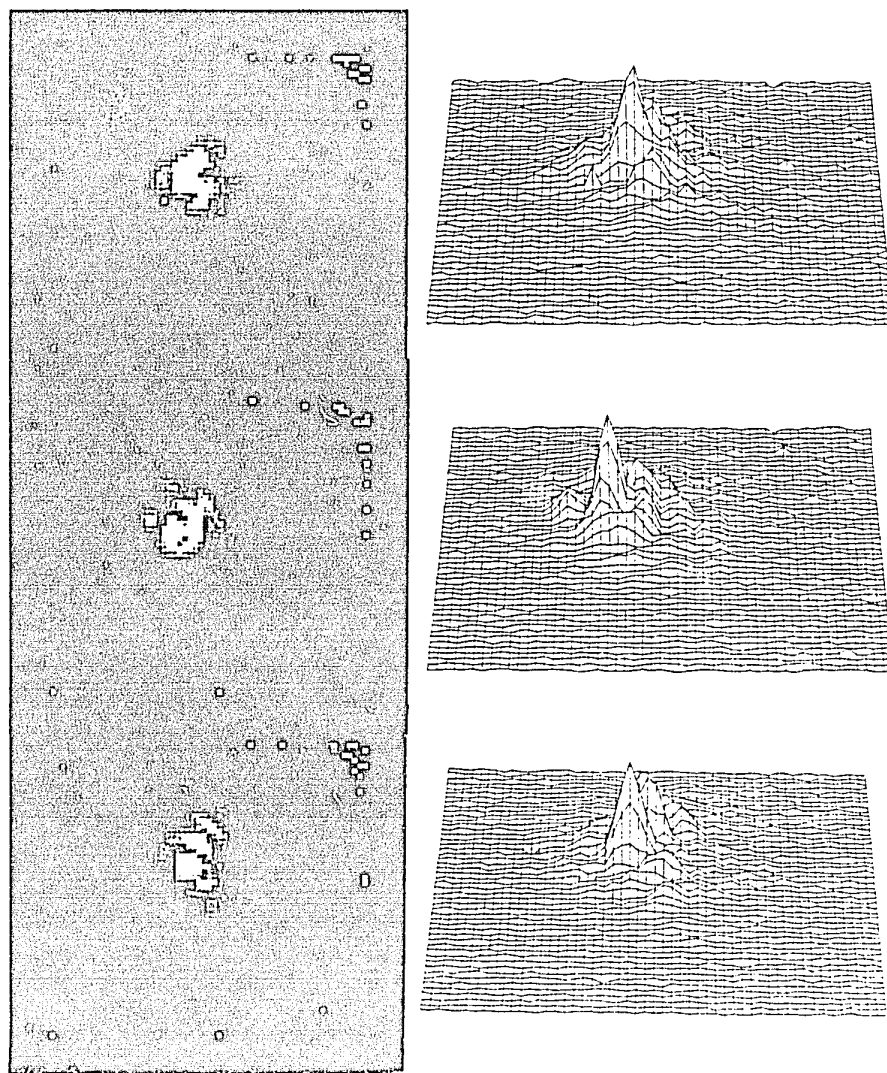


Figure 2.3 Three consecutive speckle frames taken of the survey star GL 873 at K on a night of excellent seeing. North is to the right, and east to the bottom. The right panels are surface plots of the frames shown on the left. Note the Airy ring structure.

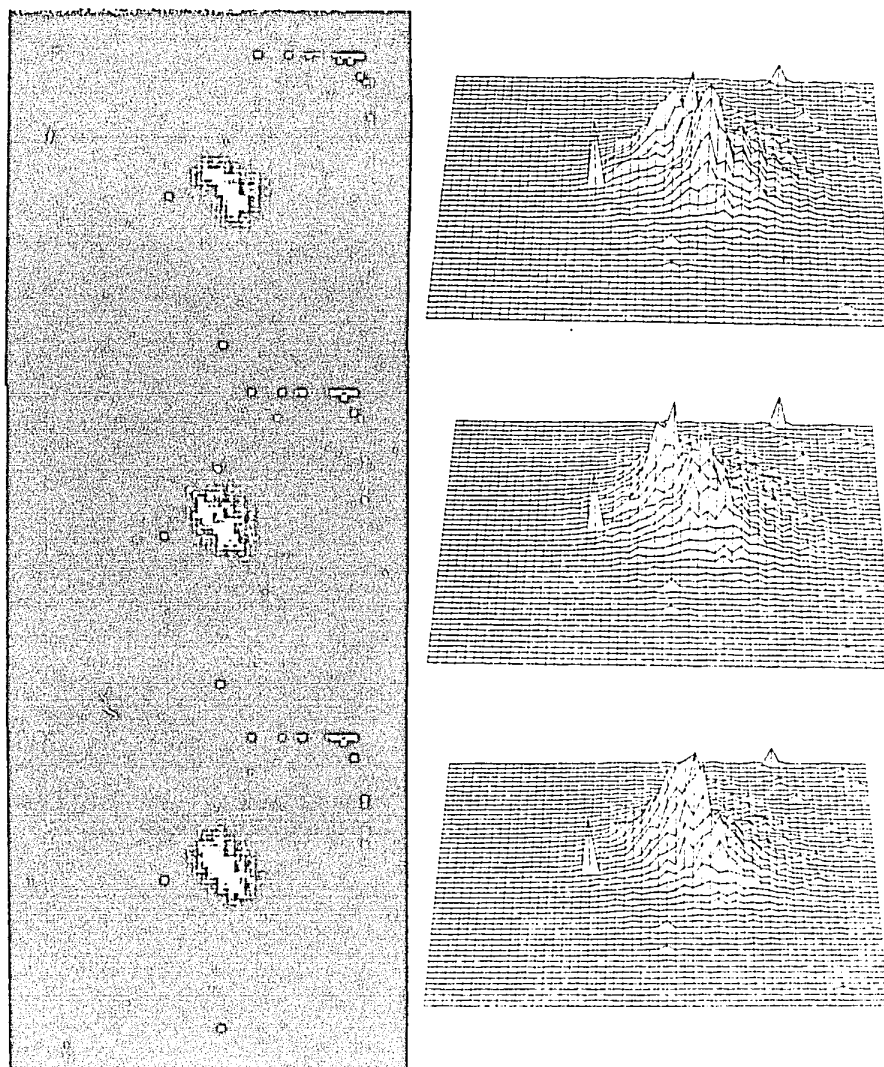


Figure 2.4 Three consecutive speckle frames taken of the binary star GL 704AB at J on a night of relatively poor seeing. The separation of the components is $0.97''$. North is to the right, and east to the bottom. The right panels are surface plots of the frames shown on the left. Note the obvious binary nature of the source, even in poor seeing.

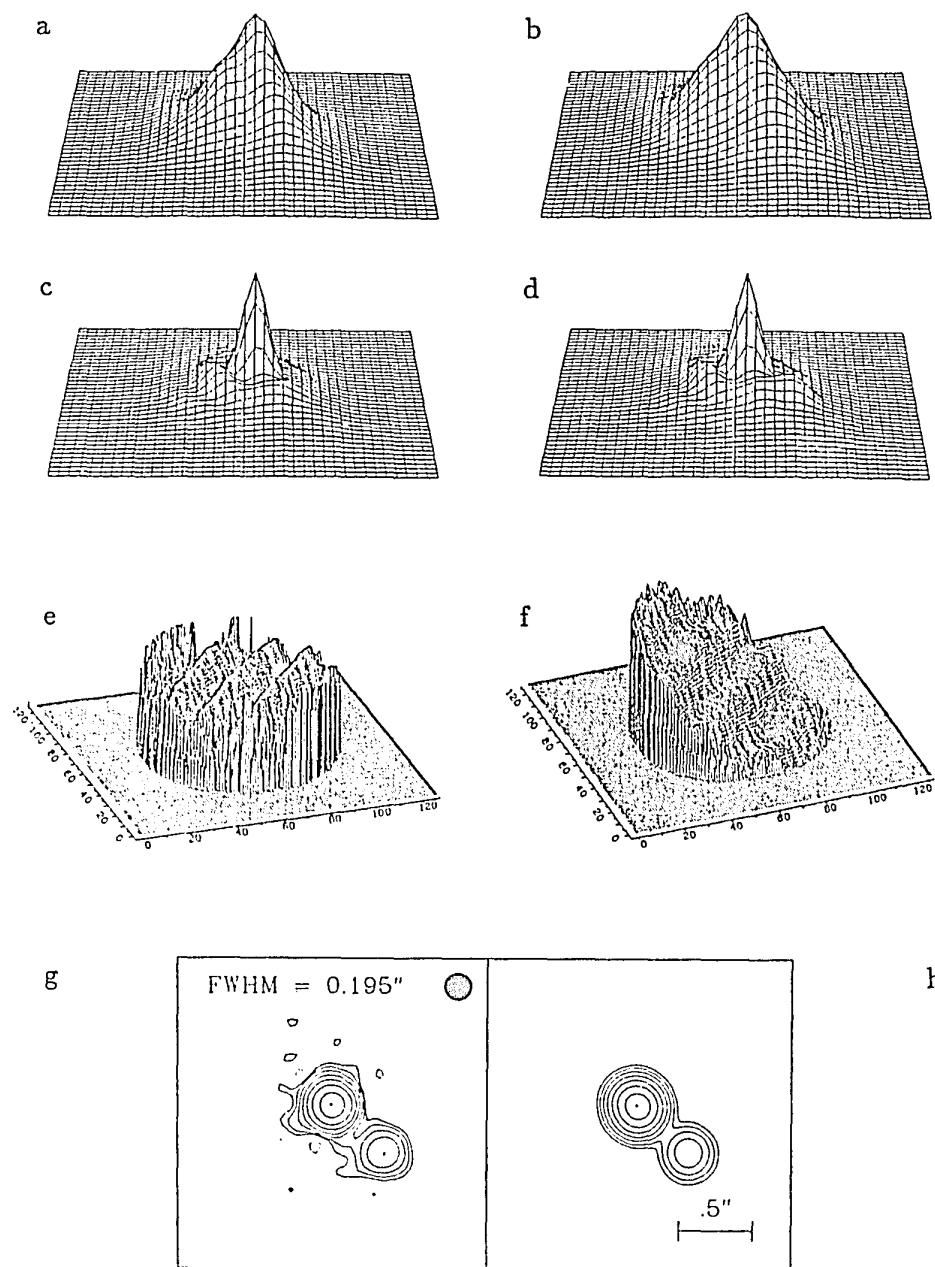


Figure 2.5 Various methods of examining images of GL 22AC and its reference point source SAO 11207 from speckle data taken at K. See text for discussion.

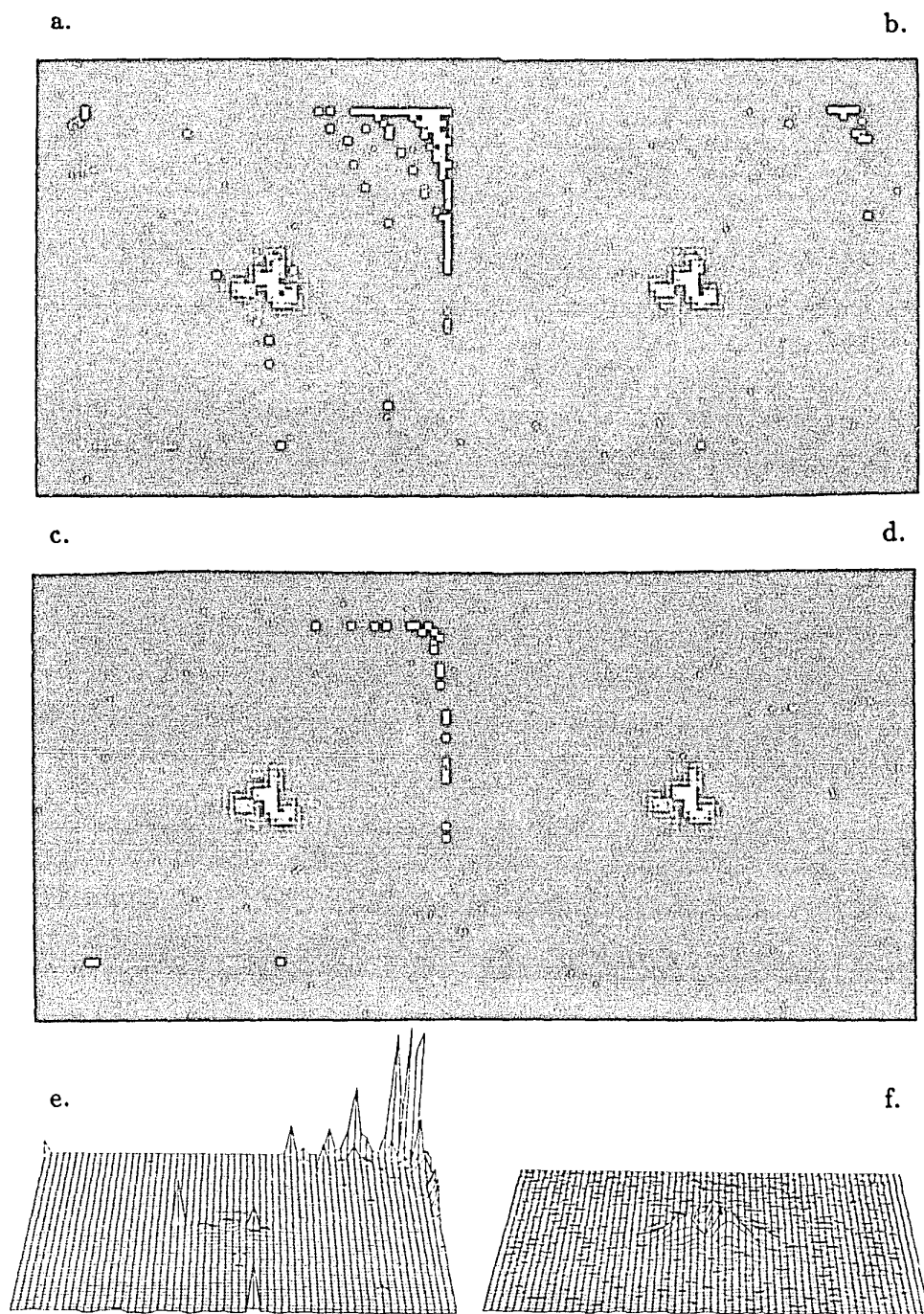


Figure 2.6 Stages in the processing of a single frame taken of the close binary GL 623AB at H. The raw data frame is shown in (a) and its surface plot in (e). It is sky-subtracted (b), flatfielded (c), and bad pixel corrected and apodized, resulting in the final product frame (d) and its surface plot (f).

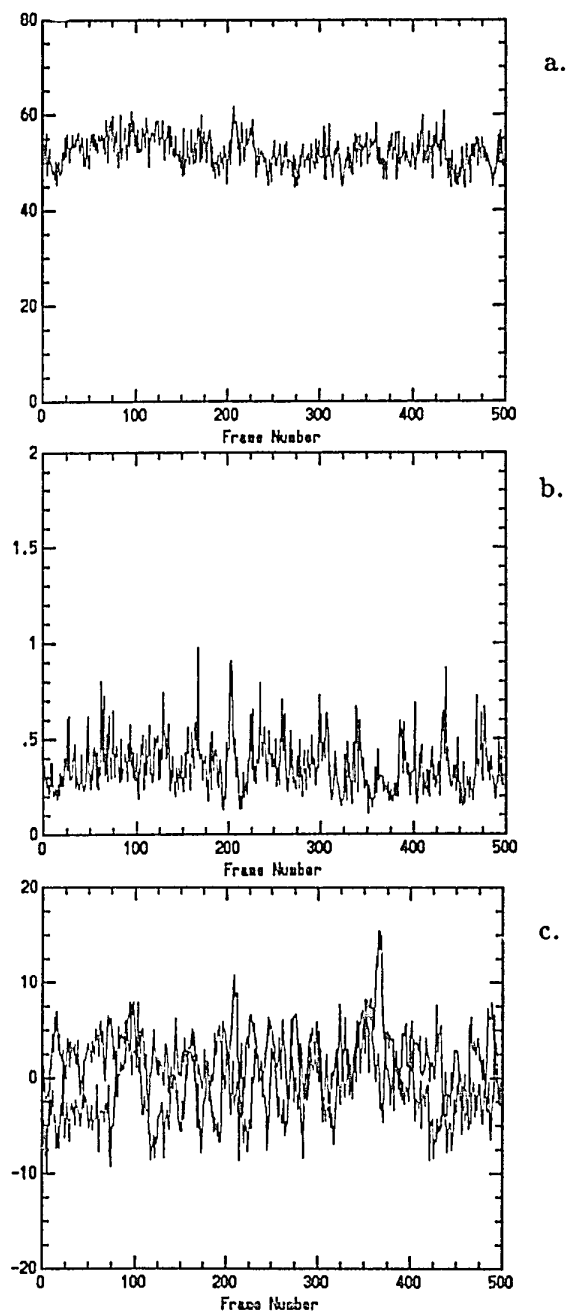


Figure 2.7 (a) The total frame power computed for each of 500 frames taken of the single star GL 873 at K. (b) Frame maximum. (c) Position of the light distribution's centroid in x and y coordinates on the array (in number of pixels).

CHAPTER 3

A Systematic Search for Low Mass Companions Orbiting Nearby Stars

3.1 An Infrared Speckle Search for Brown Dwarfs

Infrared speckle techniques are the only imaging methods that can search for BDs at the wavelengths most favorable for their detection, and within 10 AU of their primaries — the scale of our own solar system.

An infrared speckle search for low mass companions orbiting nearby M dwarfs (within eight parsecs) constitutes the bulk of this thesis. The direct detection of faint, very low mass secondaries lying within 10 AU of even the nearest stars is difficult, due to the difference in brightness between the primaries and their companions, and their subarcsecond separations. A decade ago, McCarthy (1986 and references therein) began using the technique of infrared speckle interferometry to detect low luminosity astrometric companions around nearby stars. Building on McCarthy's work, a systematic search was defined and begun by the author in 1986 to find low mass stars and high mass BDs orbiting nearby M dwarfs.

3.1.1 Scientific Rationale for an Infrared Speckle Search

The work described here complements other surveys for BDs by searching the region between 1 and 10 AU of the program stars, similar to the most effective regions examined by astrometric techniques (see Figure 1.2). The deep photometric surveys efficiently search for BDs in the field or between several tens and a few hundred AU of designated stars. Radial velocity surveys are most sensitive to companions within a few AU of their primaries. We are capable of detecting companions at near-infrared wavelengths around most of the survey stars to $M_K = 11.0$, which includes all stellar companions and probably the highest mass BDs (see §3.5.3).

While this speckle search probes regions similar to those investigated by astrometric work, the speckle technique has several distinct advantages. Perhaps the more important is that it has been done at near-infrared wavelengths (1.0–2.5 μm), rather than in the visible where traditional astrometry is done. Low mass M dwarfs and high mass BDs are brighter in the near-infrared than in the visible because they have temperatures from 4000 K to less than 1000 K. These bodies radiate most of their energy (whether it be the energy from nuclear fusion in the cores of the M dwarfs, or the release of gravitational and thermal energy from the cooling BDs) near their blackbody peaks, which fall between 1.4–2.9 μm , overlapping the near-infrared atmospheric windows (Lunine *et al.* 1986, 1989).

The second advantage answers the question: Why not use speckle techniques at visible wavelengths? Although today's infrared detectors are inherently noisier than their optical counterparts, it is advantageous to make speckle observations in the infrared, rather than in the visible, because the atmospheric coherence time is longer. This allows us to probe significantly fainter sources because we are able to integrate longer without losing diffraction-limited information. Furthermore, very red secondaries are brighter in the infrared relative to the target stars. For example, the magnitude difference in a binary composed of 0.40 M_{\odot} and 0.08 M_{\odot} dwarfs may be 9–10 mag in the visible, but only 4–5 mag at 2.2 μm .

The third advantage of the speckle search is that we are able to detect a companion in a single observation, rather than over the decades of observations that are required to confirm an astrometric companion. After “first-sighting,” the system can be placed on a high-priority list of targets

without the long wait required in astrometry to confirm a perturbation. Nevertheless, the astrometric observations, which require enduring patience, remain crucial to many of the conclusions drawn in this thesis. It is the combination of the astrometric and speckle data which yields the all-important masses and absolute magnitudes for a binary system's components. However, speckle techniques are efficient in detecting equal luminosity components which can be missed by conventional astrometry because over time there is no "wobble" of the stellar image on a photographic plate. The nearby binary GL 866AB (McCarthy *et al.* 1987) is an example.

By incorporating speckle and astrometric data, the crucial parameter which makes an object a viable BD candidate, its mass, can be determined. This is possible because we are working at separations where orbital motion is relatively rapid. For example, when observing at $2.2\ \mu\text{m}$ on the Steward Observatory 2.3m telescope, we are able to fully resolve components at separations as small as $0.20''$, which corresponds to a distance of only 1.6 AU for stars lying at the outer boundary of the survey. In some instances, e.g., GL 33, a K dwarf not in the main survey, we are actually able to "superresolve" even closer companions although brightness ratios and separations are uncertain. Currently, speckle and astrometric data are combined to yield the primary and secondary masses (see §3.4.2). Eventually, relative orbits will be fully described with infrared speckle data alone (the first example is GL 866AB, Leinert *et al.* 1990), but because the development of the technique has occurred only recently, only very short period binaries have completed full orbits since speckle data acquisition commenced.

The regions around M dwarfs between 1 and 10 AU are important because of the 32 companions included in this survey, 11 are found in that realm (see §3.7.3). The inner cutoff for the survey has been chosen to be 1 AU because most stars have been probed to that separation. Within 1 AU the radial velocity surveys are more effective than the speckle survey. In practice, we are able to resolve closer companions to some stars, and have detected 12 of the 14 secondaries within 10 AU of their primaries — the close spectroscopic binaries GL 268 and GL 643 have not been resolved.

3.1.2 Why M Dwarfs?

We have chosen to search for low mass companions to M dwarfs for several reasons. The magnitude differences between an M dwarf and a BD in the infrared H and K bands, at which BDs presumably emit most of their radiation, are smaller than for earlier type primaries, such as F, G and K dwarfs. In practice, we are able to reach to a magnitude difference of 5–6 mag for bright sources, and typically 4–5 mag for most of the survey stars, which allows us to dip into the realm of high mass BDs as companions.

The second reason to examine a group of M dwarfs is that we are able to search a large number of stars at the desired distance scales in a complete volume-limited sample, thereby allowing us to estimate the companion populations of very low mass M dwarfs and high mass BDs. In addition, because the sample is complete and large, we can determine the true luminosity and mass functions for low mass objects. Furthermore, because the M dwarfs are of lower mass than earlier main sequence stars,

the telltale wobble induced by a BD will be larger than for more massive primaries, and will allow us to concentrate on specific stars with known perturbations.

Finally, equal-mass components appear to be more common in the short-period systems for which we are searching here, than high mass ratio systems (Abt 1983), i.e., we are more likely to find a BD orbiting an M dwarf than a solar-type star. This supposition, that equal mass binaries are most common, however, is subject to selection effects which favor equal mass/equal luminosity components, because in unbiased radial velocity surveys, only 15% as many SB2s (\sim equal mass) are found as SB1s (presumably less similar components). Nonetheless, formation scenarios in binaries favor high production rates of roughly equal mass components (Boss 1988, and references therein).

3.2 The Sample

Every known M dwarf within eight parsecs of the sun, and north of -25° has been searched for companions.

The optimum sample to be searched ideally includes a complete set of stars in the solar neighborhood. To remain as objective as possible, and to maintain a statistically complete, comprehensive survey, the sample was chosen to include *every known* M dwarf within a chosen distance, regardless of brightness. The natural starting point was the traditional 5.2 pc survey, chosen as a volume-limited sample by van de Kamp (1945, 1953, 1969, 1971, 1986), further discussed by Lippincott (1978), Gliese (1982), and most recently by Batten (1990). The portion of this sample observable from

Tucson, targets north of -25° , was searched using one-dimensional infrared speckle imaging, and the results reported in 1990 (Henry and McCarthy). The survey was then expanded to include every M dwarf within 8 pc north of -25° . The expansion began in 1989 and benefitted from the development of the two-dimensional infrared speckle camera described in Chapter 2, possible because of the availability of 58×62 format infrared arrays. Two-dimensional observations provide full coverage of the sky in one observation, and do not suffer the nonlinear effects of one-dimensional scanning techniques. The observational methods are discussed in detail in Chapter 2.

The total sample includes 99 objects, 74 of which have been searched for low mass companions. The 25 objects not searched include six companions discovered during the survey, and 19 components in close ($\leq 4''$) multiple systems which were already known and could not be searched separately. The targets include all M dwarfs listed in the Gliese (1969), Gliese and Jahreiss (1979) and LHS (Luyten 1979) catalogs with parallaxes greater than or equal to $0.125''$. The completeness of the sample is unfortunately subject to the biases of the parallax surveys from which the observing list was taken, i.e., if any objects have been missed as primary targets, they will be those that are faint or lie in crowded fields, nine of which have been found to lie within 5 pc in the last 20 years (see §3.9 and Table 3.8).

3.2.1 Parallaxes and their Distribution

Counts of the 99 late-type dwarfs known within various shells making

up the eight parsec survey indicate that it is quite likely that even within the very near solar neighborhood not all stars have been found. The total survey volume, for declinations $+90^\circ$ to -25° to 8 pc includes 1370 pc^3 . If we divide this total volume into four equal parts, each accounting for 343 pc^3 , we find that the number of stars in these equal-volume shells plummets even past only six and a half parsecs! The four bins are: 0.00–5.03 pc [35 objects], 5.04–6.35 pc [29 objects], 6.36–7.27 pc [15 objects], and 7.28–8.00 pc [20 objects]. Considering only two equal volumes in order to boost the numbers in individual bins, we find 64 known survey dwarfs in the nearer volume, and only 35 in the more distant one. While it is possible that we reside within a local density enhancement of stars in the local spiral arm, it is far more likely that many faint members of the solar community remain undetected. As we shall see below (§3.9), during the last several decades, the number of M dwarfs known even within the 5.2 pc shell has nearly doubled, and the discovery rate shows no indication of slowing.

The fact that perhaps as many as 50% of the stars are missing in the outer shell of the survey volume will, of course, affect any luminosity function for the nearby stars, and this is why several luminosity functions are presented in §4.3 — the traditional 5.20 pc sample, the sample to 6.35 pc (which has a similar number density as the 5.20 pc sample), and the entire 8.00 pc sample. The dropping star counts at greater distances are due to the incomplete proper motion surveys whose members make up the parallax catalogs used to cull the observing list for this survey. Primary targets missed most likely lie in regions difficult to search for nearby stars, such as the galactic plane, and some have undoubtedly been missed due to

the lack of sensitivity of the proper motion surveys to nearby stars of both low and very high proper motion.

3.2.2 Photometry

Table 3.1 lists the 99 survey objects. Included in this list are the 74 primary targets searched for companions (labelled T in the first column), 6 new companions (C), 17 components of close, previously known, double systems (D), and 2 spectroscopic binary secondaries (S) which were not resolved during the search. The second and third columns of Table 3.1 identify the objects, the fourth and fifth columns give their positions. Columns six through nine list the apparent V, J, H and K magnitudes, and each measurement's associated error. The final column gives the references for the photometry, where the first reference is for the V magnitude, and the second (/third in some cases) is for the infrared photometry. A "J" following a photometric value indicates that the measurement includes flux from both components of a close pair, which must be deconvolved ("decon" listed for the photometry of the secondary) to recover the individual fluxes.

Visible photometric data were taken primarily from Stauffer and Hartmann, which was the first source checked, (SH, 1986) and Probst (P1, 1981 Table A.7 — averaged value of many studies). In cases where there was no photometry in those two compendia (or in the case of P1 when the value listed was that of Gliese 1969), other sources were used, including Gliese (GL, 1969), Gliese and Jahreiss (GJ, 1979), Dahn (D, 1988), McCarthy *et al.* (M+, 1988), and Ianna *et al.* (IRM, 1987).

Infrared photometry was taken from many of the same references.

Holes in the database were filled by the author using the 2D Infrared Speckle Camera discussed in §2.3.2 on the SO 2.3m telescope, or using the NICMOS 256×256 Infrared Camera kindly provided by Marcia Rieke on the SO 1.5m telescope on Mt. Bigelow, Arizona. Photometric observations were made by taking multiple blocks of tens of frames on the target stars and Elias *et al.* (1982) standards of similar airmass. All data frames were then sky-subtracted, flat-fielded and corrected for bad pixels. Quoted errors include systematics determined by comparison of standard star data, and individual target errors found from the repeatability of a measurement at a given wavelength. Photometry provided by the author is indicated by an asterisk (*) in the table. The single additional reference used for the infrared photometry was Probst (P2, 1981 Table A.2 — individual observations).

As a check on the consistency of the V photometry of the various studies, the data reported in the three primary studies used, SH, P1 and GL, were compared. For 32 stars in common between SH and P1, we find a mean (SH - P1) value of 0.006 mag, with a scatter of 0.058 mag. Comparison of 18 stars in common between SH and GL, yields (SH - GL) = 0.004, with a scatter of 0.044. The small differences in the means for the common samples indicate that there are no significant first-order *systematic* differences between the studies. However, the scatter is rather large, and is probably due to variability in the stars themselves, since the sample includes a number of known flare stars, as well as possible second-order color term differences in the photometric systems for which no check has been made here. Without an extensive examination of the entire sample

at V, it is not possible to assign each star a range in V associated with its particular flaring activity. Because of this lack of variability data, we adopt a characteristic range of visible magnitudes for the sample members, ± 0.02 mag at V, as determined by comparison of the various databases. Thus, a 3σ variance in either direction from the reported value covers the largest scatter between the datasets. All values for V magnitudes have been assigned this error, except those few known to have larger amplitudes, such as those reported by SH.

For the 57 stars with K photometry in common between SH and P1, we find $(SH - P1) = 0.003$, with a scatter of 0.033. Probst (1981, his Table II.2) also gives a comparison between his JHK photometry and others', and finds systematic differences ~ 0.03 mag, and variances ~ 0.03 mag. Comprehensive work exploring the variability of M stars in the infrared has not been done, although it is suspected not to be as significant as it is at visible wavelengths (Giampapa, 1991 private communication). This may be the reason why the variances are smaller in the infrared than they are in the visible. We adopt typical errors of ± 0.03 mag at J, H and K, in an attempt to include both the systematic differences and possible low-level infrared flaring. Some individual measurements, notably those reported in P2 and those made by the author, have larger errors in the infrared photometry for a variety of reasons (e.g., faintness, proximity to a nearby source).

Using many references, and providing infrared photometric data for stars with no published values, we have compiled a complete dataset of VJHK photometry for the nearby M stars. Deconvolution of close binaries

using speckle data permits the determination of absolute magnitudes (see §3.8.1) and the true luminosity function at V, J, H and K for all objects presently known within the survey limits (see §4.3).

3.2.3 Age

We can estimate the age of the sample constituents using the velocity diffusion coefficient of Wielen (1977). Although this dating technique cannot be applied with confidence to individual stars, it is useful when used to describe large populations such as the one surveyed here. We calculate an age for the “systems” (i.e., both single stars and multiple systems are counted only once) which have UVW space motions listed in the Gliese (1969) catalog, and estimate a mean age for the sample as a whole. This age estimate will be biased toward an older sample because the parallax catalogs were compiled primarily using proper motion surveys which are biased toward high velocity, presumably old members of the local population. With this *caveat* in mind, we find a representative age of 6.3 Gyr for the 56 systems with space motions listed, with a large formal scatter of 8.6 Gyr. A more realistic estimate may be obtained if we omit the ten systems which have ages estimated to be greater than 10 Gyr due to very high space motions, and an equal number with ages less than 1.0 Gyr. The result, which is the age range adopted for the sample, is 3.7 ± 2.0 Gyr. This age places the sample in the intermediate disk population, the same group which includes our sun.

3.3 The Visibility Curves

For binary systems, separations and position angles are found at

each epoch, and magnitude differences at each wavelength. For unresolved program stars, limits are set for the faintest companion which could have been detected.

For all stars in the survey, one of two models was adopted for the source — either an unresolved single star, or a resolved binary system. For an unresolved source, the visibility is theoretically equal to 1.00 at all spatial frequencies and at all position angles. In the case of a binary source, the separation and brightness ratio are found directly from the visibility curve, supplemented with position angle information, the phases, to resolve the 180° quadrant ambiguity. Visibility curves for resolved sources are shown in Figures 3.1 to 3.11, and for unresolved sources in Figures 3.14 to 3.80. Howell (1980, Equation 33) describes the binary star visibility as a function of spatial frequency, f , as

$$V(f) = [1 + 2BR(1 + BR)^{-2} \cdot (\cos(2\pi xf) - 1)]^{1/2} \quad (3.1)$$

where BR is the brightness ratio and x is the separation.

Graphically, the separation is simply the reciprocal of the spatial frequency point at which one period of the visibility modulation is complete. For the 1D data, only separations measured in the scan direction, either north-south (NS) or east-west (EW), are given. The brightness ratio, BR , is determined from the minimum in the visibility curve, V_{min} from

$$BR = \frac{(1 - V_{min})}{(1 + V_{min})} \quad (3.2)$$

and the magnitude difference is then

$$\Delta m = -2.5 \cdot \log(BR). \quad (3.3)$$

In the next sections, we discuss how the final visibility curves are obtained. We then elaborate on the methods used to fit the resolved sources, and how we set limits on the unresolved sources.

3.3.1. Determining Visibility Curves for Resolved Sources

In 1D speckle, the visibility curves of binaries in one direction are obtained directly from the divided power spectra. A problem identified in the 1D speckle technique is damping of the visibility curve caused by imperfect scanning (McCarthy *et al.* 1988). Non-linear mirror motions can cause the Fourier moduli to damp exponentially with increasing spatial frequency. This effect can, and has been, modelled during data fitting, and recovery of the true brightness ratios for binaries is possible. The fits done for the 1D data have been accomplished using a non-linear least squares routine described in Freeman (1990) which includes a damping constant and uses both the visibility and phase data. The phase data are required to determine the quadrant in which the secondary is found.

The error in the brightness ratio determined during fitting is representative of the quality of the data, and is directly related to how well the fitting program is able to determine a unique minimum in the visibility. The adopted errors in the reported separations are taken to be an estimate of the peak error in the total separation, 10%, due to the typical error in the scanlength calibration at the telescope, which generally overwhelms any

error in the fit to the data. Because the scans were done in either a NS or EW direction, no errors are given on the position angles for individual scans, although for data with phase information available, the location of the companion, e.g., to the north or south, is listed.

The product of 2D speckle observations is a visibility map covering all position angles. Five methods of data fitting have been explored in the case of resolved binary sources to determine the three parameters of interest obtainable from the 2D data: the brightness ratio, the separation *and* the relative position angle (measured north (0°) through east). The five methods include: 1. row summation of the 2D visibility along fringes, 2. fitting the 2D visibility only, 3. fitting the 2D visibility and phase, 4. parameter determination from the reconstructed image, and 5. a global random search method which samples points of the 2D visibility and phase. The first four methods are outlined in Henry *et al.* (1991) where they have been tested on GL 67AB, a binary with the largest brightness ratio (BR = 59:1 or 4.43 mag at K) detected to date using speckle techniques.

In all of the 2D fitting methods, the primary limiting factor on the determined separation is the accuracy of the known binary star orbits used to calibrate the detector scales. In addition to imperfect orbits, there is an added error in position angle introduced during the camera alignment procedure at the telescope, which is accomplished by trailing star images across the field in right ascension and declination. The systematic errors in the case of the SO 2.3m observations are 4% for the detector scale calibration (binary star orbits), and 2° for the position angle measurements (binary star orbits and camera alignment). During the data reduction tests,

we have found that the separations determined from all five methods are consistent to 2% (only half the error in the scale calibration), the position angles to 1.5° , and the magnitude differences to 5%. We conclude that the five reduction methods give answers which vary by less than the magnitude of the systematic errors, and thus, any of the methods will suffice in determining the binary parameters.

The methods chosen to produce visibility curves and obtain final answers for resolved sources are the first and last ones. The first, row averaging the 2D visibility map, is used in the case of very close binaries (GJ 1005AB and GL 831AB, for example) when a large portion of a one fringe can be seen by eye, and produces a single visibility curve similar to the end-product of a 1D observation. The 2D visibility map and the visibility errors are first rotated to align all fringes along rows in the Fourier plane. In practice, even with a single broad fringe or at large brightness ratios, alignment of the fringes can be accomplished by eye to 1° accuracy. Again, because the binary star orbits are rarely accurate to 1° , any error introduced by eye-alignment of the fringes is minor.

The visibility value at a given spatial frequency is then found by determining the weighted average along a row; each visibility point along a fringe should, in theory, have the same value. The error on each resulting visibility value is the formal error, as defined by

$$\sigma_{mod}^2 = \frac{1}{\Sigma(1/\sigma_i^2)} \quad (3.4)$$

where σ_{mod} is the error on the row's visibility value, and σ_i is the error

on an individual visibility point in the row. The outer cutoff radius in the data is chosen by inspection of the noise level in the visibility plane. The maximum possible outer radii, equal to the reciprocals of the diffraction limits, at J, H and K for the SO 2.3m are $8.89''^{-1}$, $6.79''^{-1}$ and $5.07''^{-1}$. The cutoffs are usually less than these values because rarely is information gained out to the diffraction limit, especially for faint sources. The outer limit chosen in each dataset can be seen on the visibility plots by the location of the final point plotted. In practice, an inner radius cutoff is chosen as well; at low spatial frequencies it is difficult to calibrate seeing fluctuations accurately. Typically, the inner radius is $\sim 0.5''^{-1}$.

The method used to fit the 2D data for all but the few closest binaries, the random sampling technique, is more rigorous. In this case, 200 samples of the complex visibility plane (including both modulus and phase points) containing 500 points each are made. Each sample is then fit for brightness ratio, separation and position angle, and the standard deviation computed for each quantity using the 200 individual samples. Tests of the method indicate that further sampling does not result in significant improvement of the fit, and therefore only 200 samples were taken for each dataset. Further details of this method can be found in Freeman (1991).

The visibility curves for the survey binaries are presented in Figures 3.1 to 3.11. The modulation of the curve, resulting in the fringe signature of a binary star, can be seen in all cases. The vertical axis in all plots indicates the visibility, and the horizontal axis, the spatial frequency. For the doubles, the three panels in each figure represent observations taken at the three infrared wavelengths used during the survey, J, H and K.

The corresponding observational data and results are provided in Table 3.2. Curves are not shown for all binaries at all wavelengths because in several cases — GJ 1005AB, GL 473 AB, GL 623AB, GJ 1245AC and GL 866AB — the data have been published previously.

As discussed above, adopted errors in separation for the 1D observations are 10%. For 2D data we adopt standard errors of 4% for binary component separations, and 2° for all position angle measurements, unless otherwise noted. Errors in magnitude difference in both 1D and 2D data are highly dependent upon data quality, and are reported for the individual observations. All data for binaries within the survey are presented in Table 3.2, and all speckle data for other binaries used in the development of the mass-luminosity relations (see §4.1) are given in Table 4.2.

3.3.2 Comparison of 1D and 2D Techniques — Gliese 67AB

For illustrative purposes, we compare in Figure 3.12 one-dimensional (UT 04 Oct 1982) and two-dimensional (UT 10 Oct 1989) speckle imaging data taken at $2.2\ \mu\text{m}$ of the binary system GL 67AB. The primary is a solar-type G2 dwarf, with an dM secondary orbiting at 8 AU. The determined north-south separation for the 1D data is $\sim 0.55''$, which is coincidentally close to the $0.62''$ total separation measured for the 2D data. Thus, the two sets of fringes are roughly equally spaced.

The improvement in the dynamic range that can be reached using 2D speckle is pronounced and obvious. While the 1D data indicate the presence of the companion, the separation and brightness ratio are difficult

to determine with confidence, primarily due to large errors in the individual visibility points. The last 2D data point shows a similar error for a single point in the 2D visibility plane, since it lies at the edge of the circular region used when row-averaging. However, because many points along a fringe are available in 2D imaging, the formal errors decrease as the root of the number of points and allow a much better determination of each visibility point, although systematic errors may still be present in a given dataset and must be considered independently. Such row-averaging is possible for binary stars, but not for more complicated sources, although radial-averaging in the Fourier plane is possible for circularly symmetric objects. It is easy to see that the relative flux and separation of the components are much better determined in 2D than in 1D. Furthermore, 2D results provide position angle information in a single observation, and allow a 2D image to be reconstructed using the 2D Fourier modulus and Knox-Thompson phases.

In the case of this system, we have demonstrated that infrared speckle techniques used to study binary stars have been pushed to new limits in dynamic range. We estimate the detectability limit for the faintest companion observable by subtracting the fit of the binary from the data, (Figure 3.13(a) for a single angle, (b) for all angles) and find that companions six magnitudes fainter than the G2 primary at K would be detected, corresponding to dwarfs of mass 0.10–0.15 M_{\odot} . This estimate has been made using neither the lowest, nor highest, quality data. For the dataset used to determine the six magnitude sensitivity, the target star has $m_K = 3.6$, the seeing was $\sim 1''$ at K, and 5000 frames each were taken of the target and reference. Further dynamic range can be achieved in better

seeing conditions, by taking more frames, and by using the next generation of lower read-noise infrared arrays.

3.4 Six New Companions — Resolved Targets

Six new companions were found during the course of the survey, ranging in mass from $0.4 M_{\odot}$ to the end of the main sequence. Three of them are very low mass brown dwarf candidates.

3.4.1 The Companions

Of the 74 stars searched for companions, six have been found to be orbited by low mass secondaries. Speckle observations of the six new companions are listed in Table 3.2 and the visibility curves are included with all doubles in the survey in Figures 3.1 to 3.11. The three reddest objects known for which masses have been determined are in the survey, and are included in the following descriptions of the newest members of the solar neighborhood.

GJ 1005B:

This astrometric binary, also known as LHS 1047AB, is only 5.3 pc distant, placing it just outside the boundary of the traditional 5.2 pc sample. The system is discussed by Ianna *et al.* (1988), where the first infrared speckle observations are reported. With a period of under five years and a semimajor axis of only 1.7 AU, this binary is difficult to resolve. The semimajor axis of the astrometric orbit is small ($\alpha = 0.073''$) and poorly determined, and results in large formal errors in the masses. Using three speckle measurements and two visual measurements by Heintz, we make mass estimates for the components of 0.137 and 0.057

M_{\odot} . The formal errors on these masses are, in fact, larger than the masses themselves. Better definition of the astrometric orbit would reduce the mass errors considerably. The secondary's mass estimate places it below the stellar/substellar break at 80 Jup, and although the error is large, it remains a viable BD candidate.

GL 570C:

The GL 570ABC system is composed of a dK primary currently separated from a pair of close M dwarfs by ~ 120 AU. At a distance of 5.6 pc, this is the fourth nearest known triple, after the Alpha Centauri, GJ 1245, and α^2 Eri systems. The B component was suspected to be a binary because it appeared overluminous for its spectral type, and was placed on the observing lists of the radial velocity and French infrared speckle groups. Because the B component is an M dwarf, it was also included in the speckle survey discussed here. The tertiary was first reported by Marcy and Benitz (1989) in their radial velocity survey. It was also detected early in our speckle survey, found to be stellar, and was not given high priority. Mariotti *et al.* (1990) give the orbit ($P = 309$ days, $a = 0.143''$) and masses (0.553 ± 0.047 and $0.390 \pm 0.032 M_{\odot}$) for the components in a thorough discussion of this interesting system.

GL 623B:

Lippincott and Borgman (1978) first reported a 3.7 year astrometric perturbation of the dM2.5 primary. McCarthy (1986) confirmed that the object was in fact a binary using infrared speckle, and continued to observe the system. In 1987, McCarthy and Henry gave the first mass estimates

for the secondary — $0.11 M_{\odot}$ dynamically and $0.08 M_{\odot}$ photometrically. At the time, the companion was the lowest luminosity red object for which a mass had been determined. It was supplanted by GJ 1245C in 1988 (see the next entry in this section).

In 1989, Marcy and Moore reported their spectroscopic work on the system, and estimated the secondary's mass four ways, all falling in the range 0.07 to $0.09 M_{\odot}$. With an additional infrared speckle observation in 1991, we provide revised dynamical mass estimates for the components of 0.52 and $0.12 M_{\odot}$. These are certainly too large, as the primary is overmassive by 30%. The error is due to a poorly determined parallax, an overestimated semimajor axis, or both. For further discussion, we adopt masses of 0.300 ± 0.032 and $0.079 \pm 0.010 M_{\odot}$ for the components (see §4.1.3). This system warrants close scrutiny in the future since the system is of relatively short period and thereby holds promise for a very accurate orbit determination. The secondary remains a BD candidate.

GJ 1245C:

Also known as G 208-44/45, this is the closest known triple (only 4.5 pc distant) beyond the Alpha Centauri system. The high proper motion, red dwarf pair is currently separated by $8''$ (~ 37 AU) with an orbital period of several hundred years. The brighter component, GJ 1245A, was reported to be an astrometric binary by Harrington (1982).

The very low mass secondary has been detected using 1D infrared speckle imaging, and a full discussion of the system is given by McCarthy *et al.* (1988). Direct determination of the masses of the close pair, GJ

1245AC, using the definitive astrometric orbit of Harrington (1990) and all available speckle data results in mass estimates of 0.118 ± 0.018 and $0.087 \pm 0.014 M_{\odot}$. The distant component, GL 1245B, is estimated from its photometry to be of mass $\sim 0.1 M_{\odot}$. GL 1245C is currently the lowest luminosity red object for which a mass has been determined, and is a strong BD candidate.

GL 891B:

Also known as Wolf 922, the dM4.5 primary was reported to be an astrometric binary by Lippincott in 1979, and has been further studied by McNamara *et al.* (1987). The system is difficult to resolve at any epoch, since the short period orbit (1.92 years) has a semimajor axis of only $\sim 0.2''$. We find that the components have a brightness ratio of ≥ 4 in the infrared, and an estimate of the component masses using the speckle observation made at H in November 1990 and the Lippincott orbit results in unrealistic masses of 0.82 and $0.24 M_{\odot}$. Using the newer McNamara orbit, the 2D infrared speckle point and an optical speckle point of Blazit *et al.* (1987) yield a scale factor of ~ 6.7 , although the measured position angles do not match the predicted angles well. Using this scale factor and their new photocentric semimajor axis results in masses even larger than in the case of the Lippincott orbit. Obviously, further work is required before a definitive mass determination can be made.

GL 866B:

Due to its southerly declination (-15°), GL 866 gave no dynamical indication of duplicity because of little astrometric coverage and because the

components are nearly identical, thereby causing a very small photocentric perturbation. The binary is truly “in our own backyard” at a distance of only 3.4 pc, and illustrates our lack of knowledge about even the nearest stars, since its binary nature was only revealed in 1985. The system was first resolved using infrared speckle, and has been discussed in detail since by McCarthy *et al.* (1987) and Leinert *et al.* (1990), the latter of which provides mass estimates of 0.22 ± 0.02 and $0.16 \pm 0.02 M_{\odot}$. The relative orbit of GL 866AB is the first to have been determined from infrared speckle data alone, and the masses have been found from the brightness ratio and by assuming a mass-luminosity relation for low mass stars.

The components are overmassive for their spectral type, indicating a possible error in the parallax, although it appears to be well-determined. Gliese (1979) lists a parallax of $0.290'' \pm 0.005''$, USNO reports $0.291'' \pm 0.003''$, and Leinert *et al.* (1990) mention an updated parallax (Gliese and Jahreiss, in preparation) of $0.294'' \pm 0.003$. It is possible that the parallax is in error because GL 866 was not known to be a binary system when its parallax was determined, or that there are more than two bodies in the system, which would lead to high mass estimates for the observed fluxes. It is interesting to note that although the GL 866 system is the fourteenth nearest, it is poorly understood! This is further evidence that there remains much work to be done on even the nearest stars.

3.4.2 Mass Determinations

Masses have been determined for the newly-resolved astrometric binaries, GJ 1005AB, GL 623AB, and GJ 1245AC, as follows. The infrared

speckle observations provide the component separation (p), the magnitude difference in the infrared (Δm_J , Δm_H and/or Δm_K), and in some cases, the position angle of the secondary (θ). The astrometric work provides the parallax and defines the photocentric orbit of the binary, including the period (P), inclination (i), eccentricity (e), epoch of periastron (T), longitude of periastron (ω), angle of the ascending node (Ω) and the photocentric semimajor axis (α).

It is the combination of the photocentric orbit and the relative separation and brightness ratio from infrared speckle observations that allows the determination of the component masses. First, the total system mass is found, followed by the determination of the fractional mass of the secondary, thereby permitting mass determinations for the system's constituents. van de Kamp (1986) discusses in detail the methods used to obtain the masses and the relative orbit of a binary system from an astrometric orbit once it has been resolved. The total system mass is given by Kepler's Third Law, $M_A + M_B = a^3/P^2$, where a is the semimajor axis of the relative orbit in AU, and P is the period in years. P is determined by the astrometric orbit, and once a binary is resolved using speckle techniques (yielding the relative separation p at a single epoch), the combination of the photocentric orbit parameters α and ρ (the photocentric perturbation at that epoch) with p yields the semimajor axis of the relative orbit: $a/\alpha = p/\rho$, or $a = \alpha \times p/\rho$. The parallax of the system must be known in order to convert the semimajor axis of the relative orbit from arcseconds to AUs.

The fractional mass of the secondary, $B = M_B/(M_A + M_B)$ is found using $p/\rho = (B - \beta)^{-1}$. β is the secondary's fractional luminosity

at visual wavelengths, where the astrometric data are acquired. In the case of infrared speckle data, β is determined by first converting from the infrared magnitude difference, Δm_J , Δm_H and/or Δm_K , to Δm_V using the relations of Probst (1977), $\Delta m_J/\Delta m_V = 0.56$, $\Delta m_H/\Delta m_V = 0.55$, and $\Delta m_K/\Delta m_V = 0.53$, which were developed by measuring magnitude differences of widely-separated binaries in the visible and infrared. An estimate of ΔV using these relations should ideally include second order terms in order to address the range of colors for the stars to which they are applied. However, no attempt has been made here to include such terms, although this is an obvious step which could be made in future work. Even when Δm_V is established, one must be careful when assigning the value of β because of the varying sensitivity, color response, granularity and inertia of photographic plates. Feierman (1971) tabulates β values for various Δm_V , because observed values of β often deviate from that predicted by the theoretical relation

$$\beta = (1 + 10^{0.4\Delta m})^{-1}. \quad (3.5)$$

The discrepancies between the theoretical and adopted β values also depend upon telescope, emulsion type and the binary separation.

The quantity $(B - \beta)^{-1}$ is often called the scale factor, and directly relates the sizes of the relative and photocentric orbits at all epochs. Typically, several measurements of p are made, ratioed to ρ at each epoch, and the mean used to determine a using α . B is then obtained since β is known, and leads to the deconvolution of the system mass once Kepler's

Third Law is solved.

A spectroscopic orbit can substitute for an astrometric one if the binary can be resolved using speckle imaging. This has been accomplished in the case of GL 570BC, and the technique is outlined in Mariotti *et al.* (1990), where they discuss the system. In perhaps the most extensive use of various techniques, Marcy and Moore (1989) combine all three types of data — radial velocity, astrometric, and infrared speckle — in their study of the GL 623AB system. It is the combination of these three types of data that is proving to be a powerful tool in the study of close binary systems.

3.5 Determining Detection Limits for Unresolved Sources

When no companion is found orbiting a program star, we set a limit to which the star is unresolved. The limits assigned for companion infrared fluxes allow us to reach to the end of the main sequence for nearly every program star, and deep into the realm of brown dwarfs in many cases.

3.5.1 Limits at 1, 2, 5 and 10 AU

Table 3.3 lists absolute magnitude limits for unseen companions orbiting the program stars. These objects include all stars which are single or in widely separated ($\geq 8''$) pairs comprised of targets that could be searched individually. The values given here supercede those reported in Henry and McCarthy (1990) due to the acquisition of new data and refined fitting techniques. The visibility curves for the unresolved targets are shown in Figures 3.14 to 3.80. The search technique used is given in the second column of the table, where 1D indicates a one-dimensional scanning result

in the north-south (NS) or east-west (EW) direction. The two-dimensional camera data are indicated by 2D 2X when the search was done using the 4'' field of the camera, and by 2D 1X when the 8'' field was used. The 1X camera magnification was used on faint sources, and while resolution was lost (no targets could be searched to 1 AU, and some not to 2 AU), the higher signal allowed at least some search to be accomplished.

Limits have been set at 1, 2, 5 and 10 AU from the primary star, determined using the parallaxes listed in Table 3.7. First, the distance from the star in arcseconds corresponding to the desired search radius is determined. For example, if we wish to search for companions orbiting a star at 2 AU, at a distance of 5 pc, the separation would be 0.4''. Inversion of this separation yields the spatial frequency at which a full cycle of the visibility is completed, $2.5('')^{-1}$. We are actually concerned with the *minimum* of the visibility curve, which occurs at half of the full cycle, so in order to search for objects at 2 AU, we set the limit at a spatial frequency of $1.25('')^{-1}$. The following equation can be used to calculate the spatial frequency (sf) at which the minimum is reached, given the parallax of the target searched in arcseconds (π) and the desired separation in astronomical units (AU):

$$sf = \frac{1}{2\pi \cdot AU}. \quad (3.6)$$

Some stars could not be searched for companions throughout the 1 to 10 AU region. Most often, this was caused by the target source faintness — all stars searched at H using the 8'' field of the 2D camera, and some

1D scans on the fainter survey stars. The two nearest stars in the survey, Barnard's Star (GL 699) and Wolf 359 (GL 406), were not searched at 10 AU, as the separations of companions would be $5.5''$ (0.09 arcsec^{-1} spatial frequency for the visibility minimum), and $4.2''$ (0.12 arcsec^{-1}), respectively.

There are no visibility curves shown for one star in the survey, G 208-45. This star was never searched independently, but was used as the standard point source for G 208-44, which did prove to be resolved. Limits for G 208-45 have been obtained by examining the sizes of the error bars on the individual visibility points at the four separations of interest, effectively measuring how good a point source G 208-45 really is. This procedure was followed for the two observations, one in each scan direction, listed in the table.

For the 1D data, separate companion magnitude limits have been determined by fitting a limit to the visibility of the object found from scans in each of the two orthogonal scan directions, NS and EW. At each step in the fitting procedure care has been taken to assure that all limits assigned are conservative. The limit in each scan direction at a given separation has been determined using *any* any spatial frequency point out to that separation. As an example, consider the visibility curve for GL 406 scanned at K in the EW direction shown in Figure 3.42. The limits found are $\Delta m_K = 4.28, 3.22$ and 3.22 at 5, 2 and 1 AU. Although the limit at exactly 1 AU could be more stringent using the spatial frequency point at that separation, in order to cover all companions between 2 and 1 AU, we adopt the least severe limit falling within that range, in this case the spatial frequency point at $0.6''^{-1}$.

The error bars plotted for the individual 1D visibilities are 1σ formal errors. At high spatial frequencies (small separations) where many visibility points must fit a curve described by Eq. 3.1 for a binary model, assigning the limit to the bottom of all visibility points' errors is an accurate, if somewhat conservative, method. However, at the lowest spatial frequencies where the 10 AU limits often fall (and some of the 5 AU limits for the nearest stars), few visibility points are available to be fit. Furthermore, these frequencies, corresponding to scales $\leq 1''$, are subject to poor seeing calibration, hence the name "seeing frequencies." The effect for some scans is an unrealistically large estimate of the magnitude difference to which a companions would have been detected. Typically the visibility point values would fall at 1.000 ± 0.002 , leading to a visibility minimum of 0.998, or to a companion detection limit of 7.50 magnitudes fainter than the primary (see Eqs. 3.2 and 3.3). In order to address the lack of visibility points, and to compensate for the small errors on the individual points, we adopt a 3σ limit, rather than 1σ at these low spatial frequencies. This corresponds to a visibility minimum of 0.994, and results in a largest possible detectable magnitude difference of 6.30 mag. We therefore impose a blanket limit for detectable secondaries orbiting the survey stars of no more than 6.30 magnitudes fainter than the primaries.

Because observations in two orthogonal scan directions have been made in the cases of targets examined by 1D techniques, we adopt a characteristic limit at each separation for an individual star by accepting the brighter of the two scan limits at that separation. Again, this is a conservative estimate of the total detection limits for the survey, as many

scans probed much deeper.

In the case of the 2D speckle data, we first manufacture a set of 1D visibility curves, and then consider the limit found from the entire set. To produce a set of 1D visibility curves from the 2D data, we rotate the visibility maps and their complementary error maps in 5° increments from 0° – 175° . The maps are symmetric when flipped 180° , so the angles 180° – 355° are redundant. Each visibility map and its error map are row-averaged separately, as outlined for resolved sources in §3.3.1, creating 36 1D visibility curves for each unresolved source, at position angles every 5° around the target. One can imagine that we have made 36 1D observations at once using 2D techniques. These 36 curves are plotted in one figure for each unresolved source.

The limits of companion detectability at each separation, 1, 2, 5 and 10 AU, are chosen by fitting to the bottom of the visibility envelope for the 36 plots. Three test cases of extreme brightness ratios at various separations have been analyzed to check that the limits found by this method are, indeed, true limits. In Figures 3.81, 3.82 and 3.83, we show the resulting visibility curves for the binaries GL 67AB at H and K, and GL 623AB at H. In all three cases, the final limits assigned at the various separations for undetected companions are not more stringent than the true companions, i.e., we do not incorrectly report that the target is unresolved to a limit fainter than the secondaries. For GL 67AB at H, we find limits of $\Delta m_H = 4.4$ [2 AU], 4.5 [5 AU] and 4.8 [10 AU]. Thus, for the range 5 to 10 AU we adopt a limit of 4.5 mag, which matches the actual magnitude difference of the companion ($\Delta m_H = 4.50$, separation $0.44''$) found at a

distance of 6.1 AU at that epoch. According to the fit at K, the limits for GL 67B are $\Delta m_K = 4.2$ [2 AU], 4.3 [5 AU] and 4.3 [10 AU] fainter than the primary, again at precisely the actual magnitude limits ($\Delta m_K = 4.30$, separation = $0.62''$) for the secondary, then found at 8.6 AU. Finally, in the case of GL 623AB at H ($\Delta m_H = 2.65$, separation = $0.19''$) the limits, $\Delta m = 2.6$ [1 AU], 2.8 [2 AU], 3.5 [5 AU] and 4.9 [10 AU], also match that of the true companion at a separation of 1.4 AU.

In summary, in both the 1D and 2D cases, each detectability limit assigned is specific to a single dataset, and will vary with the distance from the star. The limit will vary with target brightness, seeing, integration time, detector performance and the number of frames acquired on the object and its point source. Fortunately, the brighter stars in the survey provide more signal, and allow us to probe to larger magnitude differences, thereby permitting us to reach similar absolute infrared magnitudes around the survey stars as a whole. We stress again that conservative limits have been assigned in every case, and yet, we are still able to probe into the realm of BDs for most of the survey stars.

3.5.2 Flux Limits for the Survey as a Whole

In order to characterize the survey in its entirety, we estimate comprehensive M_K detectability limits for the program stars. Some stars were searched at H rather than at K in an effort to gain better signal to noise. In order to set limits for all stars at K, the H limits have been transformed to K limits using absolute magnitudes representative of blackbodies, as is shown in Figure 3.84. We have integrated the bandpasses

of the 2D camera filters (H: 1.436-1.823 μm , K: 1.956-2.430 μm) used in the observations for objects of temperatures 1000 K to 4000 K with radii of 0.125, 0.100 and 0.075 R_\odot . These radii encompass the theoretical values found for M dwarfs of mass $\leq 0.10 M_\odot$ and BDs of age 10 Gyr (Burrows *et al.* 1989), and actual radii found for M dwarfs, which are up to 25% larger than the theoretical values (Lacy 1977).

We have chosen to determine the H-K values for the conversion of the M_H to M_K limits using bodies of radius 0.100 R_\odot . We have arrived at this radius by testing blackbody fits to three of the faintest dwarfs known, VB 8, VB 10 and LHS 2924, which are the reddest objects with high quality parallaxes (thereby allowing absolute magnitude calibration). These are at least remotely similar to the objects which we would have detected, and may, in fact, be BDs themselves (see Chapter 5). In order to fit both the absolute fluxes and colors, trials of various radii required 0.11, 0.11 and 0.10 R_\odot for the three objects, respectively.

The adopted values for companion M_K limits to all stars are listed in Table 3.3. Using all of the M_K limits — conversion to K for all objects examined at H, combining the 1D scans into one set of limits for each star, and including the limits assigned directly from the 2D camera work at K — we find the characteristic survey limits. We have taken a straight mean of all limits at a given separation, and present the answers, with their standard deviations, in Table 3.4. Also given is the number of stars which were searched at that separation.

The values shown represent the limits at that separation, and for

any object with a separation out to the next bin. For example, the limit for GL 15B at 2 AU is $M_K = 12.6$. This is the limit not only for objects at a separation of 2 AU, but for any object out to 4.9 AU as well, beyond which the 5 AU bin limit, $M_K = 13.0$, should be adopted.

Returning to Figure 3.84, inspection shows that we would have imaged objects with radii $0.10 R_\odot$ with temperatures greater than 2550 K at 1 AU around the survey stars, where the survey limit is $M_K = 10.85$. The search temperatures drop significantly for larger separations: 2100 K [2 AU], 1850 K [5 AU] and 1650 [10 AU]. For comparison, the absolute K magnitudes for the benchmark red objects VB 8, VB 10, and LHS 2924, which are considered to be near or beyond the end of the stellar regime, are 9.74, 10.01 and 10.48, respectively. Thus, we typically would have seen LHS 2924 orbiting the nearby M dwarfs, at any of the separations searched. In some instances, e.g., GL 205, GL 338A and GL 884, these objects would remain undetected. Nonetheless, there are only a few stars, some of which remain suspect (see §3.10), which do not meet the limits assigned for the survey as a whole.

3.5.3 Mass Limits for the Survey as a Whole

Using the survey flux limits we can determine the mass limit to which we would have detected BDs, both empirically and theoretically. Certainly, a quick examination of the limits indicates that we would have detected any stellar companions to the M dwarfs which orbit within the search radii. In §4.1 we derive empirical mass-infrared luminosity relations using binary components with well-known masses and extensive speckle work

to determine component infrared fluxes. The mass- M_K relation indicates that the absolute magnitude at which we reach the canonical 80 Jupiter masses, the dividing line between the lowest mass stars and the highest mass BDs, is $M_K \approx 10.0$. We are effectively probing nearly a full magnitude into the realm of BDs, even at separations of 1 AU. At 2, 5 and 10 AU, we have searched to 1.4 mag, 1.9 mag and 2.4 mag fainter than the empirical stellar cutoff, respectively.

In addition to mass, age has a significant effect upon the flux emitted by a BD, as is illustrated in Figure 3.85. The total fluxes for objects of masses 0.20 to $0.03 M_\odot$ at ages of 0.1, 1.0 and 10 Gyr have been taken from the D'Antona and Mazzitelli (1985, long dash curves) and Burrows *et al.* (1989, Model D, dot-dash curves) evolutionary models for low mass stars and BDs. The conversion from total flux to M_K has been done using the very tight (correlation coefficient > 0.99) empirical M_{bol} - M_K relation of Veeder (1974) which includes 96 objects with $4 \leq M_K \leq 9.5$:

$$M_{bol} = 1.12 \cdot M_K + 1.81. \quad (3.7)$$

Similarly, Reid and Gilmore (1981) find a relation which yields slightly (0.15 mag) brighter M_{bol} at $M_K = 10.0$:

$$M_{bol} = 1.08 \cdot M_K + 2.05. \quad (3.8)$$

From the figure it is evident that at the sample age of 3.7 ± 2.0 Gyr we would have detected objects of $M_K = 10.8$ to masses of 80–90

Jupiters. For the deeper limits at 2, 5 and 10 AU, we reach to masses of 75–80, 70–75 and 70 Jupiters for the sample age. Apparently, if the theoretical models are correct, we are only probing the very high mass BD regime.

It is the opinion of the author that it is because of the plummet in luminosity at the stellar/substellar break that BDs have proven so difficult to find. BDs may simply be much fainter than their slightly more massive stellar counterparts. The dropoff in the luminosity function, which occurs at $M_K \sim 10$ (see §4.3), may be caused by a discontinuity in the mass-luminosity relation. This discontinuity is predicted by the theoretical models, and indirect evidence is provided by the significant lack of any objects in the survey with $M_K > 10.0$, although we have probed more than two magnitudes fainter for companions orbiting many stars.

3.6 Missed Objects

Objects missed during the survey include primary targets absent from the parallax catalogs, and companions with orbital semimajor axes between 1 and 10 AU which were too close to their primaries to be detected at the time of observation.

3.6.1 Missed Primary Targets

As discussed above (§3.2.1), there are 50% fewer M dwarfs known in the more distant half of the survey volume, 6.35 to 8.00 pc, than in the nearest 6.35 pc. To make the matter worse, it is entirely unclear how many faint stars within 6.35 pc are missing from the parallax catalogs. The only solution to the shortage in the outer reaches of the survey would

be a drastic one — simply adding 29 objects to duplicate the nearer shell's density — and is not pursued further. Here we merely point out the likelihood of missing primary targets, and will address the effect on the luminosity function in §4.3.

3.6.2 Orbital Presentation Selection

Chance alignment of two objects in a system along the line of sight could result in the non-detection of a companion brighter than the limits assigned for an unresolved source. To assess the number of companions missed between 1 and 10 AU, we must calculate the portion of space 1 to 10 AU searched since not all stars could be searched at all separations, and also estimate the frequency of orbiting secondaries with semimajor axes between 1 and 10 AU which were unresolvable at the time of observation.

Using the survey coverage detailed in Table 3.4, and adding in full coverage 1 to 10 AU for the six objects which were resolved, we see that at 1, 2, 5 and 10 AU we searched 59, 68, 74 and 72 stars, respectively. The volume enclosed between 1 and 10 AU for each star is 4185 AU^3 , amounting to a total of 309700 AU^3 for 74 stars. From this total volume we subtract those regions not searched: 440 AU^3 for 15 stars from 1 to 2 AU, 2940 AU^3 for 6 stars 2 to 5 AU, and 7330 AU^3 for 2 stars 5 to 10 AU. The coverage accomplished is then 96.5% of the total volume, and indicates that 3.5% of companions would be missed, assuming uniform separations throughout the 1 to 10 AU range.

An assessment of the percentage of stars missed because they fell inside the K diffraction limit of the telescope is made by examining worst

case, circular, edge-on orbits. Figure 3.86 shows the percentage of time secondaries spend within $0.2''$ of their primaries, i.e., within the diffraction limit of the SO 2.3m at K, at the distances of the survey stars, 2 to 8 pc. Because the percentage of time observable is plotted, the masses of the components are immaterial. We also plot, in Figure 3.87, the integrated time the secondaries spend at a distance where superresolution is possible ($0.1''$ at K on the SO 2.3m). For the purposes of the rest of the completeness calculation, we assume a uniform distribution of secondaries throughout the region 1 to 10 AU, and that superresolution produces a detection. The latter stipulation is supported by the fact that data taken on the targets GJ 1005 and GL 831 have revealed the companions even when the binary is not fully resolved.

One can see in Figure 3.87 that while companions within 1 AU are difficult to detect, the probability climbs steeply for slightly larger separations. At 8 pc, 41% [1 AU], to 95% [10 AU] of companions would be detected, heavily weighted to the higher probabilities. Assuming one companion every AU, we find the mean probabilities for detection at 4, 6 and 8 pc to be 92%, 88% and 84%. Again, throughout this calculation we have been conservative. First, circular, edge-on orbits have been assumed. Any non- 90° inclination will open the orbit and enhance the chances of detection (we note that 90° inclination orbits are the best candidates for discovery by radial velocity techniques). Elliptical orbits will generally cause a companion to spend a larger fraction of its time far from its primary, thus allowing detections more often. Furthermore, some of the search was done at H, where the diffraction limit is 30% smaller than at K, and finally,

multiple scans were made of some objects. With this in mind, we adopt a detection probability for companions 1 to 10 AU of 90%.

Considering both factors which affect the true number of detections permitted, 96.5% of the volume actually surveyed, and 90% of companions located at a detectable location, we arrive at a total completeness in spatial coordinates of 87%. Fischer and Marcy (1991) have gone through a rigorous determination of the effective sampling of the initial five parsec survey, including running thousands of orbits projected onto the plane of the sky, and find a less pessimistic 93% completeness factor.

The end result of this statistical treatment is that we may have missed 13% of the companions in orbits with semimajor axes between 1 and 10 AU. Since we found six, we might expect that we then missed only one.

3.6.3 Stellar Companions Missed due to Bright Limits

A few stars, notably GL 205, 338A and 884, have limits which do not reach to the end of the main sequence. The first two of these remain among stars which show suspicious data, and are discussed in §3.10. Because so few stars have limits brighter than $M_K = 10.0$, we do not feel any completeness adjustment to the survey is warranted.

3.7 Binaries

The binary fraction of the nearby M dwarfs is low when compared to other dwarfs, possibly indicating that very faint brown dwarf companions exist, but remain undetected.

3.7.1 All Secondaries

Listed in Table 3.5 are all of the secondaries found among the nearby M dwarfs. For the purposes of the following discussion, the orbital semimajor axis and period of any secondary is considered relative to the next brighter component in the system. We have listed the spectral types of the primaries in the table for reference, as well as references for the orbit, if available. The two problematic systems which have required this definition are GL 166 and GL 643/644. The former is a triple, composed of a K dwarf, a white dwarf, and the survey M dwarf GL 166C. We consider the white dwarf to be the primary, because in an earlier epoch it presumably was. For the 643/644 system we consider the primary, 644A to have three companions, 644B, 644C, and 643A. GL 643B has GL 643A as its primary.

For systems with no available orbits we have converted the present day separation directly to a separation in AU using the parallax. In the cases of GL 166C, GL 169.1A (B was the primary in times past), and GL 283B, the primary is a white dwarf. No attempt has been made to predict what the orbital separation of the companion was to the precursor primary — rather, we use the present day separation in the statistical analysis that follows.

3.7.2 Binary Frequency

Not all portions of M dwarf companion phase space have been searched identically. Fischer and Marcy (1991) have recently done a complete analysis of the searches for companions to M dwarfs, including radial velocity, visual (astrometric), infrared imaging, and the initial infrared

speckle work. They consider companions found throughout the range 0 to 1000 AU. Although the surveys all have different observational samples, they treat the incompleteness for each carefully. They find the resulting multiplicity of M dwarf systems, which are defined as two or more stars bound gravitationally in a system where an M dwarf is the primary, to be single:double:triple:quadruple+ = 62:30:7:1. This results in a multiplicity of $38\% \pm 9\%$ for M dwarf systems, which agrees well with the initial speckle survey, in which the single:double:triple ratio was found to be 19:8:2, indicating 34% multiplicity.

We make several estimates of binarity here. The fraction of all M dwarfs in multiple systems, regardless of the other system constituents, is 53 of 99, or 53.5%. Of the 32 known companions in the survey, 26 have M dwarf primaries, meaning that 81.3% of M dwarfs in multiples have M dwarf primaries. However, this estimate is subject to the incomplete knowledge of the number of M dwarfs to earlier type primaries, which is a topic of future work. To compare the multiplicity of M dwarfs with the Fischer and Marcy study, we discard those six systems in which the primary is not an M dwarf — GL 34, 105, 166, 169.1, 283, 570. We then find for 67 M dwarf systems, single:double:triple:quadruple+ = 46:19:1:1, or 31.3% multiplicity, consistent with their results.

Perhaps the most useful estimate of binarity answers the question: when looking at an M dwarf, regardless of where it is, what are the chances that it will be accompanied by a lower mass companion? This is nearly identical to the Fischer and Marcy method, although we must include the six systems in which the primary in the system is not an M dwarf. Only

one of those six, GL 570B, has a companion, so the fraction of all M dwarfs with at least one lower mass companion is 22 in 73, or 30.1%.

Regardless of the final method adopted in estimating M dwarf binarity, the fraction of M dwarfs which are multiple is 30–40%. This is significantly lower than the 58% binary frequency of solar type stars (F3–G2 IV or V) found by Abt and Levy (1976). While some problems with their analysis have been found (Morbey and Griffin 1987), deletion of the false binaries does not change their original conclusion (Abt 1987). As further support of the earlier results, Duquennoy and Mayor (1991), in their radial velocity study of 166 nearby G dwarfs, determine a nearly identical multiplicity of 57%.

It is interesting to note that while the nearest M dwarfs generally have been studied more completely than any other spectral class for binarity (in large part due to the hunt for BDs), they are more often single than not. One reason for this low binary fraction may be their inability to “hold onto” nearby companions during the star formation process because of their low mass. Another, more intriguing, possibility is that many brown dwarf companions remain undetected. Of course, a third possibility remains — perhaps M dwarfs simply do not form with companions as often as earlier type stars.

3.7.3 Semimajor Axis Distribution

In Table 3.6 we show the multiple systems broken into order of magnitude bins in separation and period. We see that most M dwarf companions are found in the bin of separations searched by the speckle

survey, 1 to 10 AU, with decreasing fractions at larger separations. The shift in numbers for the period bins, indicated by a flatter distribution toward longer periods, is simply a result of low M dwarf masses. Typically, binary M dwarfs with separations 1 to 10 AU have periods 10 to 100 years.

Of the four largest separation binaries in the sample known, none is representative of the nearby M dwarf multiples. GL 643A and GL 644C are both members of an extraordinary five-body system. Two of the faintest objects in the survey, GL 752B (VB 10) and GL 644C (VB 8) were discovered during van Biesbroeck's (1961) search for common proper motion companions to nearby stars. GL 105B is the companion to a K dwarf, itself an astrometric binary. It is quite possible, and even likely, that many wide binary companions have been missed, and we therefore caution the reader when interpreting the 1000+ AU bin in the table.

3.8 Characteristics of All Survey Constituents

We provide here absolute magnitudes at V, J, H and K for all 99 M dwarfs known within eight parsecs of the sun north of -25° . In addition, we report spectral types taken on a standard system for 43 of the constituents.

3.8.1 Absolute Magnitudes

In Table 3.7 we provide a comprehensive list of absolute V, J, H and K magnitudes for every survey member. Column 2 lists the adopted parallax with its standard error for each object, from a variety of sources which are listed at the end of the table. Columns 4 through 7 are the absolute magnitudes and their formal errors. For single objects, the errors include those in the photometry, as listed in Table 3.1, and the error

introduced by the error in the parallax. In most cases, it is the error in the parallax which dominates the final error in the absolute magnitudes. For close binaries which have been deconvolved (see Table 3.2), the error in the magnitude difference, as determined by the infrared speckle data, has also been included.

To estimate the visual magnitudes, deconvolution of the visual flux was done using the brightness ratios determined by infrared speckle, and the relations of Probst (1977): $\Delta m_J/\Delta m_V = 0.56$, $\Delta m_H/\Delta m_V = 0.55$, and $\Delta m_K/\Delta m_V = 0.53$. A mean Δm_V was found from the three infrared measurements, and the adopted error in Δm_V represents the scatter in those three measurements. For the 16 doubles with visual flux deconvolved this way, the scatter in the Δm_V estimates was typically 0.05 to 0.20 mag.

The two close spectroscopic binaries GL 268AB and GL 643AB were not resolved during the survey and warrant special attention. Flux deconvolution has been accomplished in the case of GL 268 by using the estimate of the brightness ratio, $BR \sim 0.7$ given by Tomkin and Pettersen (1986). This corresponds to $\Delta m_V = 0.39$, and permits estimates of the infrared brightness ratios utilizing the Probst relations. No flux ratio was available for the GL 643 system, and as a first guess, we have assumed identical components.

This table is a general reference for the nearby M dwarfs, and is used in the next chapter to determine the luminosity function and to estimate masses for all of the survey members, using the empirical mass-luminosity relationships.

3.8.2 Spectral Types

In Table 3.7, column 8, we provide spectral types for 43 of the survey objects on the standard system of Kirkpatrick *et al.* (1991), which is based upon the Boeshaar (1976) system. All spectra have been taken between July 1989 and March 1991 during a program to classify the reddest dwarfs known. Forty-one spectra have been acquired using the Red Channel Spectrograph, equipped with a TI CCD, on the Multiple Mirror Telescope (MMT). A 270 line mm^{-1} grating with an LP-495 order blocking filter was used to cover the range from 6300 to 9000 Å, at a resolution of 18 Å. Two additional spectra (GL 83.1 and GL 866AB) were taken at the SO 2.3m telescope, using the Boller and Chivens Spectrograph with a TI CCD, using a 400 line mm^{-1} grating with a 2-59 order blocking filter to cover the spectral region from 6900 to 9000 Å, at a resolution of 8 Å. These two spectra have been rebinned and smoothed so that the resolution matches that of the MMT spectra. The slit width at the MMT was 2.0'', and that at the 2.3m was 2.5'', wide enough to compensate for atmospheric refraction (0.5'' at 2.00 airmass between 6500 and 9000 Å), poor seeing, and to assure that the very faint objects fell in the aperture.

Data reduction procedures are discussed in detail in Kirkpatrick *et al.* (1991), where an extensive reference list of the atomic and molecular features present in the spectral region is given.

Figure 3.88 illustrates examples of the dwarf spectral sequence, every half type from M 0.0 to M 9.0, including many of the survey objects. Each spectrum has been normalized to its flux in units of F_λ at 7500 Å, and

offset vertically in the figure for clarity. A dead column in the MMT CCD chip causes the feature at 6415 Å. Absorption by telluric O₂ and H₂O has not been removed. In cases where the spectrum is of a close double, generally $\leq 1''$, the composite type in column 8 is denoted with a "c". While we assign a spectral type of K 7.0 to GL 338B, it remains in the survey because its type was given as M 0.0 in the Gliese Catalog, from which the observing list was originally obtained.

Figure 3.89 shows in detail the spectral features of three dwarfs of type M 0.0, M 4.5 and M 9.0. The early M dwarfs have relatively smooth spectra, with CaH bands and Ca II lines stronger than in redder stars. At later spectral types, the TiO bands, K I lines, and Na I lines gain strength, and at this resolution, dwarfs of type M 7.0 and later exhibit prominent VO absorption features (at higher resolution, VO can be seen at type M 5.0). At 6563Å, H α can be seen in emission in some of the spectra.

These spectra are especially useful because they have all been taken on the same instrument, and classified on the same system. We discuss in §4.2 a spectral class-mass relation which allows mass estimates to be made based upon a dwarf's spectral class alone.

3.9 The Nearby Star Census

The census of nearby stars has grown steadily for 45 years, and shows no hint of slowing down.

It is interesting to evaluate the development of the nearby star census during the last forty-five years. In Table 3.8 and Figure 3.90 we include in the counts all stars known within the traditional 5.2 pc survey,

broken into three groups: all stars, all M dwarfs, and a group of only those dwarfs which would be contained in the initial stage of the survey — M dwarfs within 5.2 pc of the sun which are north of -25° . The new additions are listed by their Gliese numbers when available. The white dwarf/red dwarf binary GL 169.1AB has not been reinstated to the 5.2 pc list because the current determination of its parallax places it at 5.6 pc.

Since the pioneering work of van de Kamp, this sample has been reported on regularly for nearly five decades. To the current day, the total number of objects over the years has climbed steadily, at a rate of one every three years. While all of the earlier additions are due to more complete parallax or proper motion surveys, we make the two most recent additions (*) using the infrared speckle technique. Of the 17 new additions since 1945, 15 are faint red dwarfs and 2 are white dwarfs. Remarkably, the pace at which objects continue to be added to the solar neighborhood has yet to slow, as new techniques are used to detect fainter, closer companions.

3.10 Objects Worthy of Special Note

Here we discuss individual survey objects for which some indication of duplicity has been noted in the past, or for which we now present new evidence of duplicity. We rely primarily upon the astrometric review of Lippincott (LIP, 1978) and the comprehensive spectroscopic work of Marcy and Benitz (MB, 1989), as well as comments found in the Gliese (GL, 1969) Catalog of Nearby Stars. In addition, Scott Kenyon (1989) has kindly provided information on some M dwarfs being followed in a nearby M dwarf radial velocity survey. Through the combination of the

speckle, astrometric and radial velocity surveys, we believe that all stellar companions that orbit the program stars within several tens of AU have been discovered. All astrometric companions which remain undetected now have severe limits placed upon their infrared fluxes. These companions, if real, must be of extremely low mass.

GJ 1005: Astrometric companion found, see §3.4.

GL 15A: GL lists as a SB, range 26 km/s. We find no evidence for the companion to $M_K = 11.8$ at 1 AU. MB find no radial velocity variability in 11 observations over 2.7 years at a level of 0.22 km/sec. Pettersen and Griffin (1980) report an identical radial velocity and no evidence for variability to 0.3 km/sec over 4.1 years. We conclude that there is probably no companion.

GL 169.1A: Reported by Strand (1977) to be an astrometric binary of period 23 years. The photocentric orbit has semimajor axis $0.07''$, and is somewhat convincing. If the companion is dark and contributes negligible light to the system, its mass is ~ 20 Jupiters. The speckle limits, $M_K = 12.2$ to 13.2 cannot eliminate such a faint companion. MB did not examine this star.

GL 205: Inspection of the visibility curve (see Figure 3.24) indicates that this star may be resolved. Note the similarity between this data and that of GL 623AB taken at H (Figure 3.83). At a position angle of 25° , we tentatively detect a companion with $\Delta m_K = 5.2$, resulting in an $M_{KB} \sim 10.2$. MB report no variability at the 0.23 km/s level in 16 observations over 1.5 years. Continued infrared speckle observations are planned.

GL 268: GL lists as SB, range 110 km/s. Tomkin and Pettersen (1986) provide the orbit ($P = 10.4$ days) which actually has a range of 80 km/s. They argue that the inclination of the system is probably between 70° and 90° , indicating a maximum separation of 0.062–0.066 AU, or $0.01''$ at 6.0 pc. The M dwarf components are similar, with $M_1/M_2 \sim 1.2$, which would lead to deep fringes in the visibility curve. The 2D speckle datapoints do have a large envelope of values, possibly hinting at the companion, but full resolution would only be possible with a very large telescope.

GL 273: Suspicious 1D data from the original speckle survey led to the further observations of this star with the 2D camera. LIP reports a “slight trend” with an 8 to 10 period which is not of large amplitude. The latest speckle observations do not support a companion less than 5.3 mag fainter than the primary at K, from 1 to 10 AU. MB find no variability in 17 observations over 3.3 years at the 0.32 km/s.

GL 338AB: The 2D speckle data are suspicious (see Figures 3.36 and 3.37). The two nearly identical objects were observed as a pair, one being the point source for the other. The resulting visibility curves exhibit complicated structure, indicating that one or both may be resolved at large brightness ratios, and relatively large separations (several AU). Interestingly, Chang (1972) found in his orbital analysis of the system that 338B was overmassive, although no astrometric perturbation was found. The SB natures of both components reported by Abt and Levy (1973) have been found to be erroneous by Morbey and Griffin (1987). They find standard deviations in 31 radial velocity observations spanning 10.9 years

of 0.83 and 0.62 km/s for A and B, respectively. While the spectroscopic companions appear to be eliminated, further speckle observations of both components should be made.

GL 388: LIP reports that the very weak astrometric perturbation reported by Reuyl is not supported by more recent data. No companion was found to $M_K = 11.0$ from the speckle data. In 20 observations over 3.3 years, MB see no variability at the 0.20 km/s level.

GL 402: GL lists as a SB, range 34 km/s, and that a suspected astrometric companion has not been confirmed. MB made one inconclusive observation of the star, which was a difficult target for their survey. The speckle data do not indicate any companion less than four magnitudes fainter at K at a separation of 1 AU for the observation epoch. A search for radial velocity variability should be done to confirm or refute the spectroscopic companion.

GL 411: Once considered an astrometric binary, LIP has dismissed the earlier interpretation. Possible nebulosity reported by McCarthy (1986) was instrumental in origin. The speckle observations now indicate no companion brighter than 4.5 mag fainter than the primary at K, to $M_K = 10.8$. In 22 observations over 3.3 years, MB see no variability at the 0.19 km/s level.

GL 493.1: Another possible SB, range 54 km/s given by GL. This faint star could not be searched at 1 and 2 AU, and therefore no spectroscopic companion would be found. MB did not observe this star.

GL 514: GL mentions a possible small perturbation. We see no

companion to $\Delta m_K = 4.7$ at any separation.

GL 570B: Companion found, see §3.4.

GL 623: Astrometric companion found, see §3.4.

GL 628: GL lists as a SB, range 25 km/s. The speckle observations indicate no companion to $\Delta m_H = 3.1$ mag, although the data are not of high quality. MB did not examine this star. Kenyon sees no radial velocity variation in 11 observations at the 0.9 km/sec level over three years. This may not be a spectroscopic binary.

GL 643: Listed by GL as a SB with range 33 km/s. Wilson (1967) indicates that it shows "clear evidence of velocity variation." This is based upon two plates differing by 11.4 km/s, with a catalog velocity reported to be 25 km/s. This star should be observed to determine the spectroscopic orbit, thereby allowing a better description of the remarkable quintuple that includes GL 644ABC.

GL 644AB: Weis (1982) reports a possible third component, using data from multiple observatories. Unfortunately, the binary is a very close one, and does not lead to multiple fringes in the speckle-determined visibilities. Therefore, modulation of the fringes due to a third component is difficult to search for.

GL 644C: This is the star, VB 8, that is largely responsible for much of the brown dwarf research being done today. McCarthy *et al.* (1985) claimed to have detected a companion, VB 8B, $1.09''$ (7.0 AU) from the primary with $M_K = 12.7$ in early 1984. In observations made 1.8 years later, Perrier and Mariotti (1987), also using 1D infrared speckle

techniques, failed to confirm any companion to $M_K = 15.4$ at that separation. Furthermore, their data were inconsistent with the existence of a companion with $M_K = 12.7$ to any separation greater than 2.6 AU. The 2D results reported here indicate no companion to $M_K = 11.8, 13.6$ and 13.9 at 2, 5 and 10 AU. It appears that the astrometric companion, first reported by Harrington *et al.* (1983), is spurious. The false detection by infrared speckle is probably due to poor seeing calibration caused by a difference in airmass between VB 8 and its reference point source. The dip in visibility presumed to be due to the binary nature of the source occurred at the “seeing frequencies,” and was therefore probably caused by the airmass-induced differential seeing effect. Nonetheless, this object has spawned its own conference, countless published papers, and at least one graduate student’s motivation.

GL 687: This M dwarf is unresolved to $M_K \geq 10.0$ at all separations. LIP discusses a possible substellar companion, and GL lists it as a SB with velocity range 16 km/s, although the spectroscopic companion is believed to be unrelated to the astrometric one. The astrometric orbit is not convincing, with a semiamplitude of the photocenter displacement less than $0.02''$. The secondary mass is estimated to be 10 Jupiters for a Δm_v greater than 5, which must certainly be the case for such a large magnitude difference in the infrared. MB did not observe this star. Kenyon reports no velocity variations in three observations over three years at the 0.7 km/sec level. If the companion is real, it must be of very low mass below the limit of detectability for infrared speckle, astrometric, and radial velocity techniques.

GL 699 (Barnard's Star): The famous star shows no indication of companions to $M_K = 12.5$ from 1 to 5 AU, although planetary-sized objects of very low mass cannot be ruled out by the observations reported here. MB report no radial velocity variations at the 0.23 km/s level in 25 observations over 3.8 years. The most recent analysis of the possible solar system, consisting of two planets of roughly Jupiter mass, can be found in van de Kamp (1986).

GL 725B ($\Sigma 2398$): LIP mentions a possible slight trend in the B component of the wide pair. GL also lists it as a possible radial velocity variable. We see no evidence for companions to $M_K = 10.7$, 1 to 10 AU. MB did not follow either component. Kenyon reports no radial velocity variation in 30 observations over three years at the 0.5 km/sec level. There is probably no companion.

GL 752B: Otherwise known as VB 10, this star was reported by Harrington *et al.* (1983) in the same paper as VB 8 to have a possible astrometric companion. The astrometric data are completely unconvincing. We see no companion to $M_K = 12.1$, 5 to 10 AU. Unfortunately, low signal to noise prevented study at smaller separations.

GJ 1245A: Astrometric companion found, see §3.4.

GL 809: GL reports it to be a SB, no further details are given. MB did not observe this M dwarf. We see no companion to $M_K = 11.0$ in a very high quality dataset.

GL 831: Astrometric companion found, see §3.4.

GL 860AB: GL lists an astrometric companion found by Lippincott.

In 1978, she reported “no sustained evidence of triplicity.”

GL 866: No mention of possible binarity by GL or LIP. Companion has been found, see §3.4.

GL 873 (EV Lacertae): This famous flare star has a weak astrometric perturbation (van de Kamp and Worth, 1972) which seems to have flattened since 1970 (Lippincott 1983). The estimated orbital period is 45 years with a secondary mass 2 to 4 Jupiters, far below the detection limit of this survey. We see no companion to $M_K \geq 10.8$ in 2D speckle data, which supercede the earlier suspicious 1D data reported in 1990. The 2D data are not of very high quality. MB do not detect variations in 9 observations over 1.9 years at the 0.24 km/sec level. This star should remain on the infrared speckle program.

GL 880: The SB report by GL (range 33 km/s) is not supported by the MB observations: 14 observations of constant velocity over 3.0 years at the 0.21 km/s.

In summary, there are several nearby M dwarfs which warrant further examination by astrometric, spectroscopic or speckle techniques, preferably by all three. Continuing astrometric observations should target GL 169.1A, 338B and 873. A spectroscopic orbit should be found for GL 643, and confirmation or refutation should be achieved for the possible spectroscopic binaries GL 402 and 493.1. Finally, we will keep four objects on the infrared speckle program: GL 205, 338A, 338B and 873.

TABLE 3.1

PHOTOMETRY OF M DWARFS WITHIN 8 PARSECS

GL#	Other Name	RA (1950.0)	DEC (1950.0)	V	J	H	K	Refs.
T 1002	G 158-27	00 04 13	-07 47 30	13.74 0.02	8.33 0.03	7.74 0.03	7.42 0.03	GL,P1
T 1005A	LHS 1047A	00 12 53	-16 24 18	11.50J 0.02	7.28J 0.03	6.71J 0.03	6.42J 0.03	IRM,IRM
C 1005B	LHS 1047B	00 12 53	-16 24 18	decon	decon	decon	decon	
T 15A	BD +43 44A	00 15 31	+43 44 24	8.07 0.02	4.86 0.03	4.25 0.03	4.03 0.03	GL,P1
T 15B	BD +43 44B	00 15 31	+43 44 24	11.08 0.02	6.78 0.03	6.22 0.03	5.97 0.03	SH,P1
T 34B	η Cas B	00 46 03	+57 33 06	7.51 0.02	4.60 0.04	4.02 0.04	3.91 0.04	GL,*
T 54.1	LHS 138	01 09 59	-17 16 24	12.05 0.02	7.27 0.03	6.73 0.03	6.42 0.03	D,D
D 65A	L 726-8	01 36 25	-18 12 42	11.98J 0.02	6.31J 0.03	5.68J 0.03	5.34J 0.03	P1,P1
D 65B	UV Ceti	01 36 25	-18 12 42	decon	decon	decon	decon	
T 83.1	LHS 11	01 57 28	+12 50 06	12.27 0.02	7.52 0.03	6.96 0.03	6.67 0.03	GL,P1
T 105B	BD +6 398B	02 33 31	+06 38 00	11.66 0.02	7.41 0.03	6.83 0.03	6.60 0.03	SH,P1

TABLE 3.1 (continued)

GL#	Other Name	RA	DEC	V	J	H	K	Refs.
T 109	Ross 556	02 41 18	+25 19 00	10.57 0.02	6.77 0.07	6.24 0.03	5.97 0.03	SH,P1/*
T 166C	α^2 Eri C	04 13 04	-07 44 06	11.17 0.02	6.91 0.07	6.29 0.07	6.00 0.07	GL,*
T 169.1A	Stein 2051A	04 26 47	+58 53 54	11.08 0.02	6.70 0.07	6.01 0.07	5.71 0.07	SH,*
D 185A	BD -21 1051A	05 00 20	-21 19 24	8.29J 0.02	5.41J 0.04	4.79J 0.04	4.59J 0.03	P1,P1/*
D 185B	BD -21 1051B	05 00 20	-21 19 24	decon	decon	decon	decon	
T 205	BD -3 1123	05 28 55	-03 41 06	7.97 0.02	4.77 0.03	4.06 0.03	3.86 0.03	GL,P1
T 213	Ross 47	05 39 14	+12 29 18	11.52 0.04	7.16 0.03	6.60 0.03	6.37 0.03	SH,P1
T 229	BD -21 1377	06 08 28	-21 50 30	8.13 0.02	5.04 0.03	4.35 0.03	4.17 0.03	GL,P1
D 234A	Ross 614A	05 26 51	-02 46 12	11.08J 0.02	6.42J 0.03	5.78J 0.03	5.49J 0.03	SH,P1
D 234B	Ross 614B	05 26 51	-02 46 12	decon	decon	decon	decon	
T 251	Wolf 294	06 51 35	+33 20 18	10.00 0.02	6.12 0.03	5.52 0.03	5.27 0.03	SH,SH
T 1093	LHS 223	06 56 29	+19 25 48	14.83 0.02	9.25 0.05	8.61 0.03	8.26 0.03	GJ,P2

TABLE 3.1 (continued)

GL#	Other Name	RA	DEC	V	J	H	K	Refs.
T 268A	Ross 986A	07 06 39	+38 37 30	11.49 0.02	6.76 0.03	6.16 0.03	5.88 0.03	SH,SH
S 268B	Ross 986B	07 06 39	+38 37 30	decon	decon	decon	decon	
T 273	Luyten's Star	07 24 43	+05 22 42	9.87 0.02	5.67 0.03	5.15 0.03	4.90 0.03	SH,SH
T 283B	L 745-46B	07 38 02	-17 17 24	16.42 0.02	10.14 0.03	9.61 0.03	9.26 0.03	P1,P2
T 285	Ross 882	07 42 04	+03 40 48	11.18 0.02	6.60 0.03	6.02 0.03	5.75 0.03	SH,SH
T 299	Ross 619	08 09 11	+08 59 42	12.83 0.02	8.42 0.03	7.90 0.03	7.67 0.03	P1,P1
T 300	L 674-15	08 10 29	-21 23 30	12.07 0.02	7.43 0.19	6.90 0.03	6.64 0.03	SH,P1/*
T 1111	G 51-15	08 26 53	+26 57 12	14.81 0.02	8.24 0.03	7.62 0.03	7.26 0.03	GJ,P1
D 1116A	G 9-38A	08 55 27	+19 57 24	13.65J 0.02	7.73J 0.04	7.19J 0.04	6.86J 0.04	P1,*
D 1116B	G 9-38B	08 55 27	+19 57 24	decon	decon	decon	decon	
T 338A	BD +53 1320	09 10 59	+52 54 06	7.62 0.02	4.88 0.03	4.27 0.06	4.06 0.05	GL,*
T 338B	BD +53 1321	09 11 01	+52 54 12	7.72 0.02	4.95 0.03	4.33 0.10	4.14 0.05	GL,*

TABLE 3.1 (continued)

GL#	Other Name	RA	DEC	V	J	H	K	Refs.
T 388	BD +20 2465	10 16 54	+20 07 18	9.37 0.02	5.42 0.03	4.82 0.03	4.60 0.03	SH,P1
T 393	BD +1 2447	10 26 23	+01 06 24	9.64 0.02	6.18 0.03	5.58 0.03	5.33 0.03	SH,P1
T	LHS 292	10 45 41	-11 03 06	15.60 0.02	8.90 0.03	8.32 0.03	7.96 0.03	D,D
T 402	Wolf 358	10 48 19	+07 05 06	11.65 0.02	7.29 0.03	6.69 0.03	6.42 0.03	SH,SH
T 406	Wolf 359	10 54 06	+07 19 12	13.46 0.02	7.09 0.03	6.45 0.03	6.08 0.03	SH,SH
T 408	Ross 104	10 57 25	+23 06 18	10.02 0.02	6.37 0.03	5.78 0.03	5.54 0.03	SH,SH
T 411	Lalande 21185	11 00 37	+36 18 18	7.50 0.02	4.10 0.03	3.56 0.03	3.35 0.03	GL,SH
T 412A	BD +44 2051	11 03 00	+43 47 00	8.77 0.02	5.54 0.03	4.97 0.03	4.76 0.03	GL,SH
T 412B	WX UMa	11 03 02	+43 46 42	14.36 0.02	8.70 0.03	8.14 0.03	7.85 0.03	SH,P1
T 445	AC +79 3888	11 44 35	+78 57 42	10.82 0.02	6.69 0.03	6.18 0.03	5.93 0.03	SH,SH
T 447	Ross 128	11 45 09	+01 06 00	11.14 0.02	6.52 0.03	5.95 0.03	5.66 0.03	SH,SH
T 450	BD +36 2219	11 48 33	+35 32 48	9.72 0.02	6.45 0.03	5.85 0.03	5.64 0.03	SH,SH

TABLE 3.1 (continued)

GL#	Other Name	RA	DEC	V	J	H	K	Refs.
T 1156	LHS 324	12 16 32	+11 24 00	13.79 0.02	8.39 0.04	7.87 0.04	7.56 0.04	GJ,*
D 473A	Wolf 424A	12 30 51	+09 17 36	12.47J 0.03	6.97J 0.03	6.40J 0.03	6.07J 0.03	SH,SH
D 473B	Wolf 424B	12 30 51	+09 17 36	decon	decon	decon	decon	
T 493.1	Wolf 461	12 58 05	+05 57 06	13.34 0.02	8.55 0.04	7.99 0.04	7.70 0.04	GL,*
T 514	BD +11 2576	13 27 27	+10 39 00	9.06 0.02	5.87 0.03	5.26 0.03	5.06 0.03	SH,SH
T 526	BD +15 2620	13 43 12	+15 09 42	8.48 0.02	5.24 0.03	4.66 0.03	4.46 0.03	P1,SH
T 555	BD -11 3759	14 31 35	-12 18 36	11.31 0.02	6.86 0.03	6.24 0.03	5.97 0.03	SH,SH
T 570B	BD -20 4123A	14 54 31	-21 11 18	7.95J 0.02	4.78J 0.03	4.14J 0.03	3.90J 0.03	P1,P1
C 570C	BD -20 4123B	14 54 31	-21 11 18	decon	decon	decon	decon	
T 581	BD -7 4003	15 16 50	-07 32 24	10.55 0.02	6.70 0.03	6.10 0.03	5.85 0.03	SH,SH
T 623A	L 1707-1A	16 22 39	+48 28 24	10.26J 0.02	6.66J 0.03	6.14J 0.03	5.91J 0.03	SH,SH
C 623B	L 1707-1B	16 22 39	+48 28 24	decon	decon	decon	decon	

TABLE 3.1 (continued)

GL#	Other Name	RA	DEC	V	J	H	K	Refs.
T 625	G 202-48	16 24 14	+54 25 06	10.10 0.02	6.63 0.03	6.06 0.03	5.84 0.03	SH,SH
T 628	BD -12 4253	16 27 31	-12 32 18	10.11 0.02	5.96 0.03	5.37 0.03	5.10 0.03	P1,P1
T 643A	Wolf 629A	16 52 45	-08 13 54	11.75J 0.02	7.57J 0.03	7.01J 0.03	6.74J 0.03	SH,SH
S 643B	Wolf 629B	16 52 45	-08 13 54	decon	decon	decon	decon	
D 644A	Wolf 630A	16 52 48	-08 14 42	9.00J 0.02	5.27J 0.03	4.63J 0.03	4.39J 0.03	P1,SH
D 644B	Wolf 630B	16 52 48	-08 14 42	decon	decon	decon	decon	
T 644C	VB 8	16 52 55	-08 18 12	16.66 0.02	9.77 0.03	9.18 0.03	8.80 0.03	GL,SH
D 661A	BD +45 2505A	17 10 40	+45 44 48	9.40J 0.02	5.57J 0.03	5.05J 0.03	4.82J 0.03	P1,SH
D 661B	BD +45 2505B	17 10 40	+45 44 48	decon	decon	decon	decon	
T 687	BD +68 946	17 36 42	+68 23 06	9.15 0.02	5.32 0.03	4.74 0.03	4.52 0.03	GL,SH
T 699	Barnard's Star	17 55 23	+04 33 18	9.54 0.02	5.33 0.03	4.82 0.03	4.56 0.03	GL,SH
T 701	BD -3 4233	18 02 28	-03 01 54	9.40 0.02	6.15 0.03	5.55 0.03	5.34 0.03	P1,SH

TABLE 3.1 (continued)

GL#	Other Name	RA	DEC	V	J	H	K	Refs.
T 1224	LHS 3359	18 04 42	−15 58 00	13.64 0.02	8.89 0.09	8.46 0.08	8.04 0.06	GL,*
T 1230A	LHS 3405	18 39 04	+24 44 12	12.21J 0.02	7.64 0.04	7.01 0.04	6.73 0.04	GL,*
D 1230B	LHS 3404	18 39 04	+24 44 18	decon	9.56 0.04	8.88 0.04	8.61 0.04	—,*
T 725A	BD +59 1915A	18 42 12	+59 33 18	8.90 0.02	5.20 0.03	4.67 0.03	4.44 0.03	GL,SH
T 725B	BD +59 1915B	18 42 13	+59 33 00	9.69 0.02	5.72 0.03	5.20 0.03	4.97 0.03	GL,SH
T 729	Ross 154	18 46 45	−23 53 30	10.95 0.02	6.20 0.03	5.63 0.03	5.34 0.03	P1,P1
T 752A	BD +4 4048	19 14 29	+05 05 48	9.12 0.02	5.50 0.03	4.88 0.03	4.66 0.03	GL,SH
T 752B	VB 10	19 14 32	+05 04 42	17.48 0.02	9.92 0.03	9.24 0.03	8.81 0.03	P1,SH
T 1245A	G 208-44A	19 52 16	+44 17 30	13.50J 0.03	7.78J 0.03	7.26J 0.03	6.89J 0.03	M+,M+
C 1245C	G 208-44B	19 52 16	+44 17 30	decon	decon	decon	decon	
T 1245B	G 208-45	19 52 17	+44 17 30	14.31 0.04	8.33 0.03	7.83 0.03	7.44 0.03	M+,M+
T 809	BD +61 2068	20 52 18	+61 58 30	8.52 0.02	5.52 0.03	4.81 0.03	4.64 0.03	P1,P1

TABLE 3.1 (continued)

GL#	Other Name	RA	DEC	V	J	H	K	Refs.
T 829	Ross 775	21 27 12	+17 25 06	10.31 0.02	6.30 0.03	5.72 0.03	5.48 0.03	SH,SH
T 831A	Wolf 922A	21 28 34	-10 00 36	12.03J 0.05	7.32J 0.04	6.74J 0.06	6.50J 0.03	SH,*
C 831B	Wolf 922B	21 28 34	-10 00 36	decon	decon	decon	decon	
D 860A	Kruger 60A	22 26 13	+57 26 48	9.59J 0.02	5.54J 0.03	4.96J 0.03	4.71J 0.03	P1,SH
D 860B	Kruger 60B	22 26 13	+57 26 48	decon	decon	decon	decon	
T 866A	L 789-6A	22 35 45	-15 35 30	12.25J 0.02	6.51J 0.03	5.88J 0.03	5.54J 0.03	P1,P1
C 866B	L 789-6B	22 35 45	-15 35 30	decon	decon	decon	decon	
T 873	EV Lacertae	22 44 40	+44 04 36	10.26 0.02	6.14 0.03	5.55 0.03	5.31 0.03	SH,SH
T 876	BD -15 6290	22 50 35	-14 31 12	10.13 0.02	5.93 0.03	5.31 0.03	5.04 0.03	P1,P1
T 880	BD +15 4733	22 54 10	+16 17 24	8.68 0.02	5.40 0.03	4.75 0.03	4.56 0.03	GL,P1
T 884	BD -23 17699	22 57 38	-22 47 36	7.89 0.02	5.26 0.03	4.60 0.03	4.45 0.03	GL,P1

TABLE 3.1 (continued)

GL#	Other Name	RA	DEC	V	J	H	K	Refs.
T 896A	BD +19 5116A	23 29 20	+19 39 42	10.23J 0.02	5.96J 0.03	5.35J 0.03	5.09J 0.03	P1,P1
T 896B	BD +19 5116B	23 29 20	+19 39 42	decon	decon	decon	decon	
T 1286	LHS 546	23 32 34	-02 39 18	14.68 0.02	9.20 0.04	8.59 0.04	8.31 0.04	GJ,*
T 905	Ross 248	23 39 26	+43 55 12	12.30 0.02	6.91 0.03	6.26 0.03	5.94 0.03	SH,P1
T 908	BD +1 4774	23 46 36	+02 08 12	8.98 0.02	5.82 0.03	5.25 0.03	5.05 0.03	GL,P1

REFERENCES:

D = Dahn (1988) via J. Liebert,

GJ = Gliese and Jahreiss (1979),

GL = Gliese (1969),

IRM = Ianna *et al.* 1987,M+ = McCarthy *et al.* 1988,

P1 = Probst (1981) Table A.7 — averaged values of many studies,

P2 = Probst (1981) Table A.2 — individual observations,

SH = Stauffer and Hartmann (1986),

* = this work

NOTE: deconvolution required for all doubles with separations less than 7 arcseconds

TABLE 3.2

INFRARED SPECKLE OBSERVATIONS OF M DWARF SURVEY BINARIES

Object(s)	λ	Tech	Date	Separation	PA	$\Delta m \pm \sigma$
GJ 1005AB	J*	2D 2X	28 Nov 90	0.203 0.009	053 02	1.53 0.07
	H*	1D EW	07 Sep 87	0.73 0.07	W	1.93 0.03
	K	1D NS	11 Oct 84	0.32 0.03	————	1.49 0.09
	K	1D EW	12 Nov 84	0.24 0.02	————	1.18 0.07
	K	1D EW	15-18 Jun 86	0.14 0.01	————	1.56 0.12
	K	adopted				1.34 0.05
GL 15AB			searched	separately		
GL 65AB	J	1D EW	09 Nov 87	0.63 0.06	E	0.62 0.07
	J*	2D 1X	29 Nov 90	2.135 0.082	005 02	0.33 0.03
	J	adopted				0.38 0.03
	H*	1D NS	08 Nov 87	2.11 0.21	N	0.30 0.02
	K*	1D EW	07 Feb 88	0.70 0.07	E	0.40 0.07
GL 185AB	J*	2D 2X	12 Feb 90	1.044 0.040	040 02	1.35 0.03
	H*	2D 2X	10 Oct 89	1.070 0.041	040 02	1.26 0.02
	K*	2D 2X	10 Oct 89	1.071 0.041	041 02	1.07 0.02
GL 234AB	J*	1D EW	07 Feb 88	0.98 0.10	E	1.79 0.03
	J	1D EW	19 Feb 89	0.81 0.08	E	1.49 0.05
	J	adopted				1.71 0.03
	H*	1D NS	30 Oct 85	1.04 0.10	————	1.64 0.05
	H	1D NS	08 Nov 87	1.12 0.11	N	1.70 0.06
	H	adopted				1.66 0.04
	K*	1D NS	30 Oct 85	1.04 0.10	————	1.51 0.05
	K	1D NS	14 Dec 86	1.04 0.10	N	1.53 0.04
	K	1D EW	14 Dec 86	0.40 0.04	E	1.50 0.04
	K	adopted				1.51 0.03
GL 268AB			searched	as single		

TABLE 3.2 (continued)

Object(s)	λ	Tech	Date	Separation	PA	$\Delta m \pm \sigma$
GJ 1116AB	J	1D NS	08 Feb 88	2.44 0.24	N	0.32 0.02
	J*	2D 1X	29 Nov 90	1.879 0.072	047 02	0.53 0.02
	J	adopted				0.43 0.01
	H	1D NS	08 Feb 88	2.50 0.25	N	0.59 0.04
	H*	2D 1X	29 Nov 90	1.875 0.072	047 02	0.48 0.02
	H	adopted				0.50 0.02
	K	1D NS	08 Feb 88	2.50 0.25	N	0.37 0.02
	K*	2D 1X	29 Nov 90	1.879 0.072	047 02	0.42 0.04
	K	adopted				0.38 0.02
GL 338AB			searched	separately		
	J	2D ph	09 Nov 90	————	————	0.07 0.04
	H	2D ph	09 Nov 90	————	————	0.06 0.12
	K	2D ph	09 Nov 90	————	————	0.08 0.07
GL 412AB			searched	separately		
GL 473AB	J	1D NS	03 May 88	————	————	0.13 0.04
	J	2D 2X	11 May 90	0.177 0.010	226 02	————
	J	adopted				0.13 0.04
	H	1D NS	21 Mar 89	0.184 0.018	————	0.33 0.06
	H	2D 2X	27 Apr 91	0.343 0.014	164 02	0.11 0.07
	H	2D 2X	28 Apr 91	0.374 0.015	164 02	0.16 0.07
	H	adopted				0.21 0.04
	K	1D NS	26 Jun 83	0.818 0.082	————	0.20 0.04
	K	1D NS	10 May 84	0.902 0.090	————	0.39 0.04
	K	1D NS	21 Mar 89	0.196 0.020	————	0.26 0.09
	K	2D 2X	07 Mar 91	0.179 0.007	248 02	0.76 0.12
	K	2D 2X	08 Mar 91	0.177 0.020	246 02	0.66 0.11
	K	adopted				0.33 0.03

TABLE 3.2 (continued)

Object(s)	λ	Tech	Date	Separation	PA	$\Delta m \pm \sigma$
GL 570BC	J	1D NS†	Jun 87	not given	not given	1.31 0.17
	J	1D NESW†	Jun 88	not given	not given	1.23 0.18
	J*	2D 2X	11 Feb 90	0.153 0.006	220 02	1.30 0.04
	J	adopted				1.30 0.04
	H	1D NS†	Jun 87	not given	not given	1.19 0.12
	K	1D NS†	Jun 87	0.090 0.010	S	1.19 0.12
	K	1D NESW†	Jun 88	0.173 0.010	SW	1.09 0.08
	K	adopted				1.12 0.07
GL 623AB	J	1D NS	14 Mar 87	————	————	3.28 0.3
	H	1D NS	14 Mar 87	0.26 0.03	————	3.00 0.3
	H*	2D 2X	27 Apr 91	0.190 0.008	338 02	2.65 0.03
	H	adopted				2.65 0.03
	K	1D NS	07 May 82	0.28 0.03	————	3.04 0.32
	K	1D NESW	20 Apr 86	0.39 0.04	NE	2.85 0.26
	K	1D NESW	18 Jun 86	0.33 0.03	NE	2.81 0.23
	K	1D NS	10 Jan 87	0.35 0.04	N	2.85 0.31
	K	adopted				2.87 0.14
GL 643AB			searched	as single		
GL 644AB	J*	2D 2X	09 May 90	0.198 0.008	121 02	0.51 0.01
	H*	1D NS	22 Mar 89	0.17 0.02	N	0.56 0.02
	K*	1D NS	10 May 84	0.25 0.03	————	0.66 0.06
GL 661AB	J*	1D NS	20 Mar 89	0.68 0.07	S	0.41 0.01
	H*	1D NS	20 Mar 89	0.70 0.07	S	0.46 0.02
	K*	1D NS	20 Mar 89	0.70 0.07	S	0.42 0.07

TABLE 3.2 (continued)

Object(s)	λ	Tech	Date	Separation	PA	$\Delta m \pm \sigma$
GL 1230AB			searched	separately		
	J	2D ph	11 May 90	————	————	1.92 0.06
	H	2D ph	11 May 90	————	————	1.87 0.06
	K	2D ph	11 May 90	————	————	1.88 0.06
GL 725AB			searched	separately		
GL 752AB			searched	separately		
GL 1245AB			searched	separately		
GJ 1245AC	J	1D EW	08 Jun 87	0.89 0.09	E	1.22 0.04
	J	1D EW	06 Sep 87	0.86 0.09	E	1.34 0.04
	J	1D EW	06 Oct 87	1.00 0.10	E	1.12 0.07
	J	adopted				1.26 0.03
	H	1D EW	18 Sep 86	0.81 0.08	E	1.15 0.04
	H	1D EW	08 Jun 87	0.90 0.09	E	1.07 0.02
	H	1D EW	06 Oct 87	1.00 0.00	E	1.04 0.07
	H	adopted				1.08 0.02
	K	1D NS	09 Nov 84	0.39 0.04	————	1.19 0.09
	K	1D EW	08 Jun 87	0.90 0.09	E	1.02 0.02
	K	adopted				1.03 0.02
GL 831AB	J*	2D 2X	08 Nov 90	————	218 03	1.88 0.5
	H*	2D 2X	29 Nov 90	0.195 0.005	227 03	1.51 0.07
	K*	1D NS	29 Oct 82	0.25 0.03	————	1.68 0.07
	K	2D 2X	30 Nov 90	————	227 03	1.19 0.15
	K	adopted				1.59 0.06
GL 860AB	J*	1D NS	07 Jul 88	2.45 0.25	S	1.19 0.10
	H*	1D NS	07 Jul 88	2.46 0.25	S	1.14 0.05
	K*	1D NS	07 Jul 88	2.41 0.24	S	1.37 0.08

TABLE 3.2 (continued)

Object(s)	λ	Tech	Date	Separation	PA	$\Delta m \pm \sigma$
GL 866AB	J	adopted		Leinert		0.56 0.04
	H	adopted		<i>et al.</i>		0.56 0.03
	K	adopted		(1990)		0.56 0.03
GL 896AB			searched	separately		
	J	2D ph	08 Nov 90	_____	_____	1.18 0.10
	H	2D ph	08 Nov 90	_____	_____	0.94 0.15
	K	2D ph	08 Nov 90	_____	_____	1.11 0.14

* = visibility curve plotted in figures

† = measurement by another group

ph = determined by photometric, rather than speckle techniques

TABLE 3.3
COMPANION MAGNITUDE LIMITS FOR M DWARFS

GL#	Tech.	UT Date	λ	1 AU	2 AU	5 AU	10 AU
1002	1D NS	29 Sep 88	H	—	12.3	12.3	12.3
	1D EW	22 Nov 85	K	13.2	13.6	14.0	15.0
		adopted	K	—	11.5	11.5	11.5
1005		companion		found			
15A	1D NS	07 Sep 87	H	12.8	12.8	12.8	12.8
	1D EW	06 Sep 87	H	12.8	12.8	12.8	12.8
		adopted	K	11.9	11.9	11.9	11.9
15B	1D NS	07 Sep 87	H	12.7	13.8	14.2	14.6
	1D EW	06 Sep 87	H	13.4	13.7	14.8	14.8
		adopted	K	11.8	12.6	13.0	13.3
34B	2D 2X	13 Oct 89	K	9.5	10.7	10.7	11.0
54.1	1D NS	07 Oct 87	H	11.3	14.9	15.1	15.1
	1D EW	17 Sep 86	K	12.5	13.2	14.3	14.8
		adopted	K	10.7	13.2	13.6	13.6
83.1	1D NS	13 Dec 86	K	11.1	14.7	14.7	14.7
	1D EW	13 Dec 86	K	11.6	14.4	14.7	14.7
		adopted	K	11.1	14.4	14.7	14.7
105B	2D 2X	11 Oct 89	K	12.2	12.5	12.7	12.7
109	2D 2X	09 Dec 89	K	10.7	11.6	11.9	12.8
166C	1D NS	06 Oct 87	H	—	13.4	14.1	14.1
	1D EW*	06 Sep 87	H	14.1	14.1	14.1	14.1
		adopted	K	—	12.4	12.9	12.9
169.1A	2D 2X	11 Dec 89	K	12.2	12.3	13.2	13.2
205	2D 2X	12 Oct 89	K	9.0	9.2	10.8	11.3
213	2D 2X	11 Feb 90	H	12.1	12.2	12.5	13.0
		adopted	K	11.4	11.4	11.7	12.0
229	2D 2X	13 Oct 89	K	11.2	11.3	11.5	11.6
251	2D 2X	11 Dec 89	K	10.4	10.4	10.6	11.2
1093	2D 1X	28 Nov 90	H	—	—	13.8	14.5
		adopted	K	—	—	12.7	13.2
268	2D 2X	09 Dec 89	K	10.7	11.0	11.4	12.8
273	2D 2X	01 Dec 90	K	12.3	13.3	13.3	13.3
283B	2D 1X	30 Nov 90	H	—	—	13.8	14.2
		adopted	K	—	—	12.7	13.0
285	1D NS	22 Jan 89	K	10.6	13.1	13.1	13.1
	1D EW	18 Feb 89	K	9.9	11.6	13.1	13.1
		adopted	K	9.9	11.6	13.1	13.1

TABLE 3.3 (continued)

GL#	Tech.	UT Date	λ	1 AU	2 AU	5 AU	10 AU
299	2D 1X	12 Feb 90	H	—	13.4	14.1	14.1
		adopted	K	—	12.4	12.9	12.9
300	2D 1X	11 Feb 90	H	—	11.5	12.0	12.9
		adopted	K	—	10.9	11.3	12.0
1111	1D NS	02 May 88	H	12.0	12.0	12.0	16.1
	1D EW	29 Dec 85	K	12.7	15.2	15.2	15.2
		adopted	K	11.3	11.3	11.3	14.4
338A	2D 2X	09 Dec 89	K	9.3	9.3	9.6	10.1
338B	2D 2X	09 Dec 89	K	10.4	10.4	11.0	11.4
388	1D NS	03 May 88	K	11.0	11.0	12.4	12.4
	1D EW*	05 May 88	K	12.4	12.4	12.4	12.4
		adopted	K	11.0	11.0	12.4	12.4
393	2D 2X	28 Nov 90	K	9.9	10.3	11.2	12.2
	and	01 Dec 90					
L292	1D NS	03 May 88	H	—	13.2	13.3	13.7
	1D EW	06 Feb 88	H	—	11.8	16.3	16.3
		adopted	K	—	11.1	12.3	12.6
402	2D 2X	25 Apr 91	K	11.3	11.7	11.8	12.9
406	1D NS	17 Mar 84	K	13.4	14.2	14.2	—
	1D EW	12 Feb 84	K	12.4	12.4	13.4	—
		adopted	K	12.4	12.4	13.4	—
408	2D 2X	11 Feb 90	K	10.2	10.7	11.1	12.1
411	1D NS	08 Apr 87	K	11.4	12.6	12.6	12.6
	1D EW	04 May 88	K	10.8	10.8	11.5	12.6
		adopted	K	10.8	10.8	11.5	12.6
412A	2D 2X	10 Dec 89	K	11.2	12.1	12.4	12.4
412B	2D 1X	26 Apr 91	H	—	14.5	14.5	15.2
		adopted	K	—	13.2	13.2	13.7
445	1D NS	07 Feb 88	H	10.3	11.1	11.3	13.6
	1D EW	06 Feb 88	H	9.6	11.6	11.9	12.9
		adopted	K	9.4	10.6	10.7	12.0
447	1D NS	07 Feb 88	H	12.0	12.9	14.6	14.6
	1D EW	06 Feb 88	H	12.5	13.0	13.7	14.6
		adopted	K	11.3	12.0	12.6	13.3
450	2D 2X	12 Feb 90	K	10.0	10.0	10.4	11.3

TABLE 3.3 (continued)

GL#	Tech.	UT Date	λ	1 AU	2 AU	5 AU	10 AU
1156	2D 1X	12 May 90	H	—	13.7	14.1	14.3
		adopted	K	—	12.6	12.9	13.0
493.1	2D 1X	25 Apr 91	H	—	—	12.6	13.6
		adopted	K	—	—	11.5	12.5
514	2D 2X	09 May 90	K	10.3	10.4	10.5	11.4
526	1D NS	07 Jun 87	H	9.1	11.8	11.9	11.9
	1D EW	08 Jun 87	H	10.8	10.8	10.9	11.5
		adopted	K	8.9	10.4	10.4	10.9
555	2D 2X	12 May 90	H	12.1	12.1	12.9	13.5
		adopted	K	11.4	11.4	12.0	12.4
570B		companion		found			
581	2D 2X	09 May 90	K	11.6	11.6	11.6	12.9
623		companion		found			
625	1D NS	21 Mar 89	K	9.6	10.9	11.6	12.8
	1D EW	20 Feb 89	K	9.9	10.7	13.1	13.1
		adopted	K	9.6	10.7	11.6	12.8
628	1D NS	07 Jun 87	H	13.3	13.6	13.6	13.6
	1D EW	06 Feb 88	H	10.4	10.4	10.4	11.2
		adopted	K	10.0	10.0	10.0	10.7
643	1D NS	22 Mar 89	H	12.0	12.2	14.2	14.2
	1D EW	22 Jun 89	H	11.7	14.2	14.2	14.2
		adopted	K	11.0	11.4	13.0	13.0
644C	2D 1X	25 Apr 91	H	—	12.7	15.1	15.5
		adopted	K	—	11.8	13.6	13.9
687	1D NS	02 May 88	H	10.3	11.1	11.5	12.6
	1D EW	03 May 88	K	10.3	10.4	12.4	12.4
		adopted	K	10.0	10.4	10.9	11.7
699	1D NS	16 Apr 84	K	13.8	14.5	14.5	—
	1D EW	30 Apr 83	K	12.5	12.7	13.7	—
		adopted	K	12.5	12.7	13.7	—
701	2D 2X	12 May 90	K	10.8	10.8	11.3	12.3
1224	2D 1X*	27 Apr 91	H	—	—	14.5	14.5
		adopted	K	—	—	13.2	13.2
1230A	2D 2X	26 Apr 91	K	11.1	12.2	12.3	13.4

TABLE 3.3 (continued)

GL#	Tech.	UT Date	λ	1 AU	2 AU	5 AU	10 AU
725A	1D NS	07 Oct 87	H	11.3	11.9	13.2	13.2
	1D EW	04 May 88	K	11.0	11.1	12.0	12.9
		adopted	K	10.7	11.1	12.0	12.2
725B	1D NS	07 Oct 87	H	11.2	11.9	13.7	13.7
	1D EW	02 May 88	K	11.0	13.3	13.3	13.5
		adopted	K	10.7	11.2	12.6	12.6
729	1D NS	01 May 88	H	12.4	12.4	13.2	14.6
	1D EW*	09 Jun 87	H	13.1	14.6	14.6	14.6
		adopted	K	11.6	11.6	12.2	13.3
752A	2D 2X	04 Jul 90	K	11.8	12.1	12.1	12.1
752B	2D 1X	28 Apr 91	H	—	—	13.1	13.1
		adopted	K	—	—	12.1	12.1
1245A		companion		found			
1245B	1D NS	09 Nov 84	K	13.3	13.7	13.7	14.1
	1D EW	07 Oct 87	H	13.5	14.1	14.5	14.5
		adopted	K	12.4	12.9	13.2	13.2
809	2D 2X	12 Oct 89	K	11.0	11.5	11.5	11.5
829	2D 2X	13 Oct 89	K	10.7	11.9	12.1	12.5
831		companion		found			
866		companion		found			
873	2D 2X	30 Nov 90	K	10.8	11.0	11.9	12.6
876	1D NS	07 Oct 87	H	—	11.4	13.2	13.2
	1D EW	30 Sep 88	H	—	11.3	11.8	11.9
		adopted	K	—	10.7	11.1	11.2
880	2D 2X	11 Dec 89	K	9.8	10.4	10.4	11.3
884	2D 2X	10 Dec 89	K	8.8	9.0	10.0	11.3
896A	2D 2X	12 Oct 89	K	11.1	11.1	11.1	12.3
896B	2D 2X	09 Nov 90	K	12.1	12.1	12.5	12.5
1286	2D 1X	09 Nov 90	H	—	—	13.5	14.1
		adopted	K	—	—	12.4	12.9
905	1D NS*	29 Sep 88	K	12.6	14.7	14.7	14.7
	1D EW	06 Oct 87	H	12.9	14.6	14.6	15.0
		adopted	K	12.0	13.3	13.3	13.6
908	2D 2X	11 Oct 89	K	10.7	10.7	11.1	12.1

* = point source possibly resolved, or poor seeing calibration

TABLE 3.4
CHARACTERISTIC SURVEY LIMITS

Sep.	# Stars	M _K Limit
1 AU	53	10.85 ± 0.96
2 AU	62	11.43 ± 1.06
5 AU	68	11.96 ± 1.06
10 AU	66	12.44 ± 0.90

TABLE 3.5
M DWARF SECONDARIES WITHIN 8 PARSECS

GL#	a (AU)	P (yr)	Primary	Reference
1005B	1.7	4.6	dM	Ianna <i>et al.</i> 1988
15B	140	2600	dM	Lippincott 1972
34B	70	480	dG	Gliese 1969
65B	5.2	26.5	dM	Geyer <i>et al.</i> 1988
105B	1200*	> 1000	dK	Gliese 1969
166C	33	248	WD	Gliese 1969
169.1A	38	350	WD	Gliese 1969
185B	10.9	42.7	dM	Heintz 1978
234B	3.8	16.6	dM	Probst 1977
268B	< 1	10.4 d	dM	Tomkin and Pettersen 1986
283B	170*	> 1000	WD	Gliese 1969
1116B	23*	250	dM	Gliese and Jahreiss
338B	103	975	dM	Chang 1972
412B	150*	> 1000	dM	Gliese 1969
473B	3.1	16.2	dM	Heintz 1989
570B	120*	> 1000	dK	Gliese 1969
570C	0.8	0.85	dM	Mariotti <i>et al.</i> 1990
623B	2.1	3.7	dM	McCarthy and Henry 1987
643A	470*	> 1000	dM	Gliese 1969
643B	< 1	< 1	dM	Wilson 1967
644B	1.4	1.7	dM	Heintz 1984
644C	1400*	> 1000	dM	Gliese 1969
661B	4.5	13.0	dM	Heintz and Borgman 1984
1230B	46*	100-1000	dM	Gliese 1969
725B	49	408	dM	Heintz 1987
752B	430*	> 1000	dM	Gliese 1969
1245B	37*	100-1000	dM	Gliese and Jahreiss 1969
1245C	3.6	15.2	dM	McCarthy <i>et al.</i> 1988
831B	~ 1.1	1.9	dM	Lippincott 1979, this work
860B	9.4	44.7	dM	Heintz 1986
866B	1.2	2.2	dM	Leinert <i>et al.</i> 1990
896B	44	360	dM	Heintz 1984

* = current separation, no orbit

TABLE 3.6
DISTRIBUTION OF M DWARF SECONDARIES

Bin	# with a (AU)	# with P (yr)
0 - 1	3	3
1 - 10	11	5
10 - 100	9	7
100 - 1000	7	9
1000 +	2	8

TABLE 3.7

PARALLAXES, ABSOLUTE MAGNITUDES AND SPECTRAL TYPES
FOR ALL SURVEY OBJECTS

GL#	$\pi \pm \sigma$	Ref.	M _V	M _J	M _H	M _K	Spec.
1002	0.214 007	GJ	15.39 0.07	9.98 0.08	9.39 0.08	9.07 0.08	—
1005A	0.189 005	IRM	12.95 0.07	8.90 0.07	8.26 0.07	8.08 0.07	M 4.0c
1005B	0.189 005	IRM	15.87 0.50	10.43 0.09	10.19 0.07	9.42 0.08	—
15A	0.290 006	GJ	10.38 0.05	7.17 0.05	6.56 0.05	6.34 0.05	—
15B	0.290 006	GJ	13.39 0.05	9.09 0.05	8.53 0.05	8.28 0.05	—
34B	0.171 004	GJ	8.68 0.05	5.77 0.06	5.19 0.06	5.08 0.06	—
54.1	0.261 012	GJ	14.13 0.10	9.35 0.10	8.81 0.10	8.50 0.10	—
65A	0.375 006	GHW	15.32 0.06	9.76 0.05	9.16 0.05	8.78 0.06	M 5.5
65B	0.375 006	GHW	15.98 0.09	10.14 0.05	9.46 0.05	9.18 0.07	M 6.0
83.1	0.224 004	GJ	14.02 0.04	9.27 0.05	8.71 0.05	8.42 0.05	M 4.5
105B	0.137 007	GJ	12.34 0.11	8.09 0.11	7.51 0.11	7.28 0.11	—
109	0.129 006	GJ	11.12 0.10	7.32 0.12	6.79 0.11	6.52 0.11	—
166C	0.207 003	GJ	12.75 0.04	8.49 0.08	7.87 0.08	7.58 0.08	M 4.5
169.1A	0.180 004	GJ	12.36 0.05	7.98 0.09	7.29 0.09	6.99 0.09	M 4.0
185A	0.129 009	GJ	8.97 0.16	6.24 0.16	5.64 0.16	5.49 0.16	—
185B	0.129 009	GJ	11.21 0.24	7.59 0.16	6.90 0.16	6.56 0.16	—
205	0.170 006	GJ	9.12 0.08	5.92 0.08	5.21 0.08	5.01 0.08	M 1.5

TABLE 3.7 (continued)

GL#	$\pi \pm \sigma$	Ref.	M _V	M _J	M _H	M _K	Spec.
213	0.166 004	GJ	12.62	8.26	7.70	7.47	M 4.0
			0.07	0.06	0.06	0.06	
229	0.173 009	GJ	9.32	6.23	5.54	5.36	M 1.0
			0.11	0.12	0.12	0.12	
234A	0.243 002	P	13.08	8.55	7.92	7.66	M 4.5c
			0.03	0.04	0.04	0.04	
234B	0.243 002	P	16.05	10.26	9.58	9.17	—
			0.11	0.05	0.05	0.05	
251	0.168 006	G	11.13	7.25	6.65	6.40	M 3.0
			0.08	0.08	0.08	0.08	
1093	0.130 004	GJ	15.40	9.82	9.18	8.83	—
			0.07	0.08	0.07	0.07	
268A	0.166 004	GJ	13.17	8.51	7.91	7.63	M 4.5c
			0.06	0.07	0.07	0.07	
268B	0.166 004	GJ	13.56	8.73	8.13	7.84	—
			0.06	0.07	0.07	0.07	
273	0.266 006	GJ	11.99	7.79	7.27	7.02	M 3.5
			0.05	0.06	0.06	0.06	
283B	0.125 010	GJ	16.90	10.62	10.09	9.74	M 6.0
			0.17	0.18	0.18	0.18	
285	0.167 007	GJ	12.29	7.71	7.13	6.86	—
			0.09	0.10	0.10	0.10	
299	0.147 004	GJ	13.67	9.26	8.74	8.51	—
			0.06	0.07	0.07	0.07	
300	0.171 016	G	13.24	8.60	8.07	7.81	—
			0.20	0.28	0.21	0.21	
1111	0.278 004	GJ	17.03	10.46	9.84	9.48	M 6.5
			0.04	0.04	0.04	0.04	
1116A	0.192 004	GJ	15.49	9.71	9.14	8.86	M 5.5c
			0.06	0.07	0.07	0.07	
1116B	0.192 004	GJ	16.29	10.14	9.64	9.24	—
			0.09	0.07	0.07	0.07	
338A	0.162 004	GJ	8.67	5.93	5.32	5.11	M 0.0
			0.06	0.06	0.08	0.07	
338B	0.162 004	GJ	8.77	6.00	5.38	5.19	K 7.0
			0.06	0.06	0.11	0.07	

TABLE 3.7 (continued)

GL#	$\pi \pm \sigma$	Ref.	M _V	M _J	M _H	M _K	Spec.
388	0.206 006	GJ	10.94	6.99	6.39	6.17	—
			0.07	0.07	0.07	0.07	
393	0.130 015	G	10.21	6.75	6.15	5.90	—
			0.25	0.25	0.25	0.25	
L292	0.217 005	DLH	17.28	10.58	10.00	9.64	M 6.5
			0.05	0.06	0.06	0.06	
402	0.145 006	GJ	12.46	8.10	7.50	7.23	M 4.0
			0.09	0.09	0.09	0.09	
406	0.421 006	GJ	16.58	10.21	9.57	9.20	M 6.0
			0.04	0.04	0.04	0.04	
408	0.151 013	G	10.91	7.26	6.67	6.43	—
			0.19	0.19	0.19	0.19	
411	0.397 004	GJ	10.49	7.09	6.55	6.34	M 2.0
			0.03	0.04	0.04	0.04	
412A	0.186 007	GJ	10.12	6.89	6.32	6.11	—
			0.08	0.09	0.09	0.09	
412B	0.186 007	GJ	15.71	10.05	9.49	9.20	—
			0.08	0.09	0.09	0.09	
445	0.193 007	GJ	12.25	8.12	7.61	7.36	—
			0.08	0.08	0.08	0.08	
447	0.298 006	GJ	13.51	8.89	8.32	8.03	—
			0.05	0.05	0.05	0.05	
450	0.125 013	GJ	10.20	6.93	6.33	6.12	—
			0.23	0.23	0.23	0.23	
1156	0.153 004	GJ	14.71	9.31	8.79	8.48	—
			0.06	0.07	0.07	0.07	
473A	0.233 004	Hz	14.87	9.50	8.89	8.51	M 5.5c
			0.10	0.06	0.06	0.05	
473B	0.233 004	Hz	15.28	9.63	9.10	8.84	—
			0.13	0.06	0.06	0.06	
493.1	0.126 010	GJ	13.84	9.05	8.49	8.20	—
			0.17	0.18	0.18	0.18	
514	0.131 010	G	9.65	6.46	5.85	5.65	—
			0.17	0.17	0.17	0.17	
526	0.192 007	GJ	9.90	6.66	6.08	5.88	—
			0.08	0.08	0.08	0.08	

TABLE 3.7 (continued)

GL#	$\pi \pm \sigma$	Ref.	M _V	M _J	M _H	M _K	Spec.
555	0.160 007	GJ	12.33	7.88	7.26	6.99	—
			0.10	0.10	0.10	0.10	
570B	0.180 012	G	9.36	6.34	5.73	5.51	—
			0.15	0.15	0.16	0.15	
570C	0.180 012	G	11.56	7.64	6.92	6.63	—
			0.18	0.16	0.18	0.16	
581	0.153 009	G	11.47	7.62	7.02	6.77	—
			0.13	0.13	0.13	0.13	
623A	0.132 006	GJ	10.87	7.31	6.83	6.59	M 2.5c
			0.11	0.11	0.11	0.11	
623B	0.132 006	GJ	16.23	10.59	9.48	9.46	—
			0.53	0.31	0.11	0.17	
625	0.159 009	GJ	11.11	7.64	7.07	6.85	M 2.0
			0.12	0.13	0.13	0.13	
628	0.247 007	GJ	12.07	7.92	7.33	7.06	—
			0.06	0.07	0.07	0.07	
643A	0.154 006	HKD	13.44	9.26	8.70	8.43	M 3.5c
			0.09	0.09	0.09	0.09	
643B	0.154 006	HKD	13.44	9.26	8.70	8.43	—
			0.09	0.09	0.09	0.09	
644A	0.154 006	HKD	10.28	6.73	6.08	5.80	—
			0.10	0.09	0.09	0.10	
644B	0.154 006	HKD	11.34	7.24	6.64	6.46	—
			0.16	0.09	0.09	0.10	
644C	0.154 006	HKD	17.60	10.71	10.12	9.74	M 7.0
			0.09	0.09	0.09	0.09	
661A	0.158 006	GJ	10.82	7.13	6.59	6.38	M 3.0c
			0.09	0.09	0.09	0.10	
661B	0.158 006	GJ	11.61	7.54	7.05	6.80	—
			0.10	0.09	0.09	0.10	
687	0.213 006	G	10.79	6.96	6.38	6.16	—
			0.06	0.07	0.07	0.07	
699	0.545 003	GJ	13.22	9.01	8.50	8.24	M 4.0
			0.02	0.03	0.03	0.03	
701	0.136 007	GJ	10.07	6.82	6.22	6.01	—
			0.11	0.12	0.12	0.12	

TABLE 3.7 (continued)

GL#	$\pi \pm \sigma$	Ref.	M _V	M _J	M _H	M _K	Spec.
1224	0.133 006	GJ	14.26 0.10	9.51 0.13	9.08 0.13	8.66 0.11	—
1230A	0.131 013	GJ	12.84 0.22	8.23 0.22	7.60 0.22	7.32 0.22	—
1230B	0.131 013	GJ	16.30 0.23	10.15 0.22	9.47 0.22	9.20 0.22	—
725A	0.282 004	G	11.15 0.04	7.45 0.04	6.92 0.04	6.69 0.04	M 3.0
725B	0.282 004	G	11.94 0.04	7.97 0.04	7.45 0.04	7.22 0.04	M 3.5
729	0.345 012	G	13.64 0.08	8.89 0.08	8.32 0.08	8.03 0.08	—
752A	0.174 005	HKD	10.32 0.07	6.70 0.07	6.08 0.07	5.86 0.07	M 3.0
752B	0.174 005	HKD	18.68 0.07	11.12 0.07	10.44 0.07	10.01 0.07	M 8.0
1245A	0.221 002	Ha	15.37 0.05	9.80 0.04	9.32 0.04	8.97 0.04	M 5.5c
1245C	0.221 002	Ha	17.42 0.16	11.06 0.05	10.40 0.04	10.00 0.04	—
1245B	0.221 002	Ha	16.03 0.04	10.05 0.04	9.55 0.04	9.16 0.04	M 6.0
809	0.135 004	GJ	9.17 0.07	6.17 0.07	5.46 0.07	5.29 0.07	M 0.0
829	0.150 007	GJ	11.19 0.10	7.18 0.11	6.60 0.11	6.36 0.11	M 3.5
831A	0.134 010	G	12.73 0.18	8.13 0.19	7.62 0.18	7.36 0.17	M 4.5c
831B	0.134 010	G	15.76 0.34	10.01 0.46	9.13 0.19	8.95 0.18	—
860A	0.253 004	GJ	11.73 0.06	7.87 0.06	7.30 0.05	7.00 0.05	M 3.0
860B	0.253 004	GJ	13.99 0.26	9.06 0.09	8.44 0.06	8.37 0.08	M 4.0
866A	0.290 007	GJ	14.92 0.06	9.33 0.07	8.70 0.07	8.36 0.07	M 5.0c
866B	0.290 007	GJ	15.94 0.07	9.89 0.07	9.26 0.07	8.92 0.07	—

TABLE 3.7 (continued)

GL#	$\pi \pm \sigma$	Ref.	MV	MJ	MH	MK	Spec.
873	0.200 004	GJ	11.77 0.05	7.65 0.05	7.06 0.05	6.82 0.05	M 3.5
876	0.209 007	GJ	11.73 0.08	7.53 0.08	6.91 0.08	6.64 0.08	—
880	0.146 006	GJ	9.50 0.09	6.22 0.09	5.57 0.09	5.38 0.09	M 1.5
884	0.130 009	G	8.46 0.15	5.83 0.15	5.17 0.15	5.02 0.15	—
896A	0.155 013	G	11.35 0.19	7.23 0.19	6.68 0.19	6.38 0.19	—
896B	0.155 013	G	13.32 0.27	8.41 0.20	7.62 0.22	7.49 0.22	—
1286	0.139 006	GJ	15.40 0.10	9.92 0.10	9.31 0.10	9.03 0.10	—
905	0.314 004	GJ	14.78 0.03	9.39 0.04	8.74 0.04	8.42 0.04	—
908	0.180 009	GJ	10.26 0.11	7.10 0.11	6.53 0.11	6.33 0.11	—

REFERENCES:

DLH = Dahn *et al.* (1986),

G = Gliese (1969),

GHW = Geyer *et al.* (1988),

GJ = Gliese and Jahreiss (1979),

Ha = Harrington (1990),

Hz = Heintz (1989),

HKD = Harrington *et al.* (1983),IRM = Ianna *et al.* (1987),

P = Probst (1977)

TABLE 3.8
THE NEARBY STAR CENSUS

Reference	# Stars	# dMs	# North dMs	Objects Added
van de Kamp (1945)	51	32	24	
van de Kamp (1953)	55	35	27	65AB, 440, 526
van de Kamp (1969)	59	38	30	83.1, 169.1AB, 234B
van de Kamp (1971)	60	39	31	1002
Lippincott (1978)	63	43	35	54.1, 1111, 1116AB, 1245AB (169.1AB, 526 omitted)
Gliese (1982)	64	44	36	526 readmitted
Batten (1990)	67	47	38	LHS 292, L 143-23, 866B*
today (1991)	68	48	39	1245C*

* = new member added by infrared speckle work

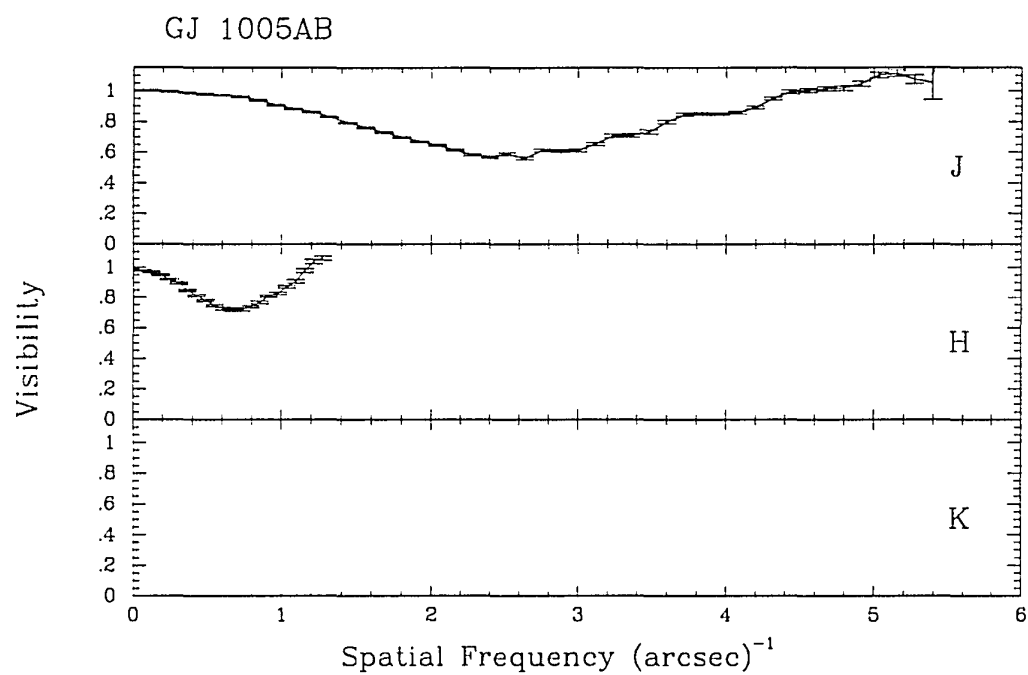


Figure 3.1 Visibility curves for GJ 1005AB.

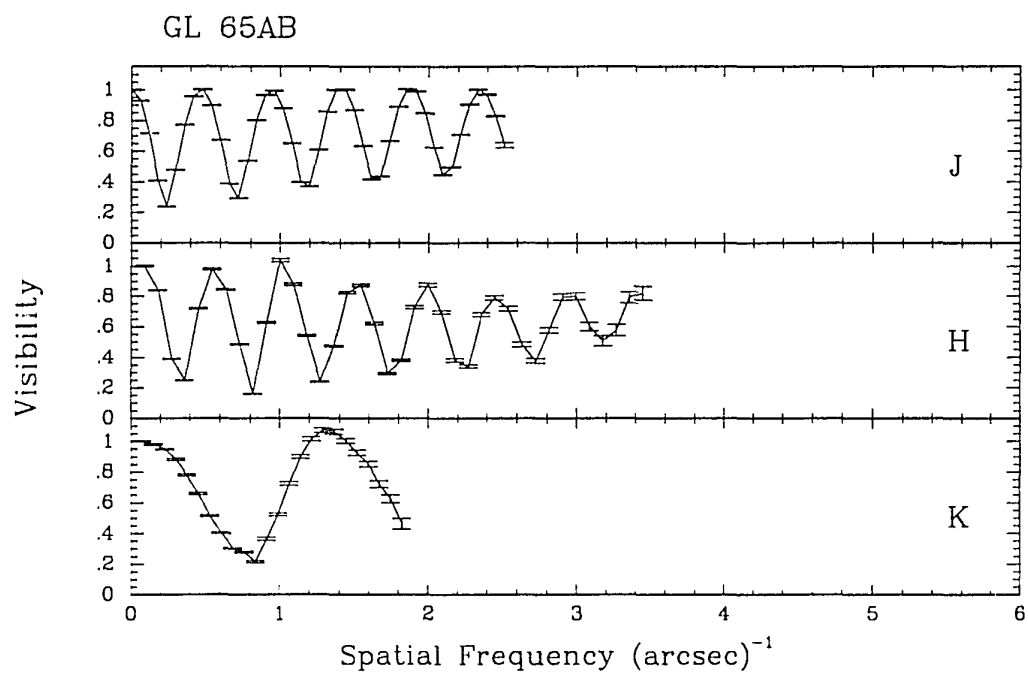


Figure 3.2 Visibility curves for GL 65AB.

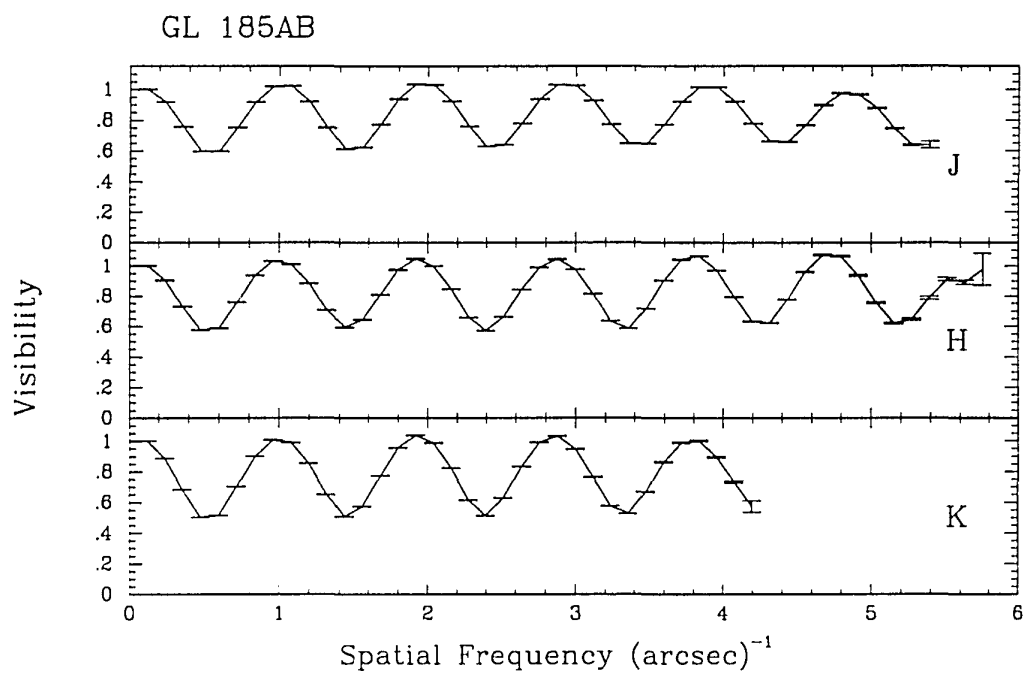


Figure 3.3 Visibility curves for GL 185AB.

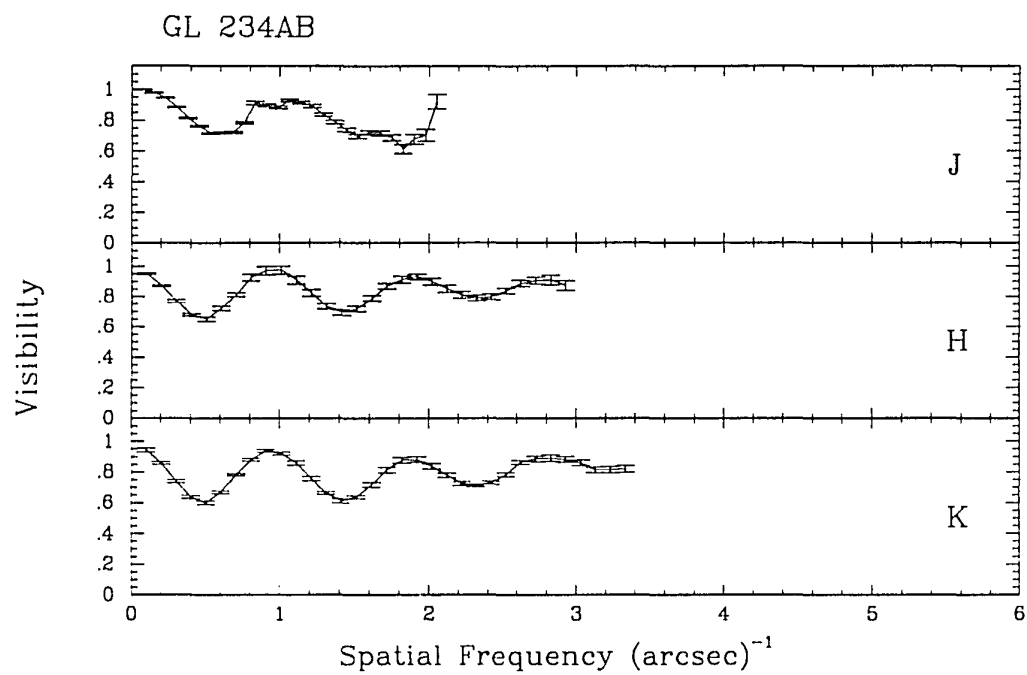


Figure 3.4 Visibility curves for GL 234AB.

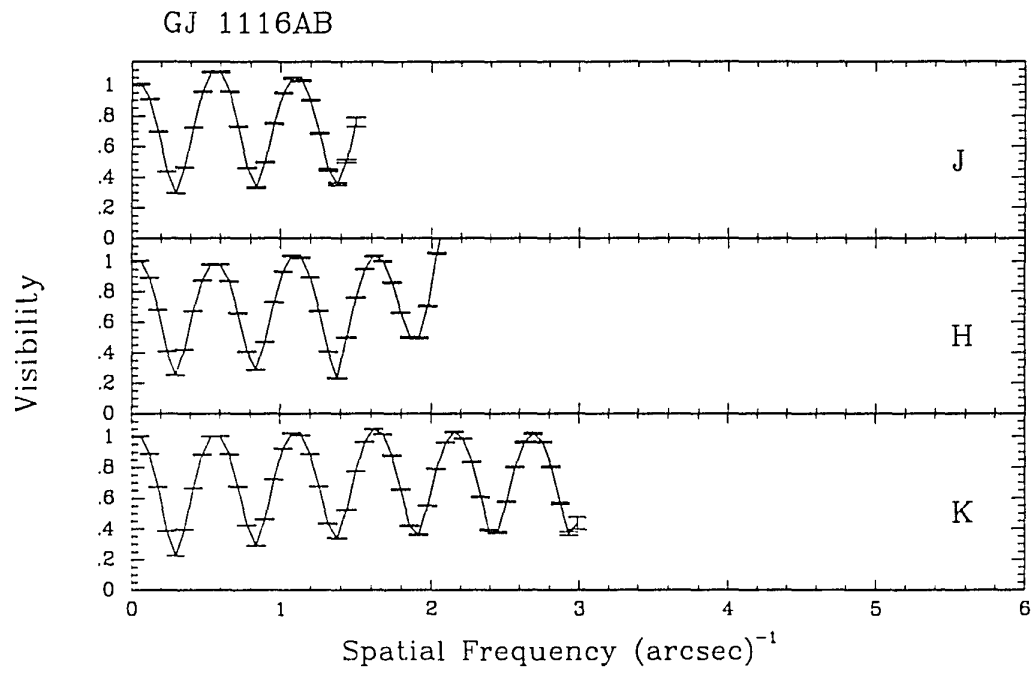


Figure 3.5 Visibility curves for GJ 1116AB.

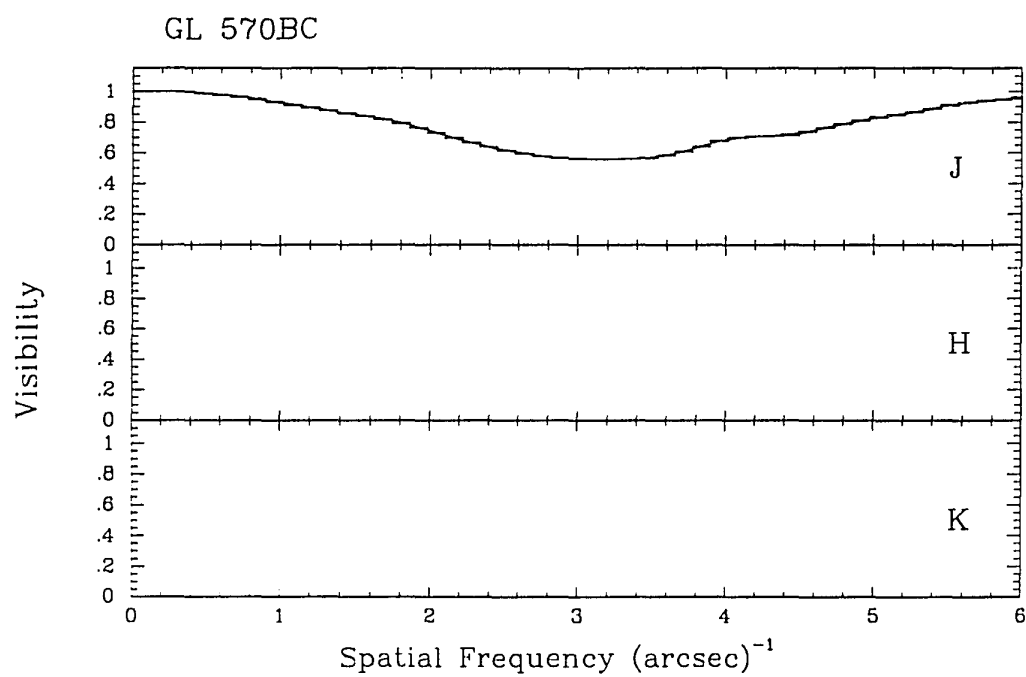


Figure 3.6 Visibility curves for GL 570BC.

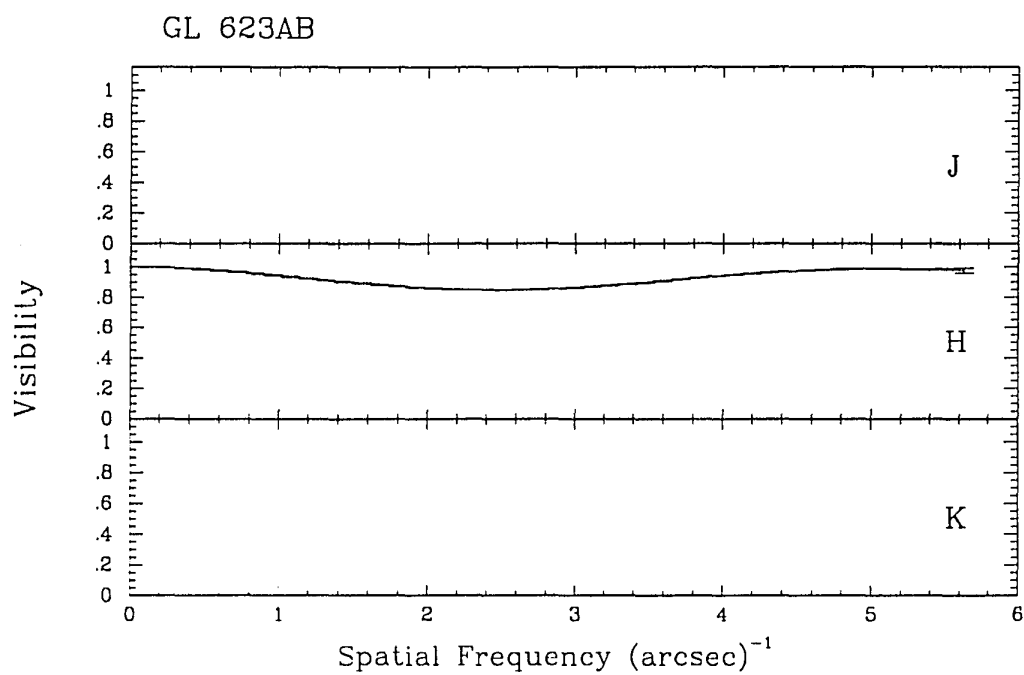


Figure 3.7 Visibility curves for GL 623AB.

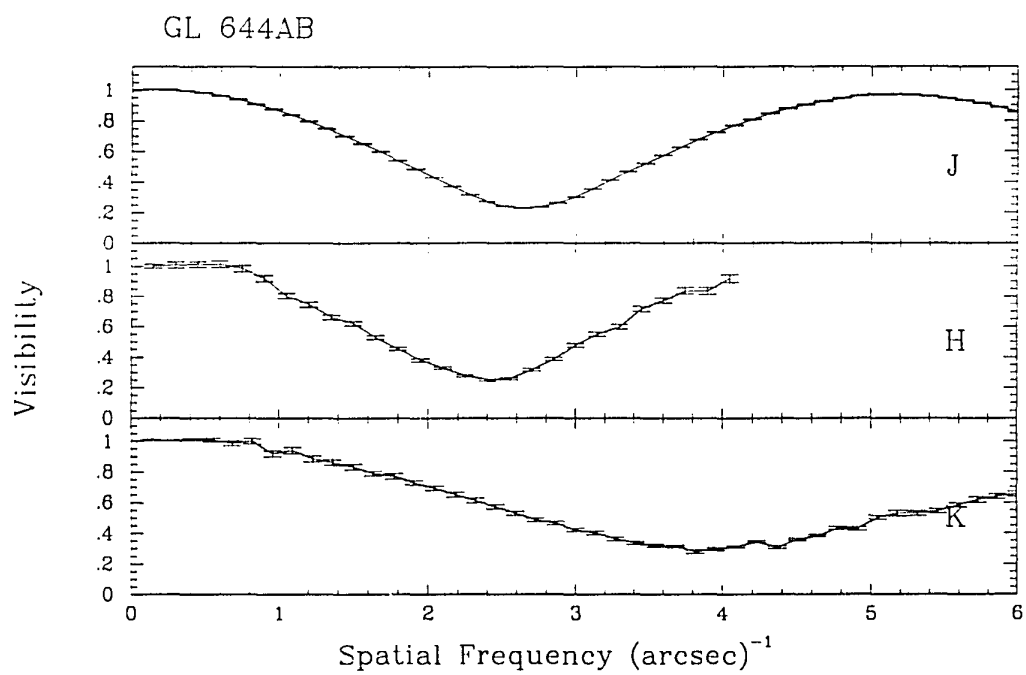


Figure 3.8 Visibility curves for GL 644AB.

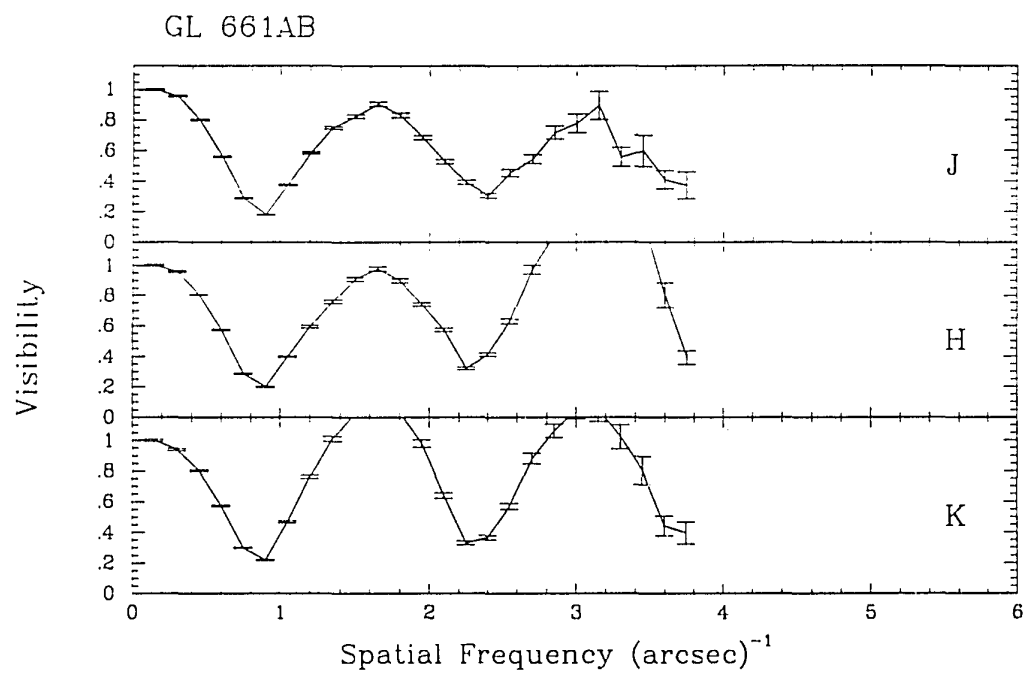


Figure 3.9 Visibility curves for GL 661AB.

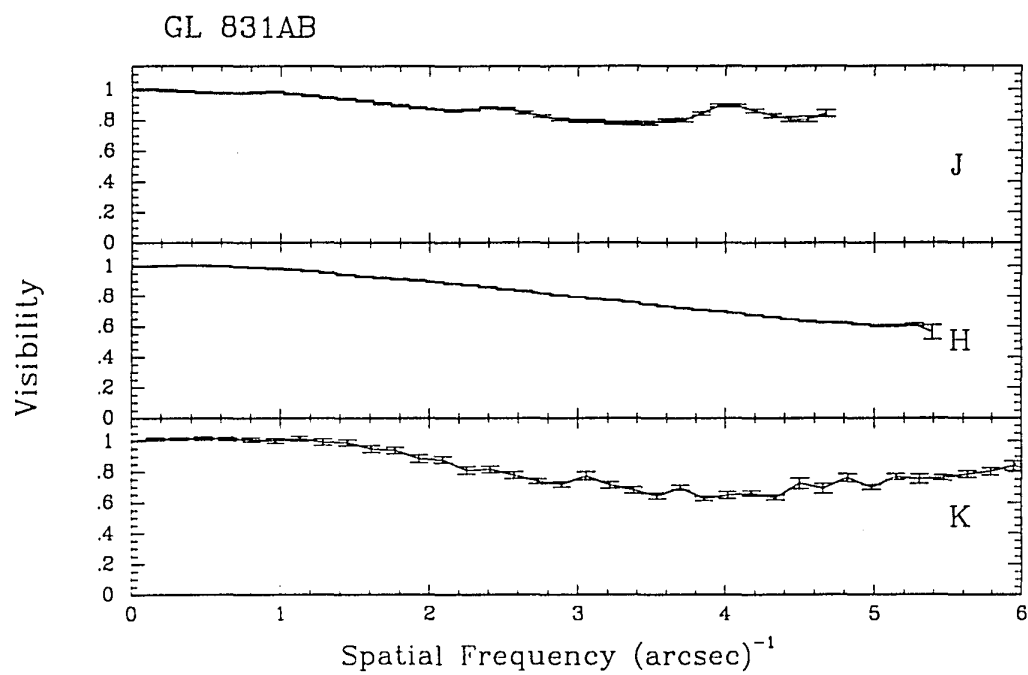


Figure 3.10 Visibility curves for GL 831AB.

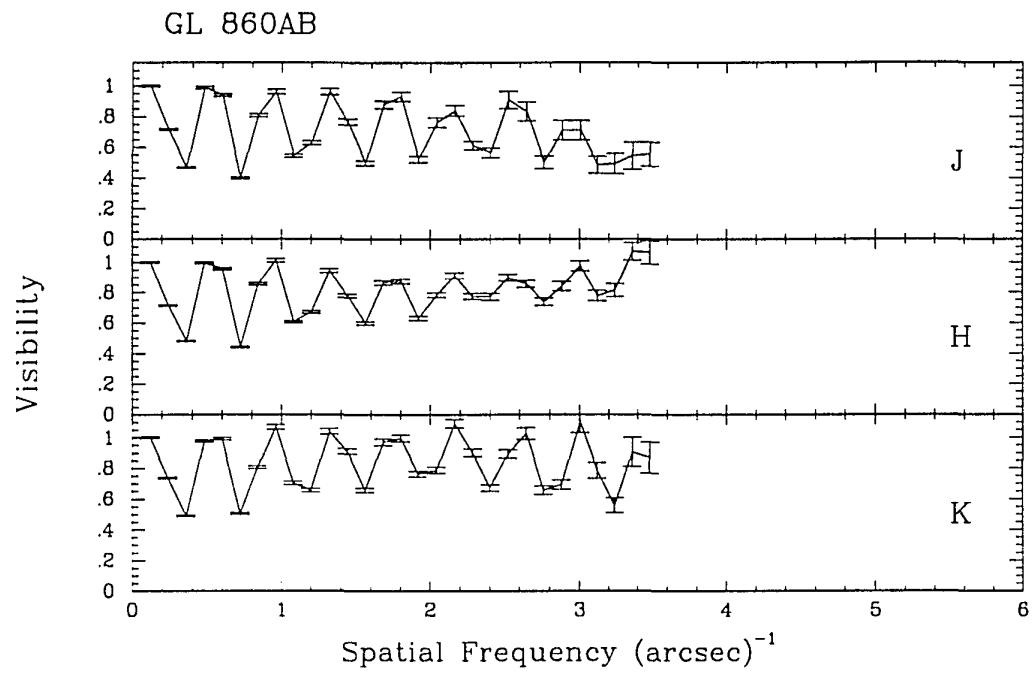


Figure 3.11 Visibility curves for GL 860AB.

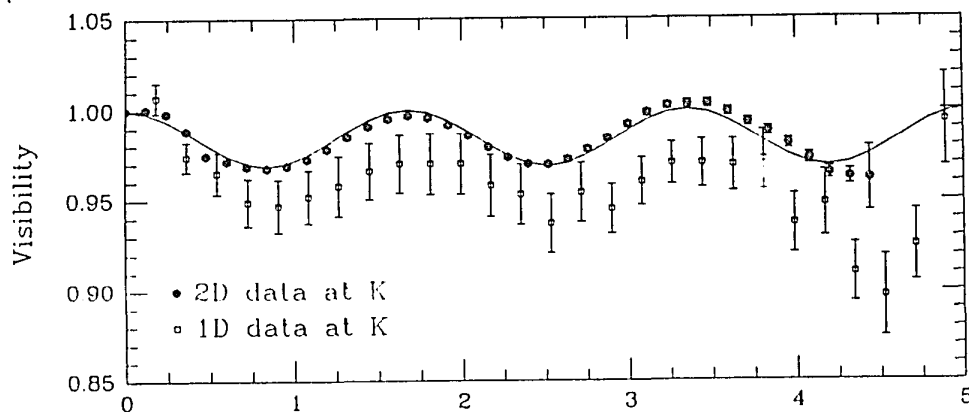


Figure 3.12 Comparison of 1D and 2D speckle data taken of GL 67AB. The curved line is the fit to the 2D data, with a magnitude difference of 4.5 at K and a separation of $0.62''$. The separation of the binary in the north-south direction when the 1D data was taken was $\sim 0.55''$. Note the much higher quality of the 2D data.

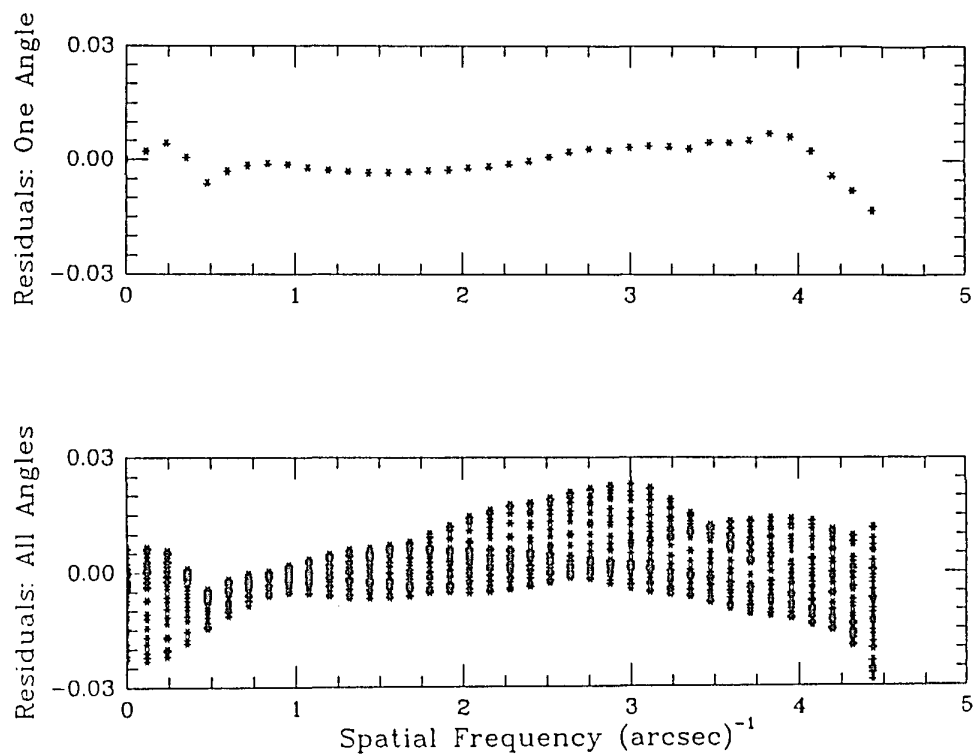


Figure 3.13 (a) Residuals from the fit to the 2D speckle data of GL 67AB observed at K, at the position angle of the secondary. (b) Residuals from the same 2D fit at 36 position angles, every 5° from 0° to 175°.

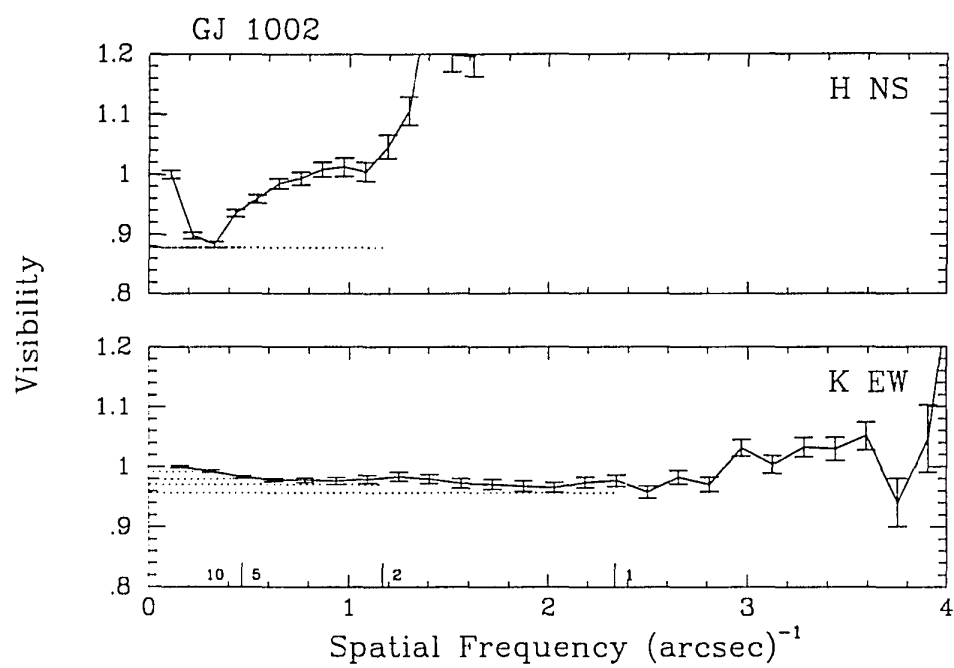


Figure 3.14 Visibility curves for GJ 1002.

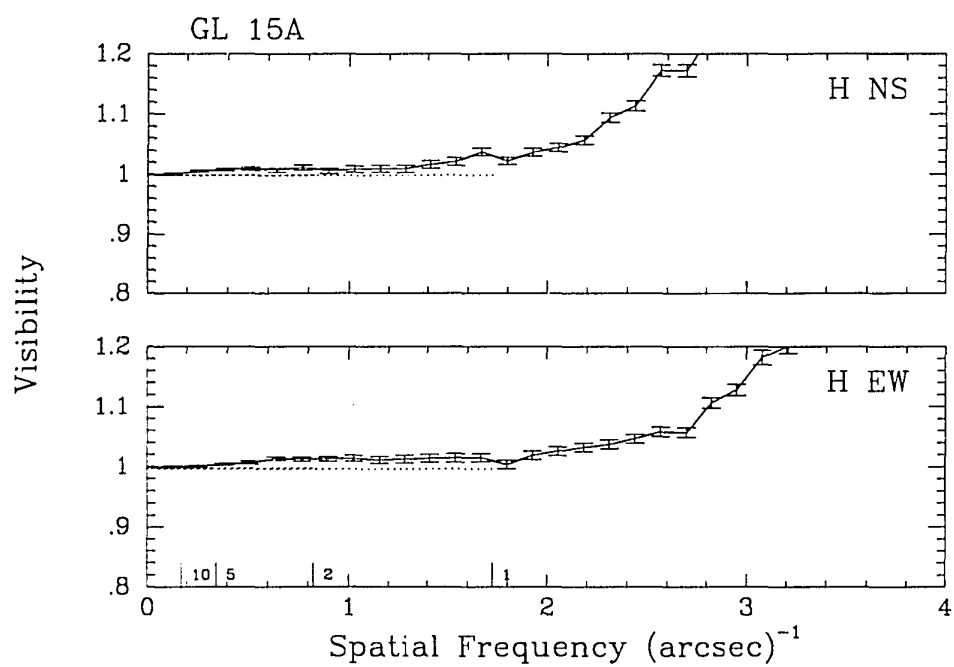


Figure 3.15 Visibility curves for GL 15A.

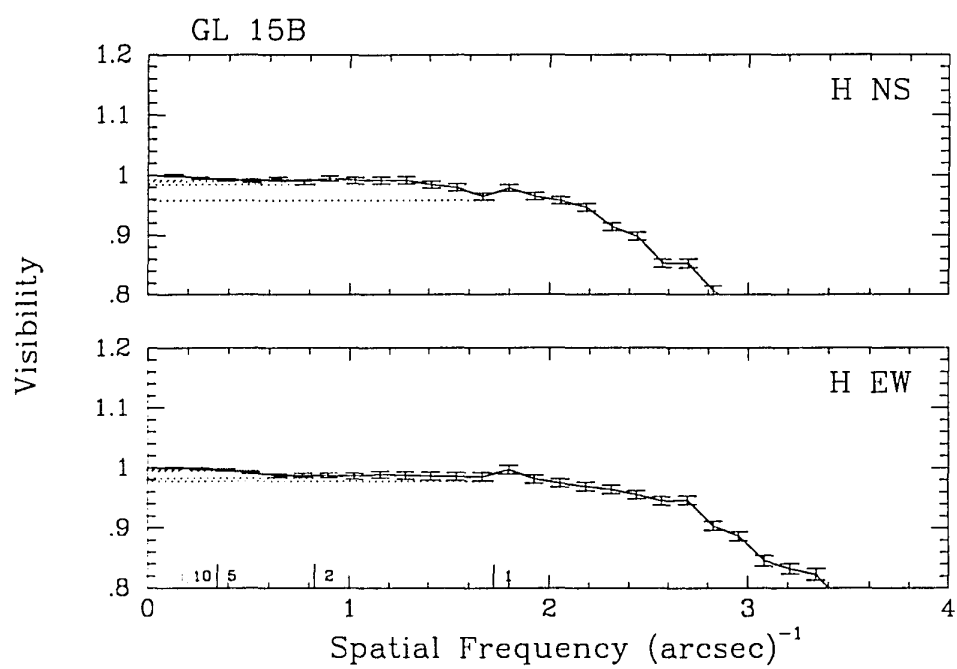


Figure 3.16 Visibility curves for GL 15B.

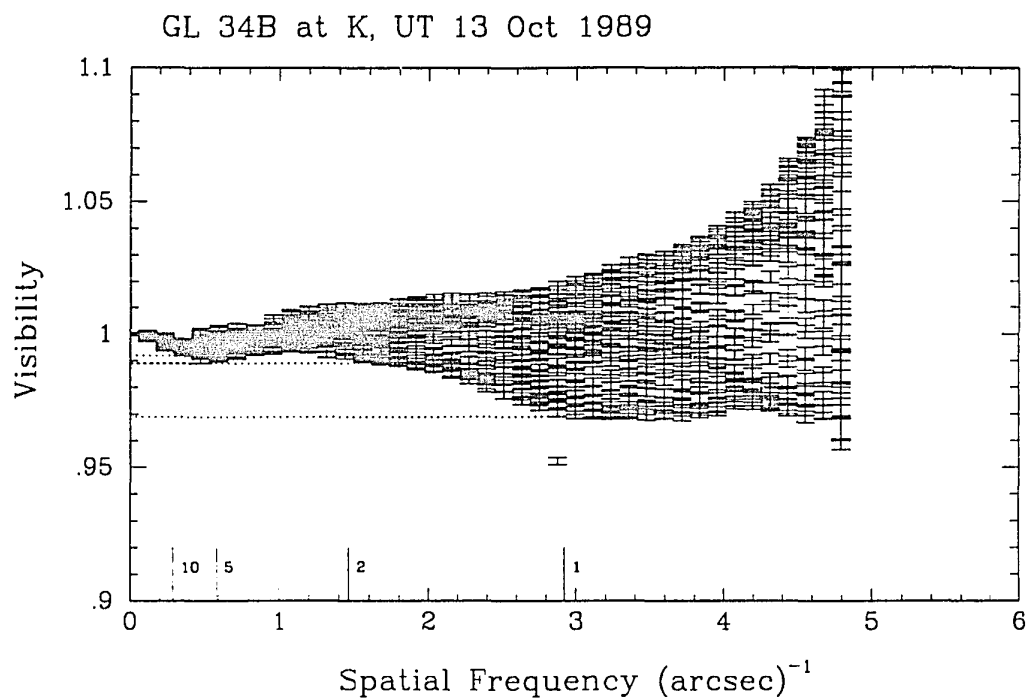


Figure 3.17 Visibility curves for GL 34B.

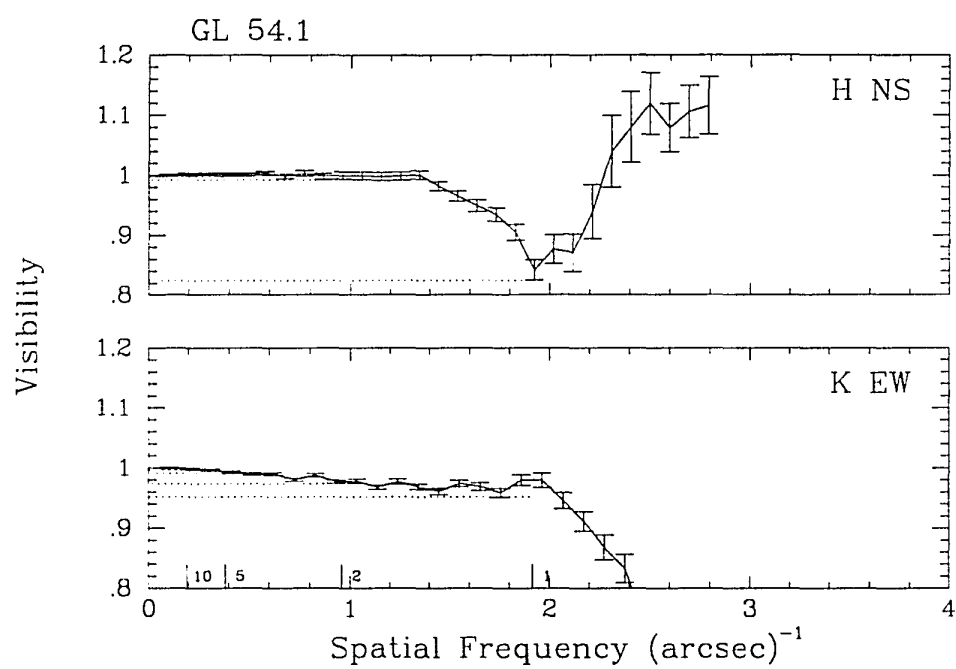


Figure 3.18 Visibility curves for GL 54.1.

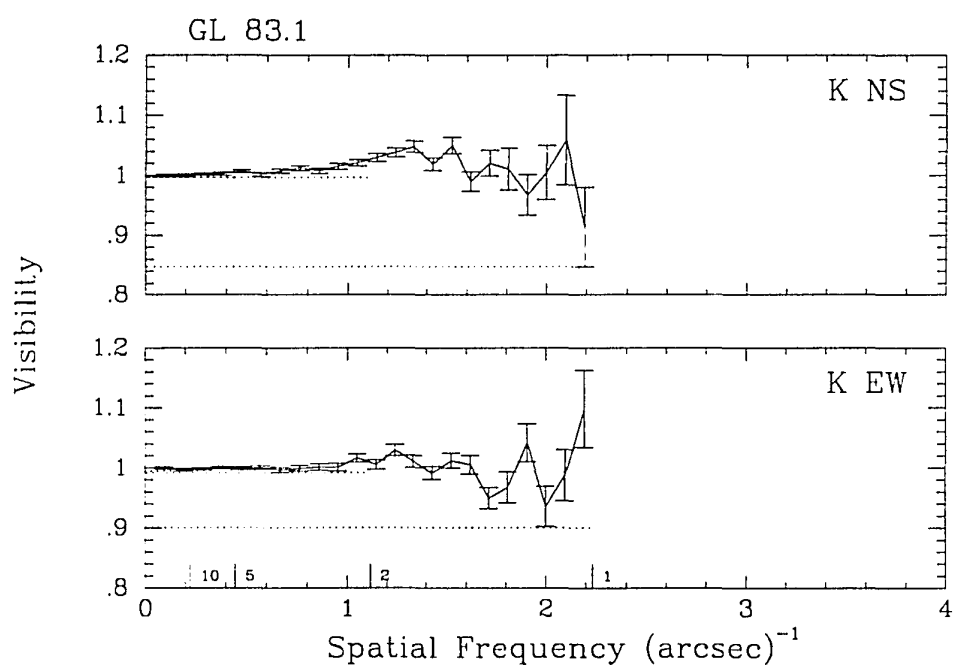


Figure 3.19 Visibility curves for GL 83.1.

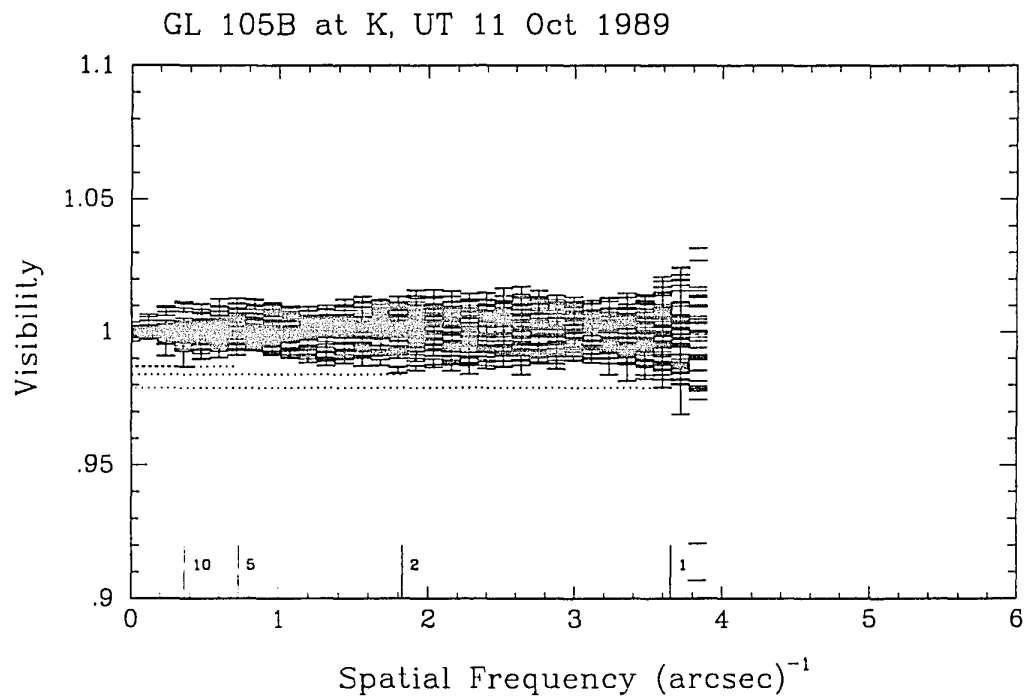


Figure 3.20 Visibility curves for GL 105B.

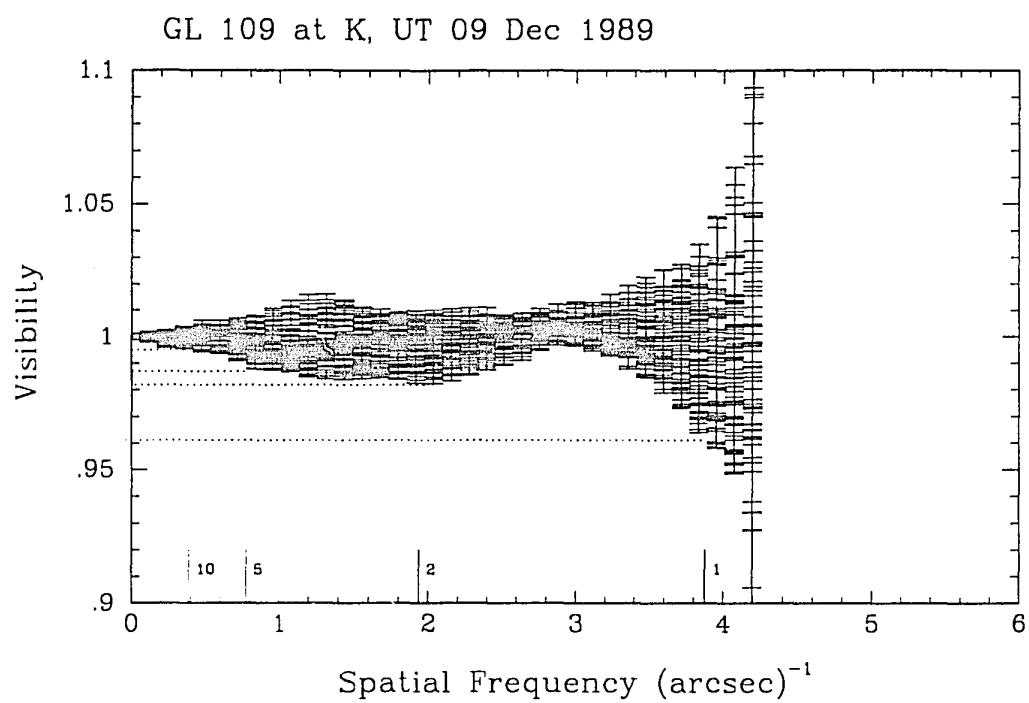


Figure 3.21 Visibility curves for GL 109.

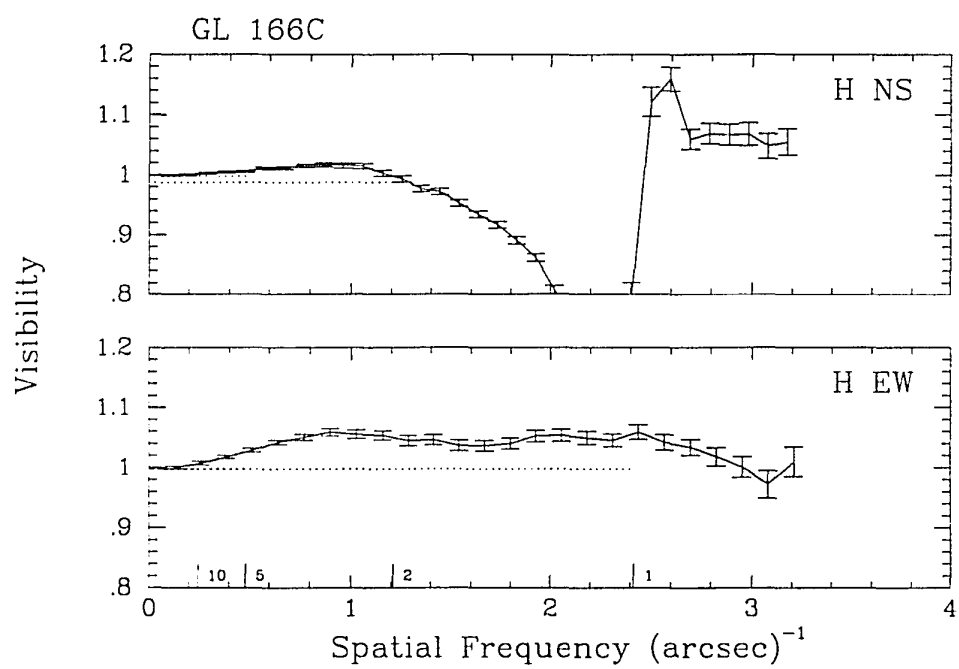


Figure 3.22 Visibility curves for GL 166C.

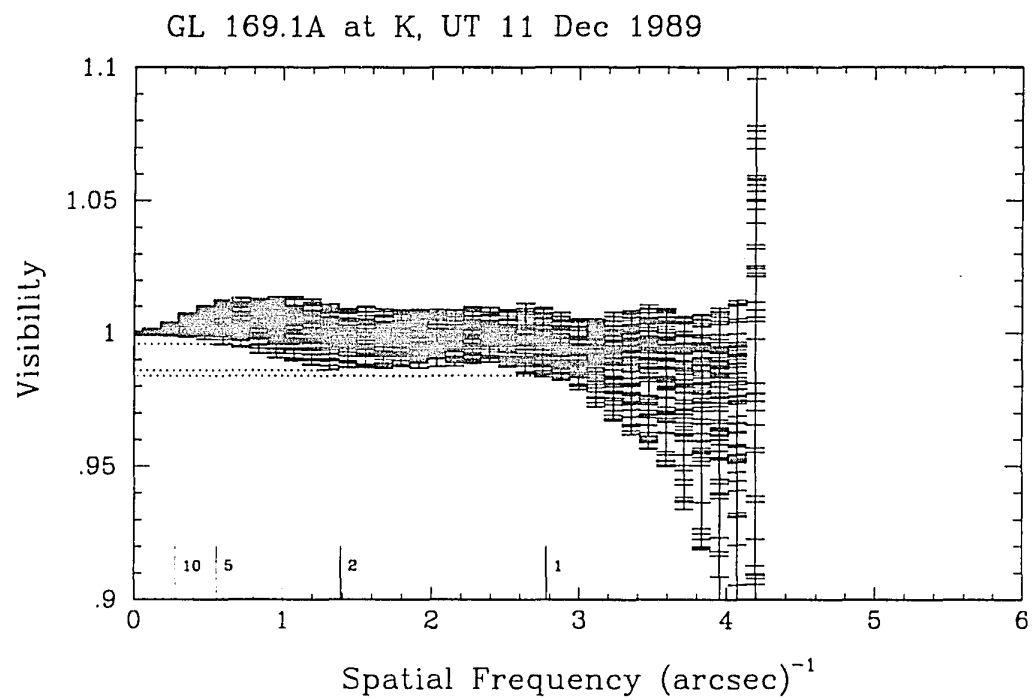


Figure 3.23 Visibility curves for GL 169.1A.

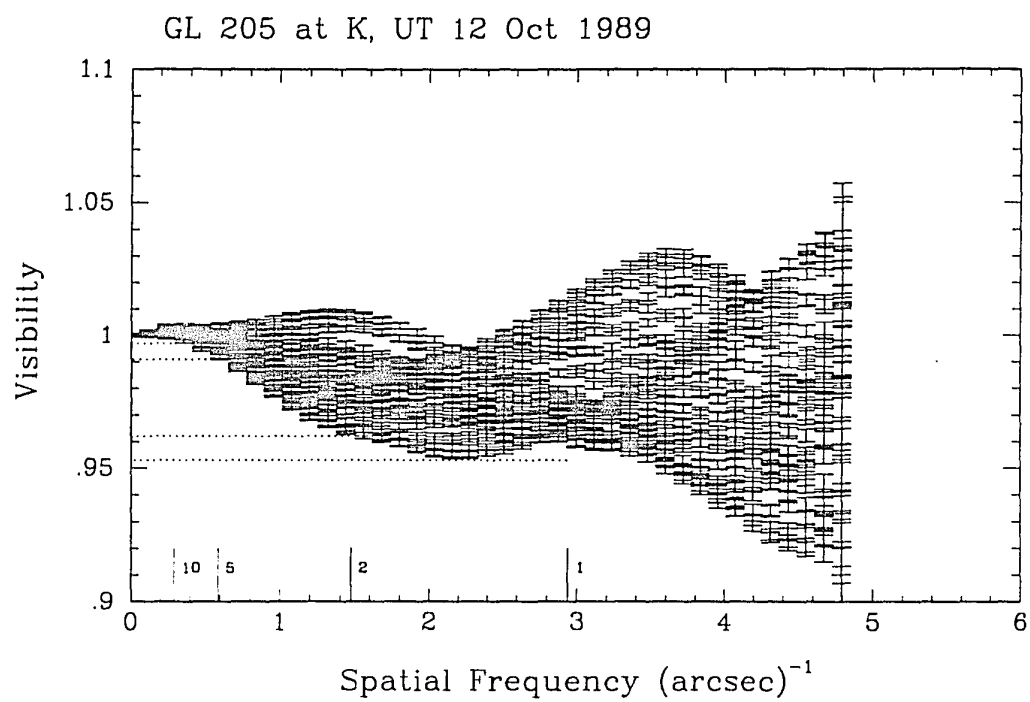


Figure 3.24 Visibility curves for GL 205.

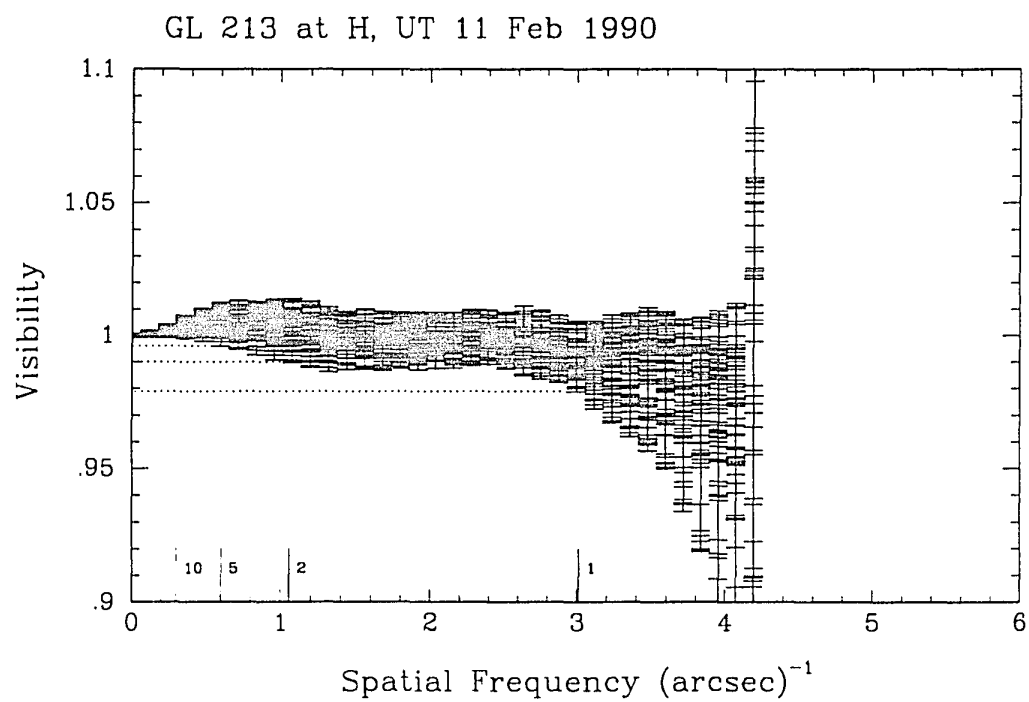


Figure 3.25 Visibility curves for GL 213.

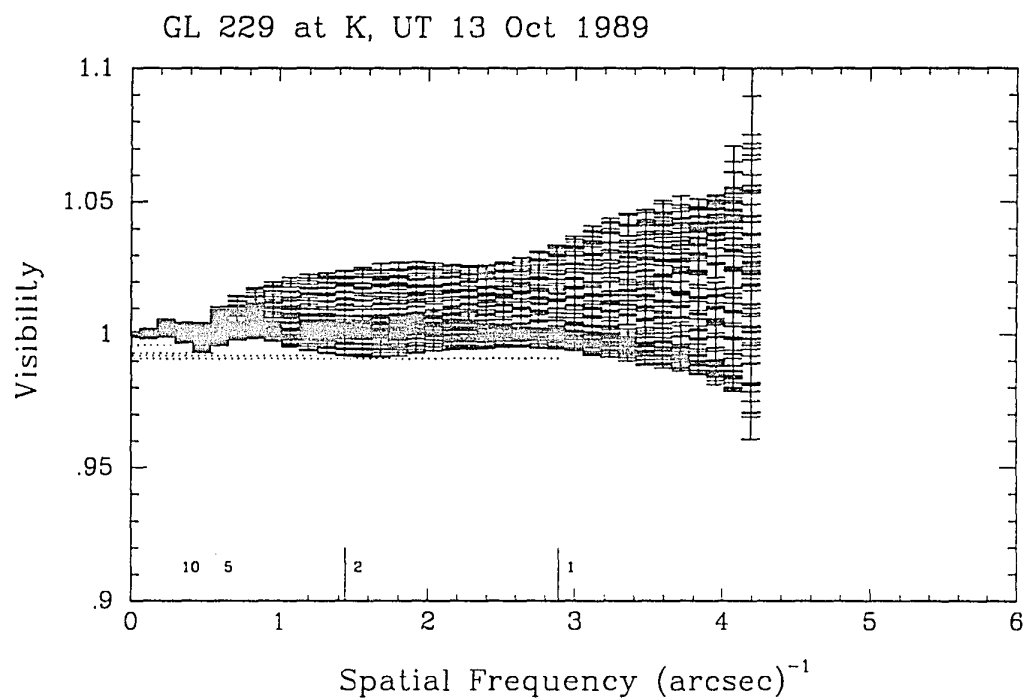


Figure 3.26 Visibility curves for GL 229.

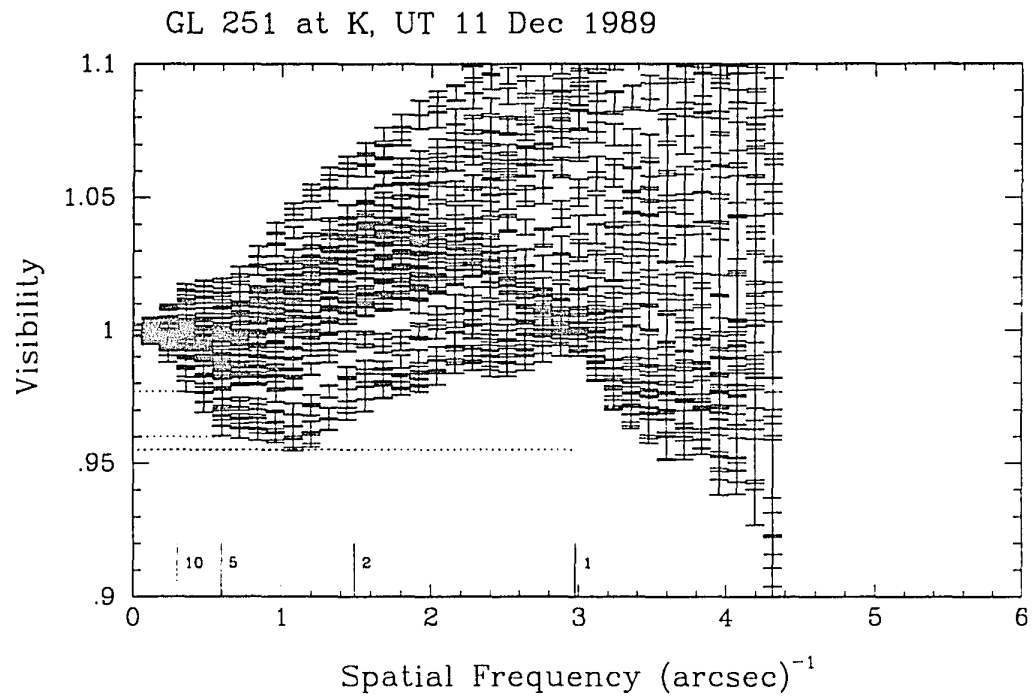


Figure 3.27 Visibility curves for GL 251.

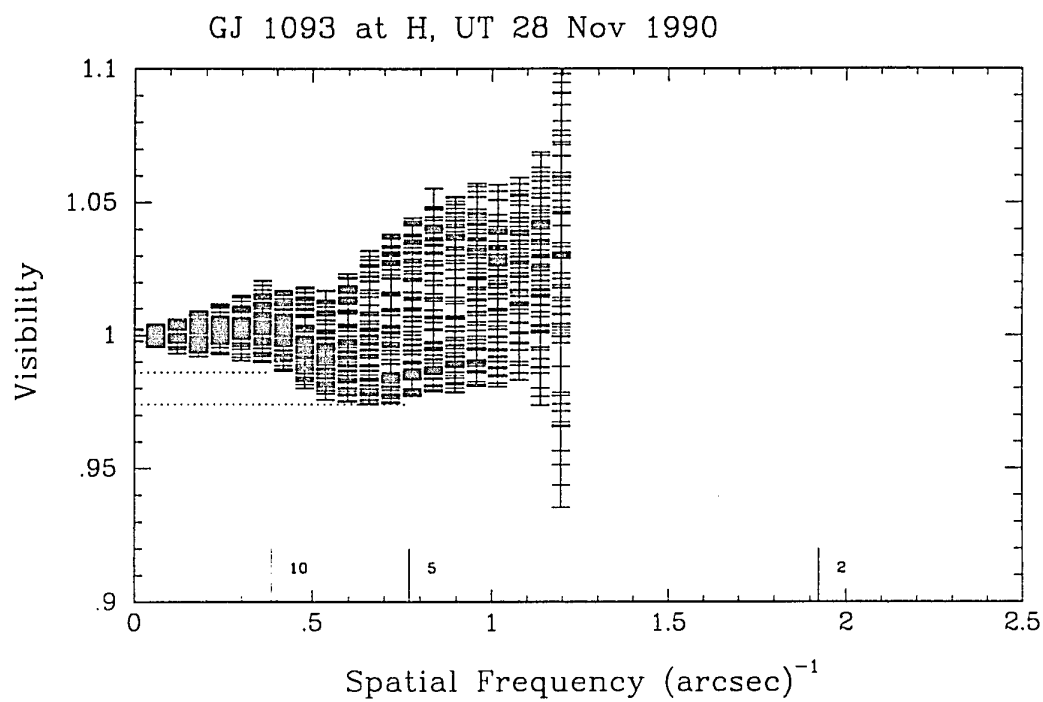


Figure 3.28 Visibility curves for GJ 1093.

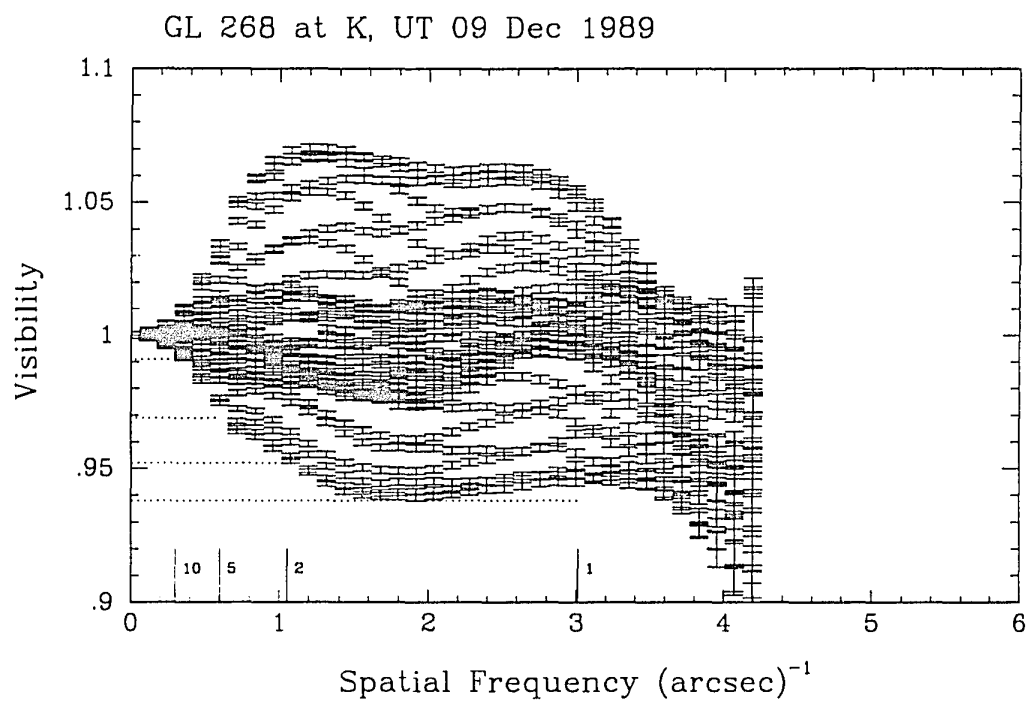


Figure 3.29 Visibility curves for GL 268.

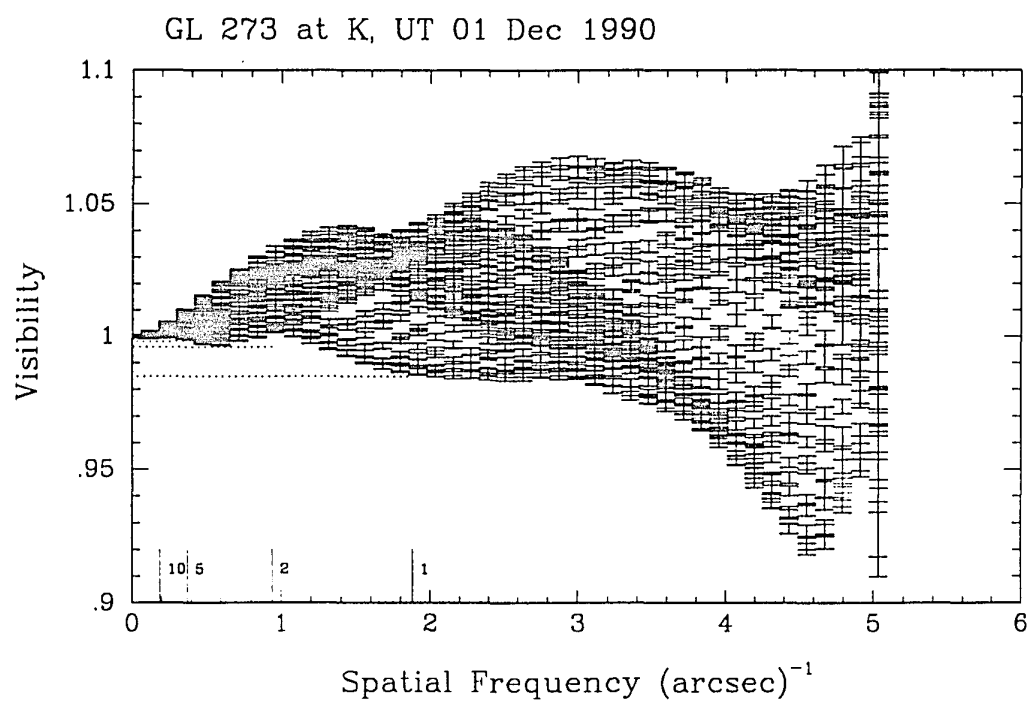


Figure 3.30 Visibility curves for GL 273.

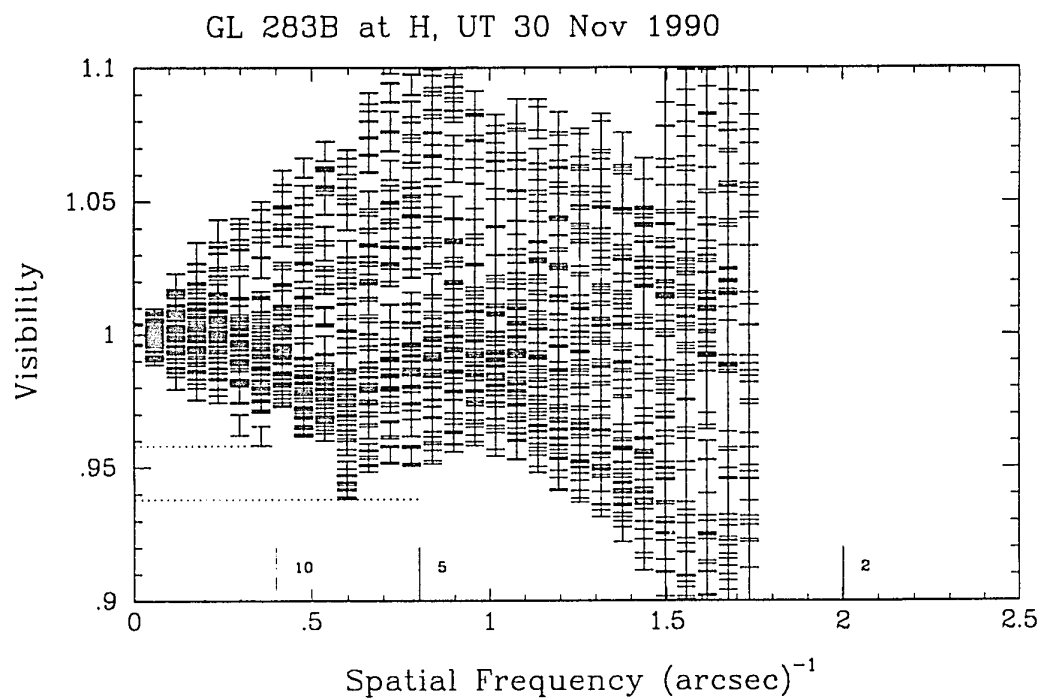


Figure 3.31 Visibility curves for GL 283B.

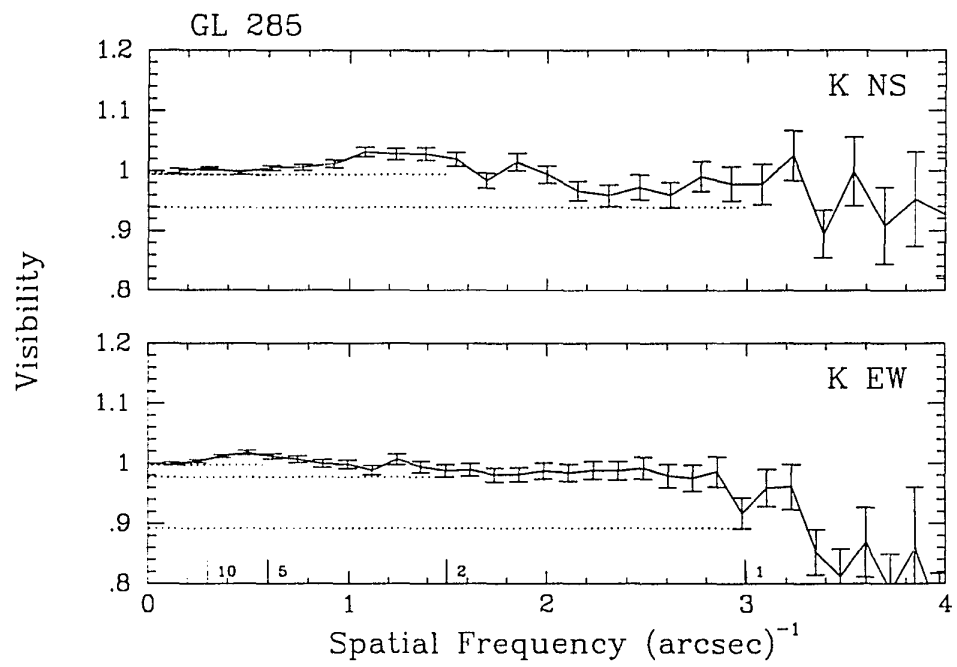


Figure 3.32 Visibility curves for GL 285.

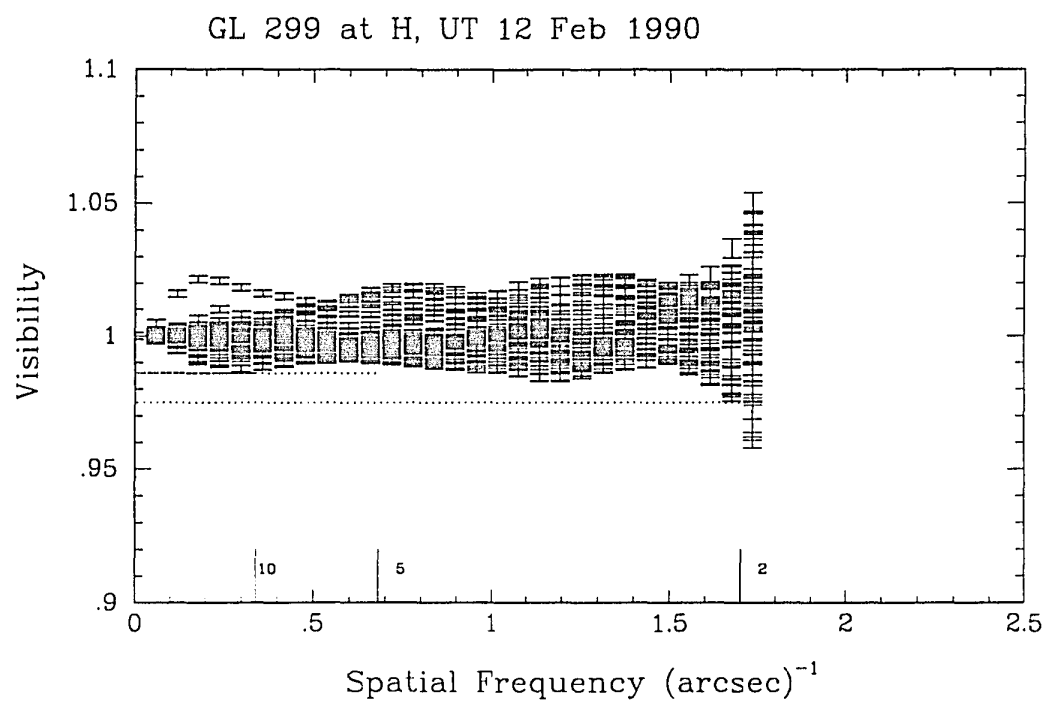


Figure 3.33 Visibility curves for GL 299.

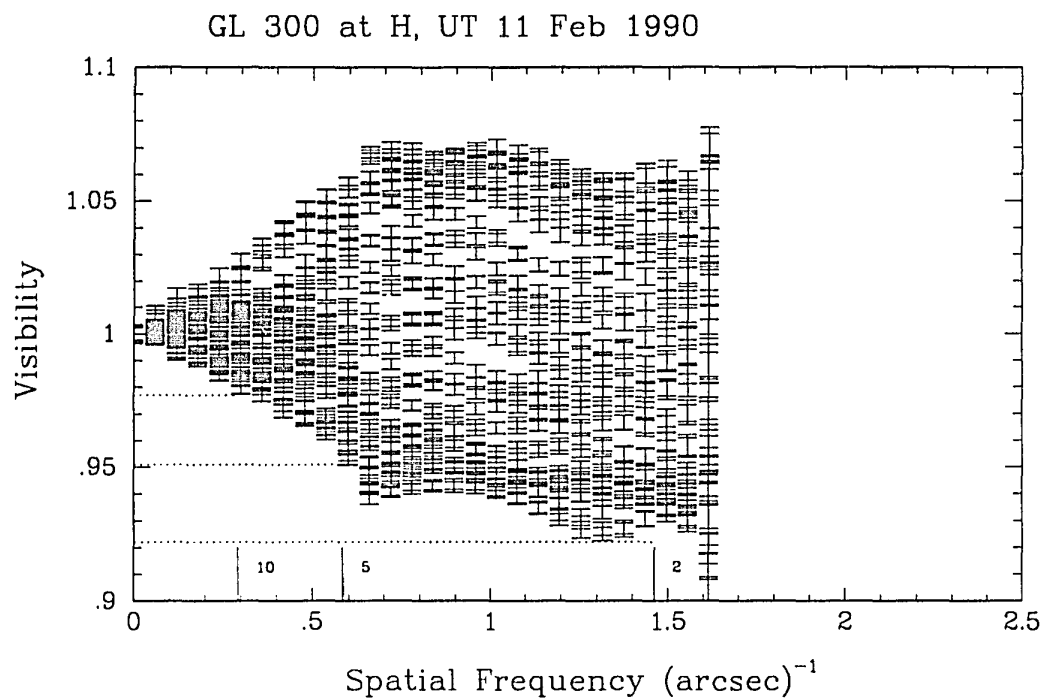


Figure 3.34 Visibility curves for GL 300.

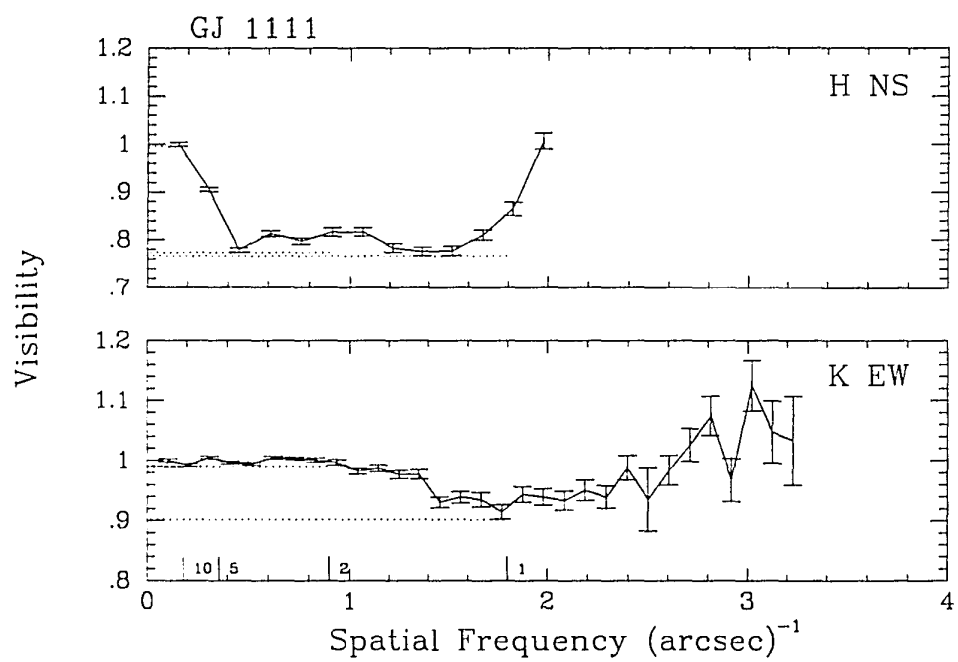


Figure 3.35 Visibility curves for GJ 1111.

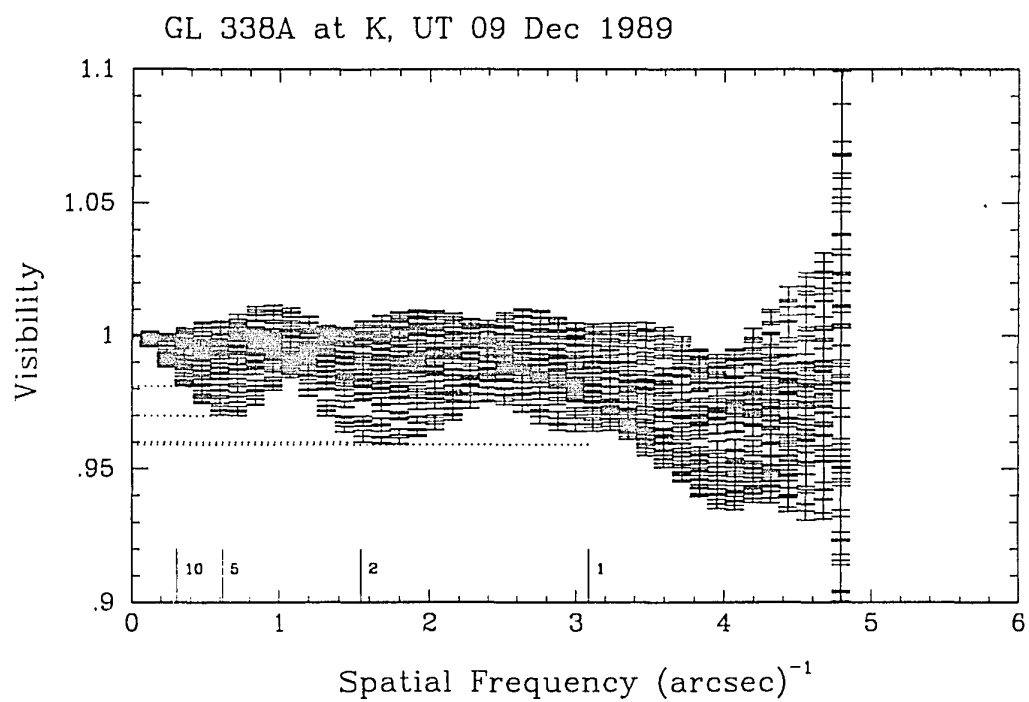


Figure 3.36 Visibility curves for GL 338A.

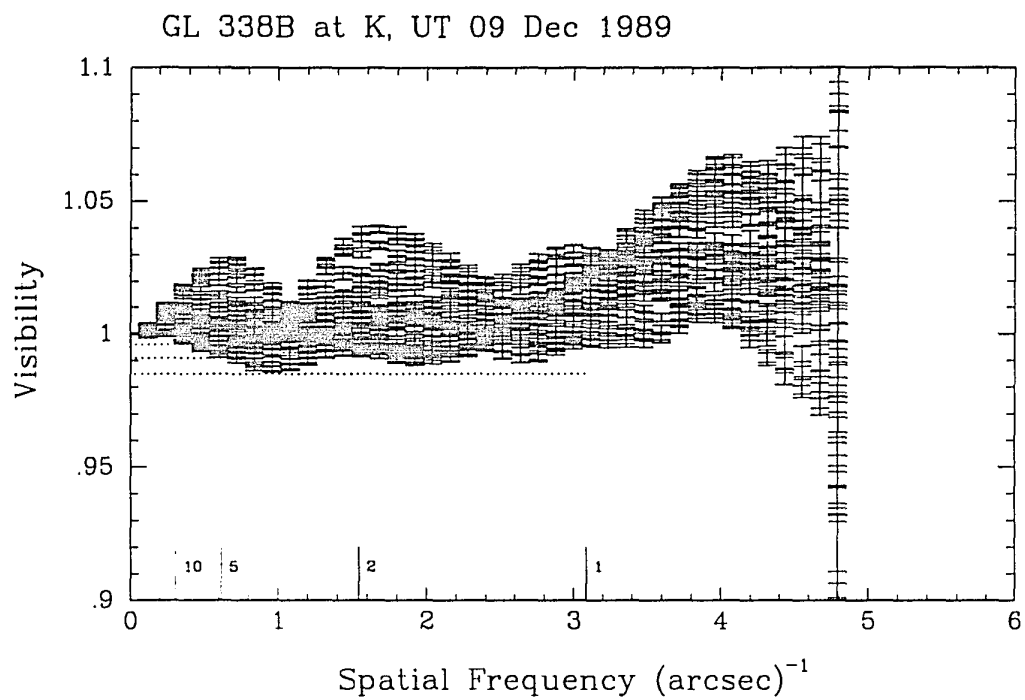


Figure 3.37 Visibility curves for GL 338B.

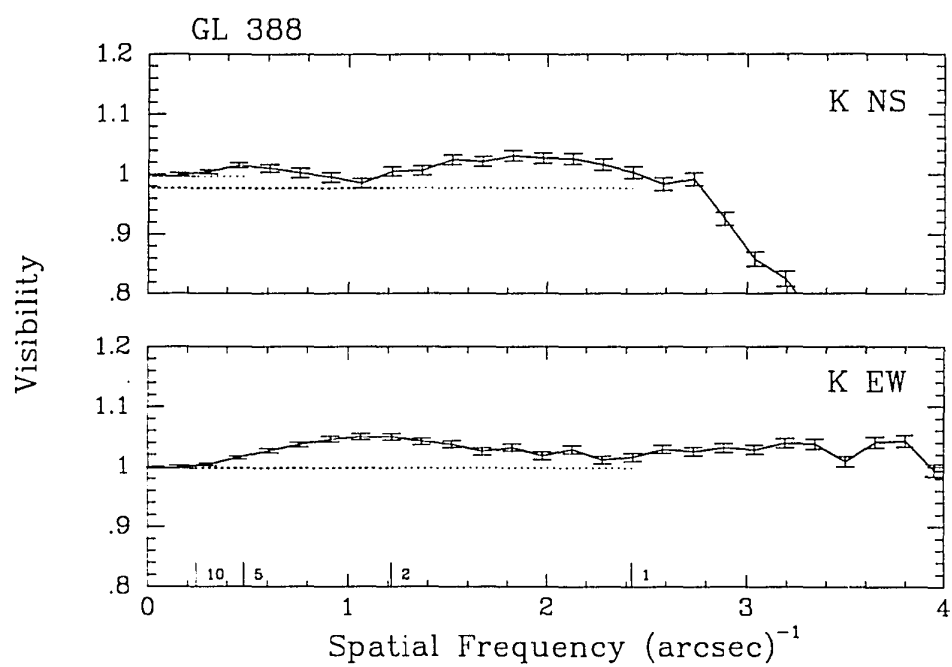


Figure 3.38 Visibility curves for GL 388.

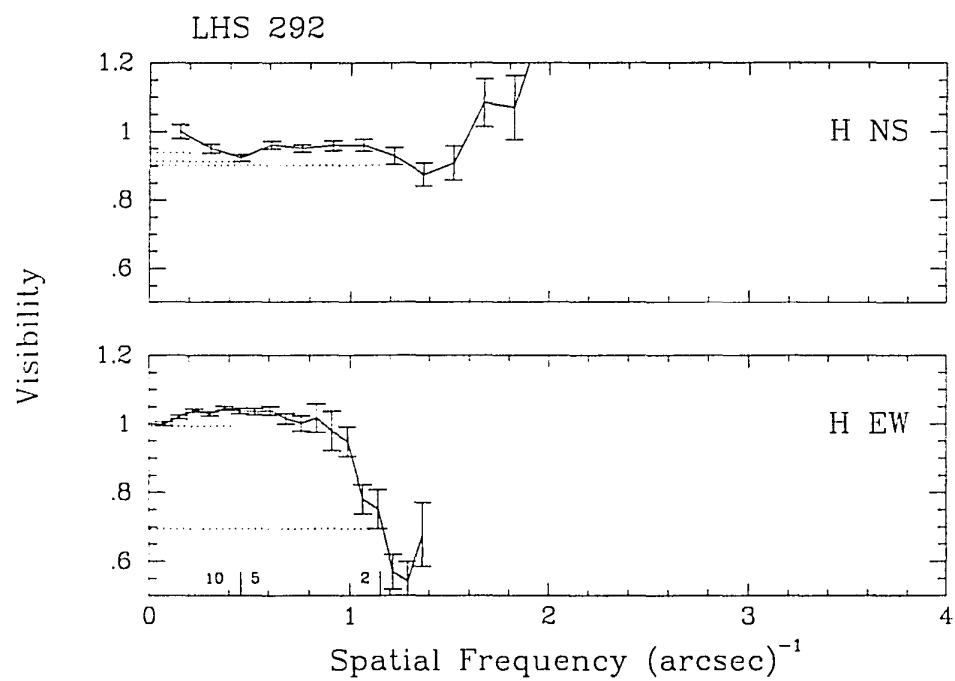


Figure 3.39 Visibility curves for LHS 292.

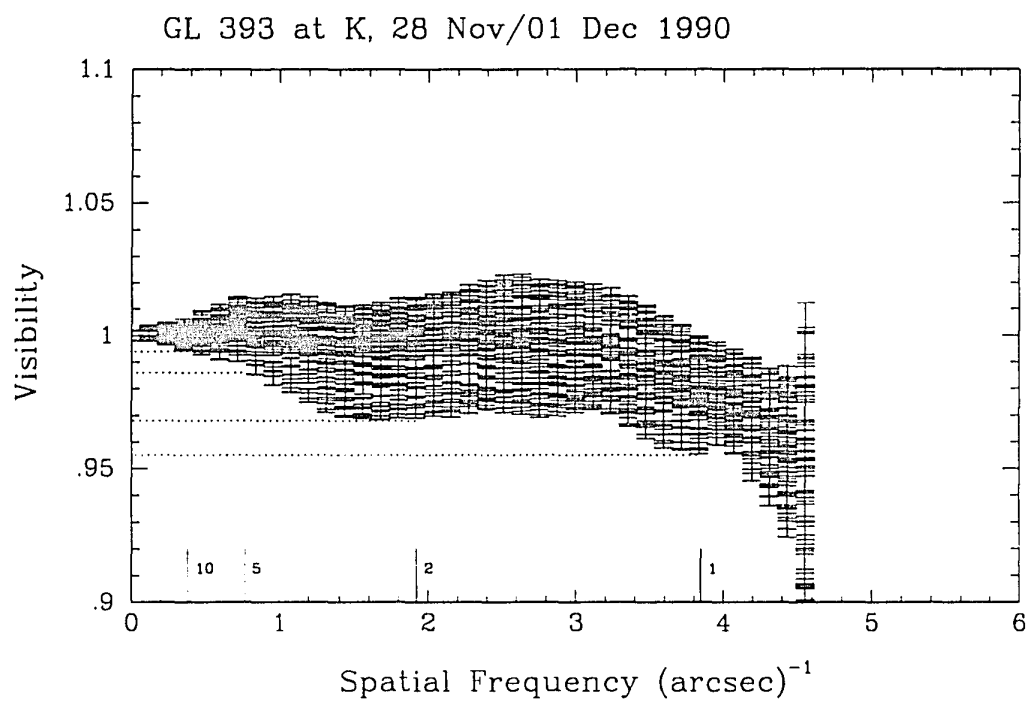


Figure 3.40 Visibility curves for GL 393.

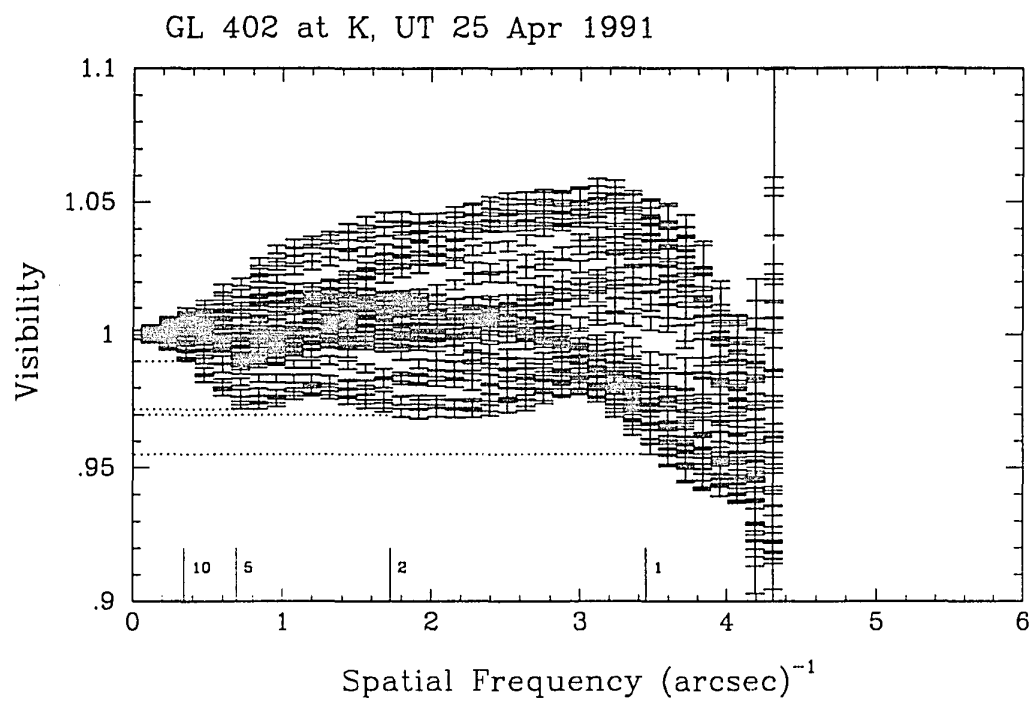


Figure 3.41 Visibility curves for GL 402.

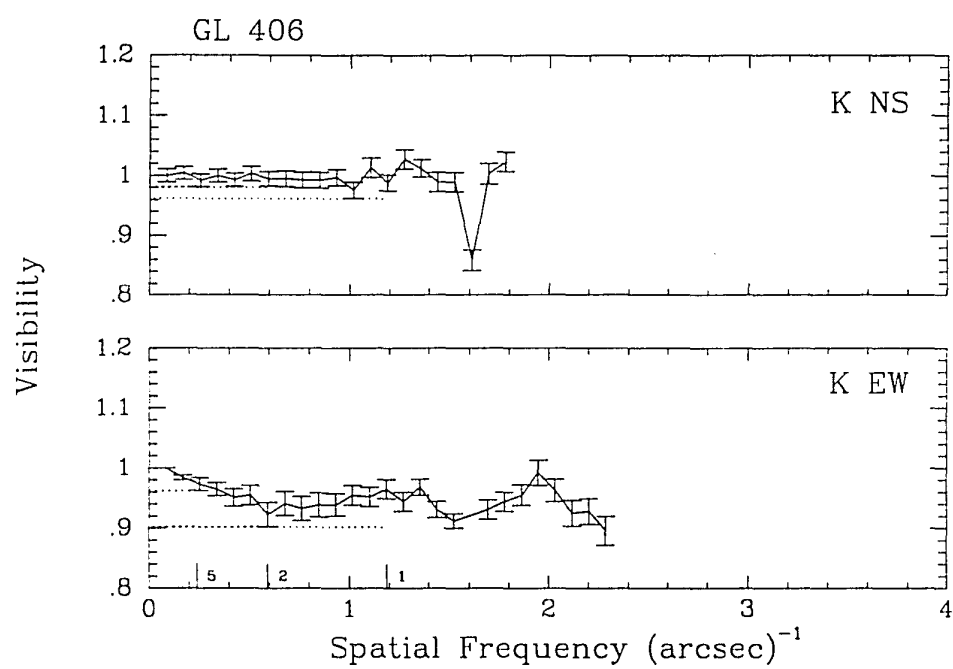


Figure 3.42 Visibility curves for GL 406.

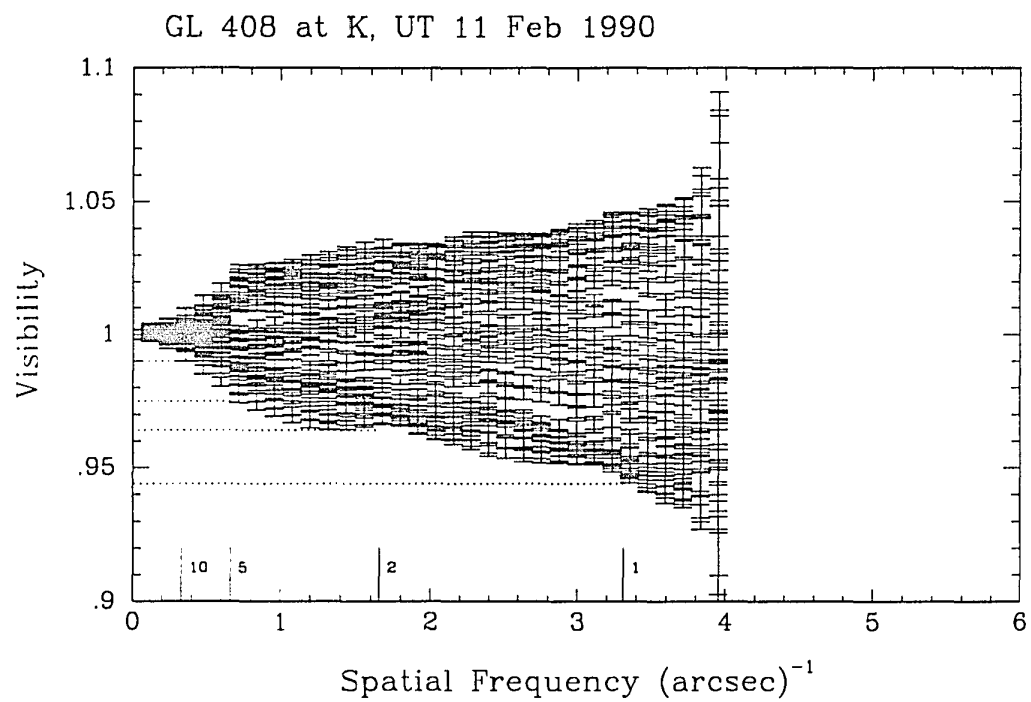


Figure 3.43 Visibility curves for GL 408.

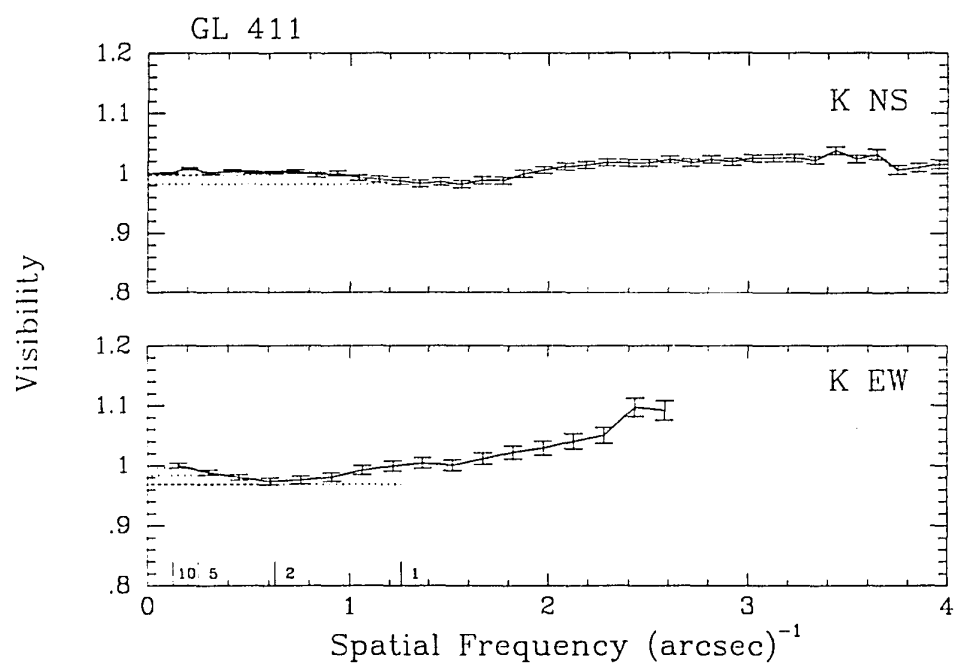


Figure 3.44 Visibility curves for GL 411.

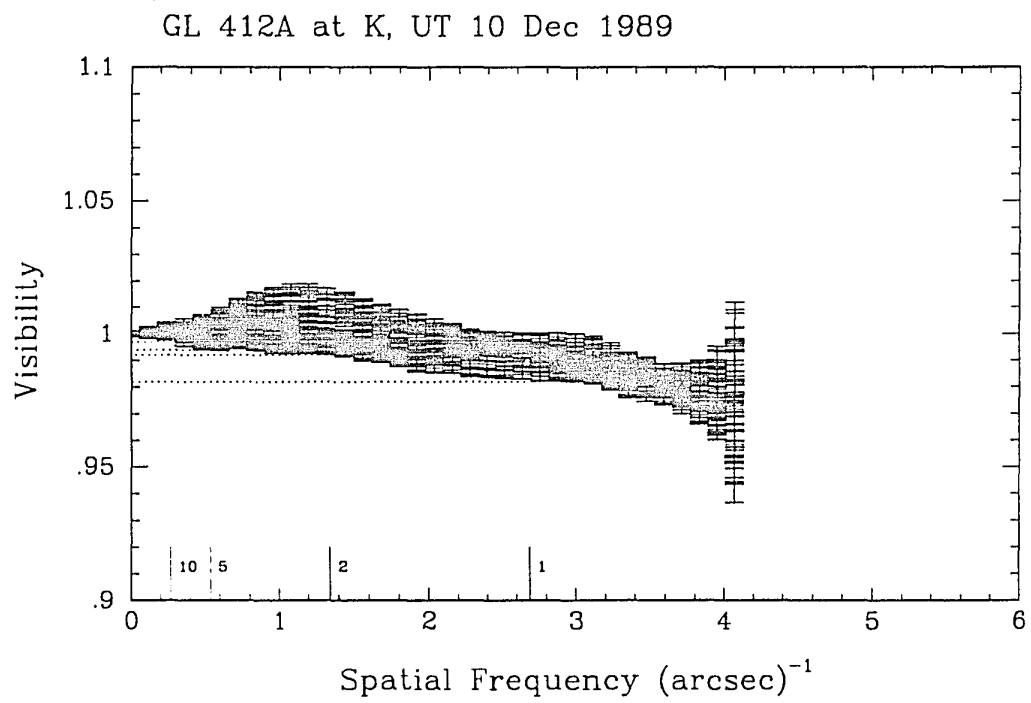


Figure 3.45 Visibility curves for GL 412A.

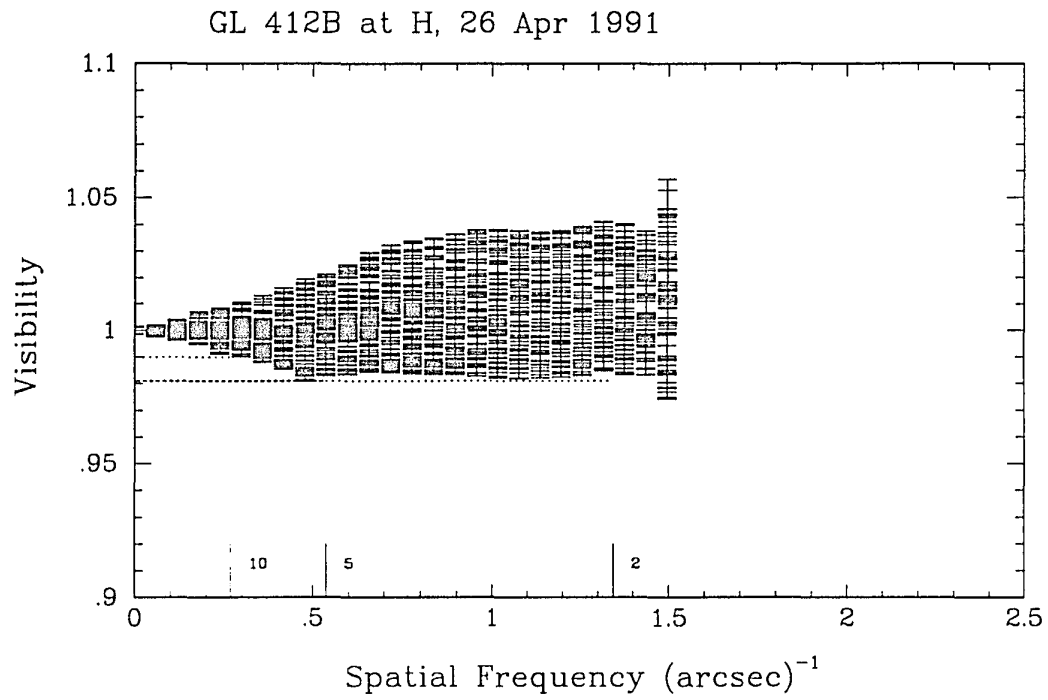


Figure 3.46 Visibility curves for GL 412B.

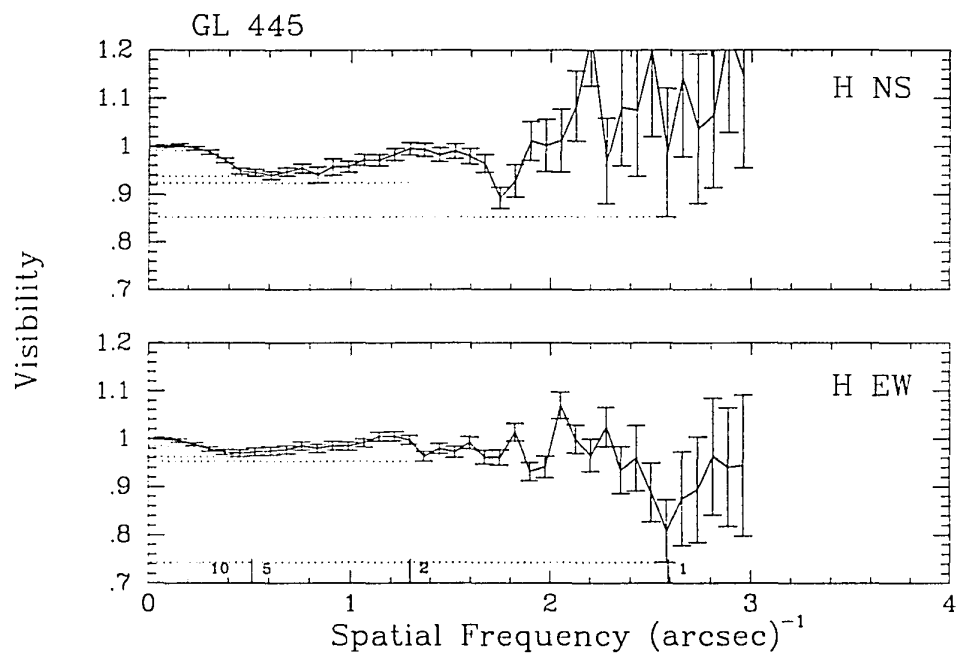


Figure 3.47 Visibility curves for GL 445.

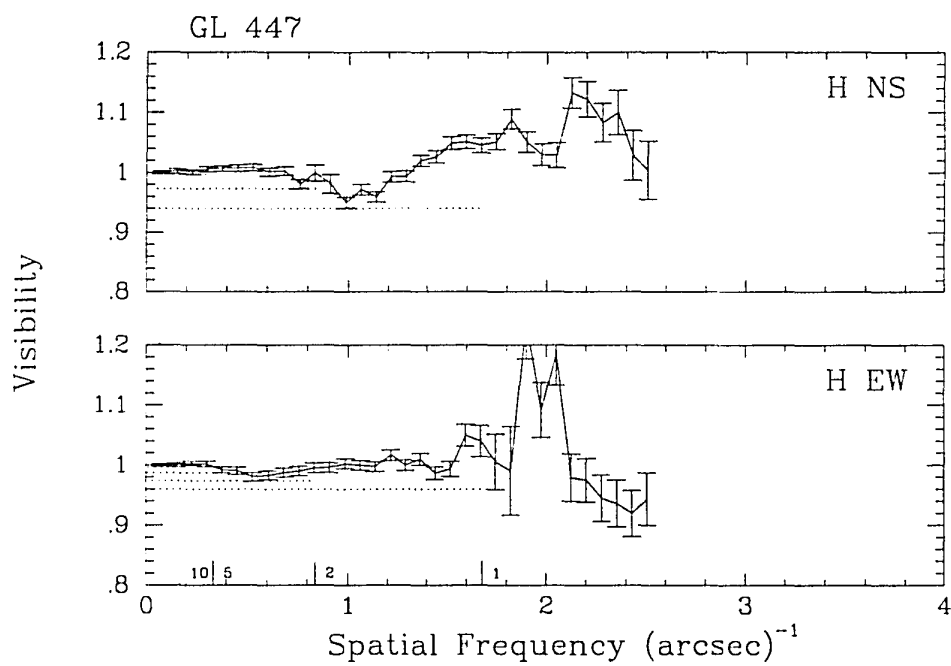


Figure 3.48 Visibility curves for GL 447.

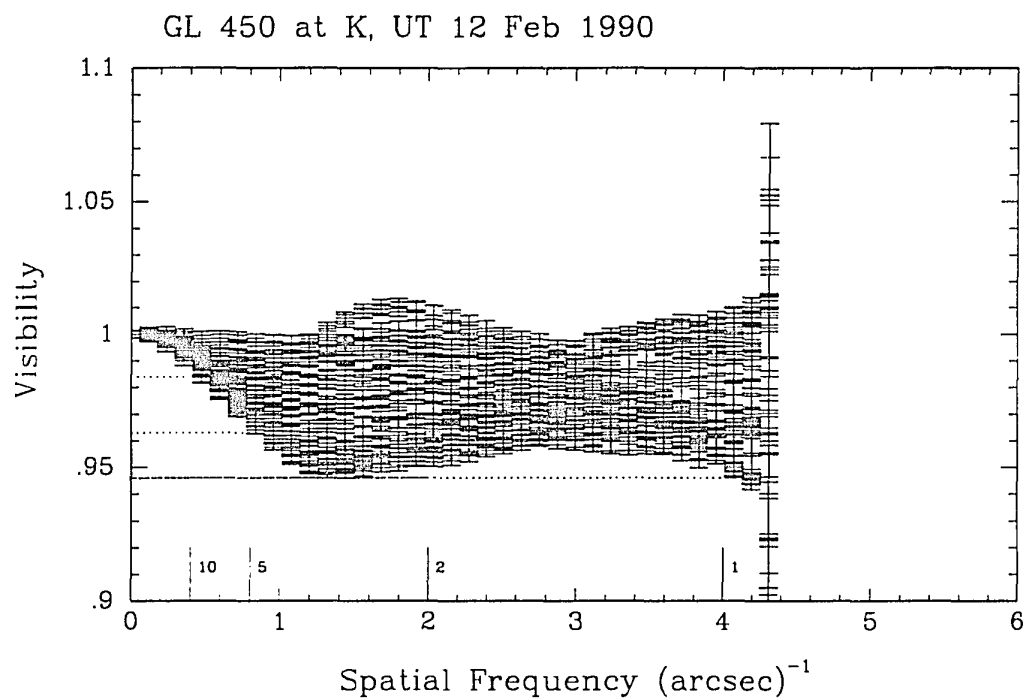


Figure 3.49 Visibility curves for GL 450.

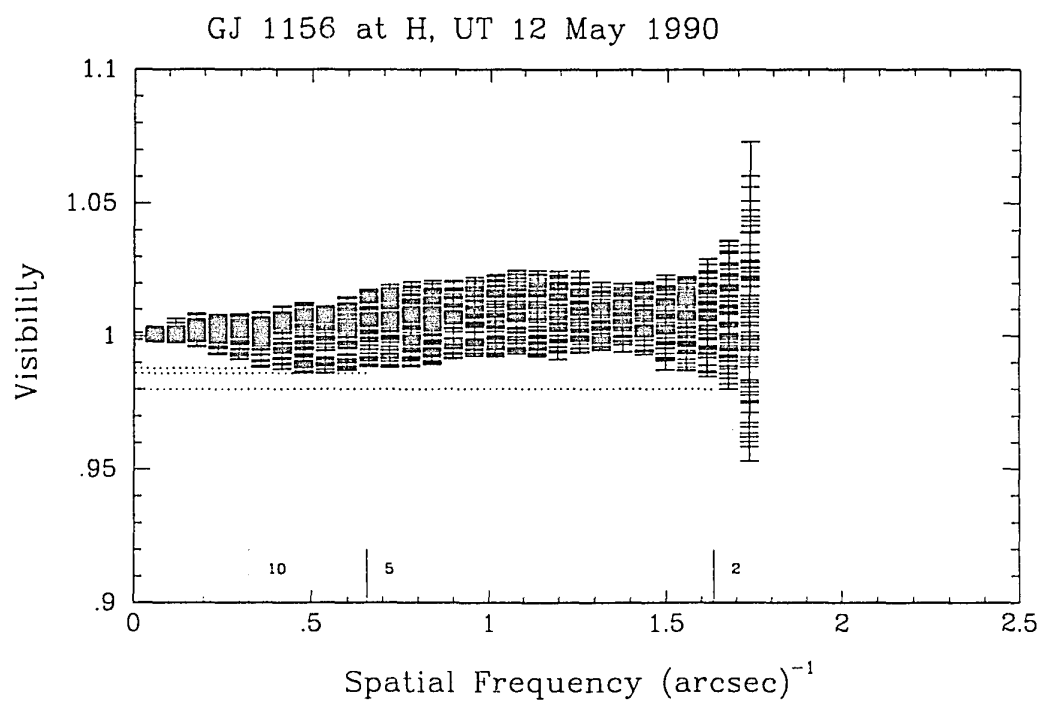


Figure 3.50 Visibility curves for GJ 1156.

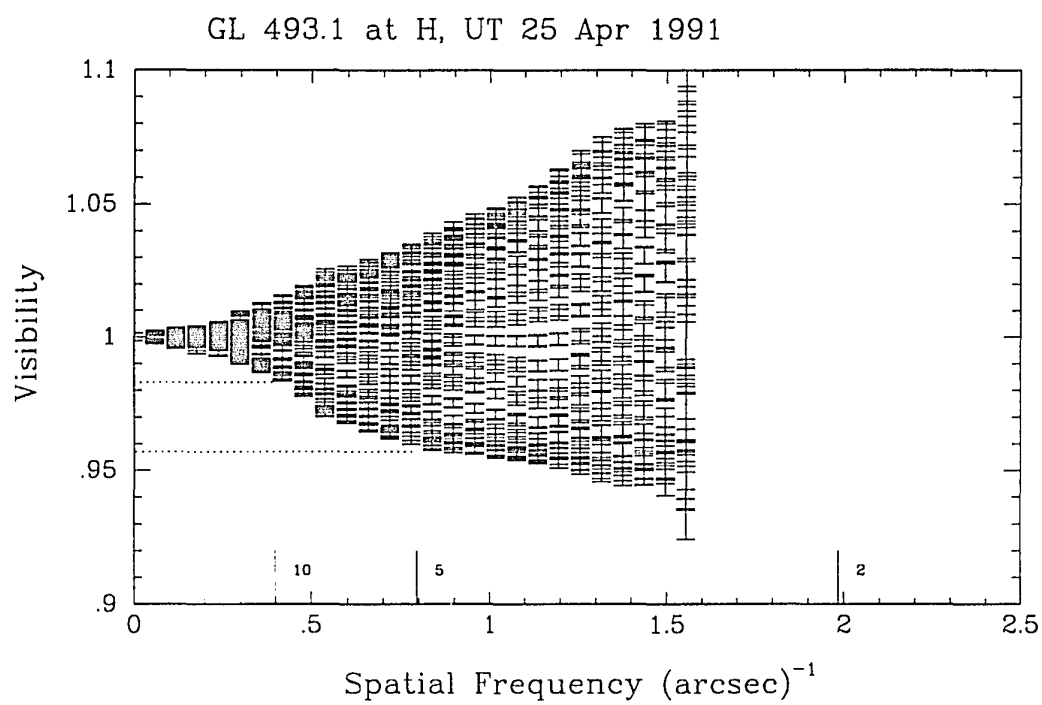


Figure 3.51 Visibility curves for GL 493.1.

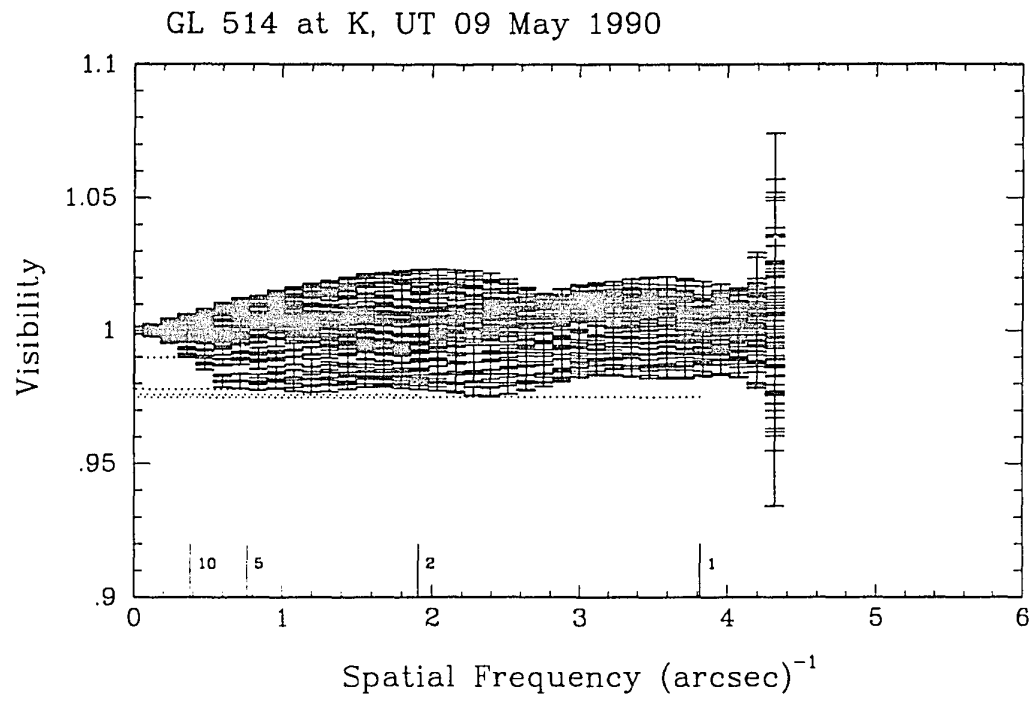


Figure 3.52 Visibility curves for GL 514.

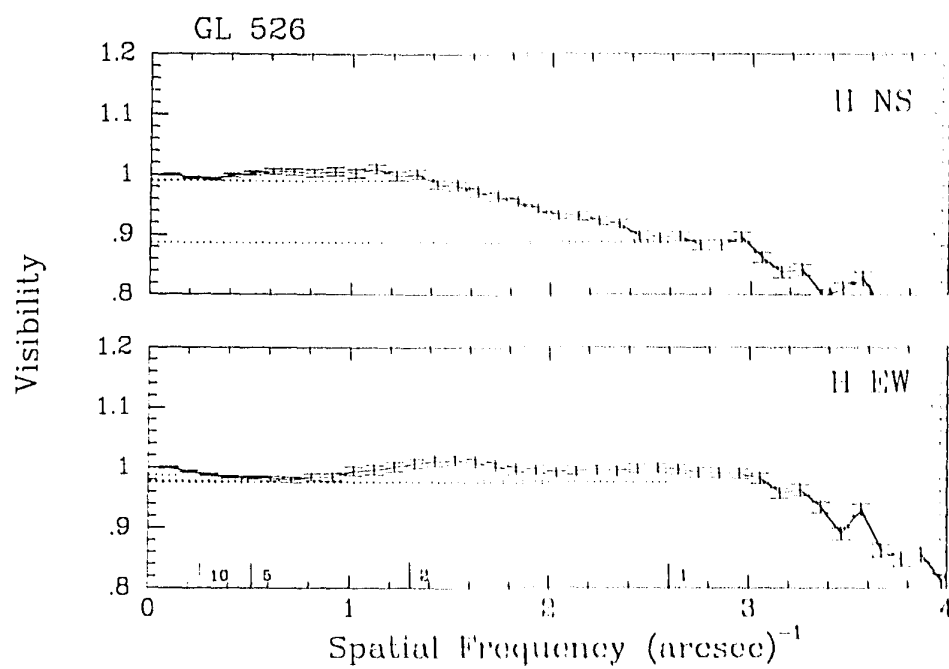


Figure 3.53 Visibility curves for GL 526.

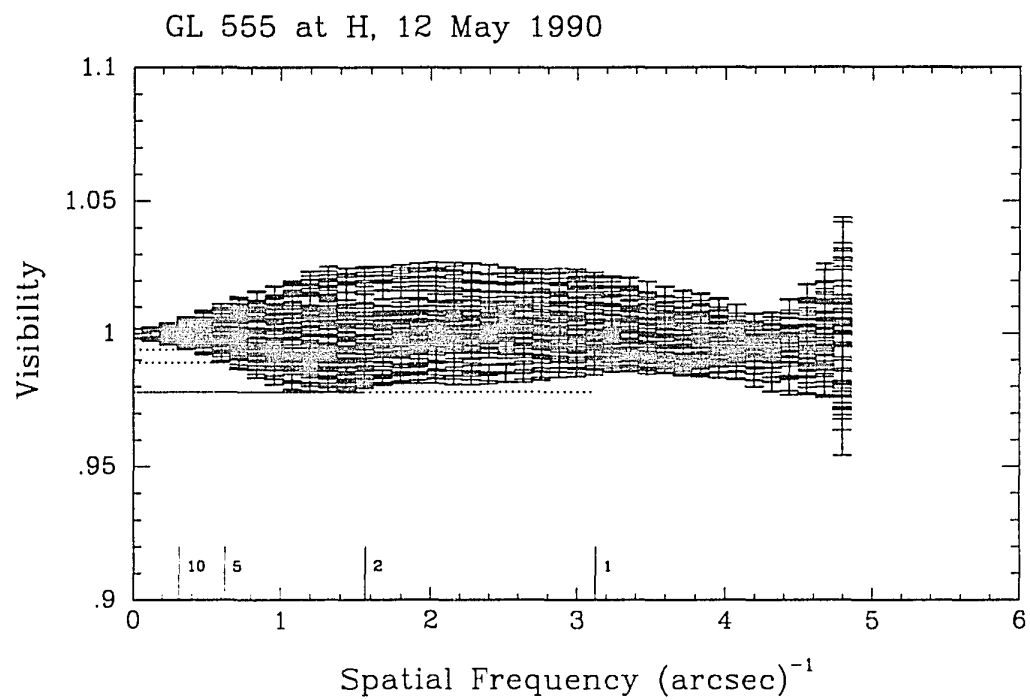


Figure 3.54 Visibility curves for GL 555.

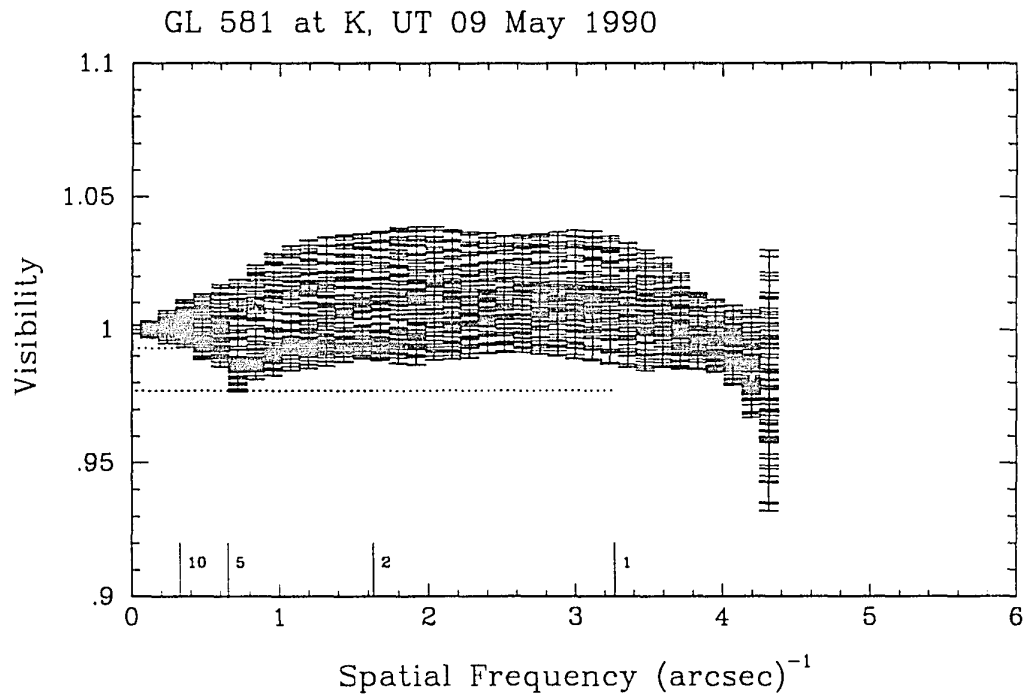


Figure 3.55 Visibility curves for GL 581.

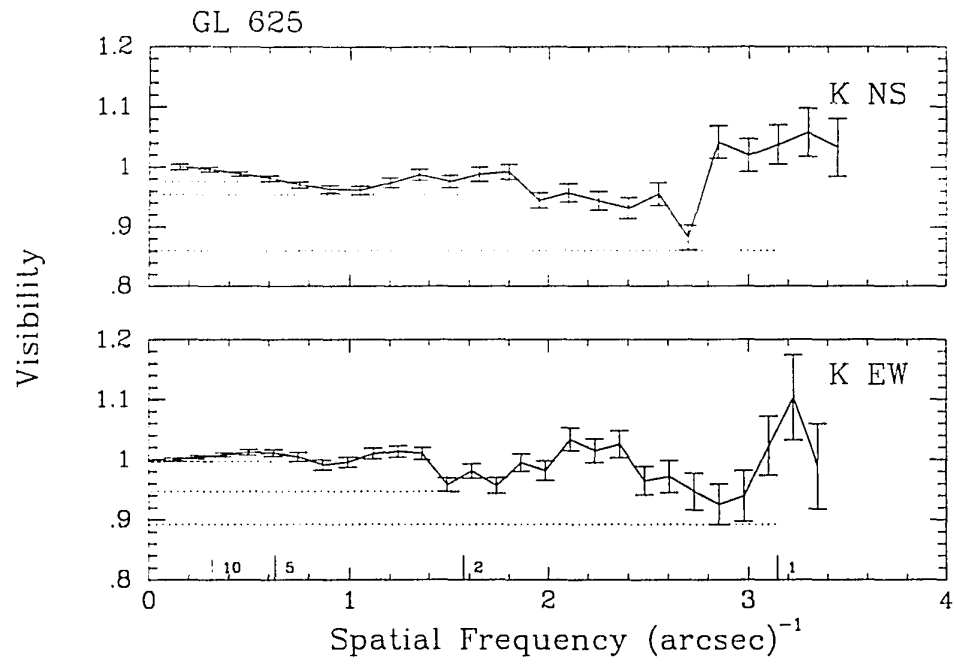


Figure 3.56 Visibility curves for GL 625.

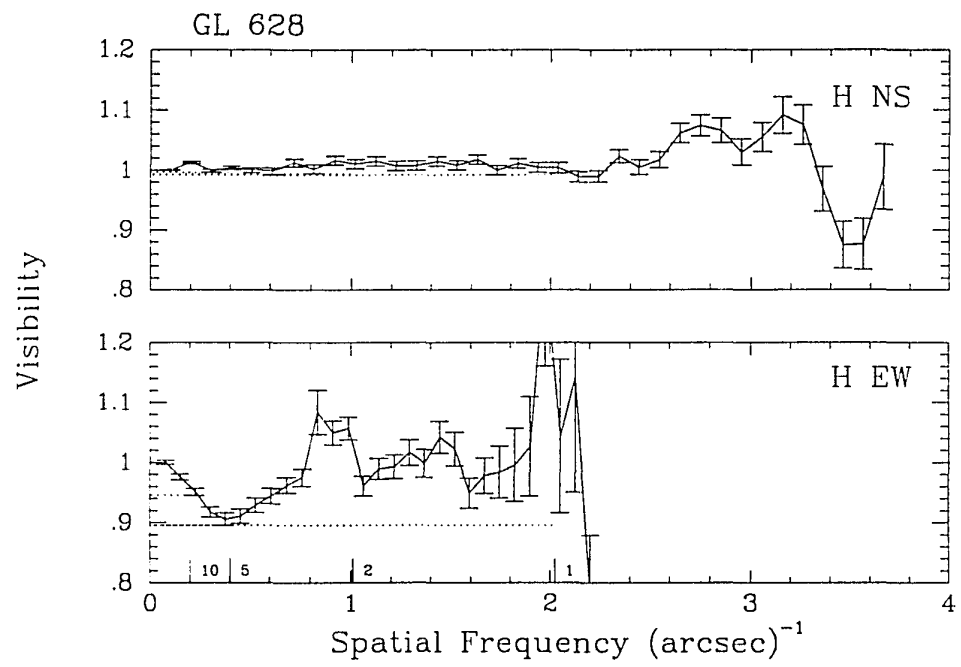


Figure 3.57 Visibility curves for GL 628.

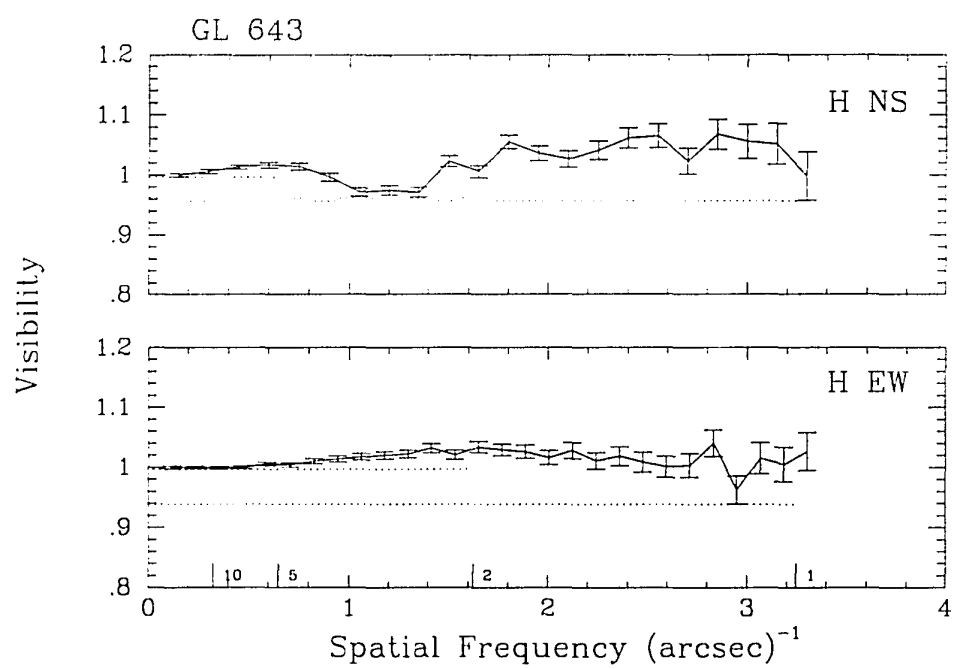


Figure 3.58 Visibility curves for GL 643.

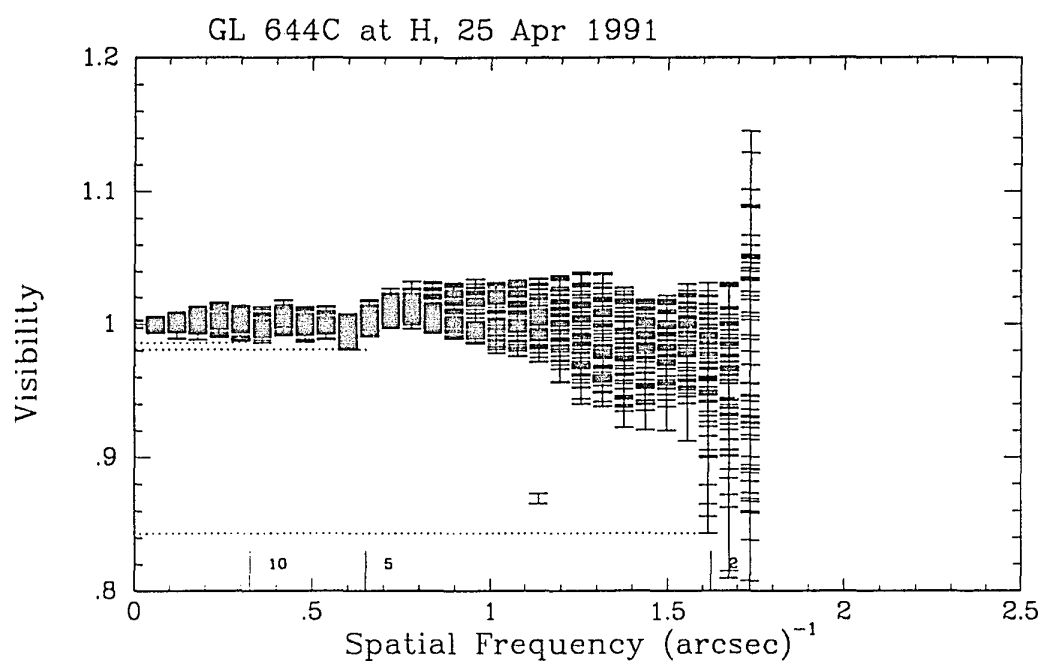


Figure 3.59 Visibility curves for GL 644C.

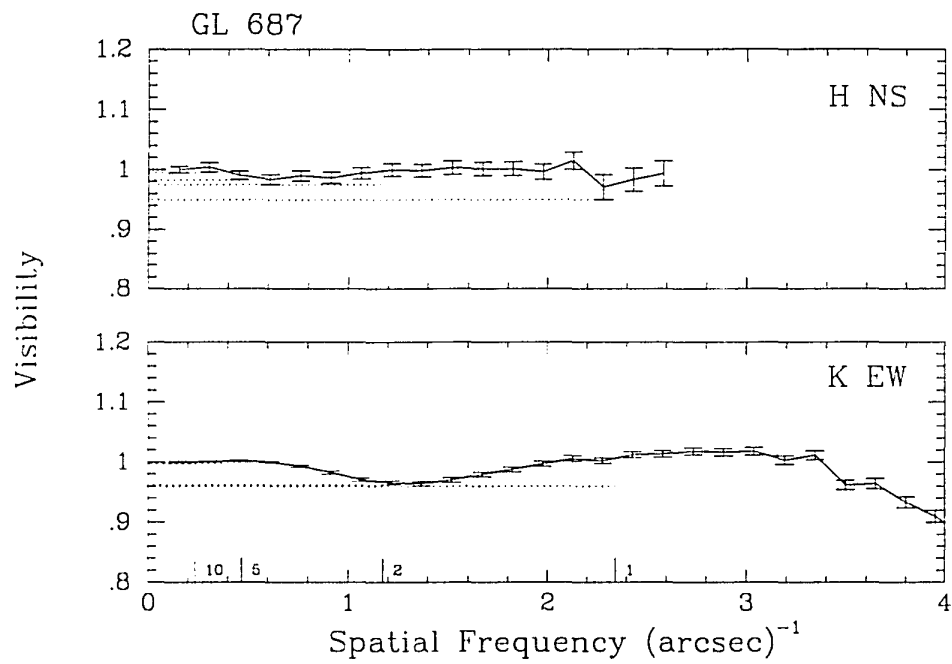


Figure 3.60 Visibility curves for GL 687.

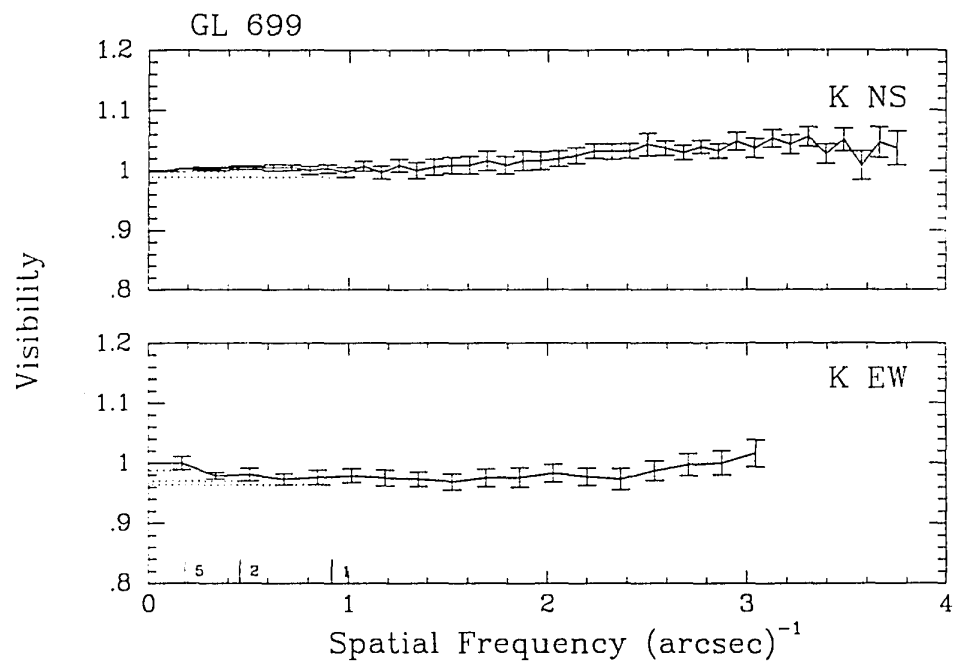


Figure 3.61 Visibility curves for GL 699.

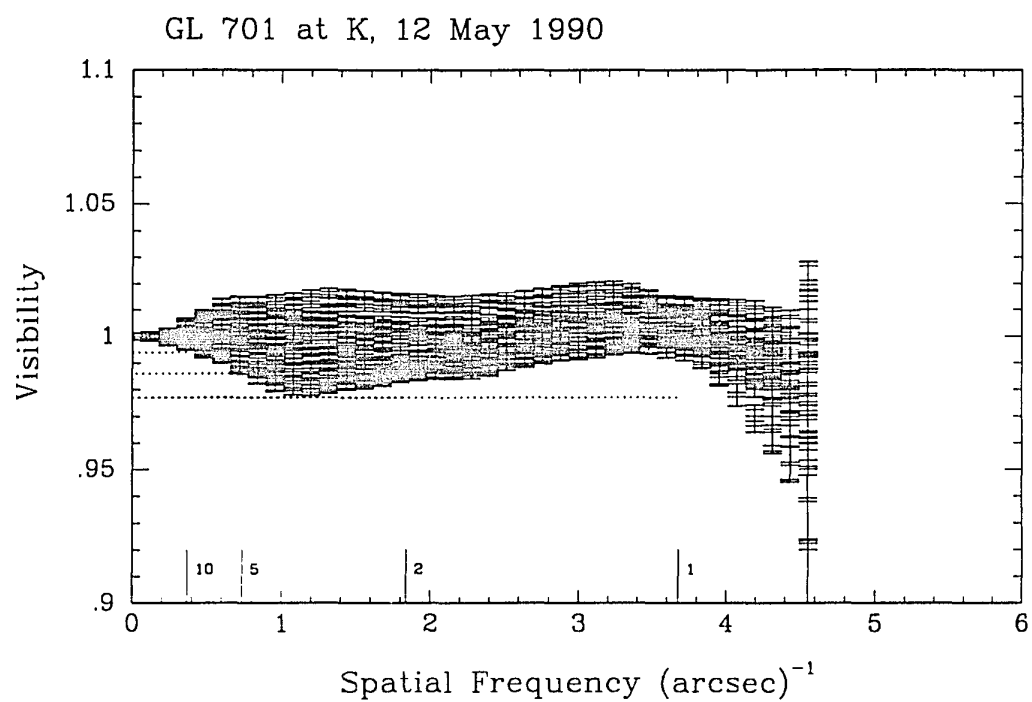


Figure 3.62 Visibility curves for GL 701.

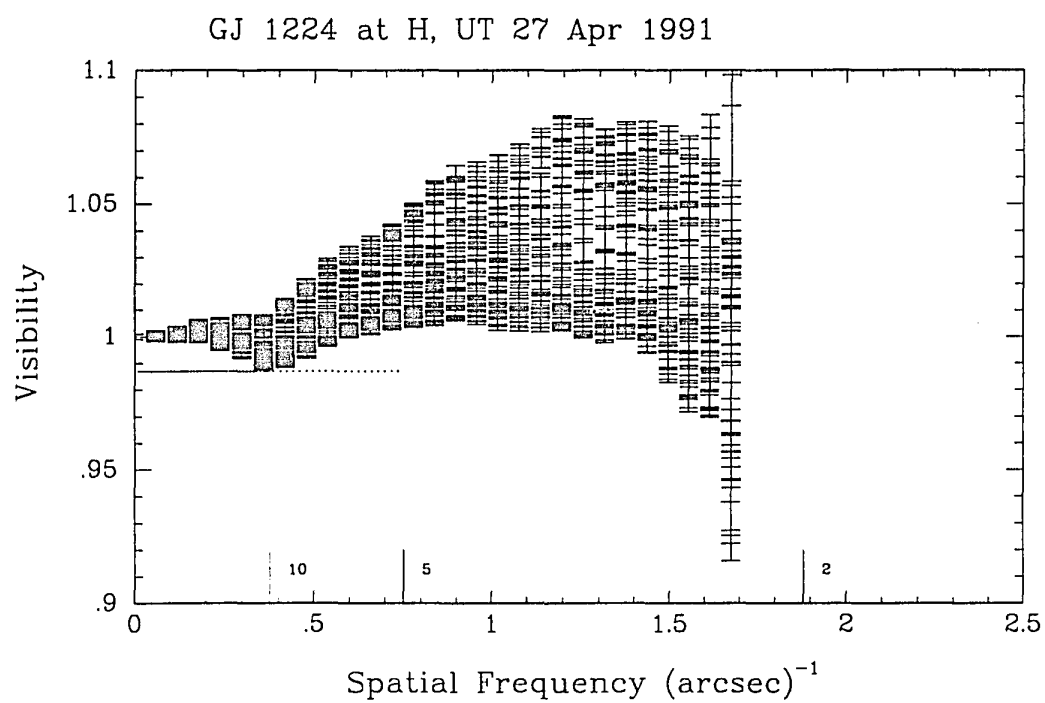


Figure 3.63 Visibility curves for GJ 1224.

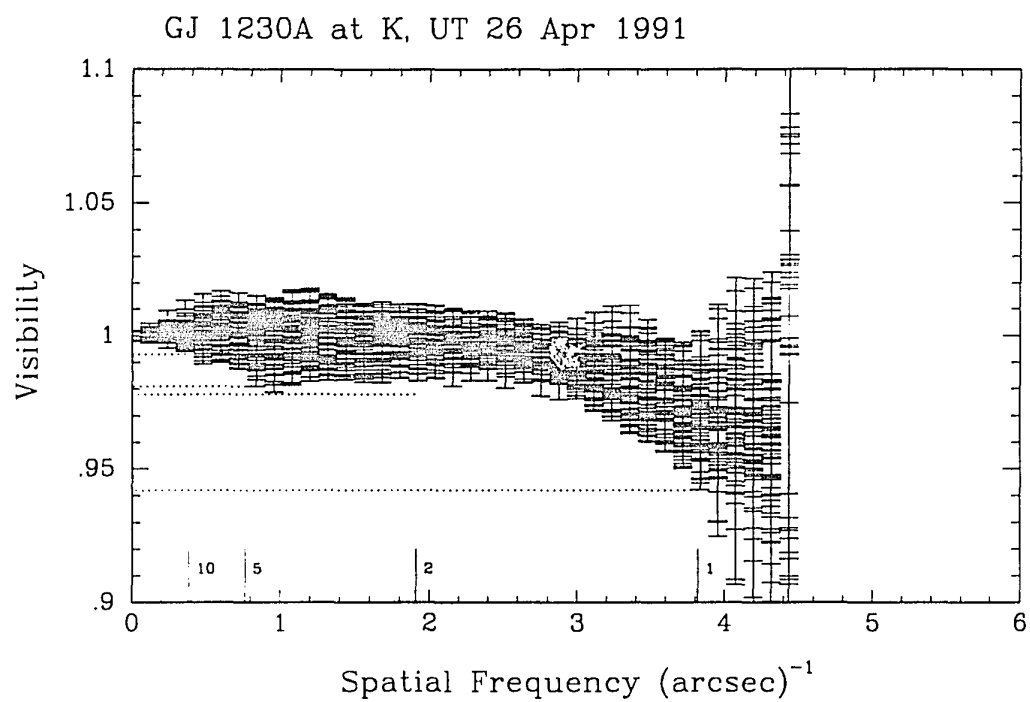


Figure 3.64 Visibility curves for GJ 1230A.

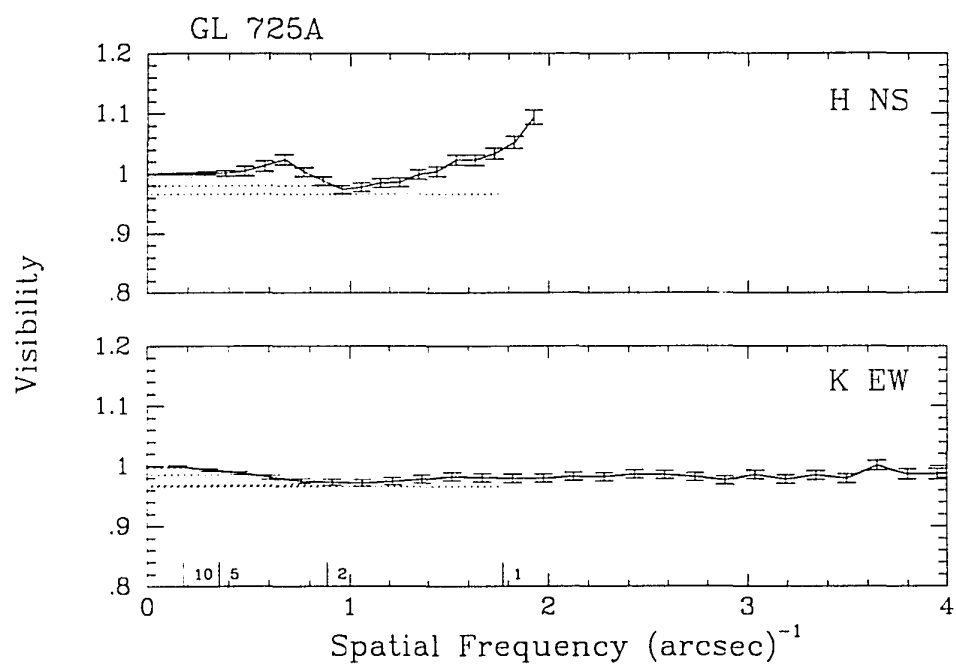


Figure 3.65 Visibility curves for GL 725A.

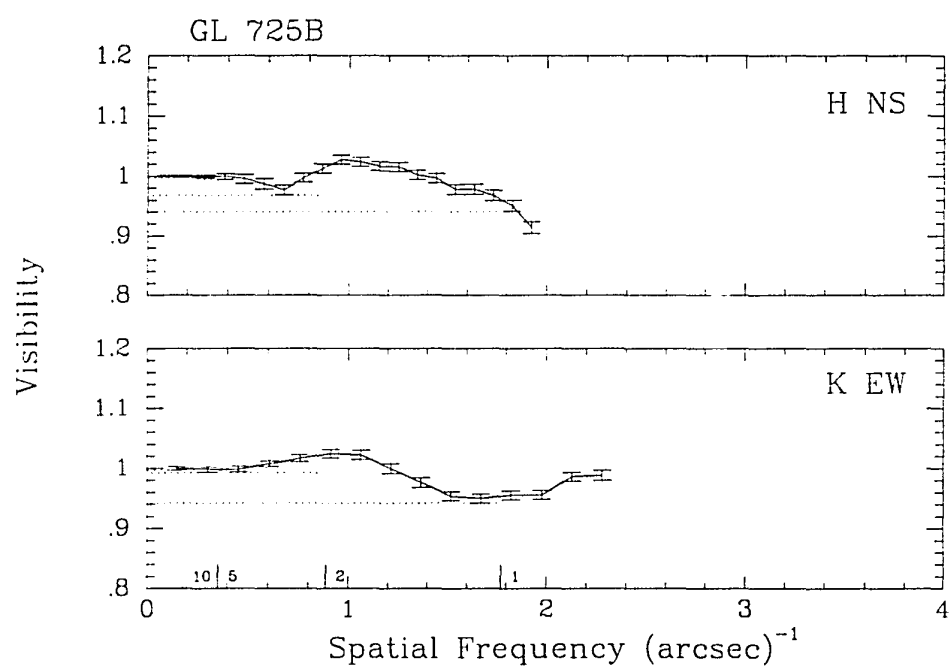


Figure 3.66 Visibility curves for GL 725B.

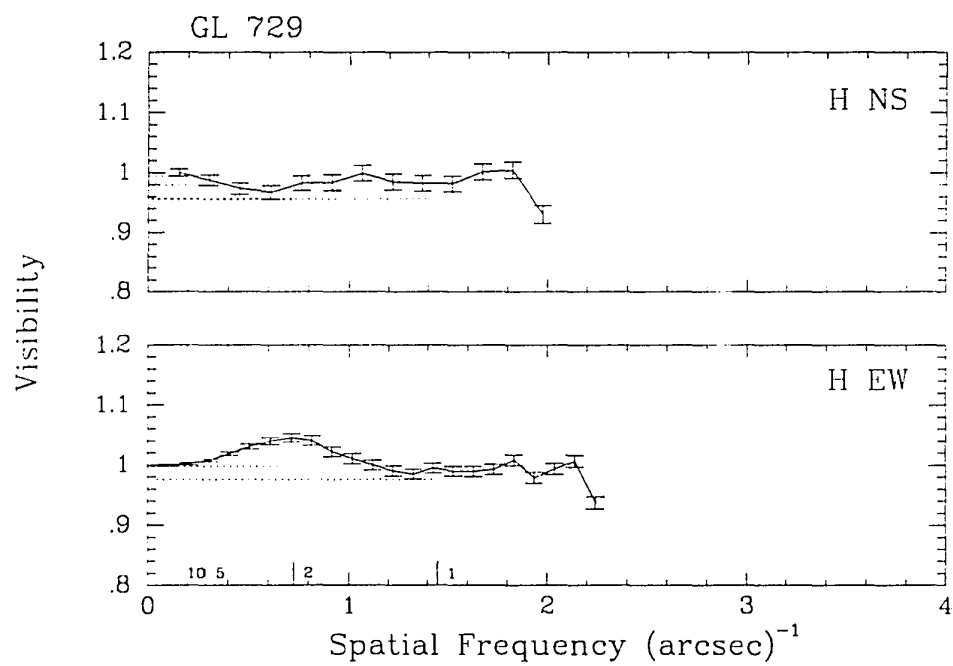


Figure 3.67 Visibility curves for GL 729.

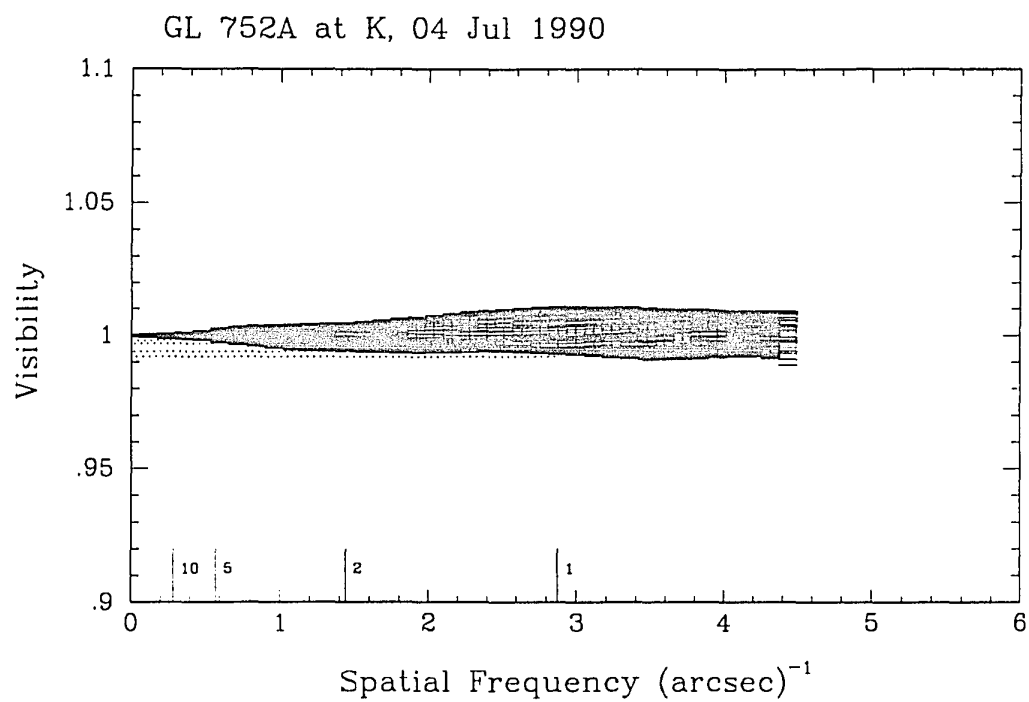


Figure 3.68 Visibility curves for GL 752A.

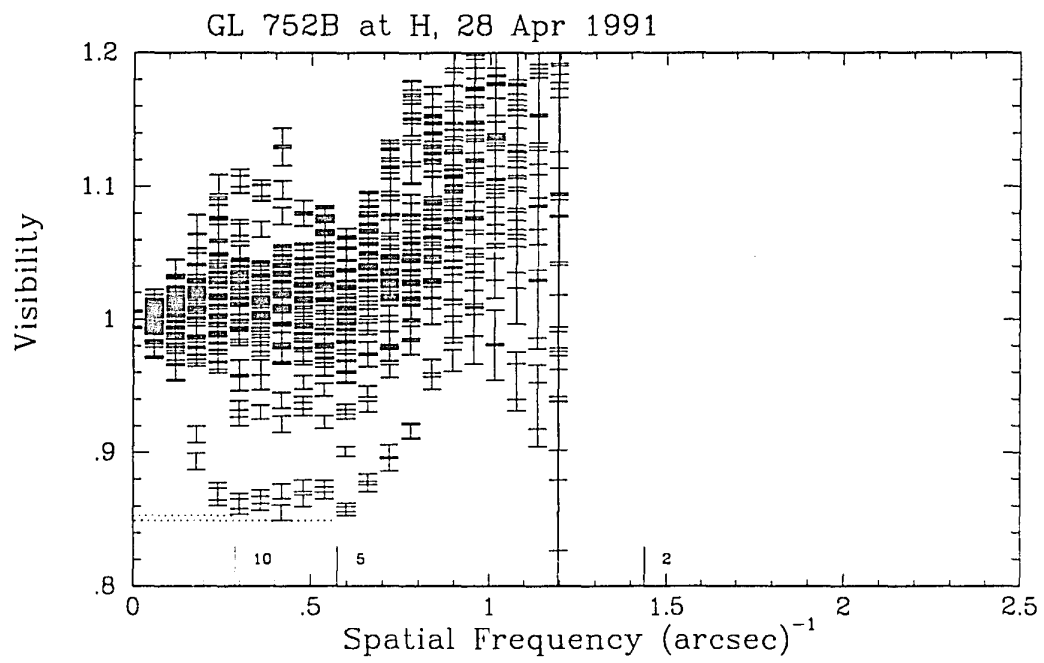


Figure 3.69 Visibility curves for GL 752B.

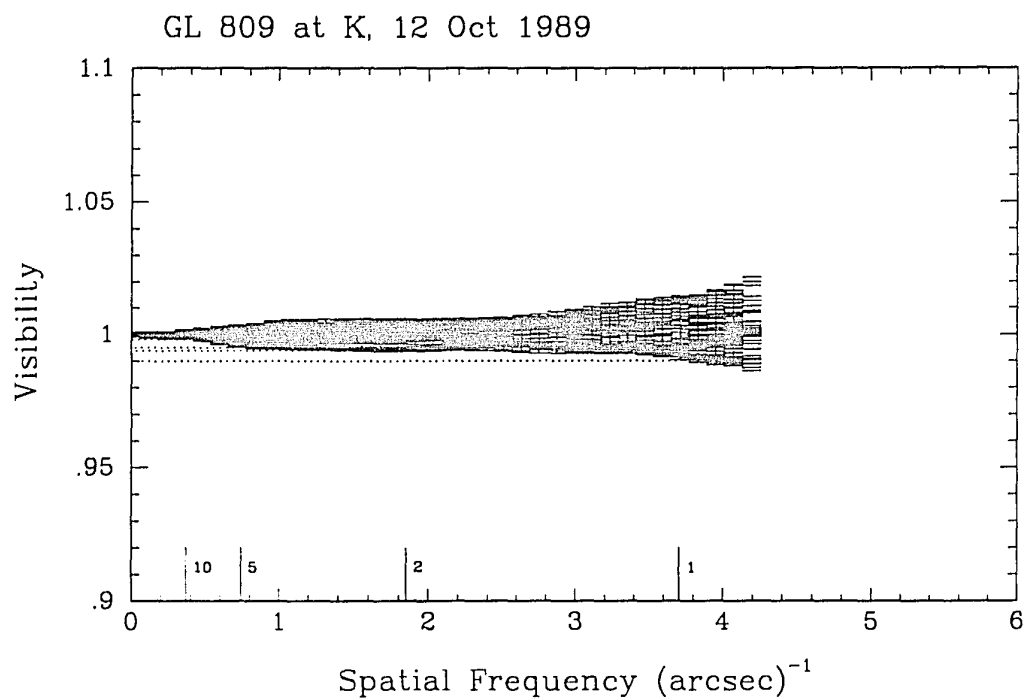


Figure 3.70 Visibility curves for GL 809.

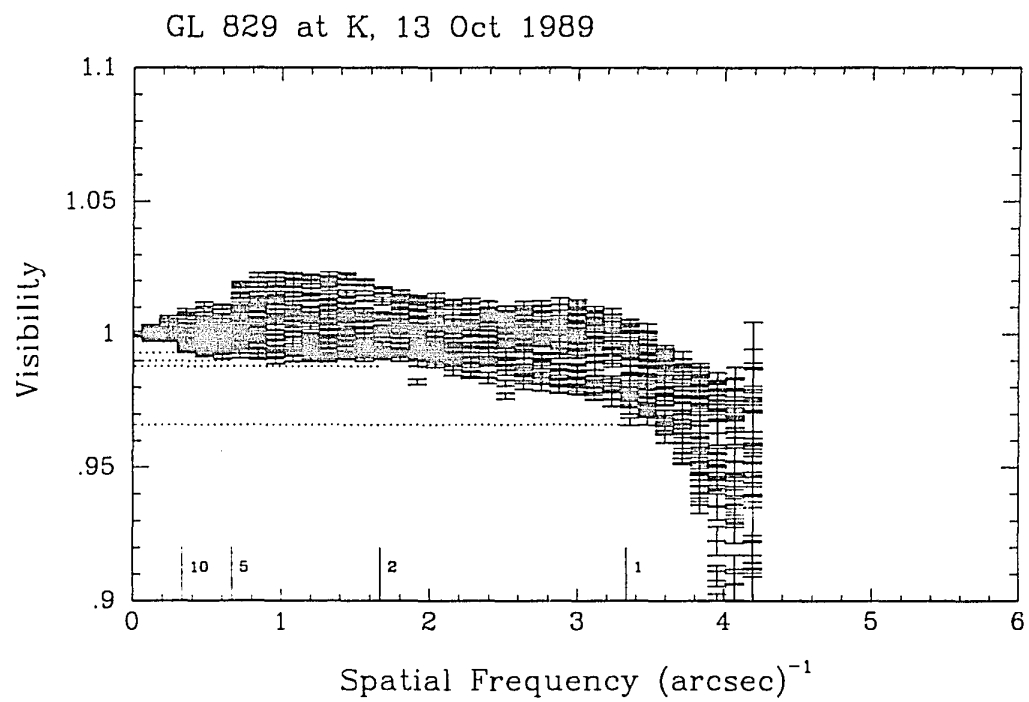


Figure 3.71 Visibility curves for GL 829.

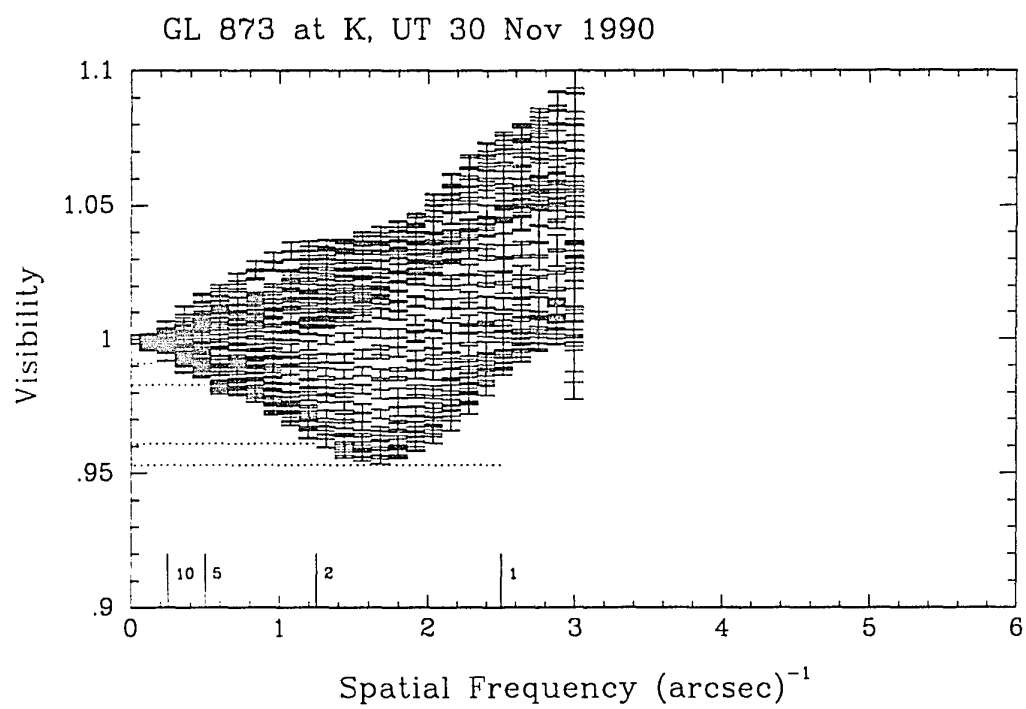


Figure 3.72 Visibility curves for GL 873.

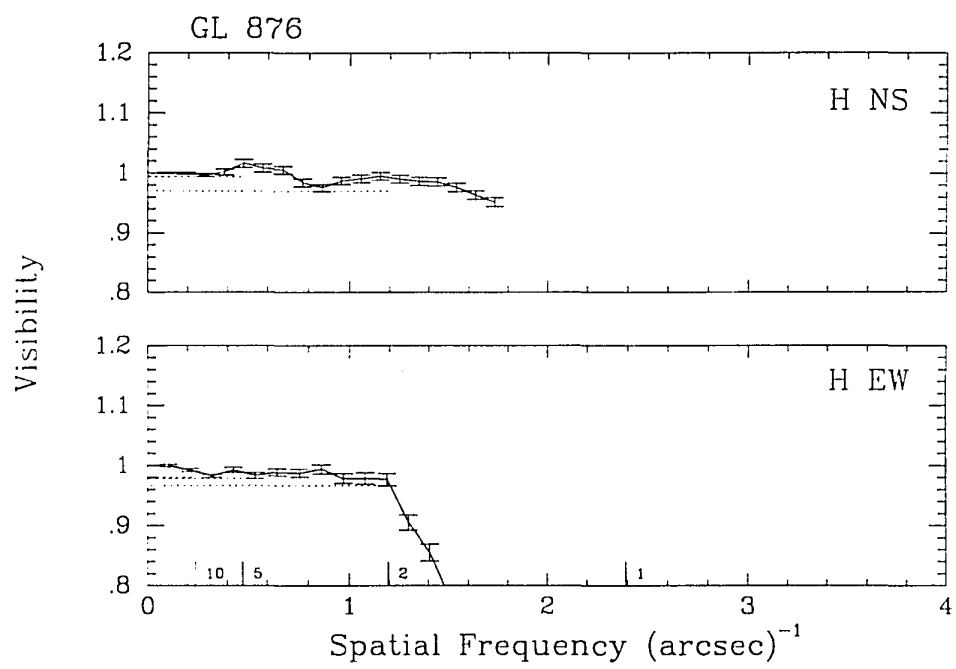


Figure 3.73 Visibility curves for GL 876.

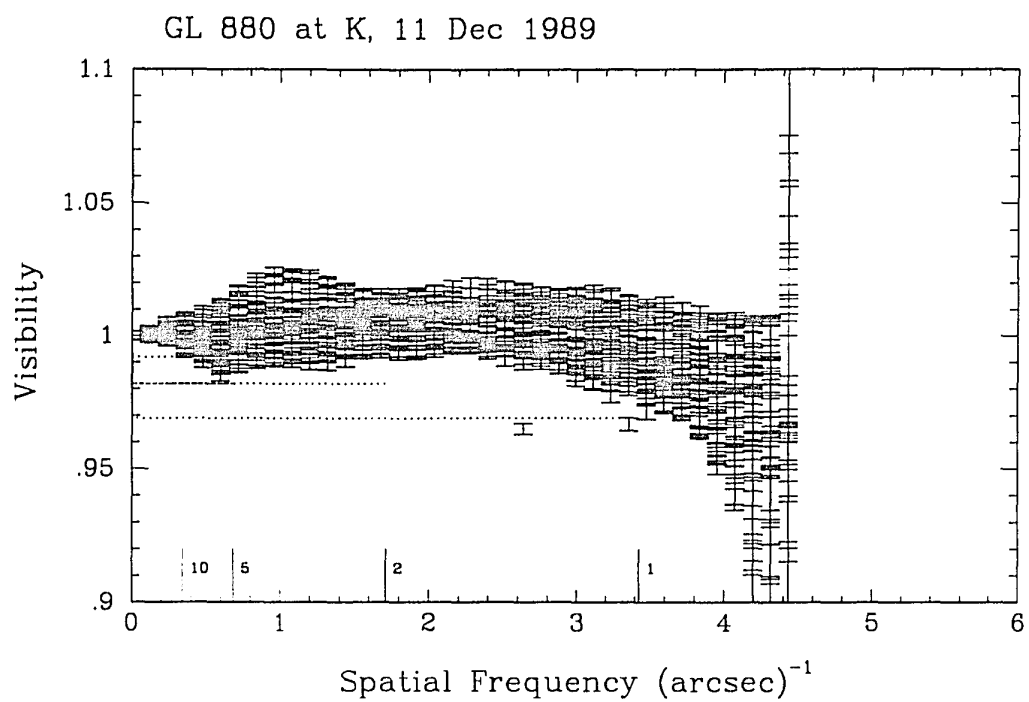


Figure 3.74 Visibility curves for GL 880.

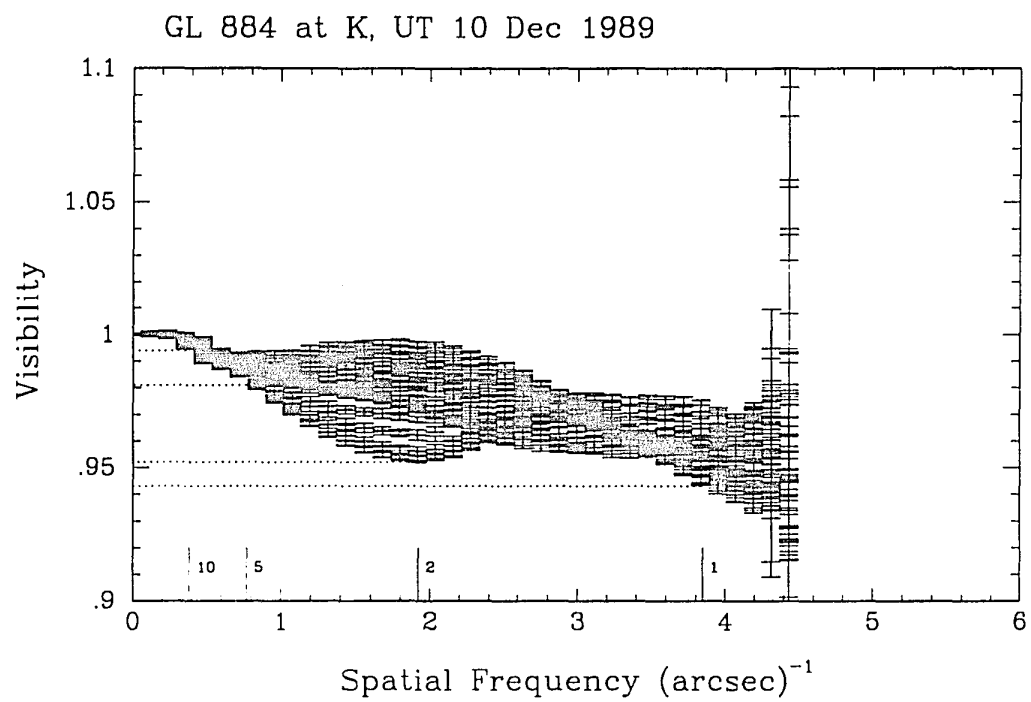


Figure 3.75 Visibility curves for GL 884.

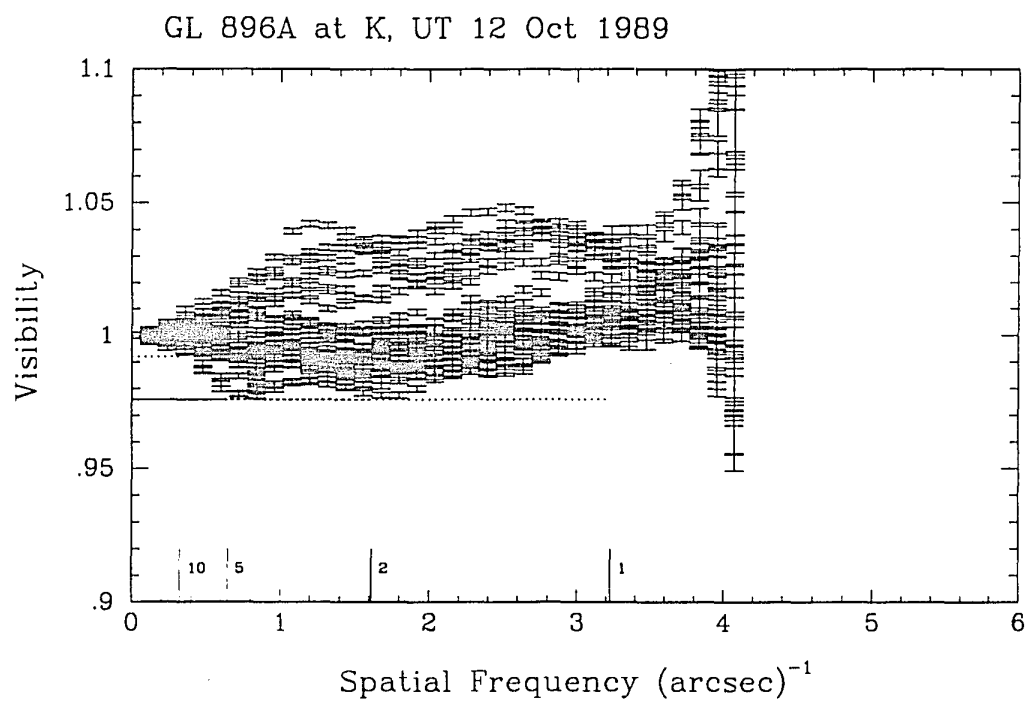


Figure 3.76 Visibility curves for GL 896A.

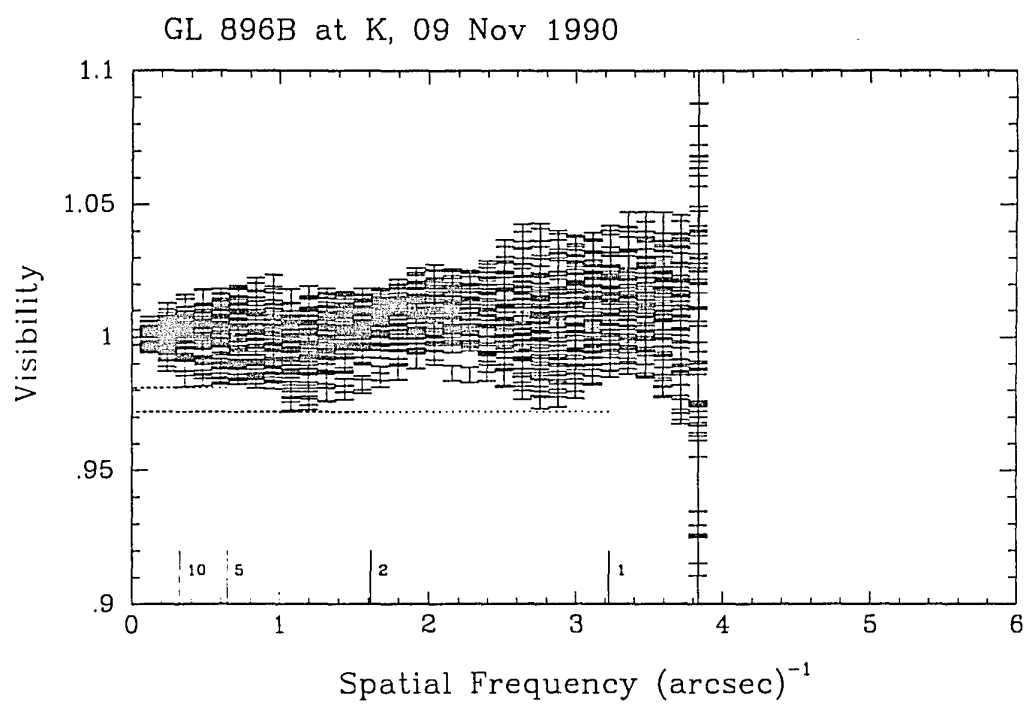


Figure 3.77 Visibility curves for GL 896B.

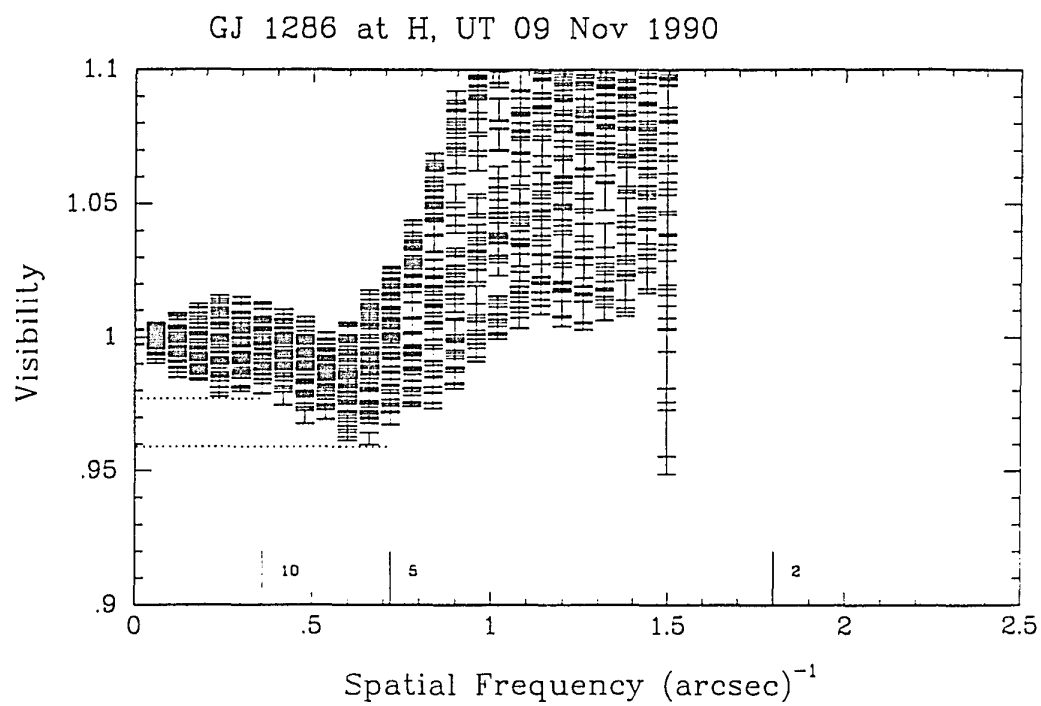


Figure 3.78 Visibility curves for GJ 1286.

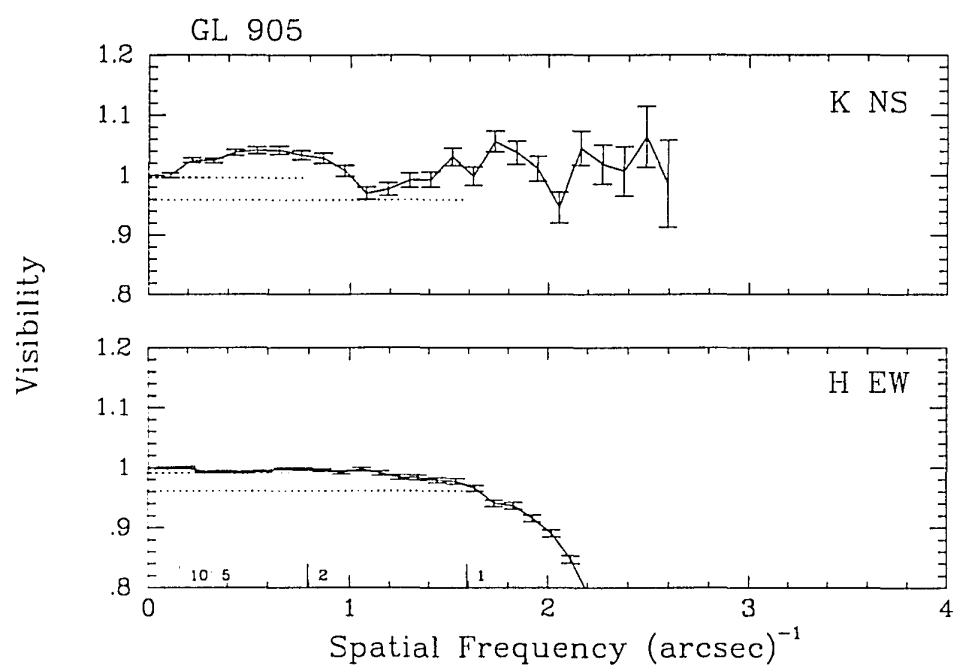


Figure 3.79 Visibility curves for GL 905.

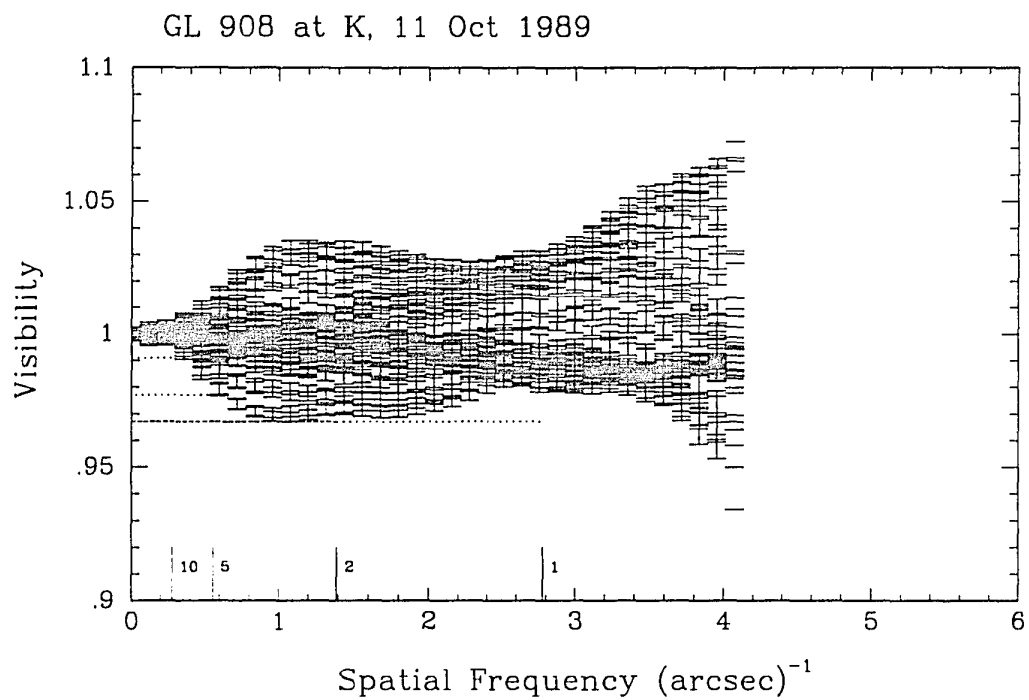


Figure 3.80 Visibility curves for GL 908.

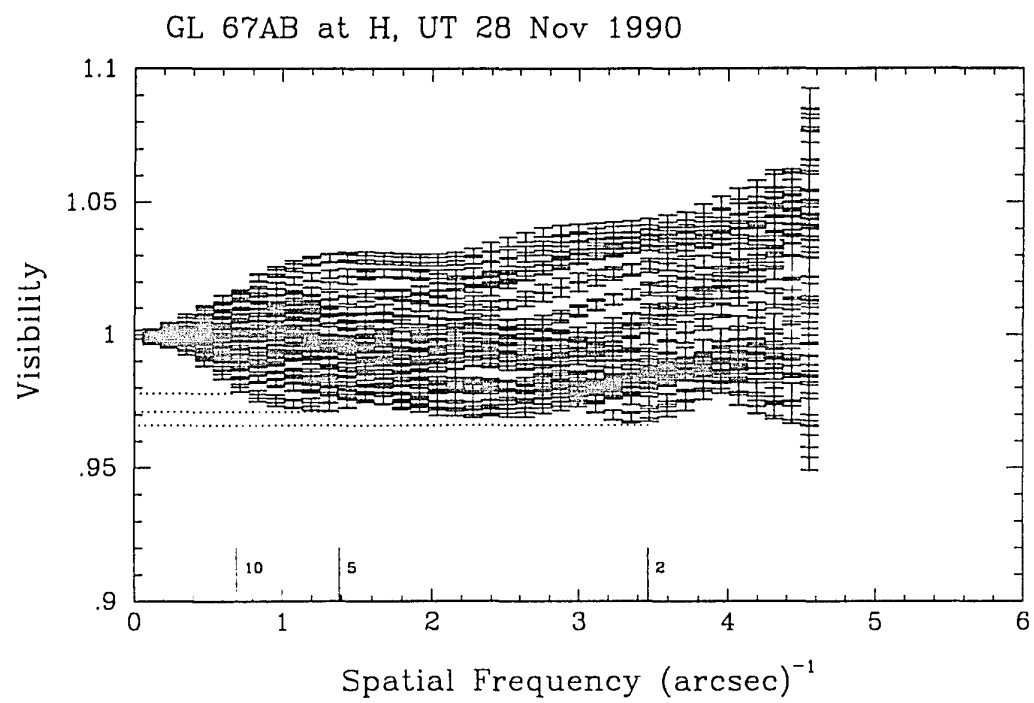


Figure 3.81 Detectable companion limit tests for GL 67AB at H using the 2D visibility curves.

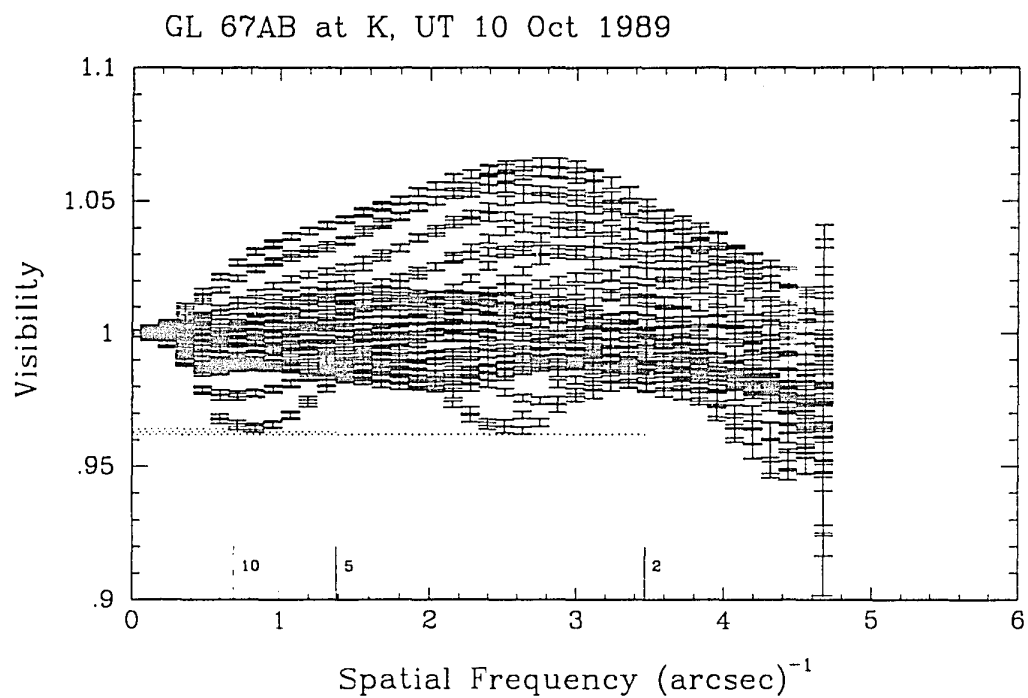


Figure 3.82 Detectable companion limit tests for GL 67AB at K using the 2D visibility curves.

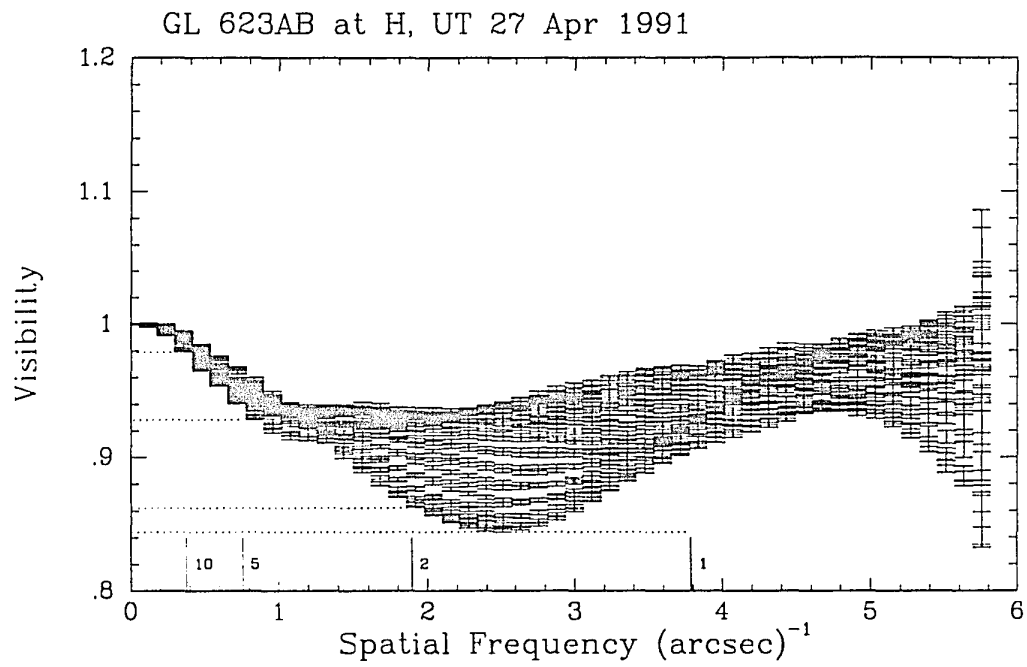


Figure 3.83 Detectable companion limit tests for GL 623AB at H using the 2D visibility curves.

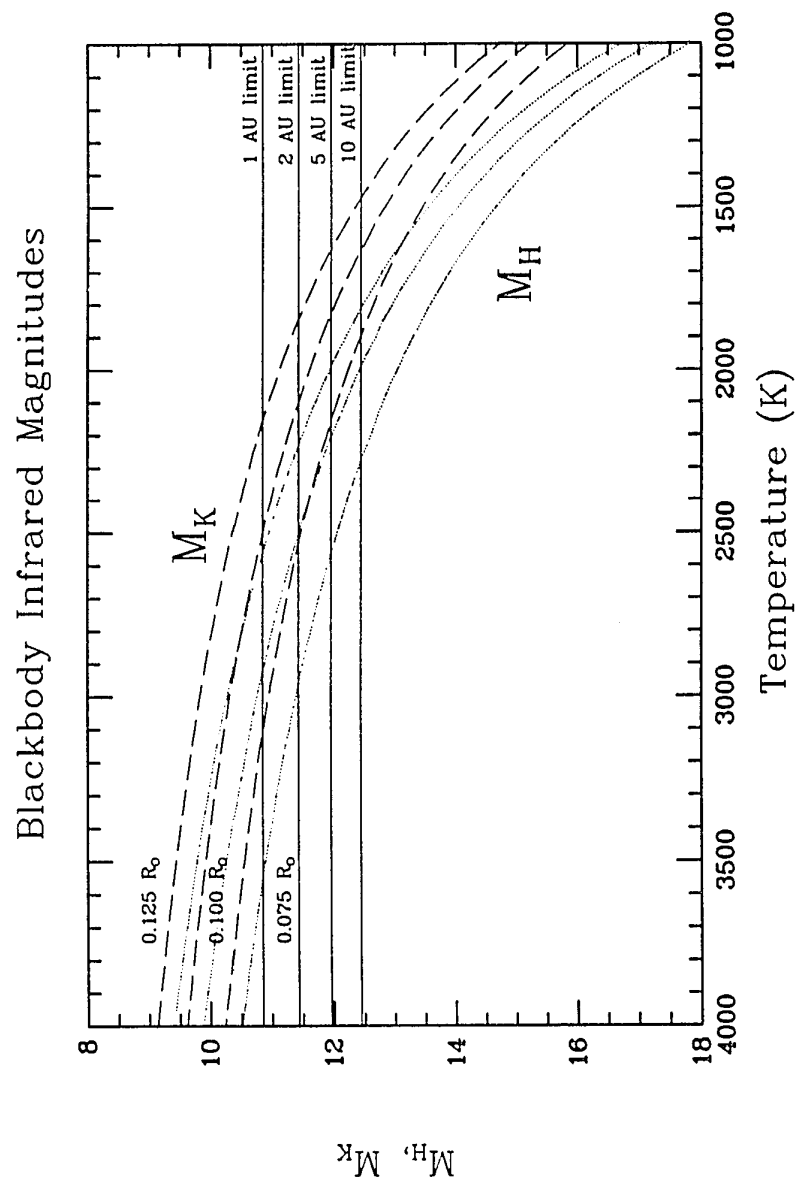


Figure 3.84 Blackbody infrared magnitudes for objects of radii 0.075, 0.100 and $0.125 R_\odot$. Dashed curves are for M_K , dotted curves for M_H . The survey M_K limits are labelled.

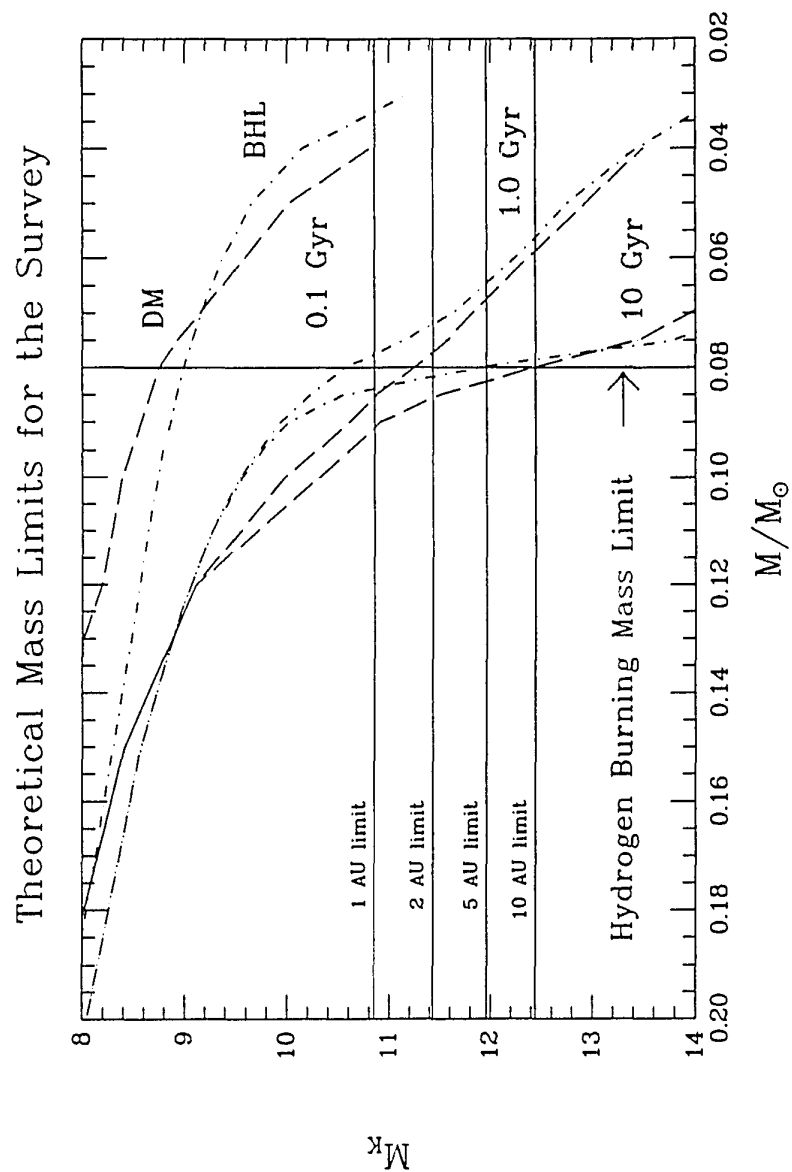


Figure 3.85 The theoretical mass-luminosity-age diagram is shown for very low mass stars and brown dwarfs. Theoretical isochrones are shown at ages of 0.1, 1.0 and 10 Gyr as found by D'Antona and Mazzitelli (1985, DM, dashed curves) and Burrows *et al.* (1989, BHL, dot-dash curves). The speckle survey M_K limits are shown.

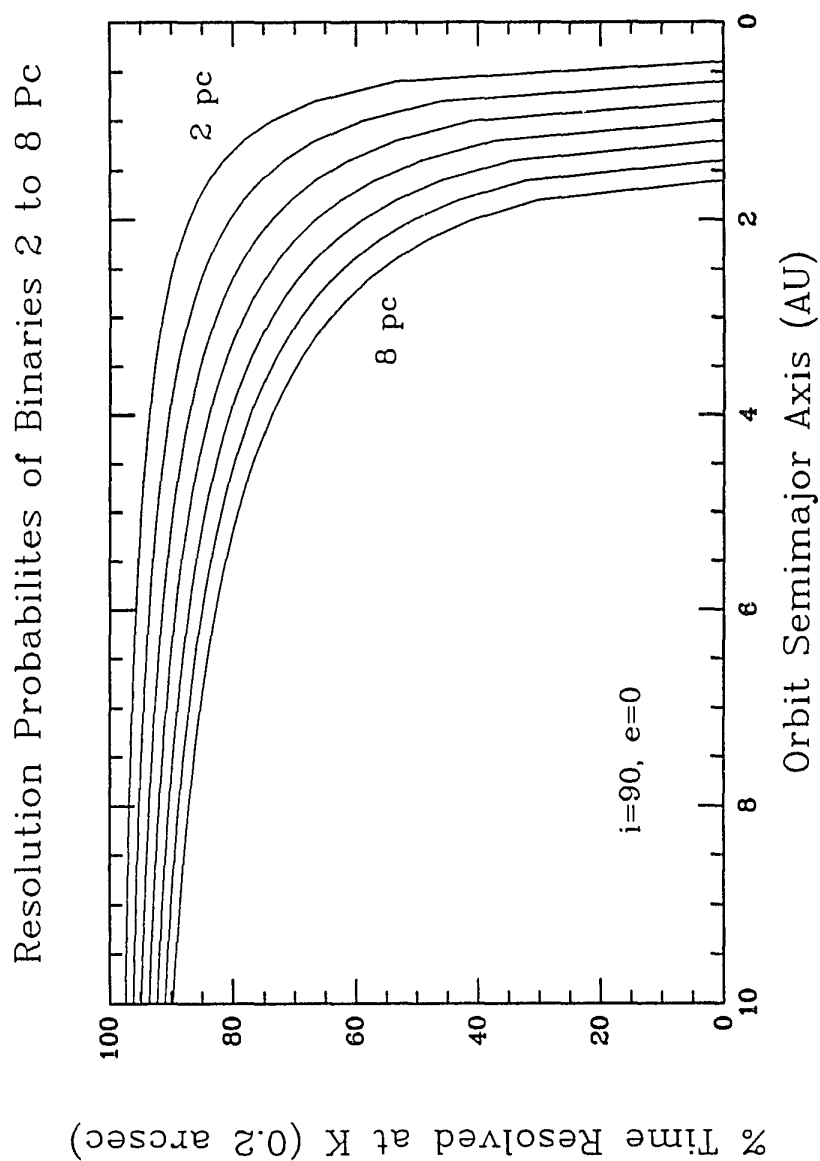


Figure 3.86 The percentage of time a secondary spends more than $0.2''$ from its primary is plotted as a function of distance (2 to 8 pc) for edge-on, circular orbits. A companion was deemed “observable” if it was more than $0.2''$, the diffraction limit of the SO 2.3m telescope at K, from the target star.

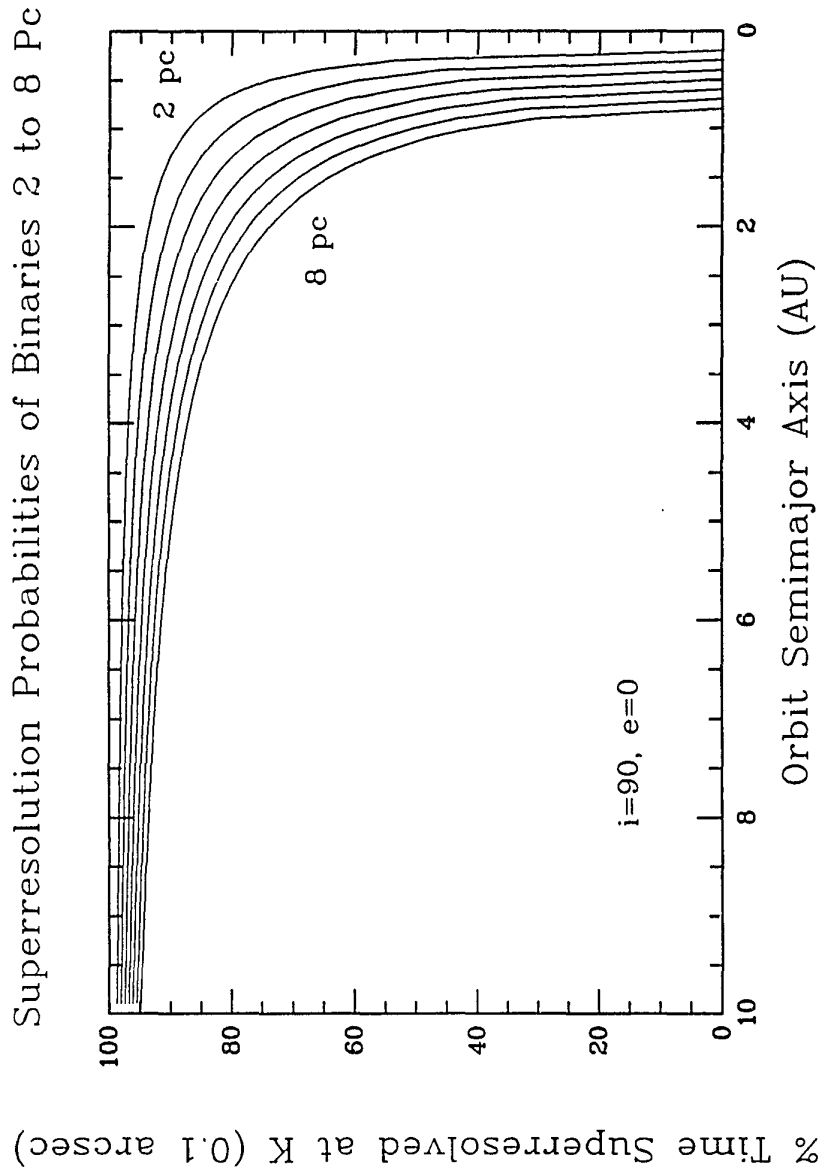


Figure 3.87 The percentage of time a secondary spends more than 0.1'' from its primary is plotted as a function of distance (2 to 8 pc) for edge-on, circular orbits. In this case, which is that adopted for the survey, a companion was deemed "observable" if it was able to be "superresolved" by the SO 2.3m telescope at K.

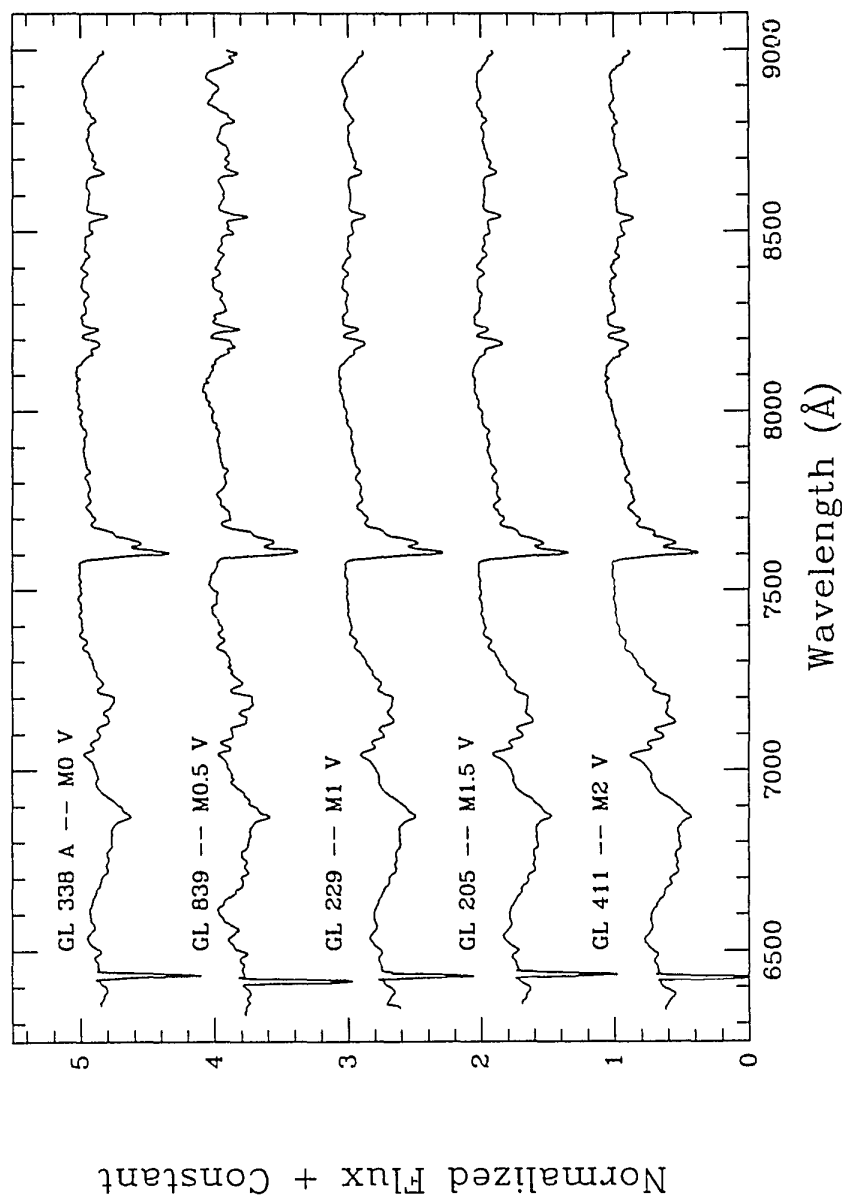
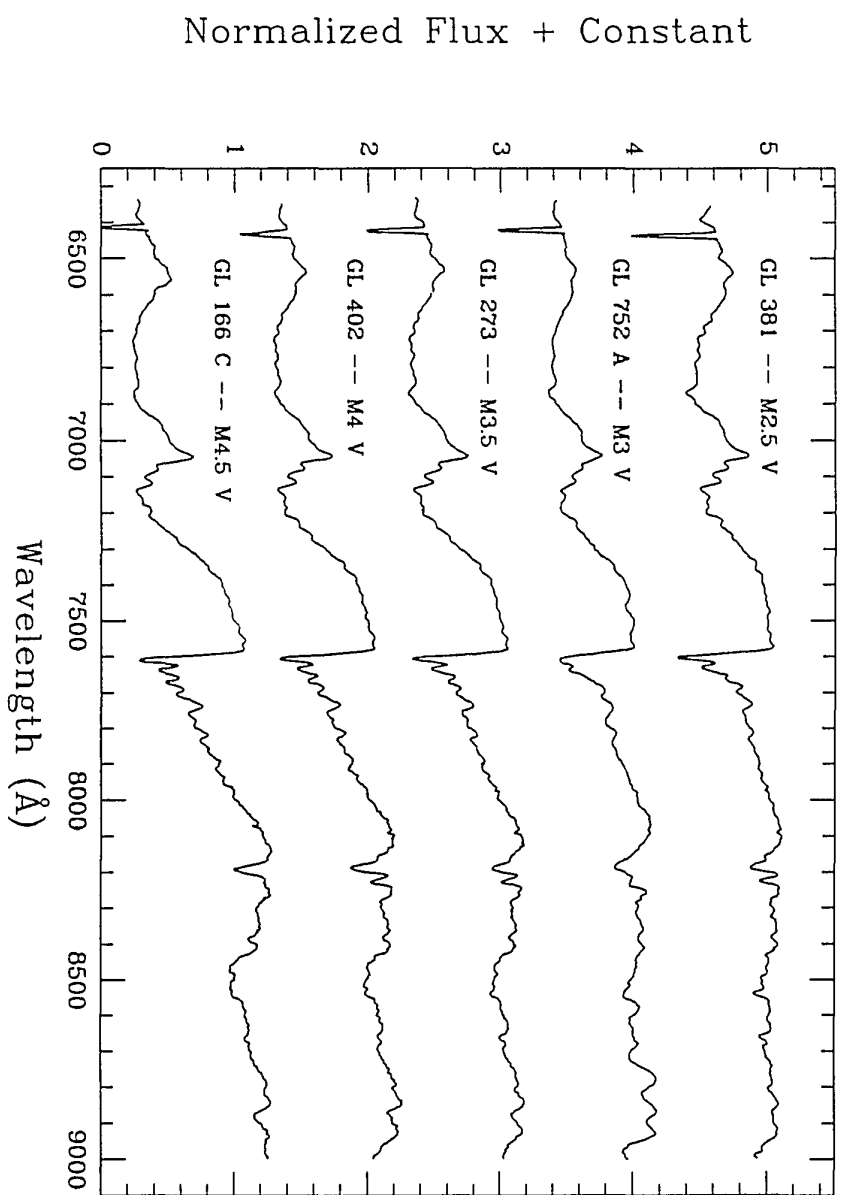
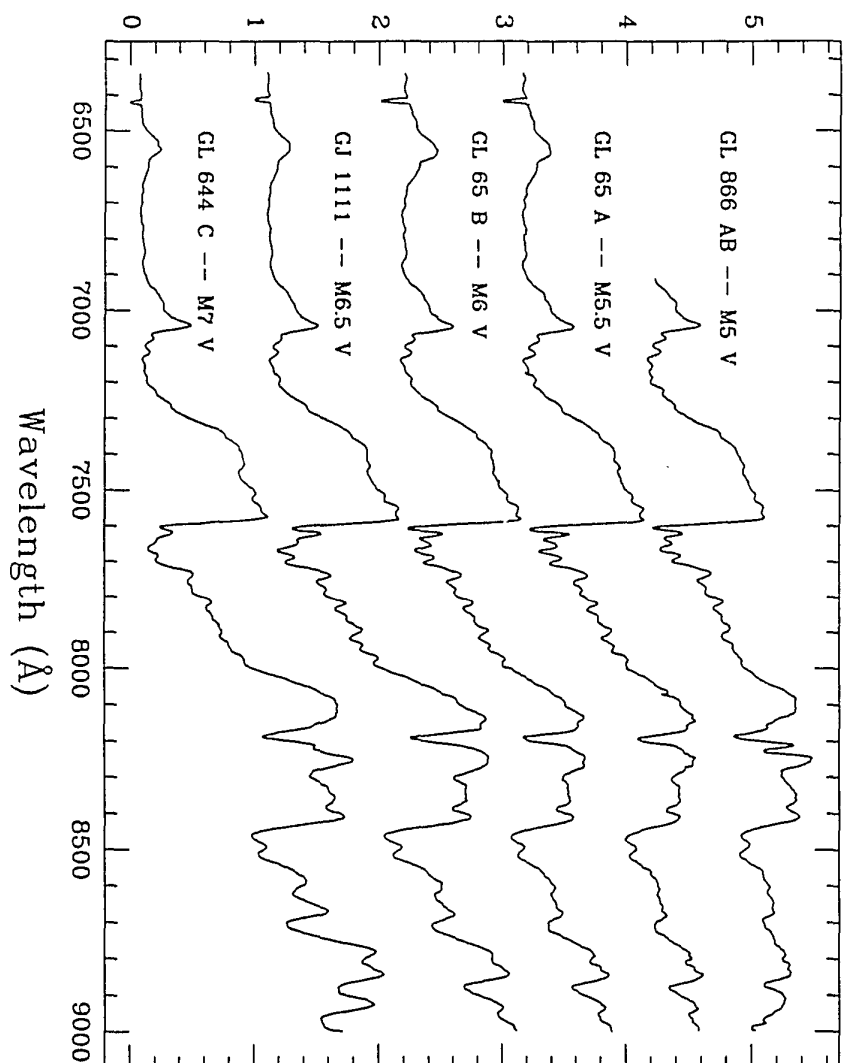
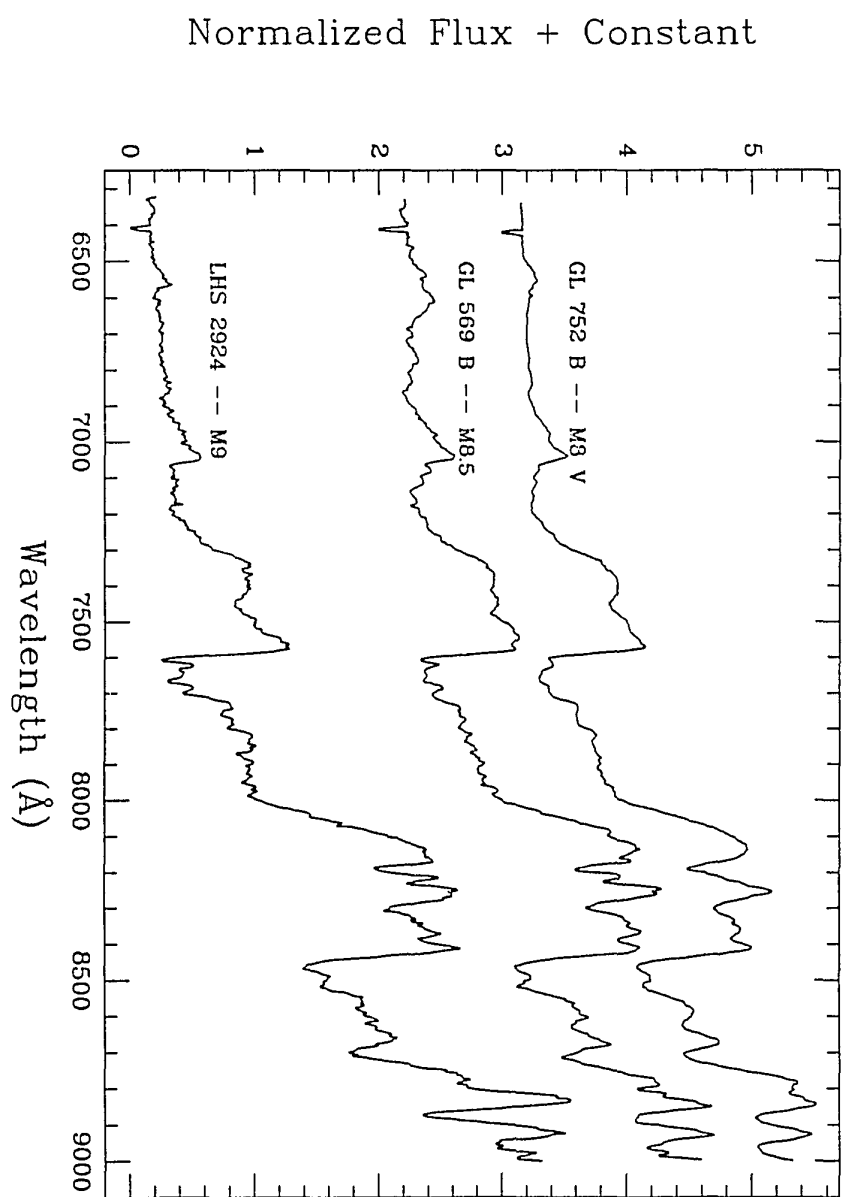


Figure 3.88 The standard spectral sequence for M0 to M9 dwarfs. See text for discussion.



Normalized Flux + Constant





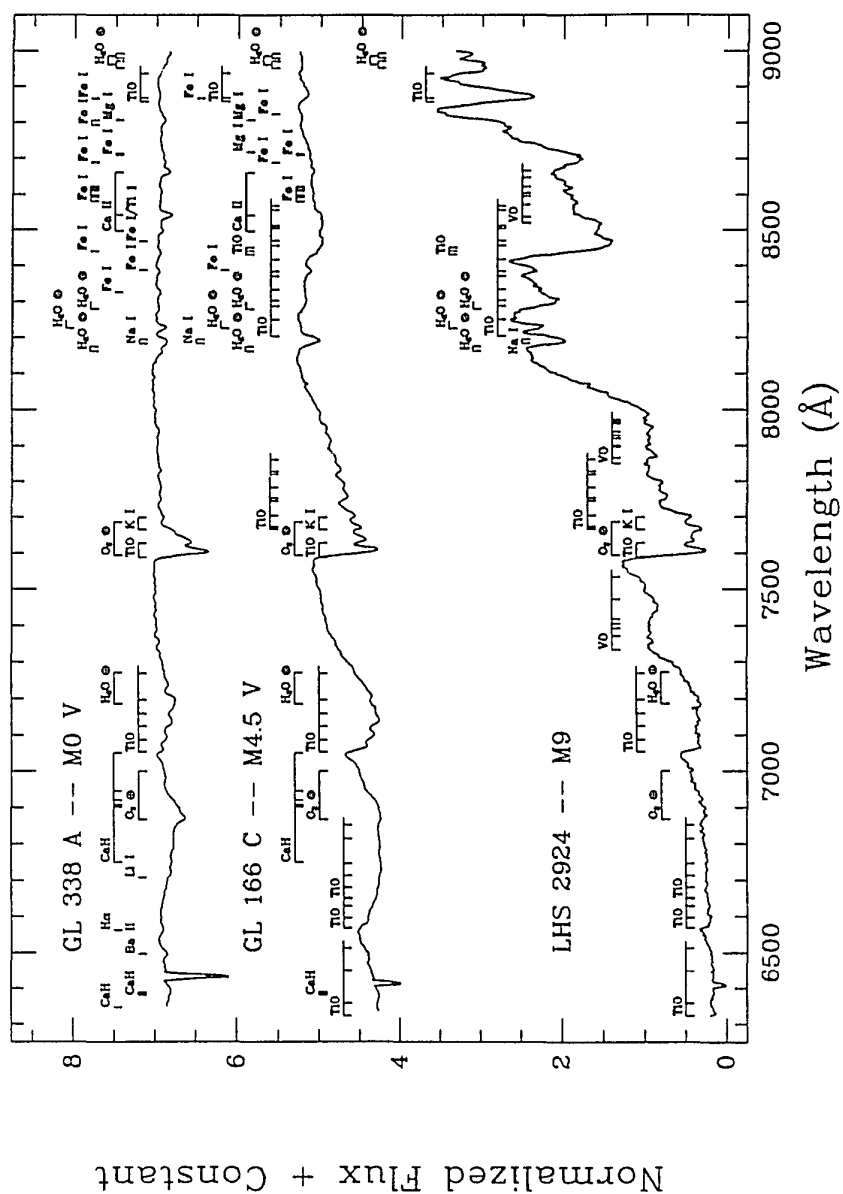


Figure 3.89 Examples of three dwarf spectra, with features labelled. Note the strong VO features evident in the spectrum of LHS 2924, a brown dwarf candidate.

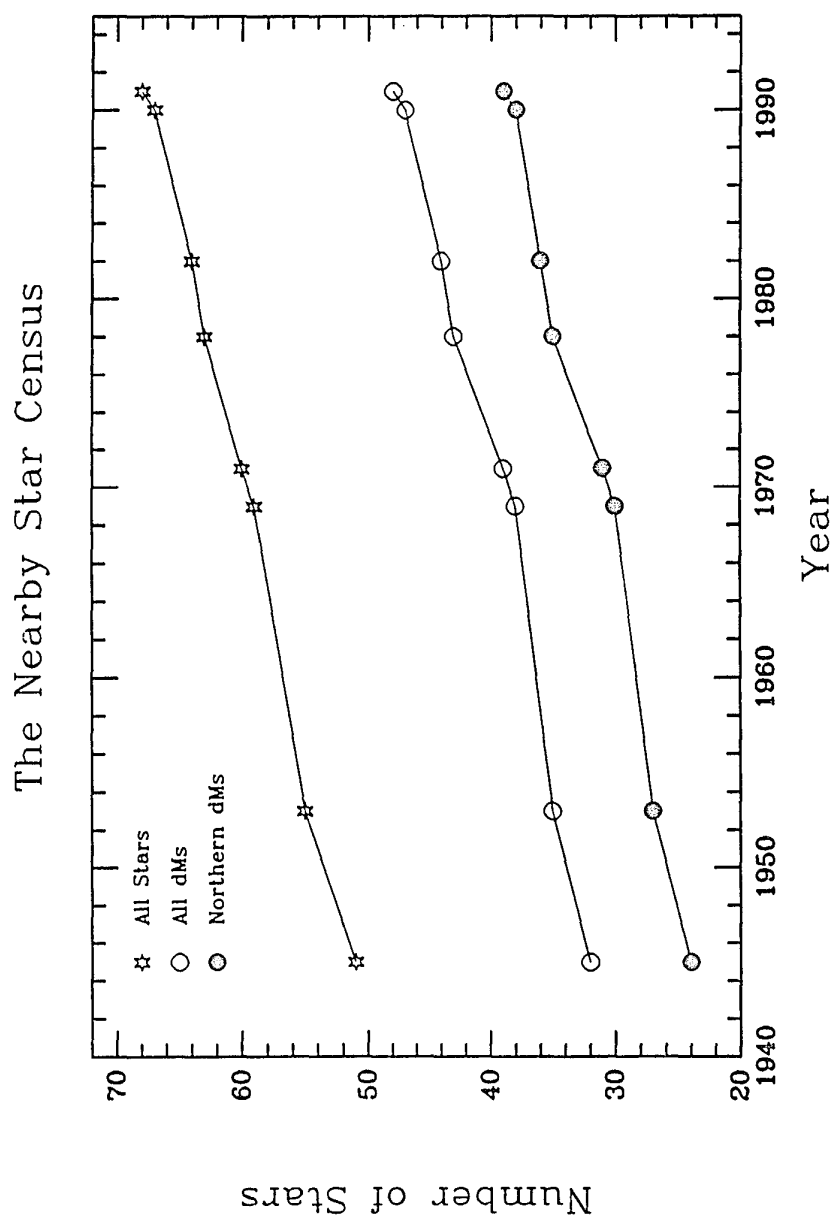


Figure 3.90 The growth of the nearby star census is shown over the last 45 years. The samples include all stars, all dMs, and all dMs north of -25° within the traditional 5.2 pc sample. Note the steady increase in the population of stars known near the sun.

CHAPTER 4

Characterizing the Population of Low Mass Dwarfs

4.1 The Mass–Infrared Luminosity Relations

In an effort to define the end of the main sequence, we have developed mass–infrared luminosity relations for stars of mass 1.2 to 0.08 M_{\odot} .

As the survey for brown dwarfs continued, it became obvious that the calibration of exactly what a brown dwarf *is* was crucial. Because we were working in the infrared and on binaries where masses could be determined, we began to calibrate empirically the characteristics of objects near the substellar border by developing much-needed mass–infrared luminosity relations. The establishment of definitive mass–luminosity relations in the infrared for low mass stars is fundamental to our understanding of the physics involved in transition objects near the star/BD border.

Until the present study the mass–luminosity relation (hereafter MLR) has been poorly determined for M dwarfs. Liebert and Probst (1987) have provided the most comprehensive assessment of the problem in their Figure 1. Shown in that figure, which compares M_{bol} and mass, is the empirical fit of Smith (1983), which relies on few points lying below a few tenths of a solar mass. Today, there are far more masses known for the M dwarfs, and the development of a strong relation, even at very low masses, is possible.

Because the M dwarfs are of low mass and temperature, it can be argued that the most useful MLR should be obtained in the infrared, where such low mass objects are most easily studied. In fact, the development of a satisfactory MLR for the reddest stars has been particularly problematic because of their weak flux in the visible, where the MLRs are usually

determined. We provide here infrared MLRs, at J ($1.25\ \mu\text{m}$), H ($1.6\ \mu\text{m}$) and K ($2.2\ \mu\text{m}$).

With these relations and a well-determined luminosity function (§4.3), an accurate mass function for low mass stars can be found (§4.5), and the contribution of low mass stars to the mass of the galactic disk in the solar neighborhood can be calculated (§4.6).

4.1.1 Selection of Systems

While it is straightforward to determine the absolute brightness of a star, given its apparent brightness and distance, the determination of a crucial parameter, its mass, is limited to only those stars found in multiple systems. Unfortunately, accurate mass determinations are only possible for stars in close ($\leq 2''$) binaries, where orbital motion is relatively rapid, and the flux of the individual components is difficult to obtain. This is especially true of the red M dwarfs, which are of low mass and therefore orbit slowly. What is required is a technique that can measure component fluxes accurately at small spatial scales. Infrared speckle imaging is such a technique, and has the additional advantage that it is done at wavelengths where the lowest mass stars are brightest.

A sample of close binaries with components of spectral types F6 and later was chosen to produce the infrared MLRs. Special care was taken to include only systems with well-determined parallaxes and high quality orbits. The final sample includes 41 objects, all of which are members of binaries with main sequence components, except for GL 166C, in which case the primary is a white dwarf. For stars of type F6 to K7, the Worley

and Heintz (1983) *Fourth Catalog of Orbits of Visual Binary Stars* was searched for binary systems with quality 1 orbits, which are considered to be definitive. Systems with quality 2 and 3 orbits which had M dwarf primaries were then added in order to concentrate upon the very late, most abundant, main sequence stars. Finally, systems which have become known since the publication of the catalog, many of them astrometric binaries resolved by infrared speckle (e.g., GL 22AC, GL 67AB, GL 623AB, GJ 1245AC), were added.

4.1.2 Mass Determinations

Table 4.1 shows the orbital parameters and the references used in determining the masses and errors of the 41 stars used in the MLRs. Column 1 identifies the system by Gliese number (except for ADS 3475), columns 2 and 3 list the right ascension and declination, and given in columns 4 and 5 are the adopted parallax and reference. When no reference is given in column 5, the parallax has been taken from the orbit reference, which is given in the last column. The next three columns list the orbital parameters required to determine component masses — the period (P), semimajor axis (a), and fractional mass (f), and their errors. When errors were not given for period or semimajor axis in the original papers, they were estimated as follows. One percent errors in both P and a were assumed for well-observed binaries whose orbital motion has been followed for two or more full revolutions. Three percent errors were assigned to those systems followed for at least 90% of a full orbit, but less than two orbits. Five percent errors were adopted in P and a for GL 166BC, which has been followed for only half a revolution, and 10% errors for the GL 725 system,

which has only been observed for one third of an orbital period. The magnitudes of these estimated errors, which are presented in italics in the table, correlate well to the errors reported by authors for various systems in which the errors are given.

The component masses are given in columns 9 and 10, with their formal errors. The errors include standard errors in the parallax, the period, the semimajor axis and the fractional mass. Because the errors on the semimajor axis enter into Kepler's Law as the cube, the final masses are critically sensitive to both the axis measured and the parallax, both of which are required to find the relative semimajor axis.

4.1.3 Systems with Very Low Mass Components

Here we give special consideration to four systems containing very low mass secondaries: GJ 1005AB, GL 234AB, GL 623AB and GJ 1245AC. These systems, in fact, contain the four least luminous secondaries for which reliable masses have been determined, and all have been examined extensively by infrared speckle techniques. *The low masses of all four secondaries make them viable brown dwarf candidates.*

GJ 1005AB has proven problematic when determining masses because of an ill-defined astrometric orbit. Ianna *et al.* (1988) have studied the system, and determine masses of 0.17 ± 0.12 and $0.055 \pm 0.032 M_{\odot}$ for the components. Here we make a revised estimate, using two 1D speckle observations, two visual observations (the two reported in their work), and a new 2D camera measurement. Two of the 1D observations listed in Table 3.2 (those on 12 Nov 1984 and 07 Sep 1987) yielded nonsensical masses,

and were not used. Using the five good observations, We derive masses of 0.137 ± 0.183 and $0.057 \pm 0.079 M_{\odot}$. Note that the formal errors are larger than the masses themselves! In the MLRs, these large errors result in very low weight for these points.

GL 234AB is the well-studied, nearby double Ross 614AB. There are seven 1D speckle observations (see Table 3.2) and five visual measurements (see Probst 1977) in which the system is resolved. Using the astrometric orbit and parallax of Probst (1977), and discarding the high and low extreme points (the Worley 1965 visual point, and the 1988 speckle point), we determine the scale factor, p/ρ to be 3.278 ± 0.359 , which yields a semimajor axis of $1.013 \pm 0.113''$. With $\beta = 0.016 \pm 0.003$ as determined from the speckle measurements and the procedure outlined in §3.4.2, we find the fractional mass, f , to equal 0.324 ± 0.033 . The masses are then 0.177 ± 0.060 and $0.085 \pm 0.030 M_{\odot}$, indicating that Ross 614B should be considered a brown dwarf candidate.

The binary GL 623AB has been studied extensively by McCarthy and Henry (1987) and Marcy and Moore (1989). The problem with the masses identified by both groups is the disagreement of the primary's mass with similar stars. This has been proposed to be due to either a poorly determined parallax, or an incorrect semimajor axis determination from the speckle work. We now have an additional speckle point using the 2D camera, which results in masses of 0.202 ± 0.054 and $0.064 \pm 0.017 M_{\odot}$. This is quite different from the dynamical masses given in McCarthy and Henry — 0.51 ± 0.16 and $0.111 \pm 0.028 M_{\odot}$ — which relied upon 1D speckle measurements. Marcy and Moore derived independent measures of

the secondary's mass using an adopted mass for the primary of $0.34 \pm 0.04 M_{\odot}$ assigned by photometric techniques. They find $M_B = 0.080 \pm 0.030$ using their radial velocity data, and $M_B = 0.081 \pm 0.014$ from the astrometry and the adopted primary mass. Here we adopt the following masses, which are the weighted means of the above three measures for the primary, and four measures for the secondary — 0.300 ± 0.032 and $0.079 \pm 0.010 M_{\odot}$.

GJ 1245AC has perhaps the best determined masses of the four systems. We have rederived the masses using the original 1D speckle data (McCarthy *et al.* 1988) and the new orbit provided by Harrington (1990), which is considered definitive. The final masses are 0.118 ± 0.018 and $0.087 \pm 0.014 M_{\odot}$.

4.1.4 Luminosity Determinations

The infrared luminosities for the components have been determined using infrared photometry of the systems, deconvolution of the photometry using speckle techniques, and the adopted parallaxes. Table 4.3 lists the final infrared absolute magnitudes for the stars used in the MLRs. The apparent photometry for the system (except in the cases of GL 166C, 559AB and 725AB which are in wide binaries allowing individual photometry to be done on the components) is given in column 3, and the photometric reference in column 4. An asterisk (*) indicates photometry provided by the author, and has been determined as discussed in §3.2.2. The infrared speckle results are given in Table 4.2, and the visibility curves are shown in Figures 4.1 to 4.10, and in Chapter 3 for those binaries within the survey.

Of special interest are the visibility curves of GL 508AB. The curves at all three wavelengths do not damp, as is sometimes the case with 1D data, but they do show a general downward slope. We attribute this to a possible third component in the system, and await future 2D observations to search for the tertiary. The first visibility minimum, at which point the offset due to the slope is minimal, has been used to determine the brightness ratio for the two known components. The absolute magnitudes and their formal errors for all objects are given in the final two columns of Table 4.3.

Several sources of error have been considered in the calculation of the individual absolute magnitudes. The errors in the apparent photometry are as quoted in the reference, but were never taken to be less than 0.03 mag. This is in order to allow for flaring activity in the infrared, which is currently uncalibrated, and for minor differences in photometric systems, for which no corrections have been applied (see §3.2.2). Errors in the final values also include errors in the speckle-determined magnitude differences and errors in the parallaxes.

4.1.5 The Relations at J, H and K

Figures 4.11, 4.12 and 4.13 show the empirical M_K , M_H , and M_J versus mass relations. A weighted (in the mass coordinate only) least-squares linear fit was made to each of the infrared magnitude-log mass relations, and is shown in the figures. Higher order fits were not considered, because the errors in the individual masses would not support a more elaborate treatment at the present time. The solid lines are the fits detailed in Equations 4.1, 4.2 and 4.3, and the dotted lines represent the

positive and negative mass offsets for errors in the slope and intercept values at the one sigma level. We find the three relations (r is the correlation coefficient of each fit):

$$\log (M/M_{\odot}) = -0.166 M_K + 0.560 \quad (r = 0.981), \quad (4.1)$$

$$\log (M/M_{\odot}) = -0.161 M_H + 0.560 \quad (r = 0.979), \quad (4.2)$$

$$\log (M/M_{\odot}) = -0.150 M_J + 0.578 \quad (r = 0.976). \quad (4.3)$$

These relations supercede those reported in Henry and McCarthy (1990). The higher correlation coefficients indicate the strength of these relations relative to the earlier ones, which had only 29, 17 and 14 data points, whereas we now present 41, 37 and 35 points at K, H and J, respectively. These relations can be applied to stars of mass 1.2 to 0.08 M_{\odot} . The first relation, involving M_K , varies more slowly over the run of mass through the range of M_K than does the Veeder (1974) relation:

$$\log (M/M_{\odot}) = -0.204 M_K + 0.853. \quad (4.4)$$

The new fit was made with more than twice as many points as the Veeder fit, and with generally higher quality masses. The errors in the M_K relation

are 2.7% in the slope and 5.0% in the intercept. The errors for the M_H and M_J relations are substantially lower than published previously: 2.8% and 5.2% for M_H , and 2.8% and 5.0% for M_J .

A few *caveats* are in order when using these relations. First, we point out that the stars included in the sample are of intermediate disk age, so the relations can only be accurately applied to objects of similar age. Second, effects of metallicity have not been considered, as the limited sample size for subsets of stars within small mass ranges does not permit a detailed analysis. Various metallicities will affect the luminosities of the stars under consideration. Third, the application of these relations for objects with masses less than $0.12 M_\odot$ ($M_K \sim 8.9$), where the theoretical models predict a growing spread in luminosities for objects spanning a range of ages, must be done with suitable qualifications if no age estimate is available. It appears that the given relations suit stars of mass 0.08 to $0.12 M_\odot$ only if they are of age 0.1 to 1.0 Gyr, *assuming the theoretical relations are accurate*. Conversely, it is possible that the models require revision, and the relations are truly linear all the way to the end of the main sequence. This conclusion is supported by the fact that the handful of objects used to calibrate the very end of the relations does not appear to be preferentially young.

Therefore, until more very low mass objects are found, and more accurate masses and age estimates are available for those objects already known, care must be taken when applying these relations.

4.1.6 Absolute Infrared Magnitudes at the 80 Jupiter Border

With the above *caveats* in mind, and assuming the stellar/substellar break to be at $0.08 M_{\odot}$, we find the absolute magnitudes for objects with masses on the border to be $M_K = 9.98$, $M_H = 10.29$ and $M_J = 11.17$. *These values indicate that objects like LHS 2924 ($M_K = 10.48$) may have masses less than $0.08 M_{\odot}$.* Objects which may be considered BD candidates based upon their infrared luminosities will be discussed further in §5.2.2.

4.2 A Mass Spectral Type Relation

As a further effort to calibrate the end of the main sequence, we have been using the MMT Red Channel Spectrograph to obtain spectral types of nearby stars and current BD candidates. A subset of the observing list has included those stars with well-determined masses listed in Table 4.1. Here we provide a mass-spectral type relation, which is purely empirical, and useful when the distance to an object is unknown.

The dwarf spectra cover the range 6320–9170 Å for types K 5.0 to M 9.0. The observing setup and procedure are described in §3.8.2, and Kirkpatrick *et al.* (1991). Briefly, all stars have been observed using the same instrumental setup, and have been classified using not only spectral features, but the overall slope of the spectrum. The classification system is based upon the pioneering work of Boeshaar (1976).

Table 4.4 lists the spectral types determined for objects with masses given in Table 4.1. Figure 4.14 illustrates the correlation between spectral type and mass. Unfortunately, no objects are known with dynamically determined masses less than $0.1 M_{\odot}$, which corresponds to spectral type

M 6.0. Objects with redder types are either single, or in very close binary systems (e.g., the four secondaries described in §4.1.3). In practice, individual component spectra are difficult to obtain unless the two objects in the system are separated by $>2''$. Systems with larger separations necessarily have long orbital periods and hence poorly determined masses. Nevertheless, several nearby M dwarfs have separations wide enough to allow the acquisition of component spectra and reasonably accurate masses: GL 65A and B, 166C, 725A and B, and 860A and B.

To this special class of objects we have added pairs with separations less than $1''$. In most cases, the primary is much more luminous than the secondary so that its light dominates the spectrum. Thus, the composite spectra for GJ 1005AB, GL 22AC, 234AB, 508AB, 623AB and GJ 1245AC have been assigned the primary's mass. Two additional systems, GL 352AB and 661AB, are comprised of components of nearly equal mass, and presumably the composite spectrum is the same as that of the individual stars. We adopt the mean mass of the components in both cases. Because only a few objects are available with known masses and spectral types on this system, no corrections for age and metallicity effects have been attempted.

As can be seen from Figure 4.14, the trend of spectral class with mass is quickly approaching the line which separates the lowest mass stars from the highest mass BDs. If the trend were to continue to lower masses, this relation would indicate that objects of spectral class M 7.0 would be substellar. However, we point out that as plotted, the relation must become asymptotic at higher masses, and there is no *a priori* reason to believe that

it cannot do the same at very low masses, as the hydrogen burning limit is approached. Nevertheless, the mass-spectral type calibration is useful when discussing stars of types M 1.0 to M 6.0.

4.3 The Luminosity Function

The nearby star sample indicates that the luminosity function is flat or rising to the end of the main sequence.

A luminosity function (LF) describes a population of stars by binning them in groups of specific flux intervals at a given wavelength, or in the case of M_{bol} , by their total flux. The LF of the reddest stars has been a topic of hot debate in recent years. The matter has been complicated by the choice of the wavelength at which the LF is determined. Traditionally, the LF has been described at visible wavelengths, but it is perhaps more appropriate to develop the LF of very low mass stars in the infrared, where they are more easily studied. Here we present LFs for the nearby star sample at both infrared and visible wavelengths.

Two important conclusions can be reached from the results presented in the next two sections. The first is straightforward — the infrared LF (and probably the visible LF as well) is flat or rising to the end of the main sequence. The second result is that *there are no objects with $M_K > 10.0$ in the survey* even though the search for companions was sensitive to $M_K = 10.8$ to 12.4. Using the MLRs discussed in §4.1, we find that the M_K cutoff corresponds to a mass of $0.08 M_{\odot}$, the star/BD border. The cutoff in the LF is real, and leads us to believe that the theoretically predicted precipitous dropoff in luminosity through the stellar/BD transition region

(see Figure 3.85) is the cause. It is likely that BDs of disk age, as are the stars in the sample, are significantly fainter than their stellar counterparts. In fact, we may need to probe to M_K magnitudes approaching 16–18 before the highest mass BDs can be detected.

This second conclusion, however, is not absolute. The four BD candidates included in the survey all have masses which straddle the 80 Jupiter border, and none is fainter than $M_K = 10.0$. Although the possibility remains that all four are relatively old stars, it is also possible that at least one is a young, relatively bright, substellar BD. A third possible explanation, that the theoretical models are in error, and that the turnover does not occur until lower masses (if at all), appears less likely. The interior models of D'Antona and Mazzitelli (1985) and Burrows *et al.* (1989) give quantitatively similar, although not identical, luminosities for low mass stars and BD at ages 0.1 to 10 Gyr. Only further study by infrared speckle, astrometric and spectroscopic techniques will allow better mass determinations to be made, and reveal whether or not the candidates are, indeed, BDs.

Two problems in determining the LF of very low mass stars have been realized during the work presented here. The first is that even past six parsecs, the parallax catalogs are seriously incomplete. The second is the importance of binaries in the determination of the true luminosity function. When deep surveys are used to determine the LF, the LF shifts to brighter magnitudes as pairs of faint objects are incorrectly counted as single stars. Both of these pitfalls encountered when searching for the true LF are addressed below.

4.3.1 The Infrared Luminosity Function

Results from recent work examining the infrared LF have been contradictory. Hawkins and Bessell (1988), Leggett and Hawkins (1988), and Skrutskie *et al.* (1989) all find a LF that turns over near $0.2 M_{\odot}$, and subsequently drops toward lower masses. Hawkins and Bessel find a peak near $M_K = 7.5$ in a study involving deep field searches using UK Schmidt plates taken at R, and conversions made to K. The Leggett and Hawkins work points to a maximum in the LF at $M_K = 7.0$. Skrutskie and collaborators argue a falling LF at faint magnitudes due to the lack of detections in a survey of nearby stars for companions in regions 2–7'' from the targets. In all cases the data appear to indicate a decline in the LF beginning near $0.2 M_{\odot}$ that continues to the end of the main sequence. In the first two studies, they find that the LF then begins to rise near the substellar border, but the statistical basis is so weak that this conclusion is unconvincing.

We reported in the 1990 survey results that the infrared LF was actually rising to the end of the main sequence and this has recently been supported by Zuckerman and Becklin (1991) in their search for low mass companions to white dwarfs. With a larger survey now in hand, containing 99 members rather than 39, the original conclusion is supported, and more robust.

Figures 4.15, 4.16 and 4.17 illustrate the LFs for the nearby star survey at K, H and J. We have binned all objects in the survey in half magnitude groups using the absolute photometry presented in Table 3.7.

Three LFs are presented at each wavelength because of the incompleteness of star counts even within the solar neighborhood (see §3.2.1). The three volumes chosen — to 5.03 pc, 6.35 pc and to the full 8.00 pc distance — represent one quarter, one half and the full volumes of the survey. The first shell contains 35 objects, the second shell 29 more, and the third shell, which has the same volume as the first two shells combined, has only 35 additional stars. Thus, nearly 50% of the members of the outer half of the survey volume appear to be unaccounted for, assuming that the sun does not fall in the midst of a density enhancement in the local spiral arm. In the full survey LF, the brighter constituents are far more likely to be fully represented than the very low luminosity objects, and the net effect is a depression of the LF at faint magnitudes, as is indicated in the plots. For the full survey plots we also include the histogram of the 32 secondary components within the survey.

Examination of the LF at K indicates that even in the full survey, which is certainly missing objects in the low luminosity bins, the LF is flat. It is certainly not falling. One unexpected feature of the LF is apparent — there appears to be a bimodal distribution with a minimum near $M_K = 7.5-8.0$. The cause of this is unknown, but it has also been found by Zuckerman and Becklin (1991) during their survey of white dwarfs for low mass companions. If there were a discontinuity in the MLR at this luminosity, the cause would be obvious — a small change in mass would result in a large change in brightness, thereby leaving an empty bin in the LF. The empirical MLR found here and illustrated in Figure 4.11, however, has no discontinuity, so the cause of the bimodal character of the

LF remains unknown. Interestingly, this deficit is located where others see the turnover, at mass $\sim 0.2 M_{\odot}$. In neither our nearby star survey, nor in the white dwarf companion survey, are the statistics large enough to permit a firm conclusion to be reached about the reality of the feature, but considering that the two completely independent studies possess the dip, it is worthy of note. The bimodality is also present in the H (at $M_H = 8.0-8.5$) and J (at $M_J = 8.5-9.0$) LFs. One interpretation of the LF at K is that there is a turnover at $M_K = 6.5-7.0$ (at higher masses than reported by others) but there is a substantial population of stars with $M_K = 8.0-9.5$, many of them low mass secondaries.

4.3.2 The Visual Luminosity Function

The determination of the LF at visual wavelengths has a long and somewhat sordid history. Liebert and Probst (1987) give a review, and provide the relevant references. The most comprehensive recent discussion of the visual LF is given by Reid (1987). Various groups find the LF to turn over near $M_V = 12-13$. These studies include work on the nearby stars by Wielen, and deep photometric surveys by Reid and Gilmore, and Hawkins and Bessell. These surveys are all plagued by the effects of unresolved binaries, which are discussed in the next section. On the other hand, Dahn *et al.* (1986) have reported that the visual LF of the traditional 5.2 pc members is flat or rising, and in work done using I band imaging of the globular cluster NGC 6397, Fahlman *et al.* (1989) also find a flat LF to $M_I = 11.5$ ($\sim 0.12 M_{\odot}$). Finally, Simons (1991) finds the LF to be rising through $M_I = 13$ for Pleiades members, possibly corresponding to BDs of masses as low as 50 Jupiters for Pleiades age.

Figure 4.18 illustrates the visual LF for the 8 pc survey members, again presented in three panels for the three volume-limited shells. While the full survey appears to turnover at $M_V = 11-12$, the more complete subsets support a flat LF at visual wavelengths. We also note that the turnover in the full survey LF is a magnitude brighter than is usually reported. This is difficult to reconcile unless some systematic error is present in the techniques used to convert color to absolute magnitudes, since the nearby star LF is based upon stars with well-determined parallaxes. Because all of the studies which indicate a turnover in the LF suffer from incompleteness at faint magnitudes and the effects of unresolved binaries, the best estimate of the visual LF is that it is flat to $M_V = 15-16$. The dropoff evident at fainter magnitudes even in the 6.35 sample is probably due to a combination of the onset of incompleteness in the parallax surveys, and because we are approaching the stellar mass limit ($M_V \sim 18$), below which the objects may be considerably fainter. A flat visual LF is supported by the work reported here on nearby stars, and work in entirely independent samples from globular clusters and the Pleiades.

4.3.3 The Effect of Binaries

When studying the population of low mass stars we must consider the effect of binaries on any evaluation of the LF. A problem arises when determining the LF using deep photometric surveys because many faint secondaries are lost in the glare of their primaries. The net result is a depression at the faint end of the stellar regime, and a boosting of the LF at higher luminosities. This effect was first noted by Dahn *et al.* (1986).

In Figures 4.19 and 4.20, we show true and false luminosity functions for the nearby star survey members at their true distances, and when moved to the distance of the Hyades (46 pc). Moving the entire survey to the Pleiades (125 pc), where several recent estimates of the LF have been made, results in a further loss of four stars. We assume that secondaries are “lost” if they fall within $1.0''$ of their primaries. The separations adopted for the multiple systems are given in Table 3.5. When moving the survey stars to the Hyades, the final result is a loss of 21 objects, and an obvious change in the character of the LF at both V and K. At V, the false LF indicates only 14% of the stars are fainter than $M_V = 15$. The actual LF supports a much larger population, 24%, or nearly twice the fraction of the false LF. We stress again that the lowest luminosity members in the survey volume remain underrepresented, and therefore the definitive LF would likely be even flatter at faint magnitudes than plotted in Figures 4.19 and 4.20.

Comparison of the true and false LFs at K is even more revealing. The true LF at K shows no dropoff until $M_K = 9.5$, where the drop is precipitous. Of all the stars in the sample, 41% have $M_K \geq 8$. When the same sample of stars is moved to the Hyades, a definite turnover is seen at $M_K = 6.0$ – 6.5 ($0.35 M_\odot$), and only 29% of the objects are fainter than $M_K = 8$. Therefore, the LF determined by Leggett and Hawkins (1988, 1989) in the Hyades is probably erroneous, and the theoretical fits to their LF and the translation to a mass function by Hubbard *et al.* (1991) should be reconsidered (see §4.5).

We see, then, that not only should there be concern about the detection limits of any deep photometric survey which claims to define the

LF, but the consideration of unresolved binaries is absolutely required to characterize the true LF of the smallest stars.

4.4 The Mass–Luminosity–Age Diagram

In Figure 4.21 we show the mass–luminosity–age diagram for the lowest mass objects known. The isochrones are from D’Antona and Mazzitelli (1985) and Burrows *et al.* (1989) as discussed for Figure 3.85. The objects are plotted at their masses and M_K values as given in Tables 4.1 and 4.3.

We also show for reference several current BD candidates for which absolute K magnitudes are known, although masses remain unknown because they are single objects, or in wide, slow-orbiting, binaries. The standout is GD 165B, at present the best BD candidate. All of the candidates are discussed further in Chapter 5. Note the generally good agreement between the location of the theoretical curves and the actual positions of the lowest mass objects. The four points with the lowest determined masses are the BD candidates included in the speckle survey.

4.5 The Mass Function

Perhaps the truest description of our galaxy’s constituents can be made by determining the number of objects per unit mass, rather than per unit flux, which is dependent on the choice of wavelength. The so-called mass function, alias MF, for the lowest mass stars has, until now, remained virtually unknown. This has been caused by two factors — the lack of a well-determined luminosity function for the faintest stars, and a poorly calibrated mass–luminosity relation. As discussed above, we now have both

in hand, and can make an accurate empirical assessment of the low mass star MF for the first time.

We determine the MF for the sample by using the MLR defined at K (see §4.1.5 and Figure 4.11) and the absolute magnitudes for all the survey members given in Table 3.7 to estimate masses for each (see Table 4.5). No attempt has been made to adjust luminosities to a predefined age, because the effects in the final mass function of a few very old and very young objects would be minor. Furthermore, a range of ages is of consequence only for masses less than $0.12 M_{\odot}$, and all objects with masses 0.125 to $0.075 M_{\odot}$ are included in the same, lowest mass bin of the MF. Thus, these very low mass members, with $M_K \geq 8.8$, will fall in the last bin regardless of their age.

A histogram of the objects, shown in Figure 4.22 binned in increments of $0.05 M_{\odot}$, clearly shows *a rising mass function to the end of the main sequence*. We find the number of stars per unit mass, $\Psi(M) \propto M^{-0.75}$ for masses 0.1 to $0.5 M_{\odot}$. We have found this MF by fixing the number of stars equal to 12 at $0.25 M_{\odot}$, followed by test runs of various exponential values for the MF, in units of 0.05 . The minimum χ^2 occurred for an exponent of -0.75 . This is significantly different than the Salpeter relation, where the exponent is -2.35 , and in which we would predict far more low mass stars. This MF indicates that the recent determination of the initial MF of the Hyades by Hubbard *et al.* (1991) is incorrect. They found that at decreasing masses the MF does not increase, undoubtedly because they relied upon the Leggett and Hawkins (1988, 1989) database which contains unresolved binaries. In this assessment we presume, of course, that the

initial MF in the Hyades mimics that of the nearby star population.

Finally, because the probable discontinuity in the MLR near the stellar/substellar break makes BDs so difficult to observe, it is currently impossible to predict the true MF of BDs, although if the MF continues to lower masses as it does at the end of the main sequence, there should be large numbers of BDs.

4.6 The Contribution of Low Mass Objects to the Galactic Disk

By adding up the masses for the survey stars in Table 4.5 which fall into the three shells discussed earlier (to 5.03, 6.35 and 8.00 pc), we calculate three mass densities of M dwarfs in the galactic disk. The inner volume, which is presumably the most complete with its 35 members, yields a density of $0.0185 M_{\odot}$ per cubic parsec. The outer two shells (64 and 99 members) result in values of 0.0214 and $0.0172 M_{\odot}/\text{pc}^3$. The higher estimate from the middle volume is the result of an overall average member mass of $0.23 M_{\odot}$, compared to the inner shell's average of $0.18 M_{\odot}$. (The average mass for the entire survey is $0.24 M_{\odot}$.) Apparently, while the number density is higher in the inner volume ($0.102 \text{ objects}/\text{pc}^3$ versus 0.0934 for the middle volume) either the immediate solar neighborhood has lower mass stars than the second volume, or there is some bias operative which ends in placing a large number of high mass stars between five and six and a half parsecs, at least among the subset of M dwarfs. As discussed before, the outer shell is undoubtedly incomplete, hence the lower mass density.

We adopt a density of $20 M_{\odot}/1000 \text{ pc}^3$ for M dwarfs in the solar neighborhood. Current estimates of the total mass density of the galactic disk range from 110 to $290 M_{\odot}/1000 \text{ pc}^3$ (Kuijken and Gilmore, 1989 and references therein). The amount of mass actually observed as stars, added to estimates of the density of the interstellar medium, amounts to 90 to $120 M_{\odot}/1000 \text{ pc}^3$ (Spitzer 1978, Hill *et al.* 1979, Mihalas and Binney 1981, Sanders *et al.* 1984, Kuijken and Gilmore 1989). Thus, one is led to conclude that, depending upon the model adopted, either more than 50% of the mass in the galactic disk is missing, or none of it is missing.

Here our purpose is not to choose a model, but to provide data that allow an accurate assessment of the amount of mass contributed to the galactic disk by M dwarfs — 20% of that observed. Furthermore, we point out that an important facet of the speckle program has been the determination that in a binary system, low luminosity secondaries typically add 50–100% additional mass to what may be inferred by the primary component's flux alone. This will boost drastically the mass contribution to the galactic disk made by the smallest stars.

TABLE 4.1

ORBITAL PARAMETERS AND MASSES FOR CLOSE BINARIES

GL #	RA	DEC	$\pi \pm \sigma$	Ref	P (yrs)	a ($''$)	f	M _A	M _B	Ref
1005AB	00 12 53	-16 24 18	.189 .005		4.63	0.304	0.295	0.137	0.057	IRM 88, *
					0.23	0.134	0.104	0.183	0.079	
22AC	00 29 20	+66 57 48	.100 .003		15.95	0.498	0.254	0.362	0.123	H 73, MHMC 91
					0.22	0.018	0.007	0.052	0.018	
25AB	00 34 47	-25 02 30	.074 .010	G	25.00	0.670	0.5	0.594	0.594	V 37, HSW 63
					0.75	0.020	0.02	0.250	0.250	
65AB	01 36 25	-18 12 42	.375 .006		26.52	1.95	0.494	0.101	0.099	GHW 88
					0.80	0.059	0.003	0.012	0.012	
67AB	01 38 44	+42 21 48	.072 .003		19.50	0.564	0.231	0.972	0.292	LBM 83, HMFC 91
					0.28	0.038	0.014	0.233	0.072	
166BC	04 13 04	-07 44 06	.207 .003		252.1	6.943	0.262	white	0.156	H 74
					12.6	0.347	0.01	dwarf	0.029	
ADS 3475	04 48 28	+10 59 14	.023 .0033		16.30	0.202	0.483	1.318	1.232	H 69, H 86a
					0.16	0.002	0.02	0.572	0.534	
234AB	06 26 51	-02 46 12	.243 .002		16.60	1.013	0.324	0.177	0.085	P 77, *
					0.03	0.113	0.033	0.060	0.030	
340AB	09 14 56	+28 46 42	.058 .004		34.20	0.66	0.473	0.664	0.596	H 82
					1.03	0.020	0.004	0.155	0.139	
352AB	09 28 53	-13 16 06	.105 .011		18.3	0.551	0.51	0.211	0.220	H 79
					0.55	0.03	0.02	0.076	0.080	

TABLE 4.1 (continued)

GL #	RA	DEC	$\pi \pm \sigma$	Ref P	α (")	f	MA	MB	Ref
508AB	13 17 36	+48 02 24	.119 .005	48.85	1.465	0.412	0.460	0.322	H 69, H 76
				0.24	<i>0.044</i>	0.012	0.072	0.051	
559AB	14 36 11	-60 37 48	.750 .010	GJ 79.92	17.552	0.449	1.106	0.901	H 60, P 80
				<i>0.80</i>	<i>0.176</i>	0.01	0.063	0.053	
570BC	14 54 31	-21 11 18	spectroscopic/speckle solution						
							0.553	0.390	MPDD 90
							0.047	0.032	
623AB	16 22 39	+48 28 24	.132 .006	GJ 3.73	0.240:	0.26	0.300	0.079	MH 87, MM 89, *
				0.09	0.035	0.02	0.032	0.010	
661AB	17 10 40	+45 44 48	.158 .006	GJ 12.98	0.71	0.496	0.271	0.267	E 67, H 84
				0.03	0.01	0.01	0.033	0.033	
677AB	17 27 24	+29 26 00	.046 .006	60.00	0.60	0.468	0.328	0.288	L 82
				<i>1.80</i>	<i>0.018</i>	0.011	0.133	0.117	
702AB	18 02 56	+02 30 36	.203 .006	88.13	4.545	0.442	0.806	0.639	WH 74
				<i>2.64</i>	<i>0.186</i>	0.01	0.114	0.090	
704AB	18 05 08	+30 33 12	.060 .005	55.8	1.00	0.398	0.895	0.592	H 72
				<i>1.67</i>	<i>0.030</i>	0.01	0.244	0.162	
725AB	18 42 12	+59 33 18	.290 .002	408	13.88	0.46	0.356	0.303	H 87
				<i>40.8</i>	<i>1.388</i>	0.02	0.129	0.110	
1245AC	19 52 16	+44 17 30	.221 .002	15.22	0.799	0.423	0.118	0.087	M+ 88, H 90, *
				0.01	0.040	0.017	0.018	0.014	
860AB	22 26 13	+57 26 48	.253 .004	GJ 44.67	2.383	0.394	0.254	0.165	H 86a, H 86b
				<i>1.34</i>	<i>0.071</i>	0.002	0.030	0.019	

TABLE 4.1 (continued)

PARALLAX REFERENCES:

G = Gliese 1969, GJ = Gliese & Jahreiss 1979: trigonometric parallaxes only

ORBIT REFERENCES:

E 67 = Eggen (1967), GHW 88 = Geyer *et al.* (1988),
H 60, 69, 72, 74, 76, 79, 84, 86a, 86b, 87 = Heintz (various years),
H 73, 82 = Hershey (1973, 1982), H 90 = Harrington (1990),
HMF 91 = Henry *et al.* (1991), HSW 63 = Harris *et al.* (1963),
IRM 88 = Ianna *et al.* (1988), L 82 = Lippincott (1982),
LBM 83 = Lippincott *et al.* (1983), M+ 88 = McCarthy *et al.* (1988),
MH 87 = McCarthy and Henry (1987), MHMC 91 = McCarthy *et al.* (1991),
MM 89 = Marcy and Moore (1989), MPDD 90 = Mariotti *et al.* (1990),
P 77 = Probst (1977), P 80 = Popper (1980),
V 37 = Voute (1937), WH 74 = Worth and Heintz (1974),

* = see text

Italicized quantities indicate errors estimated by the author.

TABLE 4.2
 INFRARED SPECKLE OBSERVATIONS OF NON-SURVEY DOUBLES
 USED IN MASS—LUMINOSITY RELATIONS

Object(s)	λ	Tech	Date	Separation	PA	$\Delta m \pm \sigma$
22AC	H*	2D 2X	10 Dec 89	0.453 0.020	044 03	2.11 0.06
	K*	2D 2X	12 Oct 89	0.451 0.020	043 03	1.94 0.06
25AB	H*	2D 2X	11 Dec 89	0.687 0.026	110 02	0.25 0.02
	K*	2D 2X	11 Dec 89	0.687 0.026	110 02	0.16 0.01
67AB	J*	2D 2X	01 Dec 90	0.448 0.030	194 02	4.37 0.25
	H*	2D 2X	28 Nov 90	0.442 0.018	199 02	4.50 0.12
	K*	2D 2X	10 Oct 89	0.623 0.027	203 02	4.30 0.07
	K	2D 2X	07 Dec 90	0.485 0.025	196 02	4.50 0.05
	K	adopted				4.43 0.04
ADS 3475	K*	2D 2X	10 Oct 89	0.113 0.014	304 02	0.80 0.13
340AB	J*	2D 2X	27 Apr 91	0.153 0.006	295 02	0.35 0.01
	H*	2D 2X	11 Dec 89	0.203 0.010	256 02	0.42 0.01
	K*	2D 2X	11 Dec 89	0.203 0.008	256 02	0.08 0.08
352AB	J*	1D NS	22 Jan 89	0.48 0.05	N	0.33 0.05
	H*	1D NS	22 Jan 89	0.47 0.05	N	0.26 0.02
	K*	1D NS	22 Jan 89	0.48 0.05	N	0.23 0.02
508AB	J*	1D EW	18 Feb 89	0.97 0.10	W	1.08 0.07
	H*	1D EW	18 Feb 89	0.98 0.10	W	0.98 0.02
	K*	1D EW	18 Feb 89	0.98 0.10	W	0.92 0.02
677AB	J*	1D EW	21 Jun 89	0.73 0.07	W	0.30 0.02
	H*	1D EW	21 Jun 89	0.74 0.07	W	0.31 0.03
	K*	1D EW	21 Jun 89	0.72 0.07	W	0.28 0.03

TABLE 4.2 (continued)

Object(s)	λ	Tech	Date	Separation	PA	$\Delta m \pm \sigma$
702AB	J*	2D 1X	20 Aug 91	1.571 0.060	205 02	1.51 0.04
	H	2D 2X	11 Oct 89	1.484 0.057	233 02	———
	K	2D 2X	11 Oct 89	1.475 0.057	233 02	———
	K	1D NS	24 Oct 83	1.09 0.11	———	0.77 0.07
	K*	1D NS	26 Sep 83	1.03 0.10	———	0.74 0.05
	K	1D EW	25 Sep 83	1.85 0.19	———	0.72 0.05
	K	adopted				0.74 0.03
704AB	J*	2D 1X	28 Apr 91	0.971 0.037	027 02	2.53 0.02
	H*	2D 2X	10 Feb 90	1.048 0.040	024 02	2.40 0.07
	K*	1D NS	21 Mar 89	1.00 0.10	N	2.06 0.07

TABLE 4.3
ABSOLUTE MAGNITUDES OF ALL OBJECTS
USED IN MASS—LUMINOSITY RELATIONS

Object(s)	λ	App AB	Ref	Abs A	Abs B
1005AB	J	7.28 0.03	IRM	8.90 0.07	10.43 0.09
	H	6.71 0.03	IRM	8.26 0.07	10.19 0.07
	K	6.42 0.03	IRM	8.08 0.07	9.42 0.08
22AC	H	6.59 0.08	MHMC	6.74 0.10	8.85 0.12
	K	6.26 0.09	MHMC	6.43 0.11	8.37 0.12
25AB	H	3.96 0.03	*	3.94 0.30	4.19 0.30
	K	3.85 0.07	*	3.87 0.30	4.03 0.30
65AB	J	6.31 0.03	P1	9.76 0.05	10.14 0.05
	H	5.68 0.03	P1	9.16 0.05	9.46 0.05
	K	5.34 0.03	P1	8.78 0.06	9.18 0.07
67AB	J	3.80 0.04	HMFC	3.11 0.10	7.48 0.26
	H	3.56 0.04	HMFC	2.86 0.10	7.36 0.15
	K	3.53 0.04	HMFC	2.83 0.10	7.26 0.11
166C	J	6.91 0.07	*	8.49 0.08	————
	H	6.29 0.07	*	7.87 0.08	————
	K	6.00 0.07	*	7.58 0.08	————
ADS 3475	K	5.26 0.12	*	2.49 0.34	3.29 0.35
234AB	J	6.42 0.03	P1	8.55 0.04	10.26 0.05
	H	5.78 0.03	P1	7.92 0.04	9.58 0.05
	K	5.49 0.03	P1	7.66 0.04	9.17 0.05
340AB	J	5.31 0.04	*	4.72 0.16	5.07 0.16
	H	4.84 0.04	*	4.22 0.16	4.64 0.16
	K	4.71 0.04	*	4.24 0.16	4.32 0.16
352AB	J	6.39 0.03	P1	7.10 0.23	7.43 0.23
	H	5.77 0.03	P1	6.51 0.23	6.77 0.23
	K	5.53 0.03	P1	6.28 0.23	6.51 0.23

TABLE 4.3 (continued)

Object(s)	λ	App AB	Ref	Abs A	Abs B
508AB	J	5.31 0.03	SH	6.03 0.10	7.11 0.11
	H	4.69 0.03	SH	5.44 0.10	6.42 0.10
	K	4.50 0.03	SH	5.26 0.10	6.18 0.10
559A	J	-1.14 0.05	ESWS	3.24 0.06	————
	H	-1.38 0.05	ESWS	3.00 0.06	————
	K	-1.48 0.05	ESWS	2.90 0.06	————
559B	J	-0.01 0.05	ESWS	4.37 0.06	————
	H	-0.49 0.05	ESWS	3.89 0.06	————
	K	-0.60 0.05	ESWS	3.78 0.06	————
570BC	J	4.78 0.03	P1	6.34 0.15	7.64 0.16
	H	4.14 0.03	P1	5.73 0.16	6.92 0.18
	K	3.90 0.03	P1	5.51 0.15	6.63 0.16
623AB	J	6.66 0.03	SH	7.31 0.11	10.59 0.31
	H	6.14 0.03	SH	6.83 0.11	9.48 0.11
	K	5.91 0.03	SH	6.59 0.11	9.46 0.17
661AB	J	5.57 0.03	SH	7.13 0.09	7.54 0.09
	H	5.05 0.03	SH	6.59 0.09	7.05 0.09
	K	4.82 0.03	SH	6.38 0.10	6.80 0.10
677AB	J	6.62 0.04	*	5.55 0.29	5.85 0.29
	H	6.08 0.03	*	5.00 0.29	5.31 0.29
	K	5.90 0.09	*	4.84 0.30	5.12 0.30
702AB	J	2.41 0.05	*	4.19 0.08	5.70 0.09
	K	1.96 0.03	P1	3.94 0.07	4.68 0.07
704AB	J	3.66 0.07	*	2.65 0.19	5.18 0.19
	H	3.50 0.04	*	2.50 0.19	4.90 0.20
	K	3.37 0.10	*	2.41 0.21	4.47 0.22

TABLE 4.3 (continued)

Object(s)	λ	App AB	Ref	Abs A	Abs B
725A	J	5.20 0.03	SH	7.45 0.04	————
	H	4.67 0.03	SH	6.92 0.04	————
	K	4.44 0.03	SH	6.69 0.04	————
725B	J	5.72 0.03	SH	7.97 0.04	————
	H	5.20 0.03	SH	7.45 0.04	————
	K	4.97 0.03	SH	7.22 0.04	————
1245AC	J	7.78 0.03	M+	9.80 0.04	11.06 0.05
	H	7.26 0.03	M+	9.32 0.04	10.40 0.04
	K	6.89 0.03	M+	8.97 0.04	10.00 0.04
860AB	J	5.54 0.03	SH	7.87 0.06	9.06 0.09
	H	4.96 0.03	SH	7.30 0.05	8.44 0.06
	K	4.71 0.03	SH	7.00 0.05	8.37 0.08

REFERENCES:

ESWS = Engels *et al.* (1981),HMFC = Henry *et al.* (1991),IRM = Ianna *et al.* (1988),M+ = McCarthy *et al.* (1988),MHMC = McCarthy *et al.* (1991),

P1 = Probst (1981) Table A.7 — averaged values of many studies,

SH = Stauffer and Hartmann (1986),

* = this work

TABLE 4.4

SPECTRAL TYPES FOR STARS WITH WELL-DETERMINED MASSES

GL #	Type	Notes
1005AB	M 4.0	primary dominates
22AC	M 2.0	primary dominates
65A	M 5.5	
65B	M 6.0	
166C	M 4.5	
234AB	M 4.5	primary dominates
352AB	M 3.0	mean mass assumed
508AB	M 1.0	primary dominates
623AB	M 2.5	primary dominates
661AB	M 3.0	mean mass assumed
725A	M 3.0	
725B	M 3.5	
1245AC	M 5.5	primary dominates
860A	M 3.0	
860B	M 4.0	

TABLE 4.5
MASS ESTIMATES FOR ALL SURVEY MEMBERS

GL#	Mass	GL#	Mass	GL#	Mass
1002	0.113	338A	0.515	661A	0.317
1005A	0.166	338B	0.499	661B	0.270
1005B	0.099	388	0.343	687	0.345
15A	0.322	393	0.381	699	0.156
15B	0.153	L292	0.091	701	0.365
34B	0.521	402	0.229	1224	0.133
54.1	0.141	406	0.108	1230A	0.221
65A	0.127	408	0.311	1230B	0.108
65B	0.109	411	0.322	725A	0.282
83.1	0.145	412A	0.351	725B	0.230
105B	0.224	412B	0.108	729	0.169
109	0.300	445	0.218	752A	0.387
166C	0.200	447	0.169	752B	0.079
169.1A	0.251	450	0.350	1245A	0.118
185A	0.445	1156	0.142	1245C	0.079
185B	0.296	473A	0.140	1245B	0.110
205	0.535	473B	0.124	809	0.481
213	0.209	493.1	0.158	829	0.319
229	0.468	514	0.419	831A	0.218
234A	0.194	526	0.384	831B	0.119
234B	0.109	555	0.251	860A	0.250
251	0.315	570B	0.442	860B	0.148
1093	0.124	570C	0.288	866A	0.149
268A	0.197	581	0.273	866B	0.120
268B	0.181	623A	0.293	873	0.268
273	0.248	623B	0.098	876	0.287
283B	0.088	625	0.265	880	0.464
285	0.264	628	0.244	884	0.533
299	0.140	643A	0.145	896A	0.317
300	0.184	643B	0.145	896B	0.207
1111	0.097	644A	0.396	1286	0.115
1116A	0.123	644B	0.307	905	0.145
1116B	0.106	644C	0.088	908	0.323

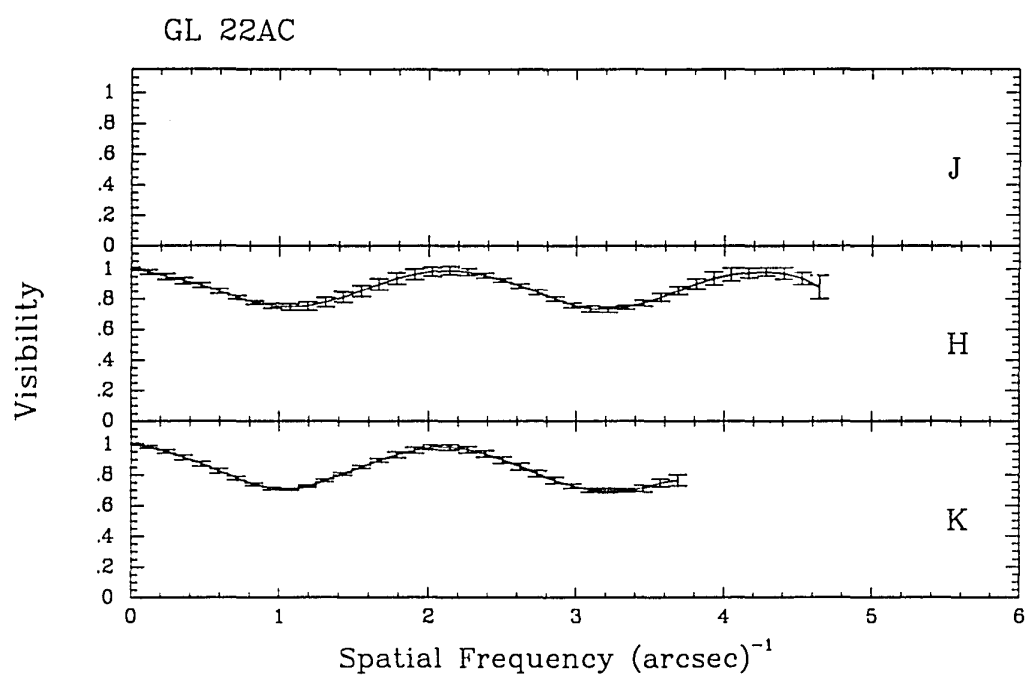


Figure 4.1 Visibility curves for GL 22AC.

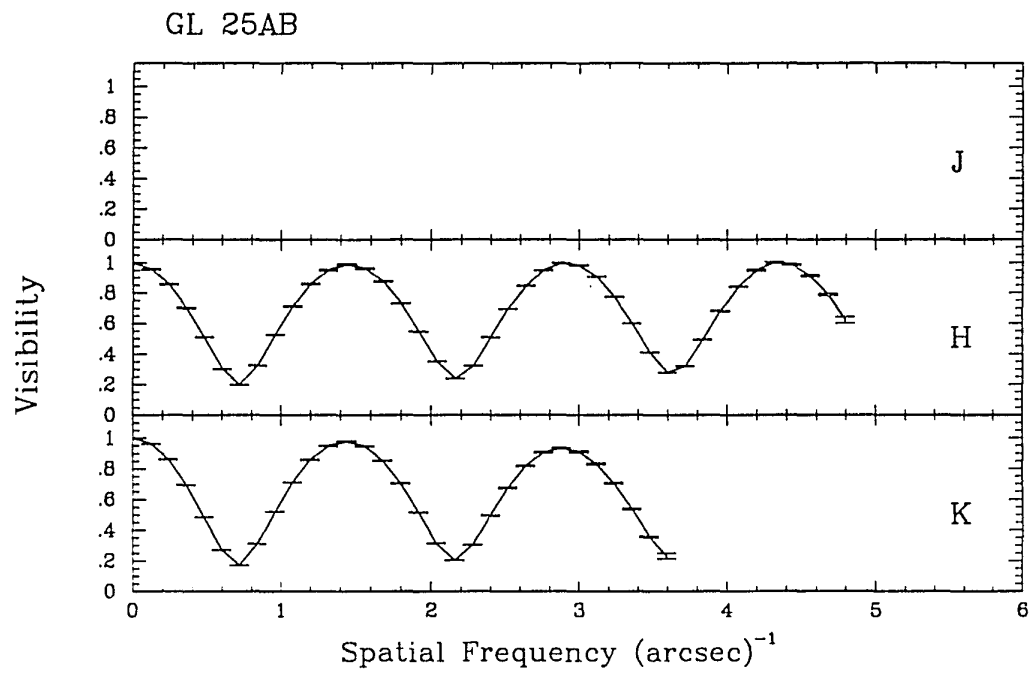


Figure 4.2 Visibility curves for GL 25AB.

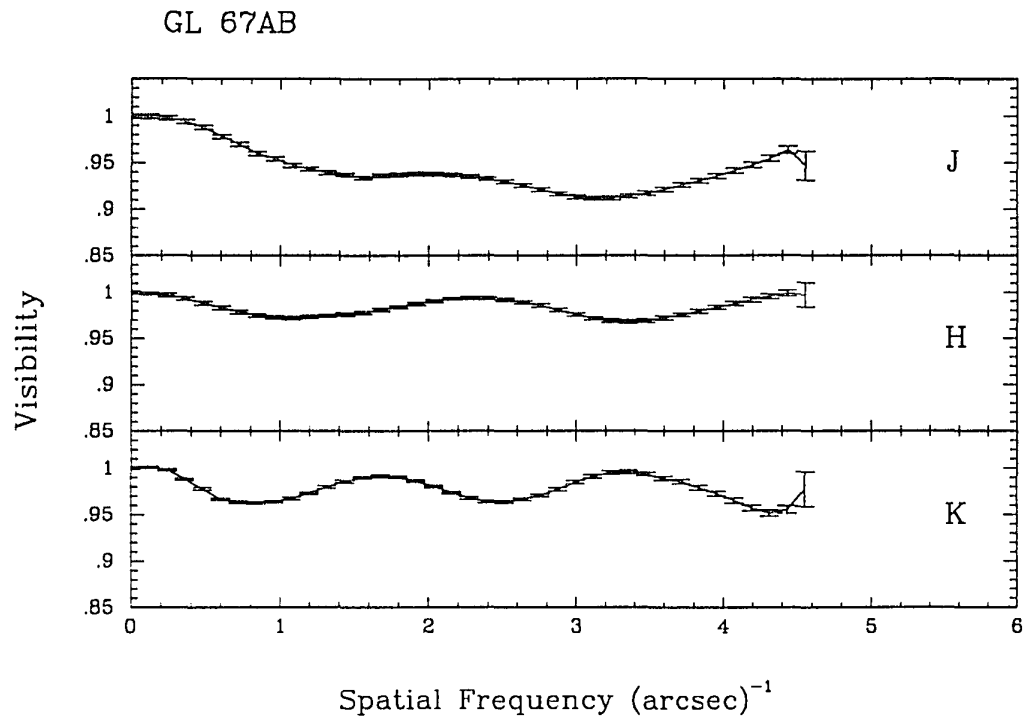


Figure 4.3 Visibility curves for GL 67AB.

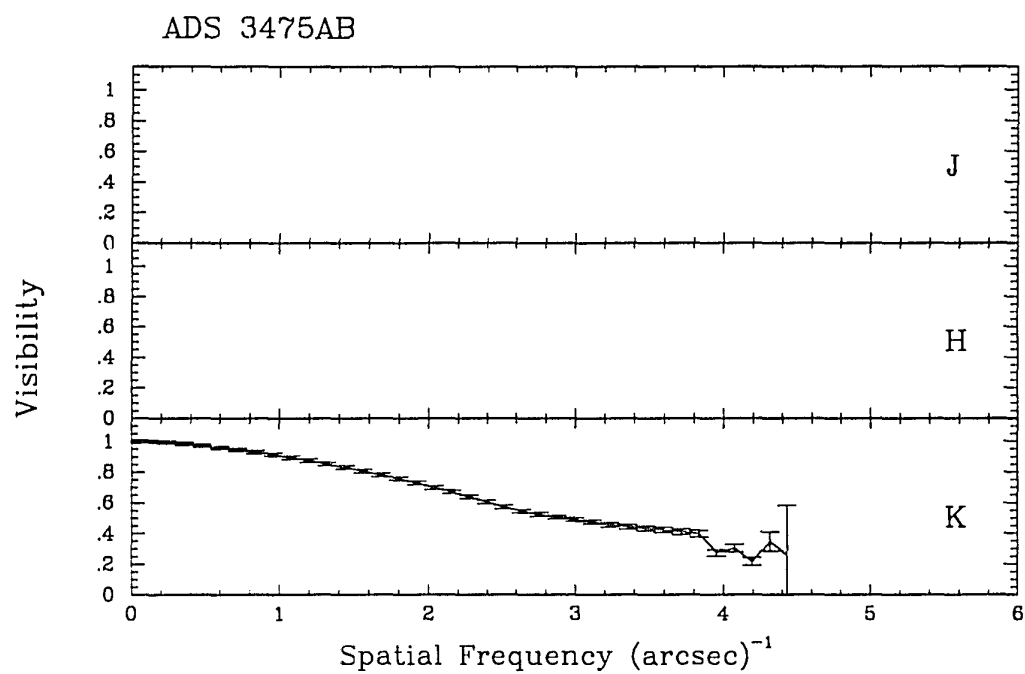


Figure 4.4 Visibility curves for ADS 3475AB.

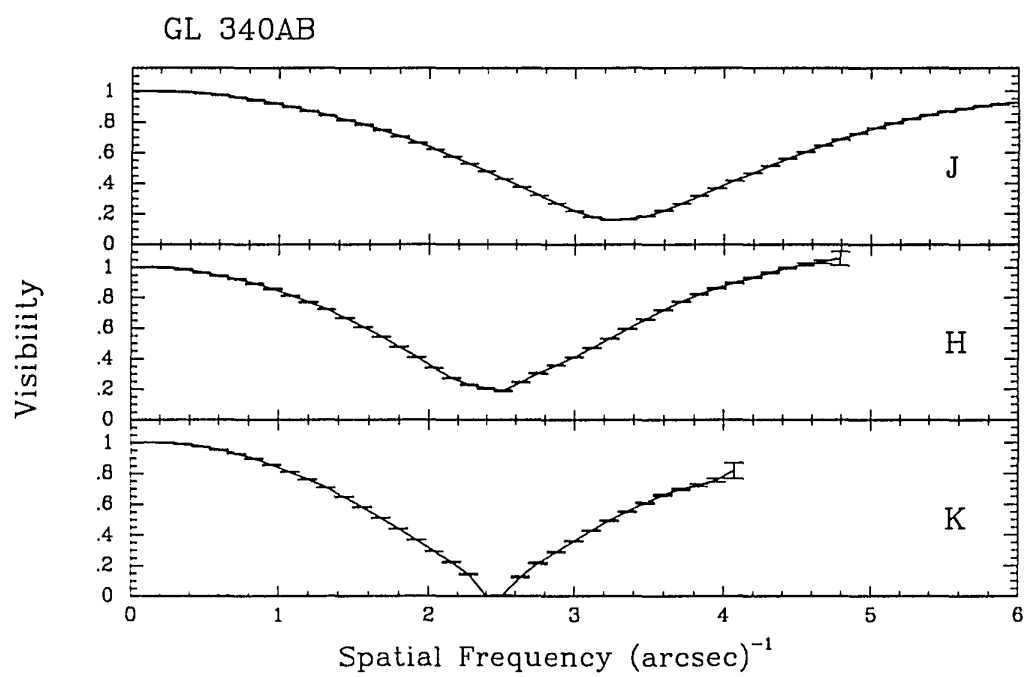


Figure 4.5 Visibility curves for GL 340AB.

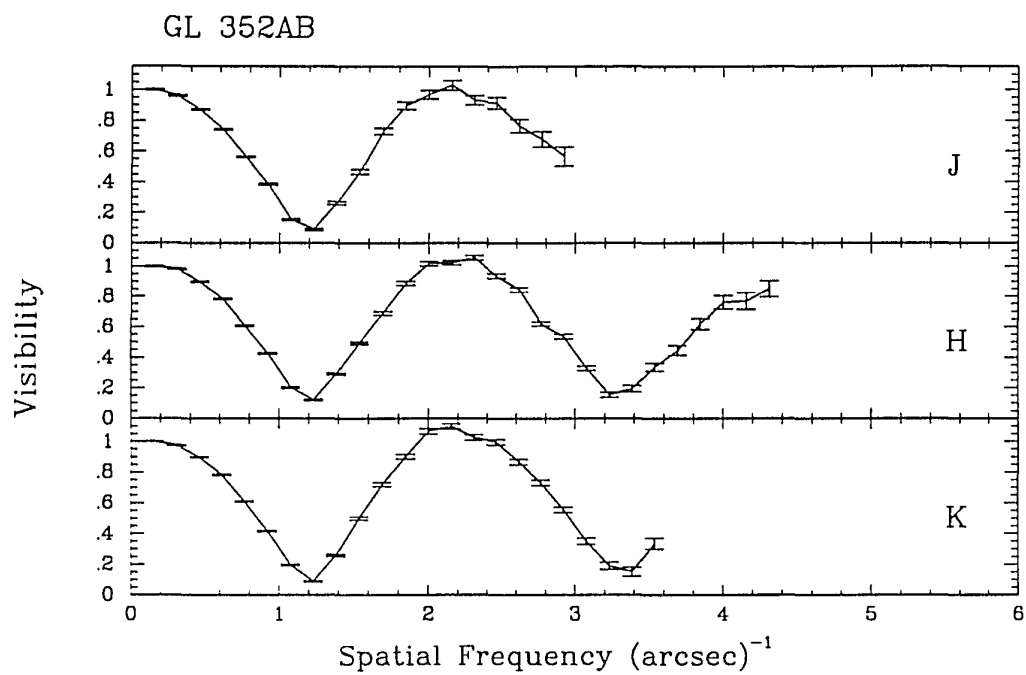


Figure 4.6 Visibility curves for GL 352AB.

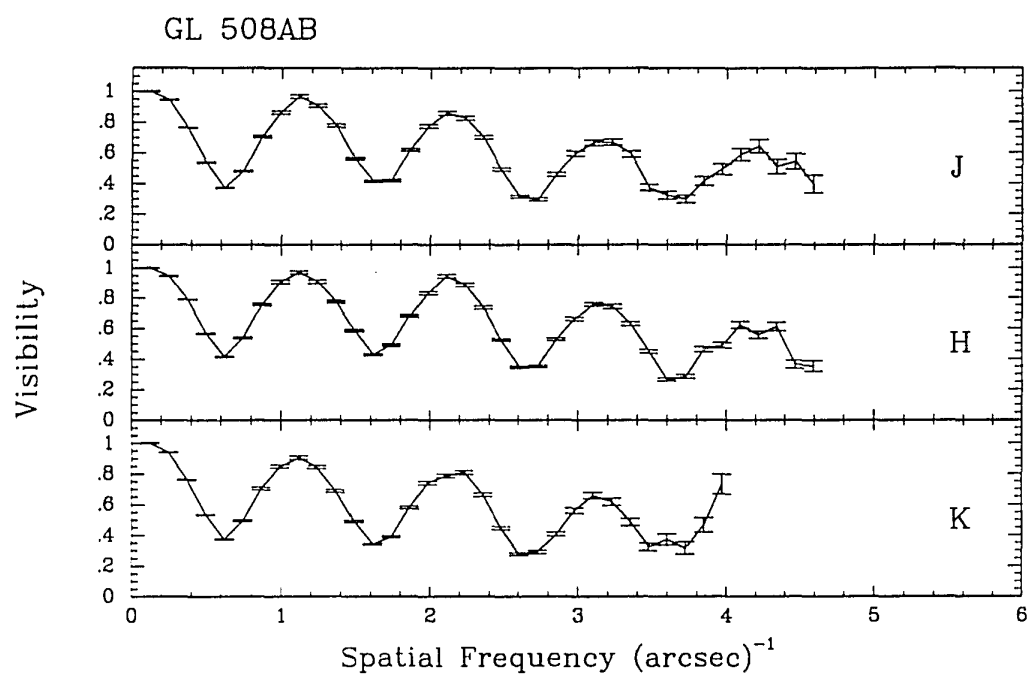


Figure 4.7 Visibility curves for GL 508AB.

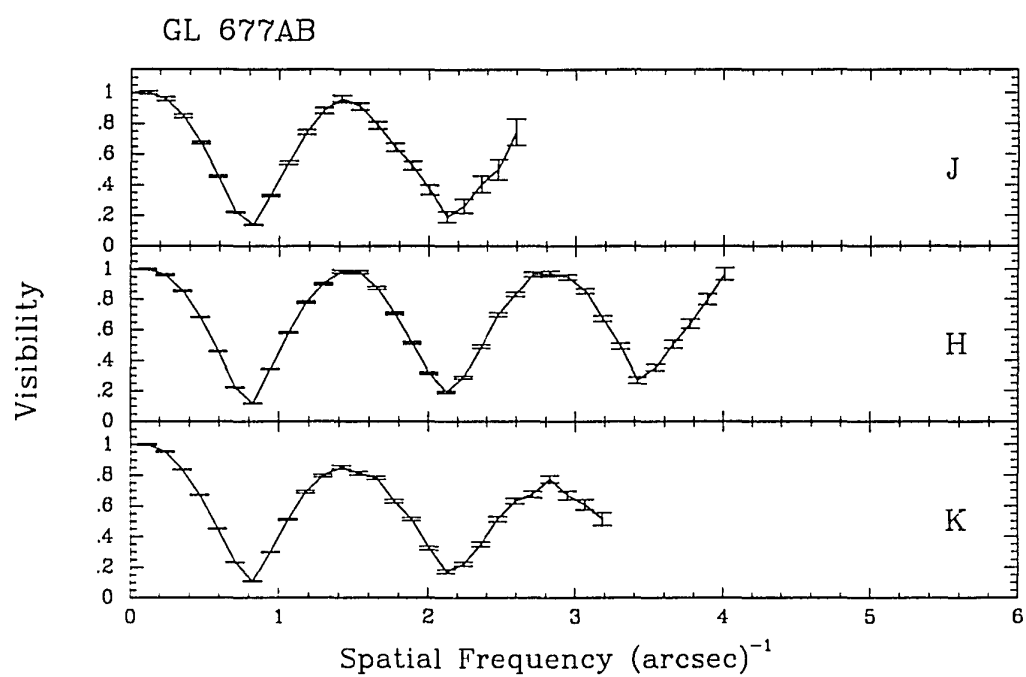


Figure 4.8 Visibility curves for GL 677AB.

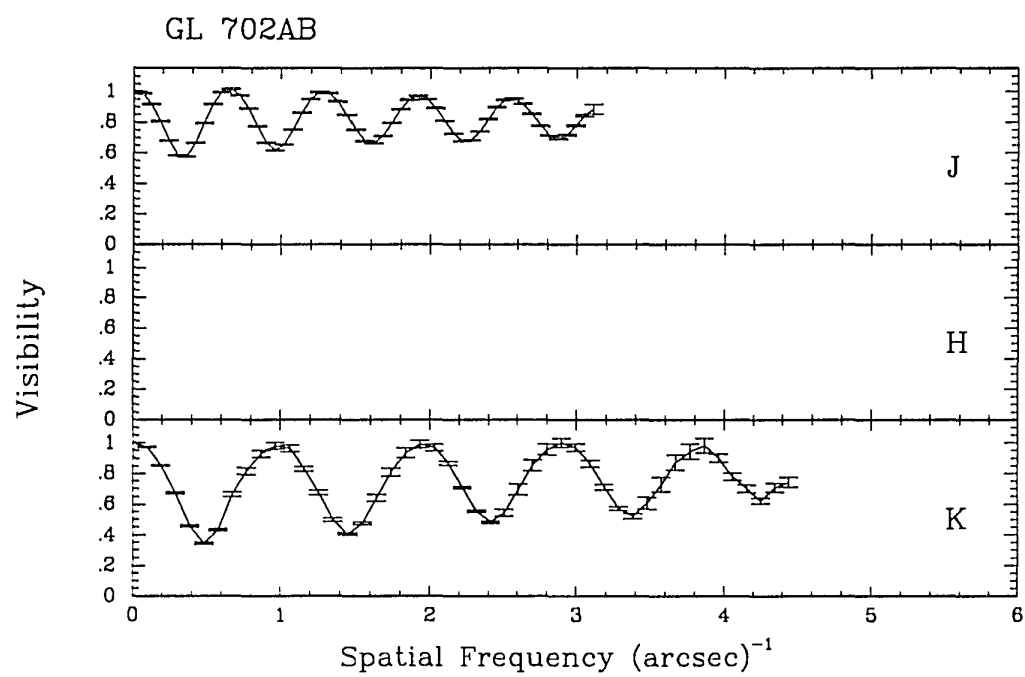


Figure 4.9 Visibility curves for GL 702AB.

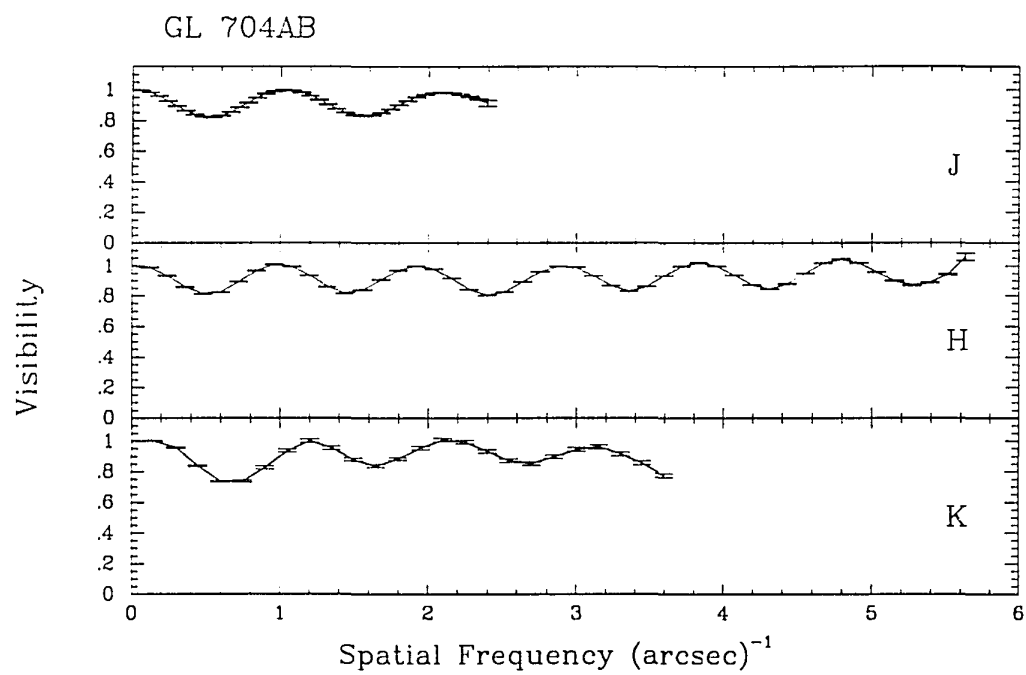


Figure 4.10 Visibility curves for GL 704AB.

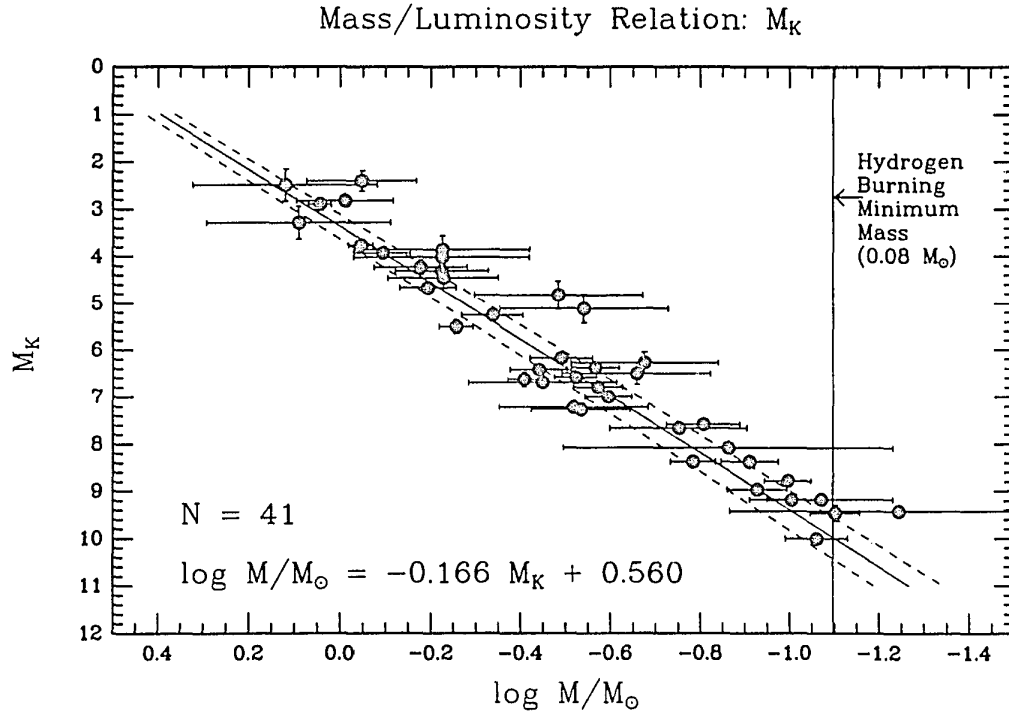


Figure 4.11 The mass-luminosity relation at K. The solid line is the weighted linear least-squares fit to the data. The dotted lines represent the fits with 1σ errors in the slope and intercept adopted.

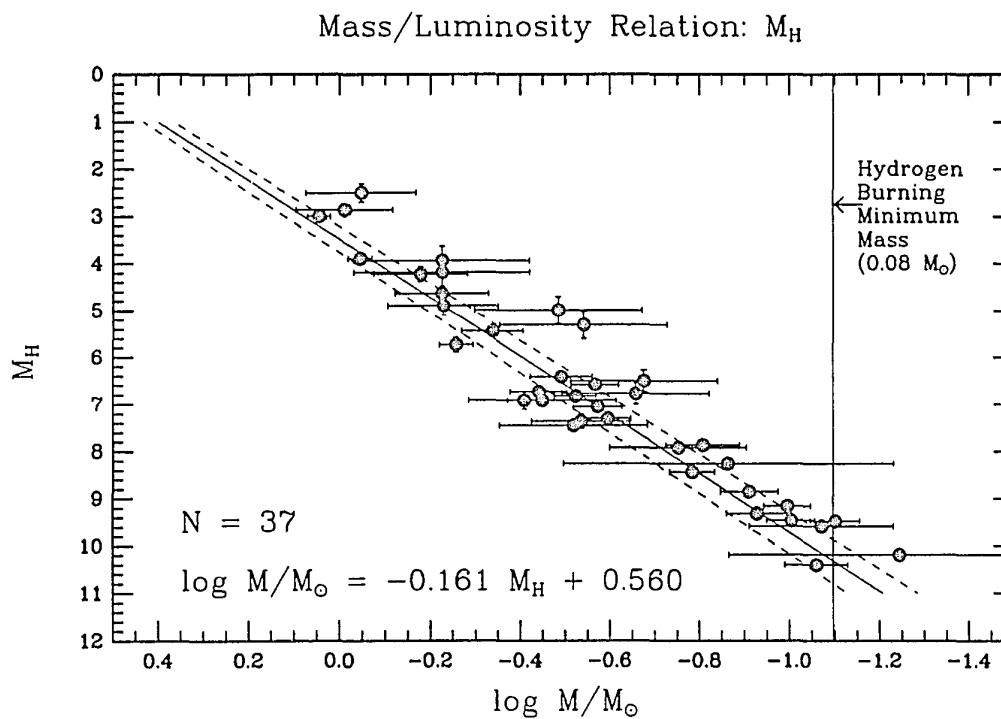


Figure 4.12 The mass-luminosity relation at H. The solid line is the weighted linear least-squares fit to the data. The dotted lines represent the fits with 1σ errors in the slope and intercept adopted.

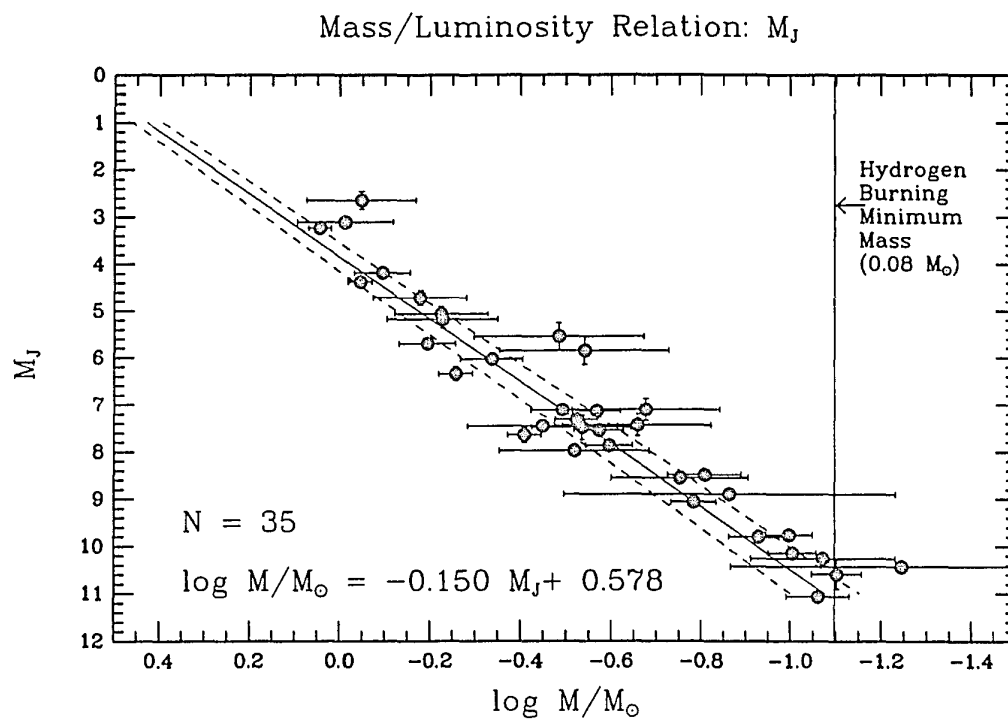


Figure 4.13 The mass-luminosity relation at J. The solid line is the weighted linear least-squares fit to the data. The dotted lines represent the fits with 1σ errors in the slope and intercept adopted.

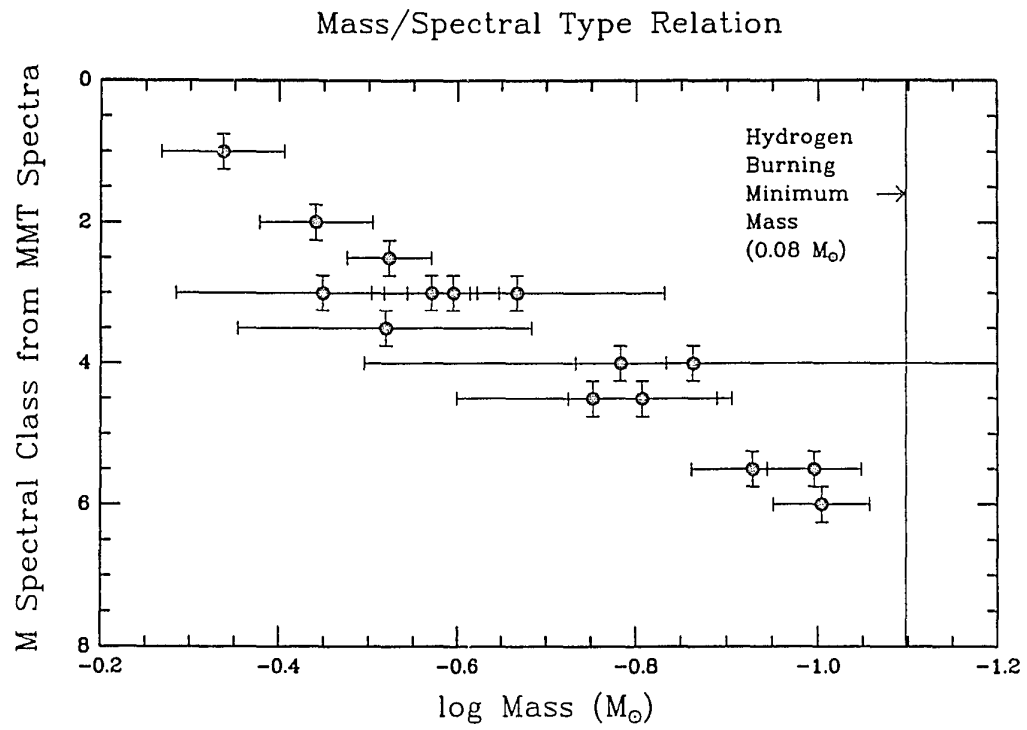


Figure 4.14 The mass-spectral type relation for stars with types M 1.0 to M 6.0.

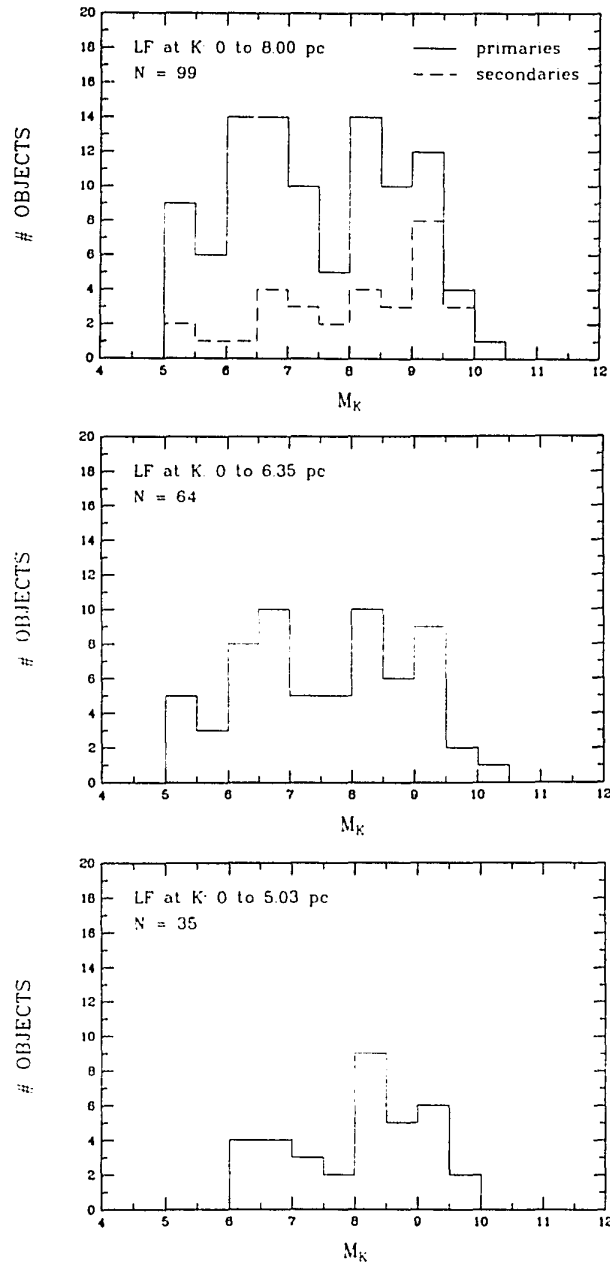


Figure 4.15 The luminosity function at K for the survey members, grouped in 0.5 magnitude bins. The top panel includes all objects to 8.00 pc, the center panel objects to 6.35 pc, and the bottom panel objects to 5.03 pc. The histogram of secondaries is shown for the complete 8.00 pc survey in the top panel.

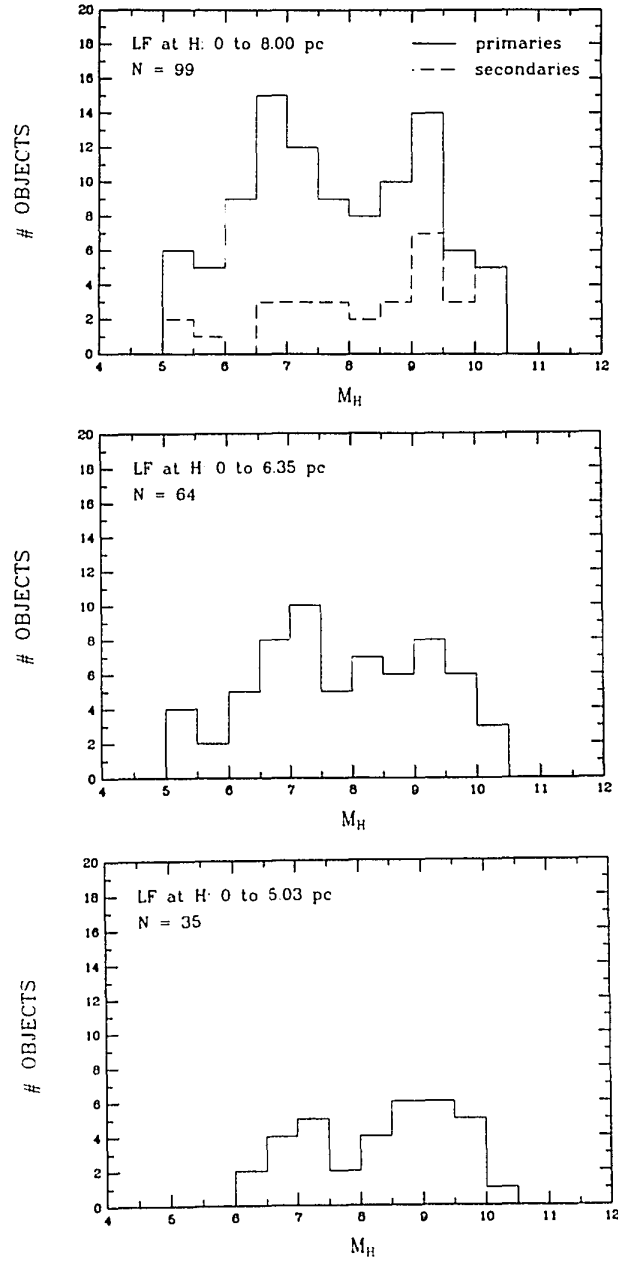


Figure 4.16 The luminosity function at H for the survey members, grouped in 0.5 magnitude bins. The top panel includes all objects to 8.00 pc, the center panel objects to 6.35 pc, and the bottom panel objects to 5.03 pc. The histogram of secondaries is shown for the complete 8.00 pc survey in the top panel.

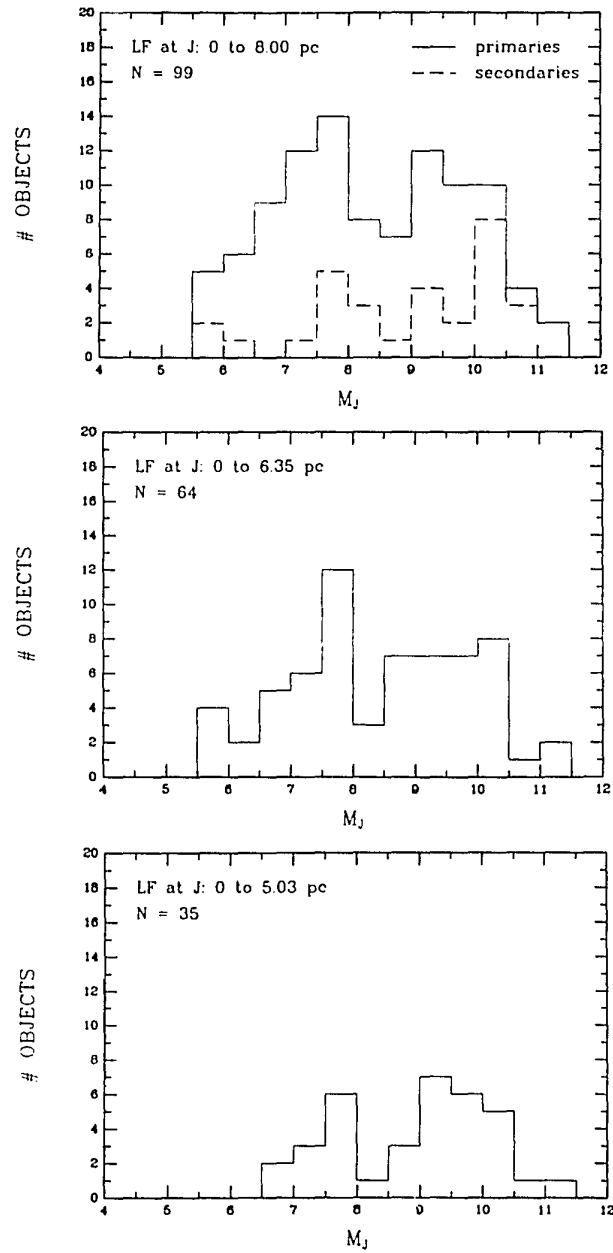


Figure 4.17 The luminosity function at J for the survey members, grouped in 0.5 magnitude bins. The top panel includes all objects to 8.00 pc, the center panel objects to 6.35 pc, and the bottom panel objects to 5.03 pc. The histogram of secondaries is shown for the complete 8.00 pc survey in the top panel.

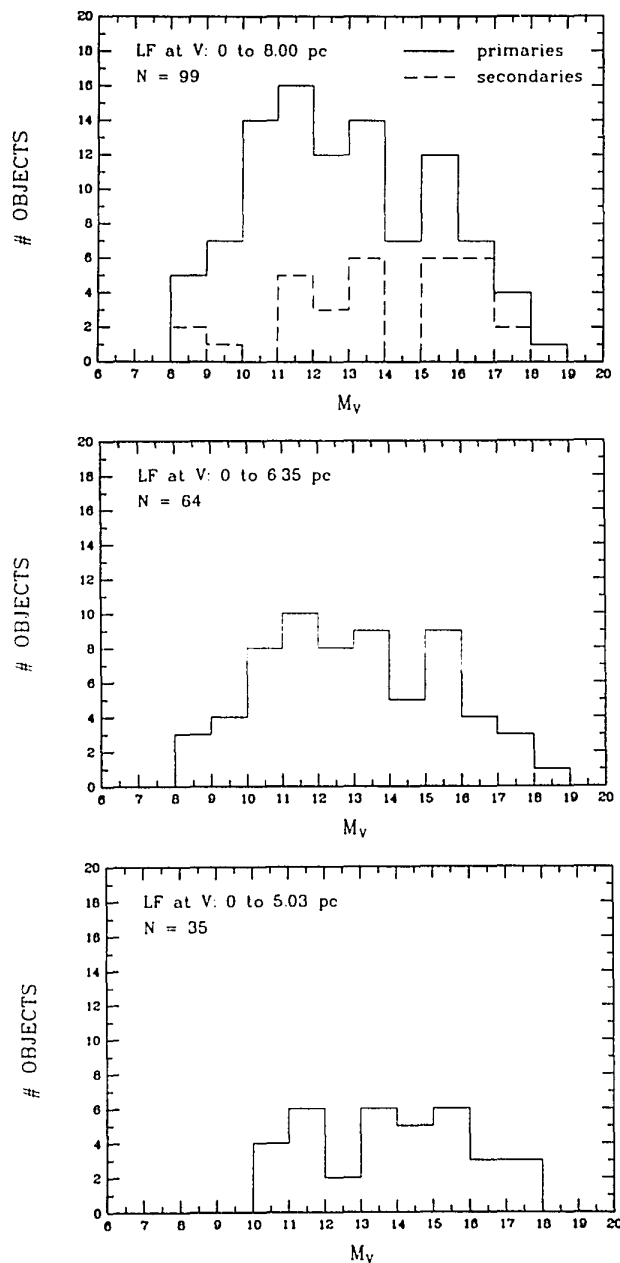


Figure 4.18 The luminosity function at V for the survey members, grouped in 1.0 magnitude bins. The top panel includes all objects to 8.00 pc, the center panel objects to 6.35 pc, and the bottom panel objects to 5.03 pc. The histogram of secondaries is shown for the complete 8.00 pc survey in the top panel.

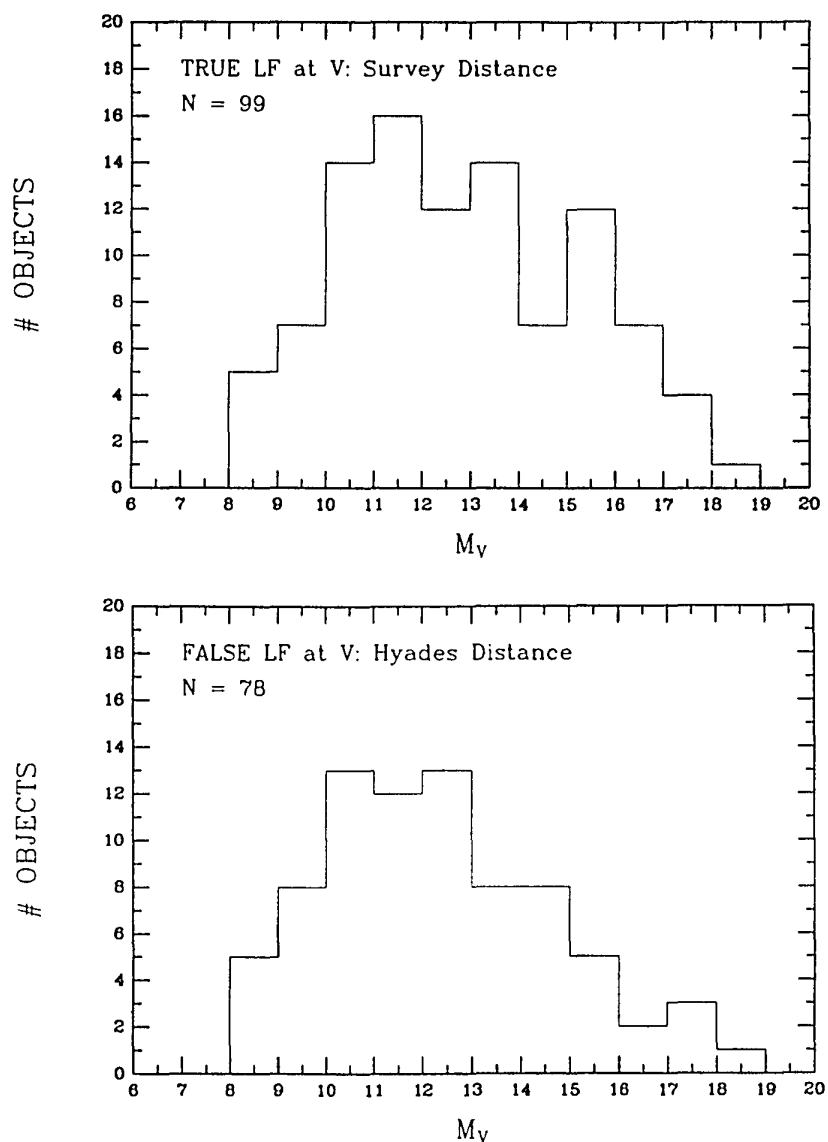


Figure 4.19 The true and false luminosity functions at V. In the top panel, the luminosity function has been determined for the sample members at their actual distances. In the bottom panel we show the incorrect luminosity function found if the sample stars were moved to the distance of the Hyades, where we have assumed binaries are not resolved if their separations are less than $1''$. Note the loss of 21 objects, and the depression of the faint end of the luminosity function.

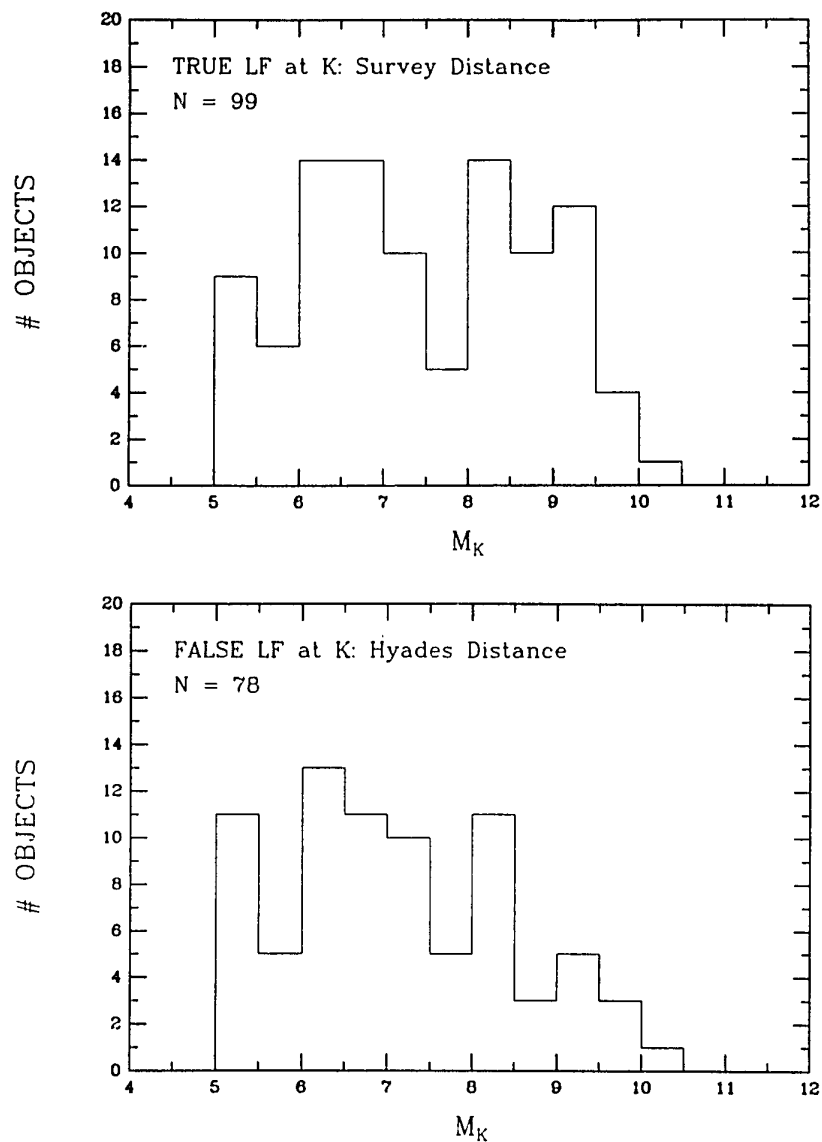


Figure 4.20 The true and false luminosity functions at K. In the top panel, the luminosity function has been determined for the sample members at their actual distances. In the bottom panel we show the incorrect luminosity function found if the sample stars were moved to the distance of the Hyades, where we have assumed binaries are not resolved if their separations are less than $1''$. Note the loss of 21 objects, and the depression of the faint end of the luminosity function.

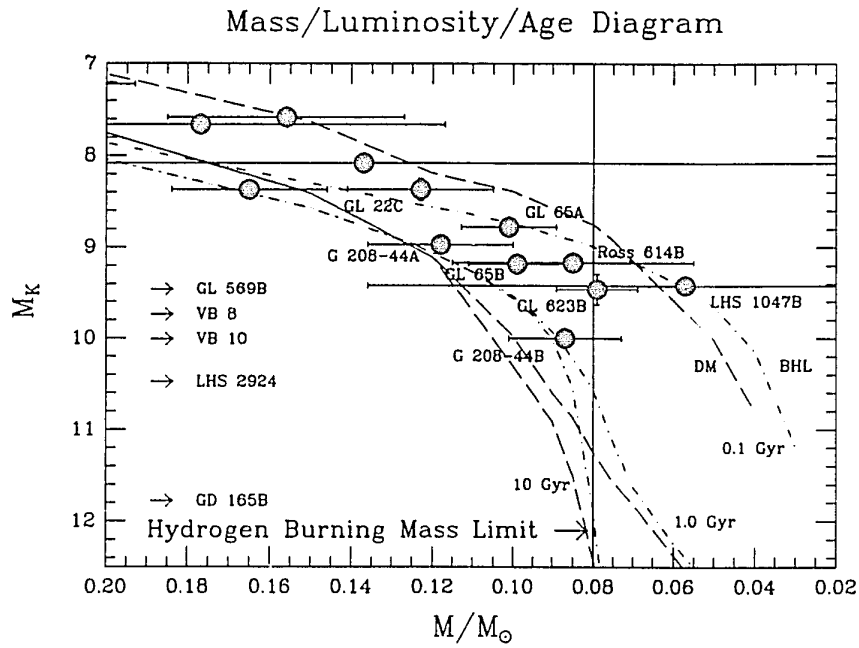


Figure 4.21 The mass-luminosity-age diagram for very low mass objects. The isochrones of D'Antona and Mazzitelli (1985, DM, dashed curves) and Burrows *et al.* (1989, BHL, dot-dash curves) are shown for ages of 0.1, 1.0 and 10 Gyr. The seven lowest luminosity red objects known with determined masses are within the speckle survey, and the four least massive are brown dwarf candidates. Other brown dwarf candidates are shown on the left at their respective M_K s.

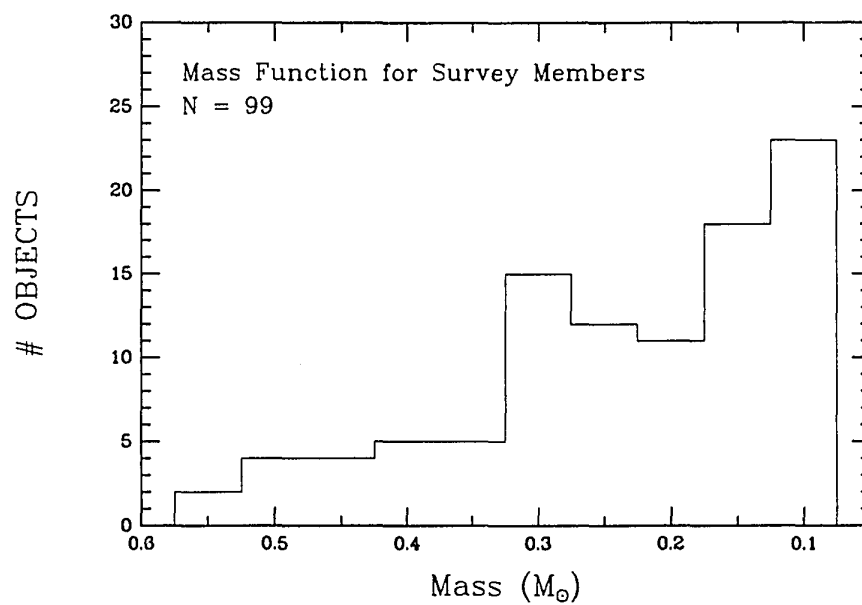


Figure 4.22 The mass function for all objects in the survey, grouped in bins of $0.05 M_{\odot}$.

CHAPTER 5

The End of the Main Sequence and Brown Dwarfs Today

5.1 The Empirical Definition of the End of the Main Sequence

We provide empirical guidelines, including absolute magnitudes, colors and spectral types, for objects with masses at the star/brown dwarf border.

In this final chapter we are concerned with the state of the search for brown dwarfs today. One of the primary goals of this thesis has been to define empirically what a BD is, and in this first section that is what we shall attempt to do — in the form of absolute magnitudes, colors and spectral types. In the final sections we discuss the BD candidates of today, summarize the results of this thesis, and outline some of the next steps to be taken in the hunt for BDs.

5.1.1 Absolute Magnitudes and Colors

As we have done throughout this work, we adopt a mass of $0.08 M_{\odot}$, or 80 Jupiter masses, as the canonical lowest mass for a star. We have provided observational support for this value in Chapter 4. Using the mass-luminosity relations of §4.1, we found that the absolute infrared magnitudes for objects of mass $0.08 M_{\odot}$ are $M_K = 9.98$, $M_H = 10.29$ and $M_J = 11.17$. These values imply infrared colors of $(J-K) = 1.19$, $(J-H) = 0.88$ and $(H-K) = 0.31$. Direct comparison of these colors to an object of similar absolute flux, VB 10 ($M_K = 10.01$, $M_H = 10.44$ and $M_J = 11.12$), indicates that the M_H value is likely to be too bright, and therefore, the

(J-H) and (H-K) values may be in error. Because of the very good match between the VB 10 absolute magnitudes at J and K, and those found for the end of the main sequence, we choose the VB 10 value to represent M_H at the star/BD border. We then adopt infrared colors (rounded to the nearest 0.05 mag) of $(J-K) = 1.20$, $(J-H) = 0.75$ and $(H-K) = 0.45$ as the empirical dividing lines between stars and BDs.

In Figure 5.1 we plot the (V-K) color versus M_K for the survey members. We have chosen M_K because it provides the strongest mass-luminosity relation, and because K is the wavelength at which speckle observations were made most often, thus the Δm_K for close binaries is often better determined than at J or H. The single point at $(V-K) > 8.0$ is VB 10, itself a BD candidate. We see that at the star/BD border ($M_K = 10.0$) the (V-K) value is ~ 8.0 , and that this translates into $M_V \sim 18.0$ for a body of mass 80 Jupiters.

5.1.2 Spectral Type

We reported in §4.2 a spectral type-mass relation using MMT Red Channel spectra of stars in binary systems. Unfortunately, the relation is only calibrated to $0.1 M_\odot$ (type M 6.0), so an estimate of the spectral type at which we approach the highest mass BDs is not straightforward. Instead, we rely upon the M_K limit of 10.0, at which we find a corresponding spectral

type of M 8.0.

5.1.3 The End of the Main Sequence

Here we summarize the empirically determined guidelines for the end of the main sequence. This is an attempt to provide a framework which *should be used primarily to identify possible brown dwarf candidates, not to determine unequivocally that an object is a brown dwarf*. Two caveats are required. First, we have assumed that $0.08 M_{\odot}$ is the breakpoint between stars and BDs. Theoretical models indicate slightly different minimum masses dividing stars from BDs at various metallicities, opacities, and mixing lengths (70–90 Jupiters for models with various galactic abundances, and 98 Jupiters for zero metallicity, Lunine 1991, private communication) and no attempt has been made here to compensate for such differences. Second, age is an important factor when discussing objects of very low mass, $\leq 0.12 M_{\odot}$, and is difficult to estimate for individual objects. Unless a mass is obtained directly for a BD candidate, the question of age is unavoidable, and must be addressed when considering the possibility that it is a true BD. While it seems reasonable that young BDs may be considerably brighter than the limits given, this hypothesis remains untested, as no mass determinations are available for very low mass objects found in young clusters. Finally, in addition to the age of a very low mass object, opacity sources will affect its luminosity, and these depend upon the object's metallicity.

The following guidelines are appropriate for objects similar in age and metallicity to those used to determine the empirical relations outlined in this thesis — members of the intermediate disk population of our galaxy. With the above reservations in mind, we find the following characteristics for the end of the main sequence:

$$\text{MASS} = 0.08 \text{ M}_{\odot}$$

$$M_K \sim 10.00$$

$$M_H \sim 10.45$$

$$M_J \sim 11.20$$

$$(J-K) \sim 1.20$$

$$(J-H) \sim 0.75$$

$$(H-K) \sim 0.45$$

$$(V-K) \sim 8.0$$

$$M_V \sim 18.0$$

$$\text{Spectral Type} \sim \text{M } 8.0$$

These empirical guidelines indicate that several brown dwarfs may already have been found, most notably GD 165B, LHS 2924, and LHS 2065.

5.2 Brown Dwarfs Today

Since the announcement of the possible companion to VB 8 in 1985,

the number of brown dwarf candidates has grown considerably, and today there are two objects known which are quite likely to be true brown dwarfs.

Table 5.1 lists today's brown dwarf candidates. These objects have been chosen because their characteristics — mass, infrared luminosity, spectral type or color — place them near or in the realm of the high mass BDs. They are listed roughly in order of their likelihood of being BDs, where GD 165B is the most promising candidate.

The spectral types given are from the standard system of Kirkpatrick (1991), who has provided the most up-to-date types for the reddest objects known (column 2). The spectra cover the range 6320–9170 Å and have been taken with the MMT Red Channel Spectrograph using the method described in §3.8.2. The third column gives the references for the spectra, a few of which were taken by other groups. The infrared photometry given in columns 4 and 5 are usually from the discovery papers (column 6). The parallax and its standard error are given in column 7 if known (reference in column 8), which allows the absolute K magnitude to be computed (column 9). The final column lists the characteristics which have led to the placement of the object on the list, and references in the cases where masses have been determined.

5.2.1 Candidates with Mass Determinations

Within the eight parsec survey, there are four objects with masses determined to be near or below the stellar/substellar break: G 208-44B, GL 623B, LHS 1047B and Ross 614B. These four objects have been discussed in detail in §4.1.3, where discussion of the infrared speckle observations and the appropriate references can be found. At the present time, all four have mass errors which could place them on either side of the 80 Jupiter border (see Figure 4.21). These four objects are the four least luminous objects known for which masses have been determined and therefore make up a very special class of objects. We recommend that speckle observations be continued to better define their masses.

The best candidate of the four is G 208-44B, with a dynamical mass found to be 87 ± 14 Jupiters, and a photometric mass estimate of 79 Jupiters. It is well known that at such low masses the objects cool in time, so their infrared magnitudes will be age-dependent. Interestingly, we have found the G208 system to be young because of the rotation properties of the components, the presence of $H\alpha$ in emission, and the space motion of the system (McCarthy *et al.* 1988; Henry and Kirkpatrick 1990). Examination of the mass-luminosity-age diagram shown in Figure 4.21 indicates that at younger ages, BDs will be brighter; thus, a low mass for G 208-44B is preferred.

The binary system Wolf 424AB is also within the speckle survey,

and has been reported by Heintz (1972, 1989) to consist of a pair of substellar components. A detailed analysis of the system is given by Henry *et al.* (1991), in which we report speckle interferometric, photometric and spectroscopic data on the system that indicate the objects are probably stars, not BDs. Specifically, the position angles measured from the speckle observations are consistently ahead of the predicted positions, indicating that the orbital parameters of Heintz require revision. Because the determination that the masses are substellar depends entirely upon the orbit, which appears to be in error, and since all other data suggest stellar masses, we believe that Wolf 424A and B should not be included in the BD candidate list. That the objects are not substellar is also supported by the infrared spectroscopy of Davidge and Boeshaar (1991) and additional infrared speckle work by Perrier *et al.* (1991).

5.2.2 Intrinsically Faint, Red Candidates

This group includes eleven objects which have M_{KS} , spectral types and/or (J-K) colors which meet or surpass the empirical guidelines for the end of the main sequence described above. Six have spectral types of M 8.0, one of which, VB 10, is within the eight parsec survey. The more interesting candidates have types M 8.5 or redder. CTI 0127+2802 was found by Kirkpatrick (1991) during a search of the University of Arizona CCD Transit Instrument database, and has been followed-up spectroscopically using the

standard system outlined in §3.8.2. GL 569B was discovered by Forrest *et al.* (1988) during a survey of nearby M dwarfs for low mass companions orbiting in regions 2–7'' from the target stars. They discuss the possibility that the companion to the M 2.5 primary is a BD. In follow-up work, Henry and Kirkpatrick (1990) reported the spectral type of the secondary to be M 8.5, making it one of the reddest objects known, although the absolute infrared magnitudes do not place it among the faintest. In a comparison of GL 569B and G 208-44B, they find that the latter is about the same age, yet fainter, and therefore is probably a better BD candidate. They also find that GL 569B is not as red as LHS 2924.

LHS 2924 and LHS 2065 are similar objects found by Luyten during his proper motion survey. LHS 2924 has been known since Probst and Liebert (1983) to exhibit a peculiar spectrum, and has been studied further by Liebert *et al.* (1984). Kirkpatrick *et al.* (1991) have classified LHS 2924 to be M 9.0 on their standard system, and have determined a similar spectral type for LHS 2065, which has a slightly redder spectrum (supporting the redder infrared photometry). At this very late spectral type, the vanadium oxide bands are quite deep, and at least in LHS 2924, little or no H α emission has been seen. According to the theoretical models, they are either old stars, or young, substellar BDs. Utilization of the empirical outlines given above indicates that these two objects are very good BD candidates.

At the top of the list we find the reddest dwarf known, GD 165B. This extraordinary object is discussed in §5.2.5, the section on “The Two Best Brown Dwarf Bets.”

5.2.3 Cluster Candidates

Because very low mass stars and brown dwarfs cool in time, their temperatures, and therefore their luminosities and spectra, are time-dependent. This has prompted many workers to look in young clusters for BDs. As pointed out in §1.6.2, these young stellar cluster searches suffer from four obstacles which are always difficult to overcome — cluster membership of the candidates, reddening in the cluster field, accurate photometry for faint objects in crowded fields, and the true age of an individual source. As listed in Table 1.1, there are now some 50 BD candidates in the Pleiades, and three in ρ Oph.

Using the recent BD cooling tracks of Burrows *et al.* (1989) and the models of D’Antona and Mazzitelli (1985), we estimate the “spectral drift” Pleiades BDs would suffer, until they become as old as the disk stars used as spectral standards. We expect Pleiades members of age 7×10^7 years and mass $0.08 M_{\odot}$ to be 500–800 K hotter than disk stars of age 5×10^9 years. Thus, a body with a mass near 80 Jupiters (spectral type $\sim M 8.0$ at intermediate disk age) should appear ~ 5 spectral subdivisions

hotter at Pleiades age (M 3.0 instead of M 8.0) than it would when at the age of the disk. Any Pleiades object with spectral type M 3.0 or later, then, may be a high mass BD. Discussions with John Stauffer and our own MMT spectra indicate types of M 5.0 to M 5.5 for some of the Stauffer *et al.* (1989) candidates, making them interesting objects, regardless of the difficulties associated with the cluster searches and in estimating the spectral type corresponding to 80 Jupiters for the Pleiades.

5.2.4 Serendipitous Discoveries of Brown Dwarf Candidates

There are a handful of BD candidates which are not the products of systematic searches, or which have proven to be highly unusual. While each of the following discoveries is interesting, each is an isolated occurrence and provides little information about BDs in general. However, one of the most positive aspects of a career in astronomical research is the surprise discovery of something you hadn't expected, where you weren't looking for it, and in recent years a few BD candidates have popped up in unlikely places using improbable techniques.

The first is the companion of mass ~ 25 Jupiters that eclipses the millisecond pulsar PSR 1957+20 (Fruchter *et al.* 1990). The companion, discovered by pulsar timing measurements, is being evaporated by the pulsar, and remains an intriguing object although it is certainly not a pristine BD.

Recently, Bailes *et al.* (1991) reported a very low mass object, perhaps only 10–12 Earth masses, orbiting the pulsar PSR 1829–10. Although the body is too small to be a BD, it certainly falls into the substellar category, and we await confirmation that it is, in fact, real. Irwin *et al.* (1989) reported a microlensing event in the gravitationally lensed quasar Q 2237+0305. They discuss the possibility that the event may be caused by a body of mass 1–100 Jupiters present in the intervening galaxy, although the data are certainly consistent with a body of mass $0.2 M_{\odot}$.

The highly unusual object PC 0025+0447 was found during a grism survey for high redshift quasars by Schneider *et al.* (1991). They argue that it may be a very young, fading BD. In this case it is the extraordinary $H\alpha$ emission ($> 250 \text{ \AA}$ equivalent width) that makes the object particularly puzzling. It has proven in follow-up work to be quite red (M 9.5, Kirkpatrick and Henry 1991), and we await further analysis.

The last object in this category is the companion to the white dwarf G 29-38, discovered by Zuckerman and Becklin (1987). The secondary has not been imaged directly, although a tentative detection at a north-south separation of $0.23''$ has been reported (Haas and Leinert 1990). However, at the present time the favored origin for the excess infrared emission is a dust shell surrounding the ZZ Ceti type white dwarf. The dust shell model is supported by pulsation timing data and by the flux measured at $10 \mu\text{m}$

(Graham *et al.* 1990). Even if the excess proves to be from a distinct object, it is quite possible that at such a small separation (≤ 5 AU) it is not a pristine BD, as it may have been affected by the evolution of the white dwarf precursor.

5.2.5 The Two Best Brown Dwarf Bets

The author believes that at this time, there are two very good bets for BDs. The first is the remarkable object GD 165B, found by Becklin and Zuckerman (1988). Imaged at a separation of ~ 120 AU from its white dwarf primary, it is known to be a distinct object, is gravitationally bound to its primary, and has probably remained unaffected by the evolution of the white dwarf precursor. Furthermore, it is truly a standout in luminosity and color, as indicated in Table 5.1, and surpasses all of the empirical criteria for the end of the main sequence discussed in this thesis. In addition, a MMT Red Channel spectrum of GD 165B has recently been obtained (Kirkpatrick and Henry 1991), and it proves to be extremely red — later in type than any object known — and very unusual.

Theoretical estimates of GD 165B's mass also indicate that it is substellar. The white dwarf's age is estimated to be 6×10^8 years (Becklin and Zuckerman 1988), and if the secondary is of the same age, the theoretical models indicate that the companion's mass is between 60

and 65 Jupiters (see Figure 4.21). This age estimate, however, remains controversial (Liebert 1991, private communication). Nonetheless, it is the opinion of the author that GD 165B is likely to be a *bona fide* brown dwarf.

The second best bet for a BD is the companion orbiting the solar-type star HD114762. Discovered to be a spectroscopic binary of period 84 days by Latham *et al.* (1989), the minimum mass for the secondary is 11 Jupiters. Unfortunately, because it is an unresolved spectroscopic binary, the mass remains uncertain because $a \sin i$ is unknown. However, the probability that the companion has a mass greater than 80 Jupiters is only 1%. We surmise, then, that the chances of the companion being substellar are very high.

5.3 Summary

We list here the more important contributions of this thesis to the studies of low mass stars and brown dwarfs.

1. We suggest that brown dwarfs be considered a third type of planet.
2. Two-dimensional infrared speckle imaging has proven effective in searching stars for low mass companions, and is superior to one-dimensional techniques.

3. It is likely that as many as 50% of the M dwarfs lying between 6.35 and 8.00 parsecs from the sun have been missed by the proper motion and parallax surveys.

4. The census of stars within 5.2 pc of the sun has grown steadily during the last 45 years, and has not yet begun to slow as new techniques are used to find faint new members of the solar neighborhood.

5. We provide a comprehensive reference of infrared photometry for all 99 sample members.

6. We give spectral types for half of the survey members on a standard system.

7. Every known M dwarf within eight parsecs of the sun, and north of -25° has been searched for low mass companions, to $M_K \sim 11$. Six new companions were found — three of them brown dwarf candidates. Limits have been set for the 68 unresolved sources at 1, 2, 5 and 10 AU.

8. Four objects are known within eight parsecs that have masses determined to be near the star/brown dwarf border.

9. No objects are known within eight parsecs of the sun with M_K between 10.0 and 11.0. This cutoff corresponds to masses ~ 80 Jupiters — the transition region between stars and brown dwarfs.

10. The theoretically predicted precipitous drop in luminosity for

objects near the stellar/substellar break is probably the cause of the paucity of brown dwarf discoveries, and is supported by the lack of objects near the sun with $M_K = 10.0\text{--}11.0$.

11. The binary fraction of M dwarfs is 30–40%, significantly lower than that of earlier type primaries. Incompleteness caused by unsearched higher mass primaries, because they are far less populous than the M dwarfs, will probably not affect the M dwarf binary fraction substantially.

12. More companions are found orbiting M dwarfs at separations between 1 and 10 AU than in any other decade interval.

13. We now have mass–luminosity relations defined in the infrared which are useful for stars of mass $1.2 M_\odot$ to the end of the main sequence, although at masses less than $0.12 M_\odot$ caution must be exercised.

14. The luminosity function of low mass stars at K is flat or rising to the end of the main sequence, and is probably flat when determined at V.

15. Any accurate determination of the luminosity function must consider the importance of binaries.

16. The mass function of the most populous members of the galaxy clearly rises to the end of the main sequence.

17. The M dwarfs contribute $\sim 0.02 M_\odot/\text{pc}^3$ to the mass of the

galactic disk.

18. We have defined empirically the end of the main sequence using infrared and visual luminosities and colors, and red/near-infrared spectra.

19. It is quite likely that at least two brown dwarfs have been discovered to date. Using the empirical definitions for the end of the main sequence, there are as many as a dozen others.

5.4 The Future

Through the many searches for brown dwarfs, whether by imaging, photometric or kinematic techniques, the existence of other solar systems with substellar, planetary-sized secondaries is being investigated. During the last decade, the hunt for brown dwarfs has become furious, and good candidates are now being discovered. Some investigators have claimed that there are very few BDs, others believe that we have not yet seen even the tip of the iceberg. The latter opinion is the one supported by the author.

Even in the immediate solar neighborhood, we have seen that the nearby star census continues to grow, and that half of the stars in the outer reaches of the survey appear to be unfound. Thus, the possibility that free-floating BDs are present in large numbers near the sun remains. As companions to nearby stars, we have only begun to scratch the surface. No systematic search for BDs orbiting stars of any type other than M

dwarfs has been completed, although a radial velocity search for G dwarf companions has been begun by Latham and collaborators. Deep imaging surveys at wide separations (a few tens to hundreds of AU) have not probed deeply enough into the realm of BDs to eliminate their existence convincingly. At smaller separations, we have been able to search only for the highest mass BDs using infrared speckle techniques, although astrometric and radial velocity work should have uncovered them if they are there. However, a 50 Jupiter mass BD orbiting an M dwarf of one-quarter solar mass has a period of 20 years at a modest separation of 5 AU, so it is not surprising that only patient work will reveal a companion. Nonetheless, although the radial velocity work of Marcy and Benitz (1989) was of short duration, it was done well, and combined with the decades of work by the astrometrists, the lack of many BD detections is disturbing.

It is an exciting time for brown dwarf research, as many techniques are just reaching the point where interesting discoveries can be made. In fact, it is the opinion of the author that a few brown dwarfs have already been found. Quite probably, finding the final answer to the question "Do brown dwarfs exist?" will require two qualities not often rewarded in today's society — patience and endurance — and we would do well to apply both to the search for the elusive brown dwarf.

It is my hope that this thesis provides a step towards finding planets

orbiting other stars. Through this work, we at least now understand the stars themselves a bit better, and may know what a brown dwarf looks like, should we find one. Finally, as a closing comment on my own and others' future work in the search for other solar systems, and on the discovery of life itself elsewhere, I end this thesis as I began it:

"... 'tis a consummation devoutly to be wished."

Hamlet Act III, Scene I

TABLE 5.1

BROWN DWARF CANDIDATES

Name	Spec	Ref	J-K	K	Ref	$\pi \pm \sigma$	Ref	M _K	Notes
GD 165B	>M9	KH	1.66	14.09	BZ	.035 004	BZ	11.78	MK, ST, color
LHS 2065	M9.0	KHM	1.34	10.75	B	—	—	—	ST, color
LHS 2924	M9.0	KHM	1.22	10.68	PL	.091 002	D	10.48	MK, ST, color
GL 569B	M8.5	HK	1.13	9.65	BZ	.096 011	FSS	9.55	ST
CTI 0127+2802	M8.5	K	—	—	—	—	—	—	ST
LHS 2397 _a	M8.0	K	1.23	10.75	B	—	—	—	ST, color
HB 2124-4228	M8.0	HB	1.22	12.18	HB	.032 006	I	9.73	ST, color
ESO 207-61	M8.0	RTR	1.19	12.21	RTR	—	—	—	ST
RG 0050-2722	M8.0	RG	1.18	12.50	RG	—	—	—	ST
HB 2115-4518	M8.0	HB	1.15	12.36	HB	.047 004	I	10.70	MK, ST
GL 623B	—	—	1.13	8.85	*	.132 006	GJ	9.46	mass: MH/MM/*
VB 10	M8.0	KHM	1.11	8.81	SH	.174 007	HKD	10.01	MK, ST
Ross 614B	—	—	1.09	7.24	*	.243 002	P	9.17	mass: P/*
G 208-44B	—	—	1.06	8.28	*	.221 002	H _a	10.00	mass: M+/*, MK
LHS 1047B	—	—	1.01	8.04	*	.189 005	IRM	9.42	mass: IRM/*

REFERENCES:

B = Bessell (1990),

BZ = Becklin and Zuckerman (1988),

D = Dahn (1989) personal communication,

FSS = Forrest *et al.* (1988),

TABLE 5.1 (continued)

REFERENCES (continued):

- I = Ianna (1991) personal communication,
 IRM = Ianna *et al.* (1988),
 GJ = Gliese and Jahreiss (1979),
 Ha = Harrington (1990),
 HB = Hawkins and Bessel (1988),
 HKD = Harrington *et al.* (1983),
 HK = Henry and Kirkpatrick (1990),
 K = Kirkpatrick (1991) personal communication,
 KH = Kirkpatrick and Henry (1991) in preparation,
 KHM = Kirkpatrick *et al.* (1991),
 MH = McCarthy and Henry (1987),
 M+ = McCarthy *et al.* (1988),
 MM = Marcy and Moore (1989),
 P = Probst (1977),
 PL = Probst and Liebert (1983),
 RG = Reid and Gilmore (1981),
 RTR = Ruiz *et al.* (1991),
 SH = Stauffer and Hartmann (1986),
 * = this work

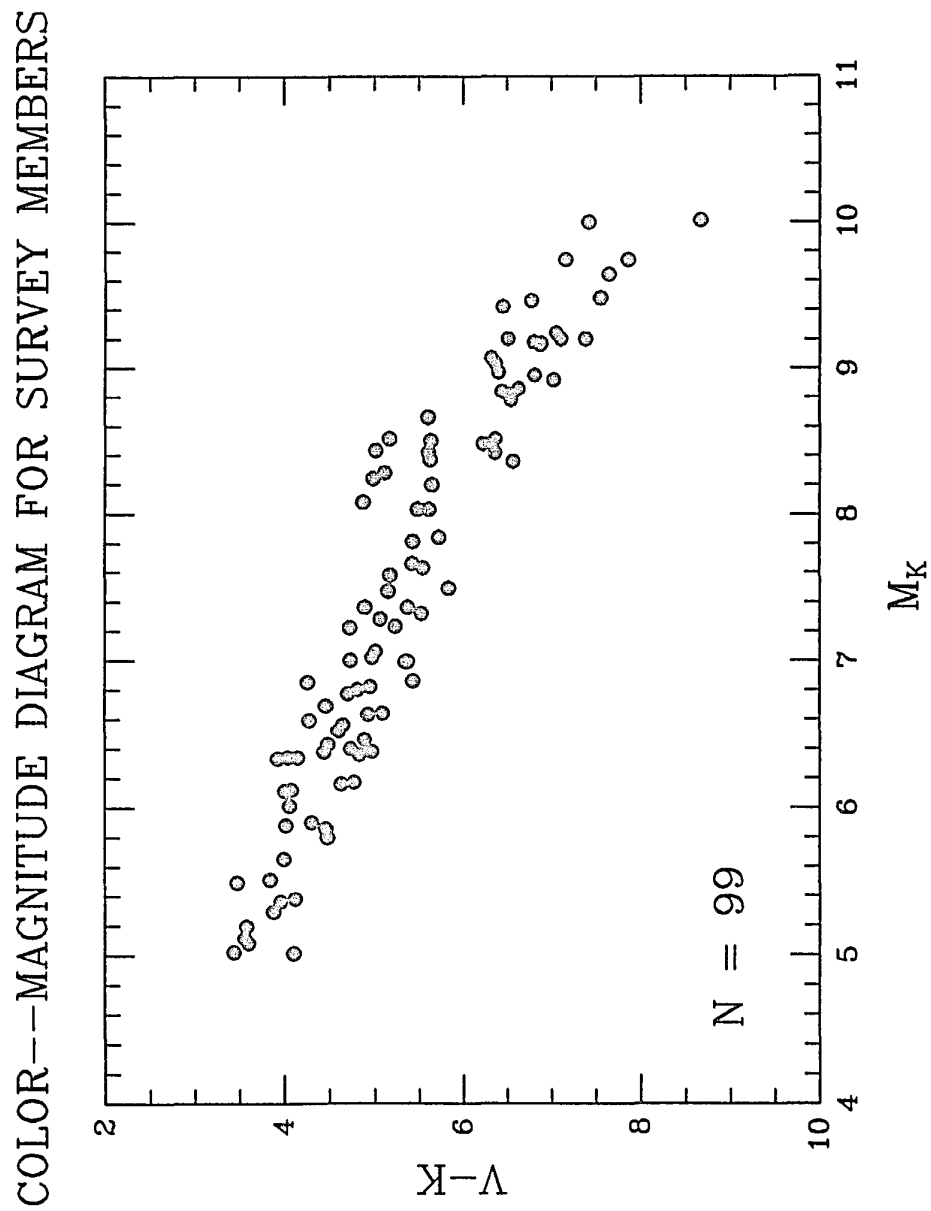


Figure 5.1 The $(V-K)$ vs. M_K diagram for all objects in the survey. The reddest point is VB 10, which is a brown dwarf candidate according to the empirical guidelines presented in this work.

REFERENCES

- Abt, H.A. 1983, ARA&A, 21, 343
- Abt, H.A. 1987, ApJ, 317, 353
- Abt, H.A. & Levy, S.G. 1973, AJ, 78, 1093
- Abt, H.A. & Levy, S.G. 1978, ApJS, 36, 241
- Bahcall, J.N. 1984, ApJ, 276, 169
- Bahcall, J.N. 1984, ApJ, 287, 926
- Bailes, M., Lyne, A.G., & Shemar, S.L. 1991, Nature, 352, 311
- Batten, A.H. 1990, in Observers Handbook, ed. R.L. Bishop
(Toronto: Royal Astronomical Society of Canada), p. 193
- Beckers, J.M., Christou, J.C., Probst, R.G., Ridgway, S.T., &
von der Luhe, O. 1988, Proc. NOAO/ESO Conf. on High-
Resolution Imaging by Interferometry, ed. F. Merkle, p.393
- Becklin, E.E. & Zuckerman, B. 1988, Nature, 336, 656
- Beichman, C.A. 1987, ARA&A, 25, 521
- Beichman, C.A., Chester, T., Gillett, F.C., Low, F.J., Matthews,

- K., & Neugebauer, G. 1990, AJ, 99, 1569
- Bessell, M.S. 1991, AJ, 101, 662
- Black, D.C. 1980, Icarus, 43, 293
- Black, D.C. 1986, in Astrophysics of Brown Dwarfs, ed. M.C. Kafatos, R.S. Harrington, & S.P. Maran (Cambridge: Cambridge University Press), p. 139
- Blazit, A., Bonneau, D., & Foy, R. 1987, A&AS, 71, 57
- Boeshaar, P.C., Tyson, J.A., & Seitzer, P. 1986, in Astrophysics of Brown Dwarfs, ed. M.C. Kafatos, R.S. Harrington, & S.P. Maran (Cambridge: Cambridge University Press), p. 76
- Boeshaar, P.C. 1976, PhD Thesis, Ohio State University
- Boss, A.P. 1988, Comments Astrophys, 91, 621
- Burrows, A.S., Hubbard, W.B., & Lunine, J.I. 1989, ApJ, 345, 939
- Campbell, B., Walker, G.A.H., & Yang, S. 1988, ApJ, 331, 902
- Chang, K. 1972, AJ, 77, 759
- Christou, J.C. 1988, in Proc. NOAO/ESO conference on High-Resolution Imaging By Interferometry, ed. by F. Merkle, p. 97

- Christou, J.C. 1991, *Exp. Astr.*, 2, 27
- Christou, J.C., Beckers, J.M., Freeman, J.D., Ridgway, S.T., & Probst, R.G. 1988, *Proc. SPIE*, 976, p. 193
- Cutri, R.M., Low, F.J., Young, E.T., Kleinman, S.G., & Gillett, F.C. 1985, *BAAS*, 17, 878
- Dahn, C.C. 1989, private communication, updated LHS Catalog via J. Liebert.
- Dahn, C.C. 1989, private communication.
- Dahn, C.C., Liebert, J., & Harrington, R.S. 1986, *AJ*, 91, 621
- Dainty, J.C. 1984, in *Topics in Applied Physics*, Vol. 9, ed. J.C. Dainty (New York: Springer-Verlag), p. 255
- D'Antona, F. & Mazzitelli, I. 1985, *ApJ*, 296, 502
- Davidge, T.J. & Boeshaar, P.C. 1991, *AJ*, 102, 267
- Duquennoy, A. & Mayor, M. 1991, accepted to *A&A*
- Eggen, O.J. 1967, *ARA&A*, 5, 105
- Elias, J.H., Frogel, J.A., Matthews, K., & Neugebauer, G. 1982, *AJ*, 87, 1029

- Engels, D., Sherwood, W.A., Wamsteker, W., & Schultz, G.V. 1981,
A&AS, 45, 5
- Fahlman, G.G., Richer, H.B., Searle, L., & Thompson, I.B. 1989,
ApJ, 343, L49
- Feierman, B.H. 1971, AJ, 76, 73
- Fischer, D. & Marcy, G.W. 1991, submitted
- Forrest, W.J., Ninkov, Z., Garnett, J.D., Skrutskie, M.F., &
Shure, M. 1989, Proc. 3rd IR Detector Workshop, ed. C.R.
McCreight (NASA Technical Memorandum 102209), p. 221
- Forrest, W.J., Skrutskie, M.F., & Shure, M. 1988, ApJ, 330, L119
- Freeman, J.D. 1989, PhD Thesis, University of Arizona
- Freeman, J.D. 1991, in preparation
- Freeman, J.D., Christou, J.C., Roddier, F., McCarthy, D.W., Cobb,
M.L. 1988, JOSA, 5, 406
- Fried, D.L. 1966, JOSA, 56, 1372
- Fruchter, A.S. *et al.* 1990, ApJ, 351, 642

- Geyer, D.W., Harrington, R.S., & Worley, C.E. 1988, AJ, 95, 1841
- Ghez, A.M., Gorham, P.W., Haniff, C.A., Kulkarni, S.R., Matthews, K., Neugebauer, G., & Weir, N. 1990, in SPIE Proc., 1237, 249
- Gilmore, G. & Reid, N. 1983, MNRAS, 202, 1025
- Gliese, W. 1969, Veroff. des Astronomischen Rechen-Instituts, Heidelberg. No. 22.
- Gliese, W. 1982, in Landolt-Bornstein Numerical Data and Functional Relationships in Science and Technology, Subvol. 2c (Berlin: Springer-Verlag), p. 168
- Gliese, W. & Jahreiss, H. 1979, A&AS 38 423
- Graham, J.R., Matthews, K., Neugebauer, G., & Soifer, B.T. 1990, ApJ, 357, 216
- Grossman, A.S. & Graboske, H.C. 1973, ApJ, 180, 195
- Grossman, A.S., Hays, D., & Graboske, H.C. 1974, A&A, 30, 95
- Haas, M. & Leinert, C. 1990, A&A, 230, 87
- Hambly, N.C. & Jameson, R.F. 1991, MNRAS, 249, 137
- Harrington, R.S. & Kallarakal, V.V. 1982, BAAS, 14, 612

- Harrington, R.S. 1990, AJ, 100, 559
- Harrington, R.S., Kallarakal, V.V., & Dahn, C.C. 1983, AJ, 88, 1038
- Harris, D.L., Strand, K.Aa., & Worley, C.E. 1963, in Basic Astronomical Data, ed. Strand, K.Aa. (Chicago: University of Chicago Press), p. 282
- Hawkins, M.R.S. & Bessell, M.S. 1988, MNRAS, 234, 177
- Heintz, W.D. 1960, Veroff. Sternw. Munchen 5, 100
- Heintz, W.D. 1969, AJ, 74, 768
- Heintz, W.D. 1972, AJ, 77, 160
- Heintz, W.D. 1974, AJ, 79, 819
- Heintz, W.D. 1976, ApJ, 208, 474
- Heintz, W.D. 1978, ApJS, 37, 515
- Heintz, W.D. 1979, AJ, 84, 1223
- Heintz, W.D. 1984, AJ, 89, 1063
- Heintz, W.D. 1984, in Calibration of Fundamental Stellar Quantities: IAU Symposium 111, ed. D.S. Hayes, L.E. Pasinetti, & A.G.

Davis Philip (Boston: Dordrecht), p. 71

Heintz, W.D. 1984, PASP, 96, 439

Heintz, W.D. 1986, AJ, 92, 446

Heintz, W.D. 1986, A&AS, 65, 411

Heintz, W.D. 1987, PASP, 99, 1084

Heintz, W.D. 1989, A&A, 217, 145

Heintz, W.D. & Borgman, E.R. 1984, AJ, 89, 1068

Henry, T.J., Johnson, D.S., McCarthy, D.W., & Kirkpatrick, J.D.
1991, accepted to A&A

Henry, T.J. & Kirkpatrick, J.D. 1990, ApJ, 354, L29

Henry, T.J. & McCarthy, D.W. 1990, ApJ, 350, 334

Henry, T.J., McCarthy, D.W., Freeman, J.D., & Christou, J.C. 1991,
AJ, submitted

Hershey, J.L. 1973 AJ, 78, 935

Hershey, J.L. 1982 AJ, 87, 145

Hill, G., Hilditch, R.W., & Barnes, J.V. 1979, MNRAS, 186, 813

- Howell, R. 1980, PhD Thesis, University of Arizona
- Huang, S.-S. 1973 *Icarus*, 18, 339
- Hubbard, W.B., Burrows, A., & Lunine, J.I. 1990, *ApJ*, 358, L53
- Ianna, P.A., Rohde, J.R., & McCarthy, D.W. 1988, *AJ*, 95, 1226
- Irwin, M.J., Webster, R.L., Hewett, P.C., Corrigan, R.T., & Jedrzejewski, R.I. 1989, *AJ*, 98, 1989
- Jameson, R.F., Sherrington, M.R., & Giles, A.B. 1983, *MNRAS*, 205, 39P
- Jameson, R.F. & Skillen, I. 1989, *MNRAS*, 239, 247
- Kamper, K.W., Legget, D., & McCarthy, D.W. 1989, *AJ*, 98, 686
- Kenyon, S. 1989, private communication
- Kirkpatrick, J.D. 1991, private communication
- Kirkpatrick, J.D. & Henry, T.J. 1991, in preparation
- Kirkpatrick, J.D., Henry, T.J., & McCarthy, D.W. 1991, *ApJS*, 77, 417
- Knox, K.T. 1976, *JOSA*, 66, 1236
- Knox, K.T. & Thompson, B.J. 1974, *ApJ*, 193, L45

- Kroupa, P., Tout, C.A., & Gilmore, G. 1990, MNRAS, 244, 76
- Kuijken, K., Gilmore, G. 1989, MNRAS, 239, 605
- Kuijken, K., Gilmore, G. 1989, MNRAS, 239, 651
- Kumar, C.K. 1987, AJ, 94, 158
- Kumar, S. 1963, ApJ, 137, 1121
- Labeyrie, A. 1970, A&A, 6, 85
- Labeyrie, A., Bonneau, D., Stachnik, R.V., & Gezari, D.Y. 1974,
ApJ, 194, L147
- Lacy, C.H. 1977, ApJS, 34, 479
- Latham, D.W., Mazeh, T., Stefanik, R.P., Mayor, M., & Burki, G.
1989, Nature, 339, 38
- Leggett, S.K. & Hawkins, M.R.S. 1988, MNRAS, 234, 1065
- Leggett, S.K. & Hawkins, M.R.S. 1989, MNRAS, 238, 145
- Leinert, C., Haas, M., Allard, F., Wehrse, R., McCarthy, D.W.,
Jahreiss, H., & Perrier, C. 1990, A&A, 236, 399
- Liebert, J., Boroson, T.A., & Giampapa, M.S. 1984, ApJ, 282, 758
- Liebert, J. & Probst, R.G. 1987, ARA&A, 25, 473

- Lippincott, S.L. 1972, AJ, 77, 165
- Lippincott, S.L. 1978, Space Sc. Rev., 22, 153
- Lippincott, S.L. 1979, PASP, 91, 784
- Lippincott, S.L. 1982, AJ, 87, 1237
- Lippincott, S.L. 1983, in Activity in Red Dwarf Stars, ed. P.B. Byrne & M. Rodonò (Dordrecht, Netherlands: D. Reidel Publishing Company), p. 201
- Lippincott, S.L. & Borgman, E.R. 1978, PASP, 90, 226
- Lippincott, S.L., Braun, D., & McCarthy, D.W. 1983, PASP, 95, 271
- Lunine, J.I., Hubbard, W.B., Burrows, A., Wang, Y.-P., & Garlow, K. 1989, ApJ, 338, 314
- Lunine, J.I., Hubbard, W.B., & Marley, M.S. 1986, ApJ, 310, 238
- Luyten, W.J. 1968, MNRAS, 139, 221
- Luyten, W.J. 1979, LHS Catalog (Minneapolis: University of Minnesota)
- Marcy, G.W. & Benitz, K.J. 1989, ApJ, 344, 441

- Marcy, G.W. & Moore, D. 1989, *ApJ*, 341, 961
- Mariotti, J.-M., Perrier, C., Duquennoy, A., & Duhoux, P. 1990, *A&A*, 230, 77
- McCarthy, D.W. 1976, PhD Thesis, University of Arizona
- McCarthy, D.W. 1984, *AJ*, 89, 433
- McCarthy, D.W. 1986, in *Astrophysics of Brown Dwarfs*, ed. M.C. Kafatos, R.S. Harrington, & S.P. Maran (Cambridge: Cambridge University Press), p. 9.
- McCarthy, D.W., Cobb, M.L., & Probst, R.G. 1987, *AJ*, 93, 1535
- McCarthy, D.W. & Henry, T.J. 1987, *ApJ*, 319, L93
- McCarthy, D.W., Henry, T.J., Fleming, T.A., Saffer, R.A., Liebert, J., & Christou, J.C. 1988, *ApJ*, 333, 943
- McCarthy, D.W., Henry, T.J., McLeod, B.A., & Christou, J.C. 1991, *AJ*, 101, 214
- McCarthy, D.W., McLeod, B.A., & Barlow, D. 1990, *SPIE Proc.*, 1237, 496
- McCarthy, D.W., Probst, R.G., & Low, F.J. 1985, *ApJ*, 290, L9
- McLeod, B.A., McCarthy, D.W., & Freeman, J.D. 1991, *AJ*, 102,

1485

- McMillan, R. 1991, private communication
- McNamara, B.R., Ianna, P.A., & Fredrick, L.W. 1987, AJ, 93, 1245
- Mihalas, D. & Binney, J. 1981, Galactic Astronomy: Structure and Kinematics (San Francisco: Freeman), p. 229
- Morbey, C.L. & Griffin, R.F. 1987, ApJ, 317, 343
- Mould, J.R. 1976, A&A, 48, 443
- Nelson, L.A., Rappaport, S.A., & Joss, P.C. 1986, 311, 226
- Perrier, C. & Mariotti, J.-M. 1987, ApJ, 312, L27
- Perrier, C., Mariotti, J.-M., Bonneau, D. and Duquennoy, A. 1991, in preparation
- Pettersen, B.R. & Griffin, R.F. 1980, The Observatory, 100, 198
- Popper, D.M. 1980, ARA&A, 18, 115
- Probst, R.G. 1977, AJ, 82, 656
- Probst, R.G. 1981, PhD Thesis, University of Virginia
- Probst, R.G. 1983, ApJ, 274, 237

- Probst, R.G. 1983, *ApJS*, 53, 335
- Probst, R.G. & O'Connell, R.W. 1982, *ApJ*, 252, L69
- Probst, R.G. & Liebert, J. 1983, *ApJ*, 274, 245
- Reid, N. 1987, *MNRAS*, 225, 873
- Reid, N. & Gilmore, G. 1981, *MNRAS*, 196, 15P
- Rieke, G.H. & Rieke, M.J. 1990, *ApJ*, 362, L21
- Roddier, F. 1988, *Physics Reports*, 170, 97
- Ruiz, M.T., Takamiya, M.Y., & Roth, M. 1991, *ApJ*, 367, L59
- Sanders, D.B., Solomon, P.M., & Scoville, N.Z. 1984, *ApJ*, 276, 182
- Scalo, J. 1986, *Fund. Cosmic Phys.*, 11, 1
- Schneider, D.P., Greenstein, J.L., Schmidt, M., & Gunn, J.E. 1991, *AJ*, 102, 1180
- Shipman, H.L. 1986, in *Astrophysics of Brown Dwarfs*, ed. M.C. Kafatos, R.S. Harrington, & S.P. Maran (Cambridge: Cambridge University Press), p. 71
- Sibille, F., Chelli, A., & Lèna, P. 1979, *A&A*, 79, 315
- Simons, D.A & Becklin, E.E. 1991, *ApJ*, submitted

- Skrutskie, M.F., Forrest, W.J., & Shure, M. 1989, AJ, 98, 1409
- Smith, R.C. 1983, Observatory, 103, 29
- Spitzer, L. 1978, in Physical Processes in the Interstellar Medium
(New York: Wiley)
- Stauffer, J., Hamilton, D., Probst, R., Rieke, G., & Mateo, M. 1989,
ApJ, 344, L21
- Stauffer, J.R. & Hartmann, L.W. 1986, ApJS, 61, 531
- Stauffer, J., Herter, T., Hamilton, D., Rieke, G.H., Rieke, M.J.,
Probst, R., & Forrest, W. 1991, ApJ, 367, L23
- Stevenson, D.J. 1978, Proc. ASA, 3, 227
- Stobie, R.S., Ishida, K. & Peacock, J.A. 1989, 238, 709
- Strand, K. Aa. 1977, AJ, 82, 745
- Tarter, J.C. 1975, PhD Thesis, University of California, Berkeley
- Tarter, J.C. 1986, in Astrophysics of Brown Dwarfs, ed. M.C.
Kafatos, R.S. Harrington, & S.P. Maran (Cambridge: Cam-
bridge University Press), p. 121
- Tomkin, J. & Pettersen B.R. 1986, AJ, 92, 1424

- van Biesbroeck, G. 1944, AJ, 51, 61
- van Biesbroeck, G. 1961, AJ, 66, 528
- van de Kamp, P. 1945, PASP, 57, 34
- van de Kamp, P. 1953, PASP, 65, 73
- van de Kamp, P. 1969, PASP, 81, 5
- van de Kamp, P. 1971, ARA&A, 9, 103
- van de Kamp, P. 1986, Space Sc. Rev., 43, 211
- van de Kamp, P. & Worth, M.D. 1972, AJ, 77, 762
- VandenBerg, D.A., Hartwick, F.D.A., Dawson, P. & Alexander, D.R.
1983, 266, 747
- van den Bos, W.H. 1937, Union Obs. Circ 4, 342
- Veeder, G.J. 1974, AJ, 79, 1056
- Weis, E.W. 1982, AJ, 87, 152
- Wielen, R. 1977, A&A, 60, 263
- Wilson, O.C. 1967, AJ, 72, 905
- Worley, C.E. & Heintz, W.D. 1983, Publ. U.S.N.O., 2nd Series, 24,

Part7, Fourth Catalog of Orbits of Visual Binary Stars

Worth, M.D. & Heintz, W.D. 1974, ApJ, 193, 647

Young, A. 1974, ApJ, 189, 587

Zuckerman, B. & Becklin, E.E. 1987, ApJ, 319, L99

Zuckerman, B. & Becklin, E.E. 1987, Nature, 330, 138

Zuckerman, B. & Becklin, E.E. 1991, ApJ, submitted